

LOUGHBOROUGH  
UNIVERSITY OF TECHNOLOGY  
LIBRARY

AUTHOR

WRIGHT, D C.

COPY NO.

006199/01

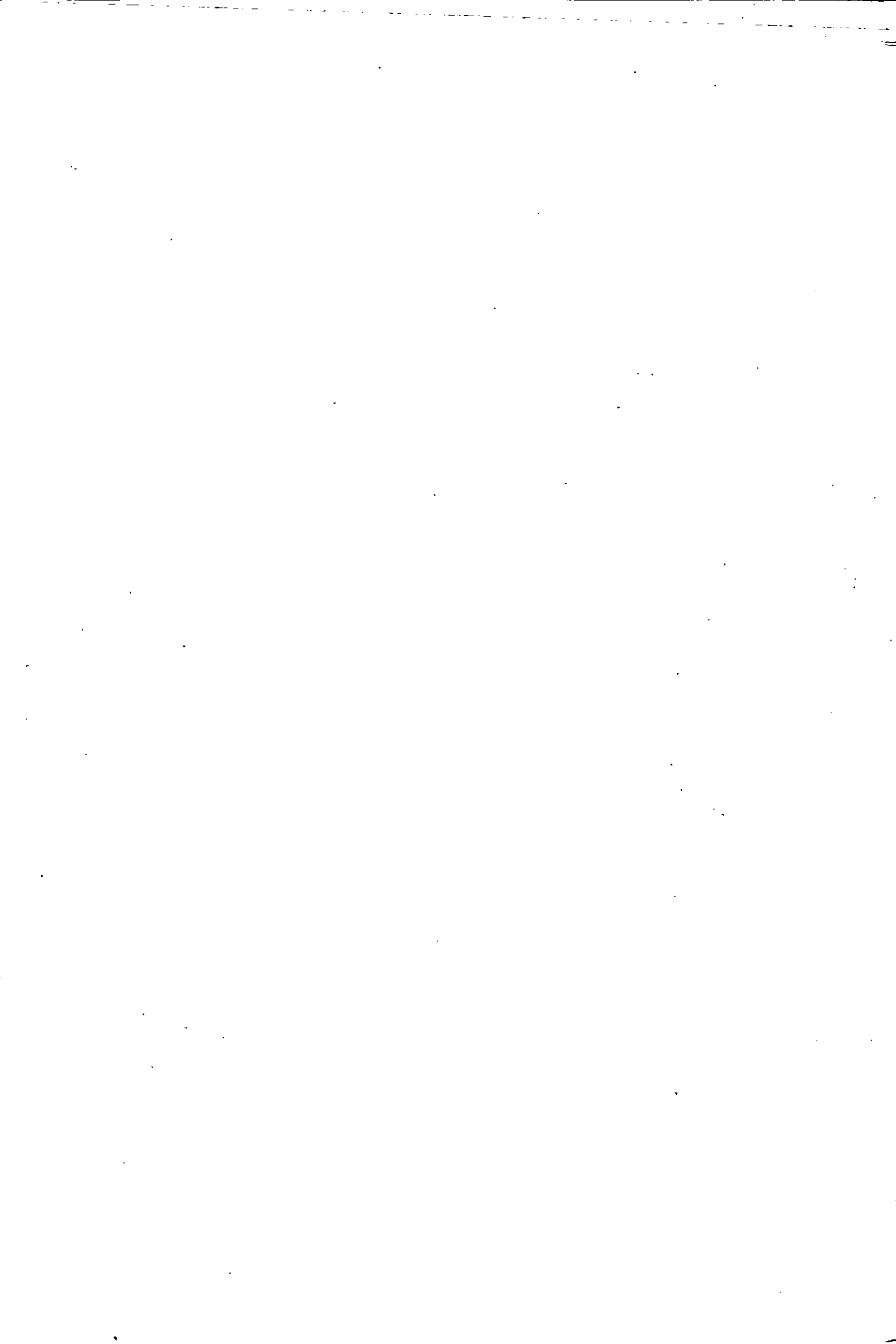
VOL NO.

CLASS MARK

ARCHIVES

COPY

FOR REFERENCE ONLY



CRAZE INITIATION AND GROWTH IN RIGID PVC

by

DAVID CHARLES WRIGHT, B.TECH., M.Sc.

A Doctoral Thesis submitted in partial fulfilment of the requirements for the award of Doctor of Philosophy of the Loughborough University of Technology, October 1975.

Supervisors: M.J.Stevens,  
Institute of Polymer Technology  
Dr. M.M.Hall,  
Rubber and Plastics Research Association



by David Charles Wright, 1975.

Loughborough University of Technology Library	
Date	July 1976
Class	
Acc. No.	006199/01

<u>CONTENTS</u>	<u>PAGE NO.</u>
Chapter 1 <u>Introduction</u>	1
Chapter 2 <u>The Mechanical Properties of Glassy</u> <u>Amorphous Thermoplastics</u>	5
2.1     A Introduction to the Glassy Amorphous State	5
2.2     Creep and Recovery	10
2.2.1     Step Input of Stress	
2.2.2     Gate Input of Stress	
2.2.3     Repeated Gate Input of Stress	
2.2.4     Craze and Crack detection by Creep Testing	
2.3     Stress Relaxation	25
2.4     Macroscopic Yielding	29
2.4.1     Yield Behaviour	
2.4.2     Post-Yield Behaviour	
2.5     Brittle Fracture	40
2.5.1     Macroscopic Fracture Theories	
2.5.2     The Fracture Process	
2.6     Fatigue	45
2.6.1     Static Fatigue	
2.6.2     Dynamic Fatigue	
Chapter 3 <u>Craze Geometry, Structure, Initiation</u> <u>and Growth</u>	54
3.1     Craze Geometry and Structure	54
3.2     The Initiation of Crazes	59
3.2.1     Sites for Craze Initiation	
3.2.2     Craze Initiation Criteria	
3.3     Craze Growth and Recovery	72
3.3.1     Growth under Static Tensile Stress	
3.3.2     Growth and Recovery under Intermittent Stress	
3.4     Crazing and Solvent Plasticization	77
Chapter 4 <u>Experimental Model and Equipment</u>	84
4.1     The Core Stress Model	85
4.2     The RAPRA Tensile Creep Machine	94
4.2.1     Design Consideration	
4.2.2     Design Details	
4.2.2.1     The Moire Fringe Extensometer	
4.2.2.2     The Optical System	
4.2.2.3     Electronics and Recording Equipment	
4.2.2.4     Machinery Hardware and Environmental Control	

Chapter 5	<u>Experimental Procedures and Results</u>	136
5.1	Thermal Conditioning of UPVC	136
5.2	The Damage Parameter in Response to Static Stress Histories	139
5.3	The Damage Parameter After a Variable Rest Period	156
5.4	The Damage Parameter in Response to Dynamic Stress Histories	157
5.5	The Effect of N-Hexane Immersion	172
5.6	Additional Test Results on Rubber Modified PPO (Noryl).	183
Chapter 6	<u>Discussion of Results</u>	185
6.1	The Damage Parameter and its Transitions	185
6.1.1	The First Transition	
6.1.2	The Growth of $\Delta R_{CR}(20)$	
6.1.3	The Second Transition	
6.2	The Relaxed Strain Criterion for Craze Initiation	192
6.3	The Relaxed Tensile Strain Criterion and Solvent Crazing	199
6.4	A Molecular Interpretation of the Relaxed Strain Hypothesis	207
6.5	Fatigue and the Relaxed Strain Criterion	214
6.6	A Engineering Design Criterion	223
Chapter 7	<u>Conclusions and Suggested Further Work</u>	232
7.1	Conclusions	232
7.2	Suggestions for further work	237
	Bibliography	240
	Appendix I Patent Specification	249
	Appendix II Creep Machine Specification	256
	Appendix III Operating Instructions	258
	Appendix IV Anomalous Post-Annealing Response of UPVC and PMMA	267
	Acknowledgments	271
	Certificate of originality	272

## 1. Introduction

Facilities and financial support for the research programme reported in this thesis have been generously provided by the Rubber and Plastics Research Association of Great Britain. This Association, with its close connections with the polymer supply and user industries is in a unique position to identify problems and opportunities connected by polymer applications. In such an environment it is therefore not difficult to devise research programmes with creditable technological objectives. However there are strong commercial pressures which tend to limit the depth and rigour of any investigation. The approach to the objective tends to be direct in deference to the law of diminishing returns. These commercial pressures do not operate to the same extent if the identified problem is a severe one. One such problem is the high incidence of brittle failure of load bearing thermoplastic components in service. These failures are generally quite unexpected because engineering thermoplastics, i.e. those chosen for load bearing applications, are invariably ductile on the evidence of standard material tests. RAPRA initiated a comprehensive research programme entitled 'Strength Criteria for Plastics' with the objectives of identifying the cause(s) of service induced embrittlement and the development of design criteria for the avoidance of this type of failure. The work reported here is one part of the strength criteria programme which concentrates on the simulation of service performance of rigid PVC (UPVC). It is reasonable to suppose that the behaviour of UPVC will be characteristic of other glassy amorphous polymers.

Research activity into the response of thermoplastics to applied stress has tended to concentrate on deformation behaviour rather than strength. Such a bias would be justified if the apparent ductility of the thermoplastic could be relied upon in service, because the design limit for extensible materials is appropriately a deformation limit as determined by the component's function. One explanation for the research bias in favour of deformation could be the faith of those researchers divorced from such activities as failure diagnosis, in the resistance of so called engineering thermoplastics to brittle failure. Also, deformation studies, which generally involve a continuum mechanics analysis, can portray a degree of elegance that is difficult to match with strength studies. A study of strength in isolation is often a very unsatisfactory pursuit. Strength data is essentially single point and therefore to generate a functional relationship between strength and a material or service variable requires many individual tests. In addition brittle strength data is relatively erratic, perhaps because of the localised nature of fracture.

The approach adopted here has been to look for discontinuities in the deformation behaviour of UPVC and to attempt to correlate these with the brittle failure process. This approach has the premise that deformation and the initiation of the failure process have a strong interaction, i.e. one perturbs the other. Evidence to support this interaction in UPVC (and other glassy amorphous polymers) is abundant. The connecting link between deformation and failure could well be craze initiation and growth. The evidence is as follows:



1. The critical flaw size for crack growth in glassy polymers is of the same order as craze dimensions.
2. The critical flaw is known not to be inherent and therefore must be generated under load. Crazes are not inherent and are also known to be generated under load.
3. The fracture surfaces of failed specimens exhibit craze like layers. Also crazes have been seen to propagate<sup>a</sup> in advance of a moving crack.
4. The growth of crazes can, if this is sufficiently rapid, perturb the deformation process. For instance there is a significant increase in creep rate after the initiation of solvent induced crazing.

The craze induced perturbation of the deformation process under simulated service conditions, where craze growth is not rapid, would not be detectable by merely examining the creep response. A special testing procedure was developed whereby the perturbation is in effect magnified and detectable. This so called  $\Delta R$  technique forms the basis of a mechanical (non-visual) method of detecting craze initiation and assessing craze growth in opaque as well as transparent polymers. The resolution of the method is such that the critical combinations of stress, strain, time and temperature for the initiation of the perturbation could be analysed in some detail. This analysis indicated that the

cause of the perturbation, and by implication craze initiation, is the generation of a critical level of relaxed tensile strain. This criterion is apparently independent of all service variables, including chemical environment. In addition the generation of the critical level of relaxed strain is shown to coincide with the initiation of the failure process where this initiation is connected with an observable mechanical instability.

The paradox raised by the observed difference in the failure of glassy amorphous polymers under laboratory and service conditions can be explained in terms of craze nucleation and growth. In the laboratory the conditions of test tend to favour craze nucleation at the expense of craze growth. In service, craze growth is encouraged by such factors as low stress levels and mechanical perturbations. It is generally accepted that a high craze (site) density precedes ductile (yield) failure and sparse crazing promotes brittle failure. It is consistent therefore to propose that under conditions which cannot be simulated in the laboratory (long service lifetimes) the primary cause of failure continues to be the initiation of crazes. Thus provided the relaxed strain criterion for craze initiation continues to operate at long times, (as its singularity under laboratory tests would indicate) a design criterion based on this should provide a rational method for avoiding in-service component failures.

## 2. The Mechanical Properties of Glassy Amorphous Thermoplastics

### 2.1 An introduction to the Glassy Amorphous State

Commercially available atactic unplasticised polyvinylchloride (UPVC) is described as a glassy amorphous thermoplastic at ambient temperatures. Other important polymers in this category include polymethylmethacrylate (PMMA), polystyrene (PS), polycarbonate (PC), styrene acrylonitrile (SAN), polyphenylene oxide (PPO), and polysulphone. In addition rubber modified polymers include high impact polystyrene (HIPS), acrylonitrile-butadiene-styrene (ABS), and modified PPO (Noryl ).

The molecular and thermodynamic characteristics typical of the glassy state can be visualised by reference to the kinematical processes that occur during the cooling of the molten polymer to the solid state. In the molten state the kinetic energy of the molecules that constitute the material is sufficient to overcome all inter- and many intra- molecular energy barriers. Thus rotation and flexing of the molecular chain, chain segments, and, where these exist, side groups, are free to occur. Thus although the molecular conformations are completely irregular and chaotic, the melt as a whole is in equilibrium with its thermal environment. On cooling, the volume of the polymer will decrease at a rate that initially maintains this equilibrium. At lower temperatures the viscosity of the melt will begin to increase significantly with the result that at high rates of cooling the volume will be unable to 'relax' at a rate sufficient

to maintain equilibrium. This condition is reached at lower temperatures at lower rates of cooling. This effect is illustrated in Figure 2.1. As the material is cooled further the viscosity increases considerably and at a level of  $\sim 10^{14}$  NS/m<sup>2</sup> the liquid is considered substantially immobile. The frozen in amorphous (liquid-like) structure that results from such a cooling process is characteristic of the glassy state. Although this state is never in thermodynamic equilibrium it is considered to be a metastable state in that changes in the direction of equilibrium (e.g. volume relaxation) generally occur so slowly that they are insignificant over the time scale of most observations.

The characteristic temperature at which the polymer changes from a liquid in equilibrium to that of a meta-stable glass is identified as the glass transition temperature  $T_g$ . The value of the glass transition temperature is both rate (1) and pressure (2) dependent. It is also dependent to some degree on the mechanical (3) and thermal (4) history of the polymer in its glassy state. Volume relaxation is only one of many transitions that can be observed and hence used as the basis of measuring  $T_g$ . Other notable parameter relaxations include; enthalpy, electrical and mechanical energy absorption, stress/strain moduli, and yield strength. The relaxation time  $\tau$ , associated with the response of the polymer to thermal, mechanical, electrical, or electromagnetic stimulation  $X(t)$  can be defined by the equation:

$$R(t) = R(\infty) e^{-\frac{t}{\tau}} \quad \text{for} \quad \begin{array}{l} X(t) = 0, \quad t < 0 \\ X(t) = X, \quad t \geq 0 \end{array}$$

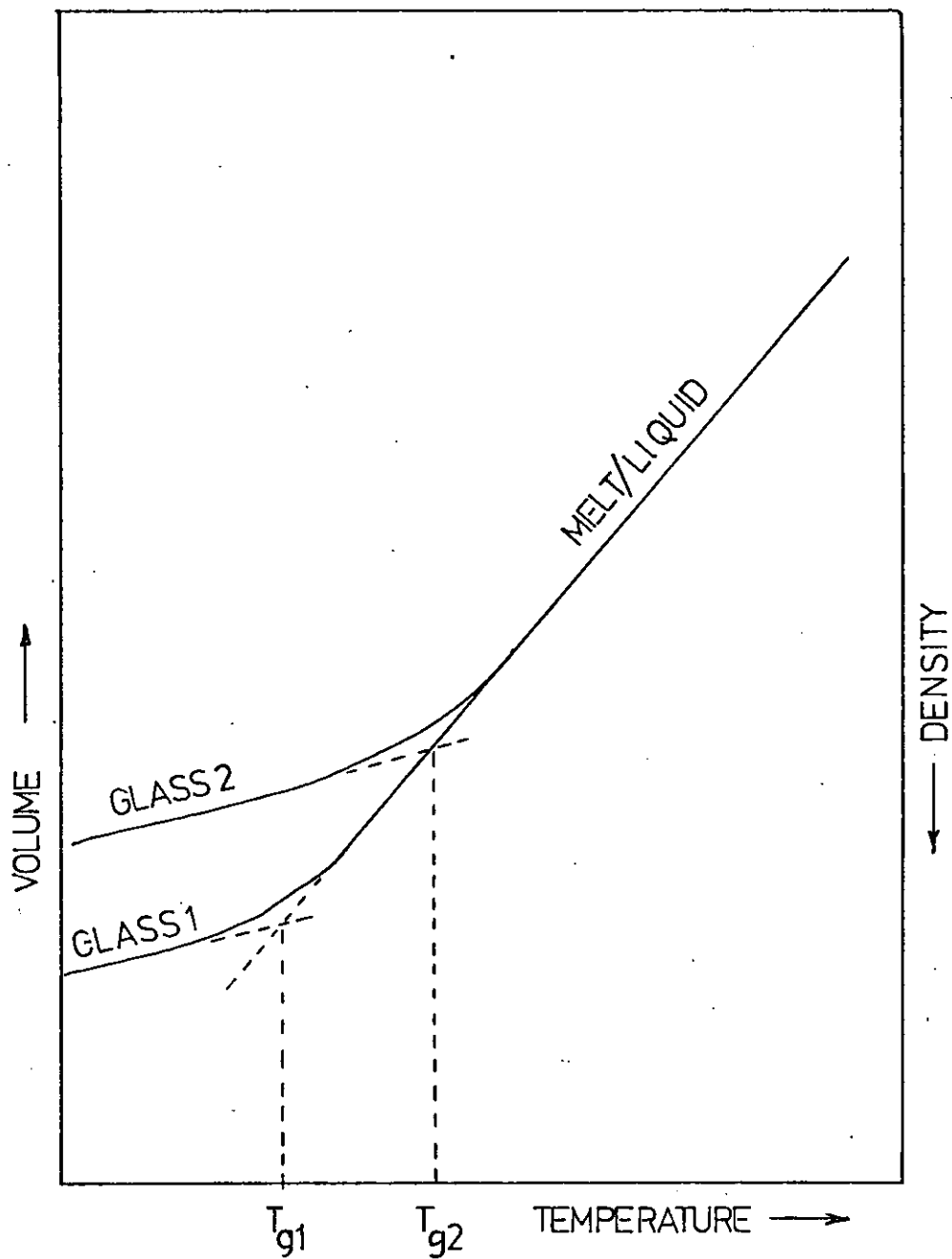
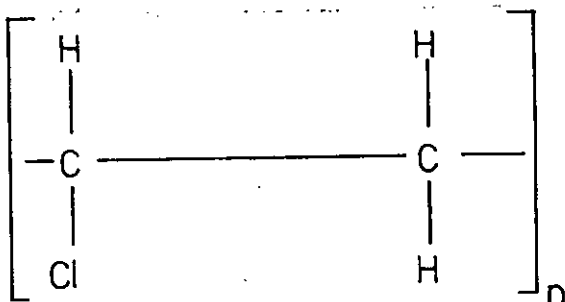


FIGURE 2.1 VOLUME TEMPERATURE RELATIONSHIP OF A GLASS FORMING LIQUID. GLASS2, FAST COOLING, GLASS1, SLOW COOLING.  $T_{g1}$  AND  $T_{g2}$  ARE GLASS TRANSITION TEMPERATURES.

where  $R(t)$  is the amplitude of the response to  $\overset{C}{\wedge}$  excitation. Formally  $\tau$  is the retardation time if the transition parameter is extensive rather than intensive.

$T_g$  is normally associated with primary (main chain) molecular relaxations. The main chain molecule of UPVC can be defined as:



Other sub-molecular units can also relax in response to  $\overset{C}{\wedge}$  excitation. These are referred to as secondary relaxations. The relaxation and retardation times are shorter, and the transitions are at lower temperatures than those associated with a primary relaxation. A labelling system has become established to assist in the identification of different relaxations, these being in order of decreasing transition temperature,  $\alpha$  (primary) and  $\beta, \delta, \epsilon, \dots$  (secondary). In the case of atactic UPVC which has no chain side groups, the source of the  $\beta$  relaxation has become associated with 'local mode relaxation of short chain segments' (5). By comparison PMMA exhibits a  $\beta$  and  $\delta$  transition which can be traced to side group rotation of  $\overset{S}{\text{ether}}$  and methyl groups.

The secondary transitions increasingly influence the mechanical behaviour of glassy polymers with decreasing temperature below  $T_g$ . This has been demonstrated for yielding in UPVC (6) (7), PC (8) and PMMA (9). Boyer (10) has proposed that the  $\beta$  transition

plays a dominant role in the craze initiation of Polystyrene. The evidence for this is that the activation energies for craze initiation (35-40 Kcal/mol) and the  $\beta$  transition (35 Kcal/mol) are similar. Similarly Sternstein and Sims (11) have reported that the respective activation energies for crazing and the  $\beta$  transition in PMMA are 20 and 21 Kcal/mol.

The pressure dependence of the  $\beta$  relaxation process in UPVC and the independence of both the  $\beta$  and  $\delta$  processes in PMMA (12) with pressure can be accounted for in terms of 'free volume'. Many other relaxation phenomena including gross effects such as macroscopic yielding (13) (14), the pressure (2) and tensile stress (15) dependency of  $T_g$  etc., have been interpreted using free volume models. The models differ generally in their quantitative definition of free volume  $V_F$  or rather their definition of occupied volume  $V_O$ . The total volume of the glass  $V$  is defined universally as:

$$V = V_F + V_O$$

$V_F$  is commonly termed the expansion volume where this is computed from the thermal expansion volume increase.  $V_O$  is the minimum (close packing) volume at 0°K. Fractional free volumes computed by using thermal expansion data for glassy polymers at  $T_g$  are in the range 0.12 - 0.14 (16). With regard to the pressure dependence of the  $\beta$  relaxation process in PVC, this is seen as evidence that local mode relaxations are volume sensitive. Side group rotations of the type responsible for the  $\beta$  and  $\delta$  relaxations in PMMA are sensibly independent of free volume in that

these can proceed without volume change.

## 2.2 Creep and Recovery

### 2.2.1 Step input of Stress

The strain response of a viscoelastic material to a step input of stress defines the creep compliance  $C(t)$  of the material.

Thus:

$$C(t) = \frac{\epsilon(t)}{H(t)\sigma_0} \quad \text{where} \quad \begin{array}{l} H(t) = 0, t < 0 \\ H(t) = 1, t \geq 0 \end{array}$$

Recommended procedures for the experimental determination of  $C(t)$  are included in BS (4618) (17). These emphasise the experimental requirements of such measurements notable of which are the need for good temperature control, low friction, and rapid but critically damped load application (18). The same set of documents (17) also recommend that creep data should be presented in a graphical format. The basic creep data  $\epsilon(t)$  <sup>are</sup> ~~is~~ plotted as a function of  $\log t$  with stress level as the parameter. This is shown diagrammatically in Figure 2.2(a). Cross-plots taken from the basic creep data are shown in Figure 2.2(b) and 2.2(c) these being termed the isochronous stress/strain, and isometric stress/time plots respectively. These reveal more obviously any non-linearity (stress or strain dependence of the compliance) in the material's response. The isometric data can be used directly in design where the maximum permissible strain is specified. <sup>They</sup> ~~It~~ can also be used as an approximation to the stress relaxation characteristic. The isochronous data can be used conveniently as design data when the life-time is specified. An additional graphical format shown in Figure 2.2(d) is  $C(t)$  versus  $\log t$  with the parameter of stress or strain. The value



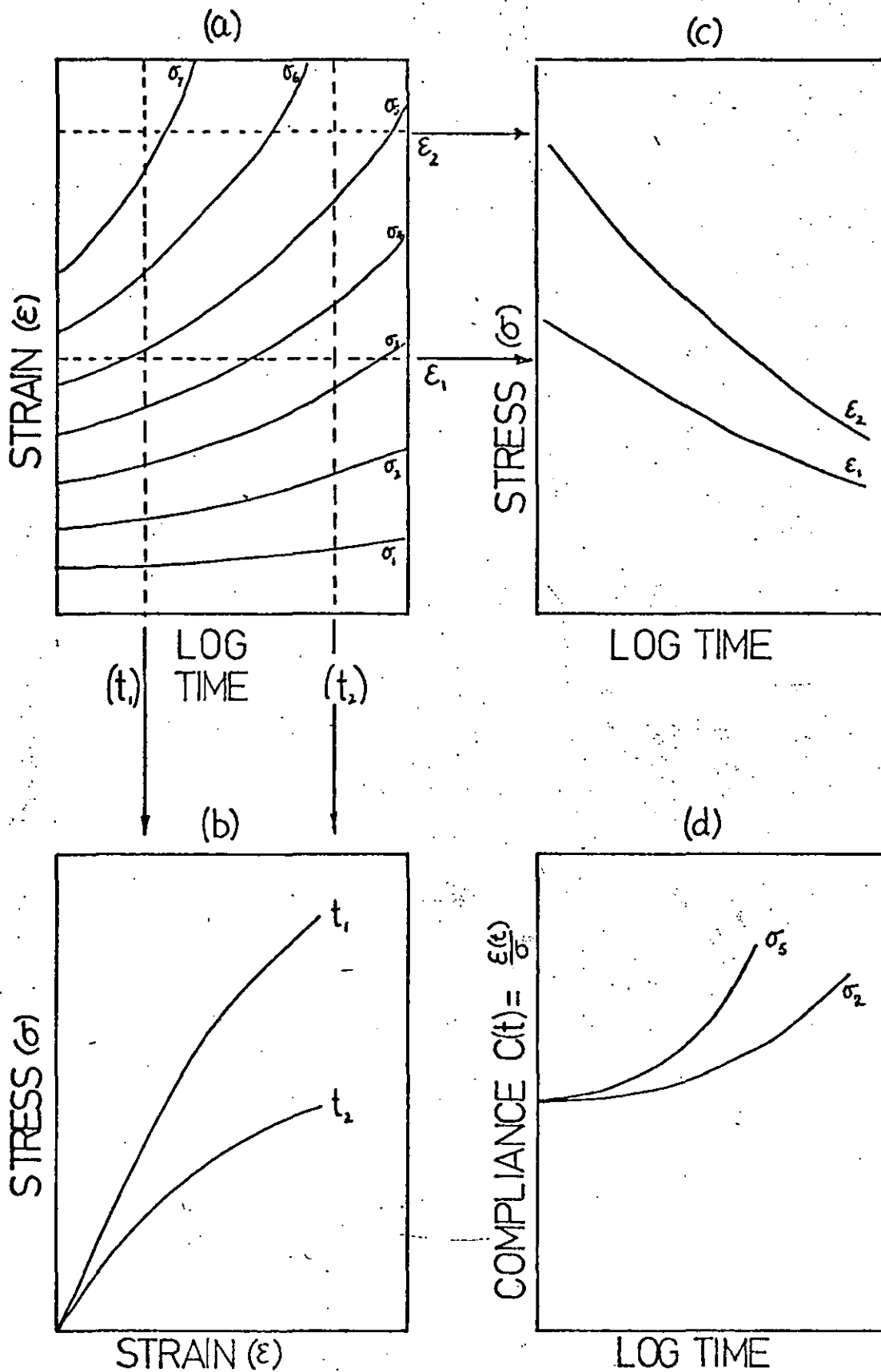


FIGURE 2.2 FORMATS FOR THE PRESENTATION OF CREEP DATA. (a) CREEP, (b) ISOCHRONOUS, (c) ISOMETRIC, (d) CREEP COMPLIANCE.

of  $C(t)$  obtained from such a plot and relevant to the specified lifetime of the designed component can be substituted as the inverse of the elastic modulus in standard elasticity equations (e.g. elastic instability, deflection of beams etc). This process has become known as pseudo-plastic design.

Apart from being temperature dependent the creep compliance is also generally stress and strain dependent at significant levels of stress, strain and time. This has been established for UPVC in tension, uniaxial compression (19) and shear (20). The bulk compression compliance for UPVC however has been reported as being independent of stress and strain (21). In tension glassy amorphous thermoplastics tend to display an apparently linear region up to experimentally significant strains and to exhibit a sharp discontinuity to non-linear behaviour (22) (23).

With reference to the difference noted (2.1) in the response of the  $\beta$  relaxation processes in UPVC and PMMA (the former being pressure dependent and the latter pressure independent) it is of interest to compare the creep response of these polymers. At low stress levels the creep characteristics are similar. At high stress levels the initial strain responses are still similar, but at longer times the creep compliance of UPVC increases dramatically in comparison to that of PMMA. This could be taken as evidence for the tensile stress dependence of  $T_g$  reported by Andrews (15) for UPVC (UPVC has a lower  $T_g$  than PMMA). The similarity of the initial compliance of the two polymers together with the differences at long times and at high stress might well also

be connected with the volume changes observed by Benham and McCammond (24). Under uniaxial tensile stress the volume of PMMA increases initially but does not increase further with time under stress. PVC however was observed to increase in volume initially and with time under stress.

The relationship between creep characteristics at different temperatures is complex and cannot be normalised by simple time/temperature super-position (25). This may be partly due to the problem of defining the reference state at different temperatures. Turner (26) has demonstrated that the preconditioning time at the temperature of test has a considerable influence on the shape of the creep characteristic of UPVC. Even after 2000 hours preconditioning time there was no evidence that a stable state was being approached. On this evidence alone it would be surprising if time-temperature superposition was ever possible with UPVC. Sternstein and Ho (3) have suggested that changes in free volume in glassy polymers do not have equal effects on different retardation processes. This may at least partially explain the phenomena. Specifically, the long term processes are preferentially affected.

The molecular processes responsible for creep in glassy amorphous thermoplastics are not known in detail. This must be due partly to the difficulty of qualifying the molecular structure or conformation of these polymers. On a macroscopic scale, shear (deviatoric) deformations occur at constant volume. Thus it might be argued that the time dependent tensile creep strain of PMMA, which occurs without volume change (24) is totally due to shear deformations and that in PVC the

deformation is partly due to shear processes and partly due to dilatational processes. This concept has been developed successfully by Bucknall and Clayton (27) as a means of assessing the dilatational contribution (crazing) to creep deformations in rubber modified glassy polymers. At a microscopic level however, particularly in the amorphous state, the nature of shear has not been established. It is conceivable for instance that the occupied (molecular) volume could change in response to an applied stress such that the total volume, which includes both free volume and occupied volume remained constant (28). This might imply, on a macroscopic level that the deformation is totally deviatoric, but at a molecular level this interpretation would not be strictly correct.

### 2.2.2 Gate Input of Stress

A gate input of stress can be formally defined as:

$$\sigma(t) = \sigma_0 H(t) \text{ where } H(t) = 0, T \leq t < \infty \\ H(t) = 1, 0 \leq t < T$$

A step input of stress, of amplitude  $\sigma_0$  is applied at  $t = 0$ ; at a time  $T$  the stress is removed step-wisely. The period  $t > T$  is known as the recovery period. The strain/time path of the recovery can be quantified in terms of either the residual strain  $\epsilon_{res}$  or the recovered strain  $\epsilon_r$ . These terms are defined in Figure

2.3. The Boltzman (29) superposition principle would predict that a linear viscoelastic material would recover along a path:

$$\epsilon_{res}(t) = C(t)\sigma_0 - C(t-T)\sigma_0 \quad \text{--- [1]} \\ \text{as } t \rightarrow \infty, \epsilon_{res} \rightarrow 0,$$

Thus the Boltzman superposition integral would predict complete recovery if sufficient time is allowed to complete this process. It is experimentally difficult to check this because at

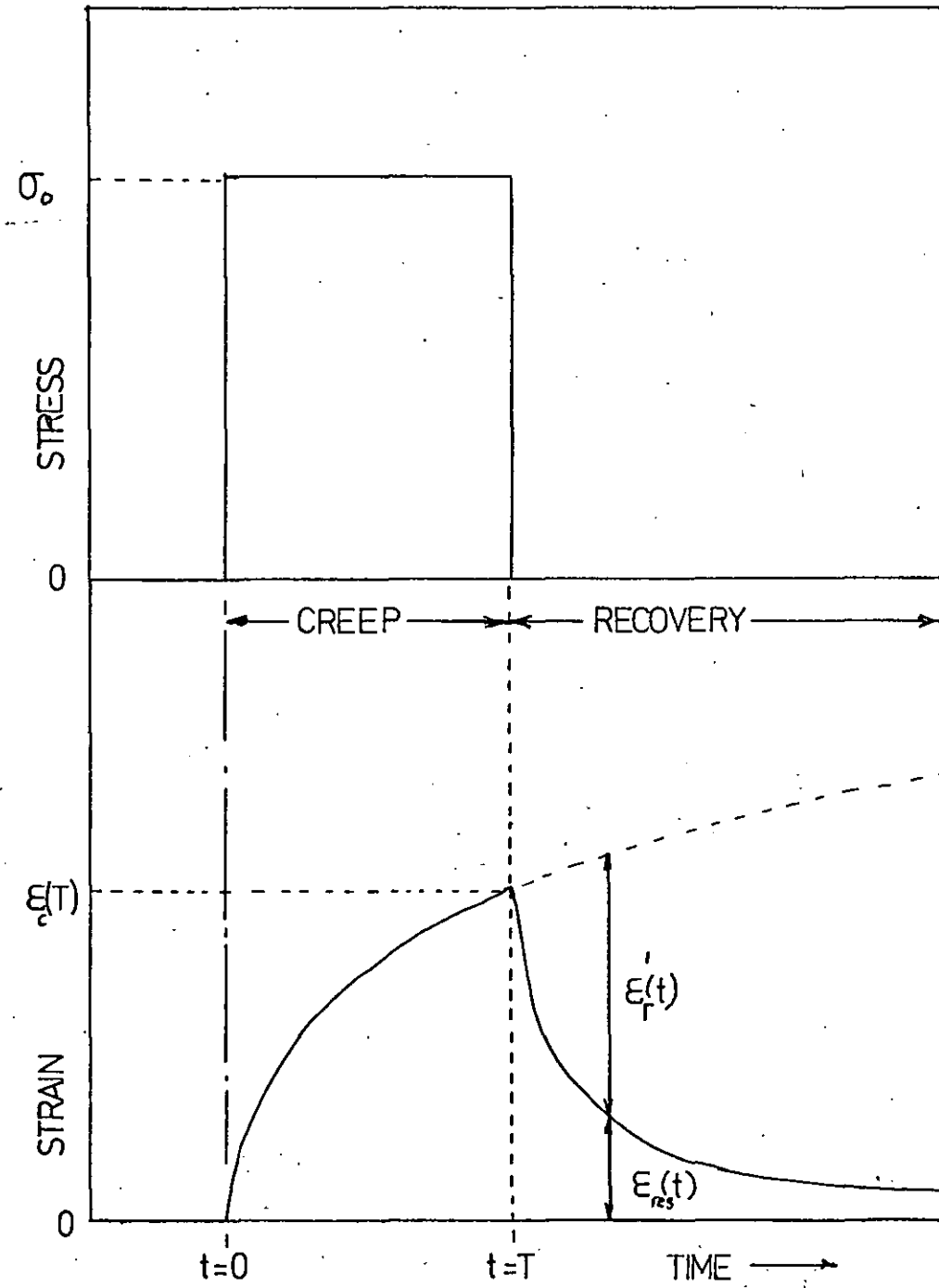


FIGURE 2.3 STRAIN RESPONSE TO A GATE INPUT OF STRESS.

low levels of residual strain the retractive forces are so weak that friction in the measuring equipment could prevent further recovery. According to Turner (18) equation [1] represents a good approximation to the measured recovery behaviour of glassy amorphous thermoplastics provided the prior creep strain and creep time are not excessive. However the recovery behaviour from 'severe' stress histories is anomalous in two respects. At small values of  $(t - T)$ , that is short recovery times,  $\epsilon_r(t)$  exceeds that predicted for linear viscoelastic materials by the Boltzman superposition integral. At large values of  $(t - T)$  the reverse is observed. Turner did not find these observations surprising. In fact he pointed out that the form of the non-linearity of these materials, that is 'strain softening', would be expected to lead to excessive initial recovery. However in the same paper he reports that although the apparent compliance of the material  $\frac{\epsilon(t)}{\sigma}$  increases with time under stress the actual compliance  $(\Delta \epsilon / \Delta \sigma)_t$  decreases with creep time. Thus the strain softening explanation for the observed high initial rates of recovery would not seem to be valid.

Menges and Schmidt (30) have proposed that incomplete recovery in glassy polymers is due to micro-damage initiation and growth during the creep period. They further propose that the initiation of such micro-damage in the form of voiding or crazing, is responsible for the onset of non-linear viscoelastic behaviour. Menges did not extend this hypothesis to explain the excessive initial recovery behaviour (which is a form of non-linear interaction). In Section 4.1 of this thesis such an explanation is proposed.

The recommended format (17) for the presentation of recovery behaviour is derived from the work of Turner (31). By the use of two

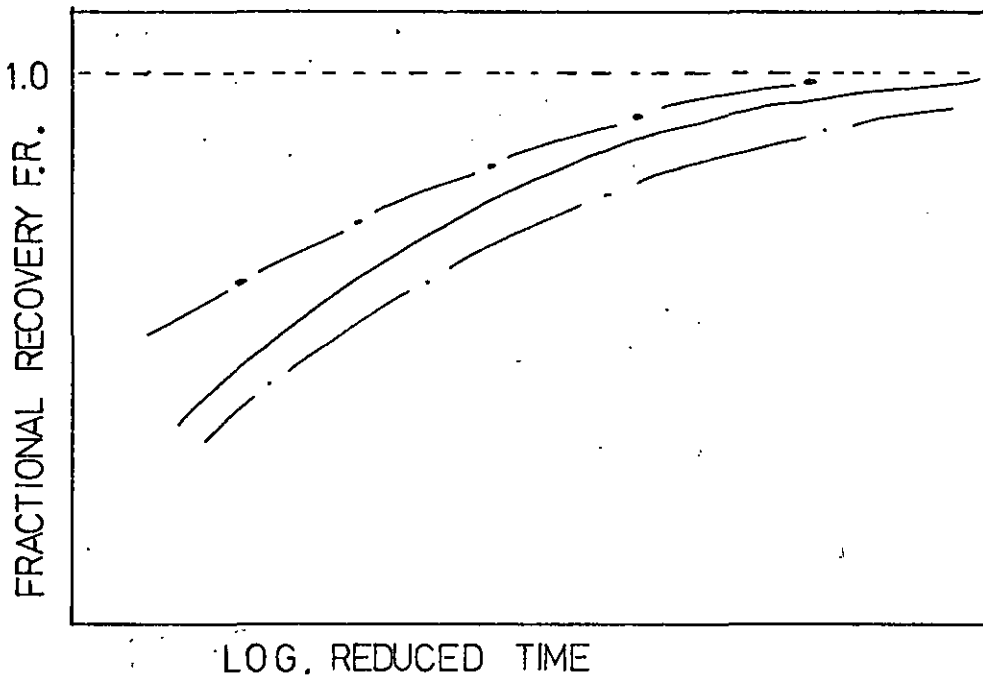


FIGURE 2.4(a) DIMENSIONLESS FORMAT FOR THE PRESENTATION OF RECOVERY DATA FULL RECOVERY, F.R. = 1 .

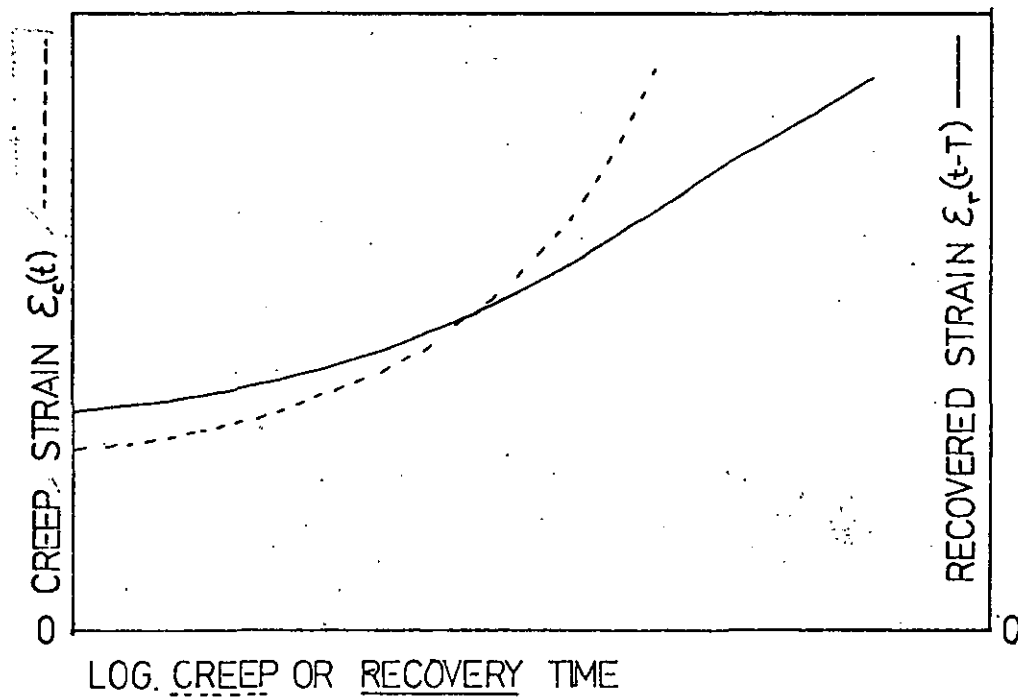


FIGURE 2.4(b) FORMAT SHOWING NON SUPERPOSITION OF CREEP AND RECOVERY DATA.

non-dimensional variables this format attempts to normalize recovery data over a wide range and combination of maximum creep strain  $\epsilon_c(T)$  and creep time (T). These two variables are defined as:

$$\text{Fractional Recovery F.R.} = \frac{\epsilon_r(t)}{\epsilon_c(T)}$$

and

$$\text{Reduced time R.T.} = \left( \frac{t-T}{T} \right)$$

The format is illustrated diagrammatically in Figure 2.4(a). The advantage of this format is that the recovery data from widely ranging creep strains and times tend to superpose. A disadvantage is that it does not reveal readily the deviation (if any) of the recovery at short recovery times compared with that predicated for a linear viscoelastic material. This can be appreciated more readily in the alternative format shown in Figure 2.4(b).

### 2.2.3 Repeated Gate input of Stress

The growth of creep strain under conditions of intermittent stresses is of relevance in many component applications. Benham and Hutchinson (19) have investigated the strain or stress response of UPVC to the following stress or strain histories:

Mode (1) Repeated gate input of tensile stress.

$$\sigma(t) = \sigma_0 H(t) \text{ where } \begin{cases} H(t) = +1 & \text{for } (2N+1)T > t \geq 2NT \\ H(t) = 0 & \text{for } (2N-1)T \leq t < 2NT \end{cases}$$

where N is the cycle number and T

= recovery period per cycle = creep period per cycle, and  $\sigma_0$  is the tensile stress amplitude.



Mode (2) Repeated tension/compression stress cycling

$$\sigma(t) = \sigma_0 H(t) \text{ where } H(t) = +1 \text{ for } (2N+1)T > t \geq 2NT \\ H(t) = -1 \text{ for } (2N-1)T \leq t < 2NT$$

where the compression stress amplitude

$$= \text{tensile stress amplitude} = |\sigma_0|$$

Mode (3) Repeated tension/compression strain cycling

$$\epsilon(t) = \epsilon_0 H(t) \text{ where } H(t) = +1 \text{ for } (2N+1)T > t \geq 2NT \\ H(t) = -1 \text{ for } (2N-1)T \leq t < 2NT$$

where the compression strain amplitude

$$= \text{tensile strain amplitude} = |\epsilon_0| = 1.25 \%$$

Benham and Hutchinson employed a superposition technique involving non-linear compliance functions and compared the experimental data with the predicted response. The non-linear compliance functions were established by generating compressive and tensile creep data at stress levels equal to the stress amplitudes as used in Modes (1) and (2) above. The stress relaxation modulus at a strain of 1.25% was used via a similar superposition technique to predict the stress response to the Mode (3) strain history. During the initial period of the cycling programmes the predicted and experimental strain responses were in close agreement particularly for Mode (1) stressing. The observed strain did however increase more rapidly than the predicted response after an extended period of cycling at high stress amplitudes. Under Mode (2) stress conditions this transition to higher than predicted strain growth rate occurred earlier, at lower stress amplitudes, and was observed to be so severe that it could be readily associated with the onset of fatigue failure. The authors established by additional

experimentation that this so-called 'cyclic softening' phenomenon was not the effect of temperature increase. PMMA was observed (32) to exhibit this phenomenon but to a lesser extent than UPVC.

The above observations are of particular interest here because the transition to cyclic softening represents a rational stability criterion for design against cyclic fatigue. The proposition that the transition is not thermally induced promotes some confidence in the extension of such a criterion to apply to 'low stimulus' fatigue situations i.e. realistic fatigue lifetimes.

Jaksch (33) studied the strain response of polyethylene under intermittent tensile stressing. Although the polymer is not glassy amorphous, the detail of his study is such that it is useful to include a reference to it here. Jaksch observed that the main contribution to strain growth under stress conditions defined by Mode (1) above was due to the increase in the instantaneous (unrelaxed) strain response with successive cycling. The time-dependent response (relaxed strain component) remained reasonably cycle-independent for extended periods. Jaksch attributed this to 'additional retardation mechanisms with very short retardation times arising from the amorphous regions'.

#### 2.2.4 Craze and crack detection by creep testing

Apart from the visual detection of micro-damage during creep, which will be discussed fully in the next Chapter, two basically mechanical techniques have been used to detect, and assess the growth of, crazes during tensile creep. These techniques are only adequate if the

craze contribution to apparent deformation is considerable.

Bergen (34) has compared the tensile creep behaviour of UPVC and other glassy amorphous polymers in air and immersed in organic solvents. The solvents induced severe crazing or cracking in the polymers. The stress, strain and time, coordinates for the initiation of this damage could be ascertained by the transition from a comparatively slow creep rate to a fast creep rate. One set of creep data, for UPVC in air and isopropanol is reproduced in Fig. 2.5. Bergen proposed on the evidence of this and other similar sets of data on ABS, PC, HIPS and SAN in environments of either n-Hexane or isopropanol that craze and crack initiation occurred at a characteristic level of tensile strain. He further proposed that these critical strains, tabulated in Table 2.1, are independent of stress level.

	CRITICAL STRAIN %	
	in propanol	in N-Hexane
PVC	1.20	0.80
ABS	0.30	0.48
PC	1.15	1.09
HIPS	0.36	Swelling
SAN	0.30	0.40

Table 2.1. The critical tensile strains for craze or crack initiation in solvents. (After Bergen (34) ).

The form of the craze instability in UPVC and the strain range for its initiation are similar to that observed for cyclic softening (discussed in 2.2.3).

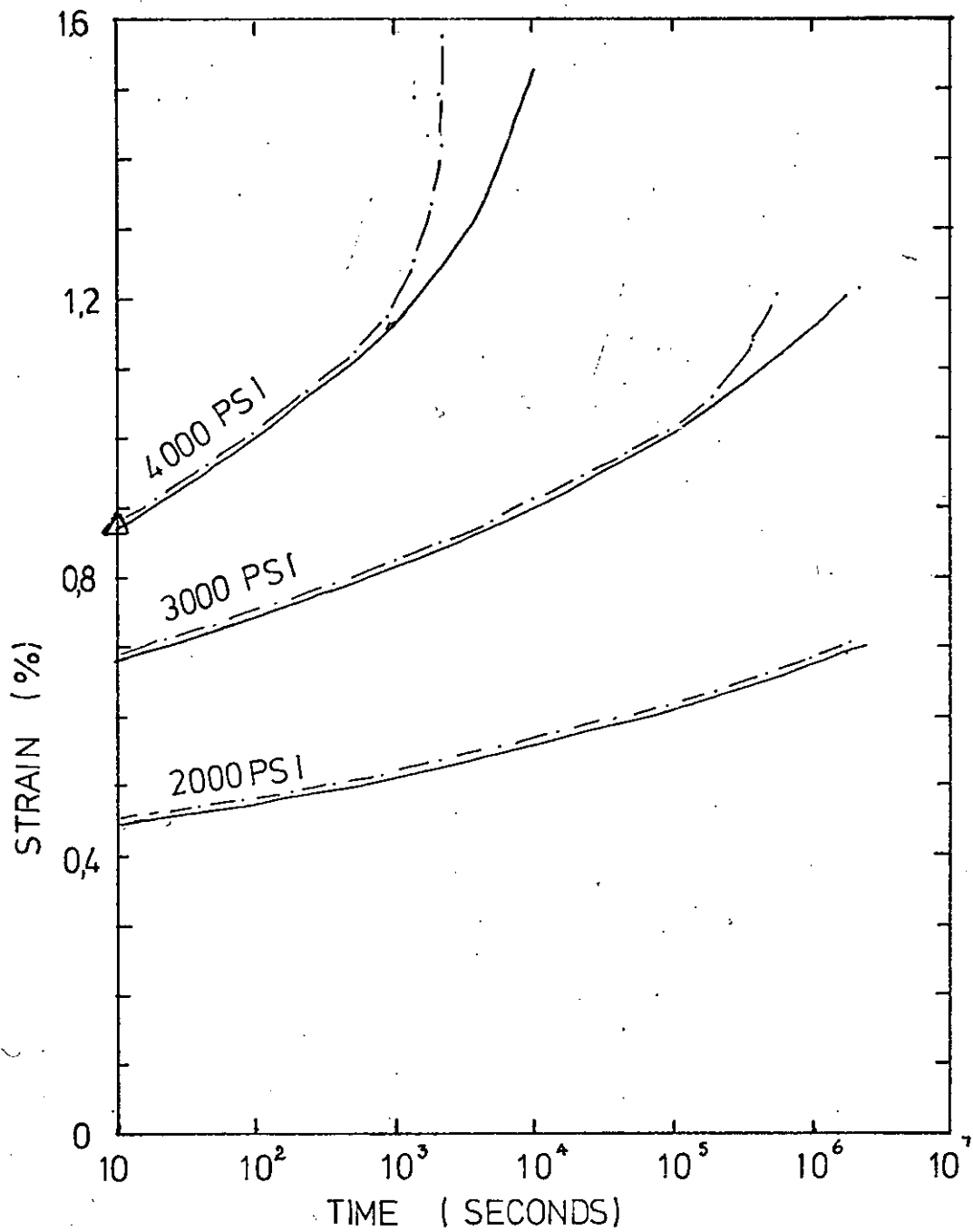


FIGURE 2.5 TENSILE CREEP OF UPVC IN;  
 — AIR,  
 - - - ISOPROPANOL  
 BERGEN (34)

Bucknall (35) and Bucknall and Clayton (27) have developed a different technique for assessing the separate contributions of dilatational and shear deformations to total uniaxial tensile creep strain, suitable for rubber modified glassy amorphous polymers in an air environment. Dilatational deformations were assumed to arise from cavitation mechanisms such as crazing, cracking or voiding. On the evidence obtained from microscopy, crazing was shown to be the predominant mechanism.

The technique involved the simultaneous measurement of both lateral and longitudinal creep strains. The volume strain during tensile creep was thus established. From <sup>these</sup> ~~this~~ data Bucknall and Clayton (27) were able to make the following deductions regarding craze initiation and growth in HIPS.

1. Crazing is the major factor in the non-elastic creep deformation of HIPS. For instance at a total tensile creep strain of 5% the crazing processes were responsible for an estimated 3.8% strain. Other contributions were, instantaneous elastic strain 1.1%, and time dependent elastic strain 0.1% (shear 'viscoelastic effects').
2. Crazing was initiated at between 0.9% and 1.1% tensile creep strain.
3. The induction time  $t_c$  for craze initiation increased with decreasing stress level  $\sigma$  such that:

$$t_c^{-1} = A e^{b\sigma}$$

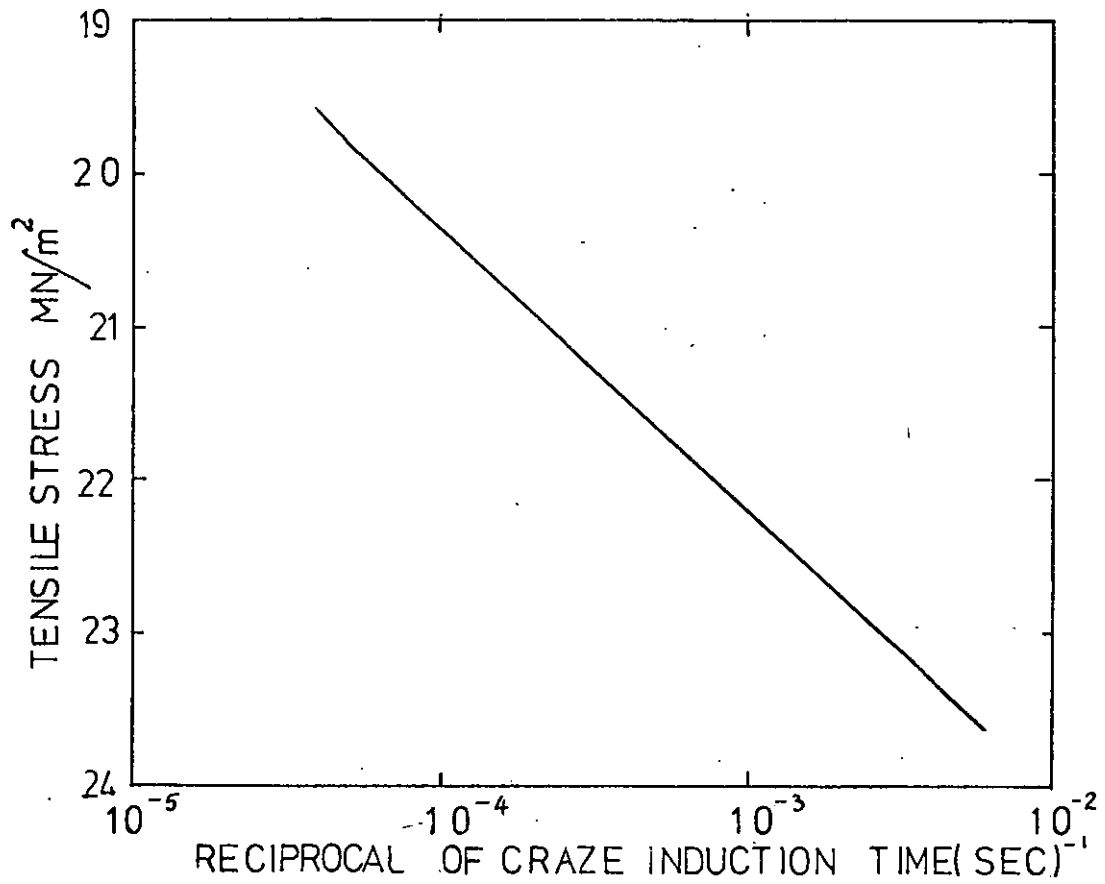


FIGURE 2.6 RELATIONSHIP BETWEEN STRESS AND CRAZE INDUCTION TIME FOR HIPS. BUCKNALL AND CLAYTON (27)

where A and b are constants. This approximates to the Eyring (36) rate equation. A similar relationship was established for the rate of dilation (crazing). Both processes had the same apparent activation volume. Thus craze initiation and craze growth were concluded to be one and the same process, this being void nucleation and growth.

4. The yield drop (yield instability) observed in glassy polymers is due to craze growth.

If craze initiation is responsible for an instability in the behaviour of a glassy amorphous polymer after long service lifetimes then the induction time for this instability shown in Figure 2.6 might offer a more rational design criterion than for instance static fatigue data. Unfortunately Bucknall and Clayton's technique would not be suitable for detecting craze initiation in unmodified glassy polymers in a passive-environment because the level of dilatational strain would be small and the crazes widely dispersed.

### 2.3 Stress Relaxation

The stress relaxation modulus  $M(t)$  is defined by the stress response  $\sigma(t)$  to an applied step input of strain  $H(t) \epsilon_0$  such that:

$$M(t) = \frac{\sigma(t)}{H(t) \epsilon_0} \quad \text{where} \quad \begin{array}{l} H(t) = 0, \quad t < 0 \\ H(t) = 1, \quad t \geq 0 \end{array}$$

Oberst and Retting (37) have evaluated  $M(t)$  for UPVC over a wide range of temperature. Some of their data <sup>are</sup> included in Table 2.2. The applied tensile strain was 0.5%.

t secs	M(t)	
	23°C	70°C
1	3200	1000
10	3100	600
10 <sup>2</sup>	3000	200
10 <sup>3</sup>	2900	50
10 <sup>4</sup>	2800	-

Table 2.2. The tensile relaxation modulus M(t) of UPVC (after Oberst and Retting (37)).

Oberst and Retting established the 'long term' relaxation spectrum H( $\tau$ ) using the equation:

$$H(\tau) = - M(t) \frac{d(\log M(t))}{d \log t} \Big|_{t=\tau}$$

and extended the spectrum to short times by measuring the loss modulus E'' over a range of frequencies. The equation used was:

$$H(\tau) = \frac{2}{\pi} E''(\omega) \Big|_{\omega = \frac{1}{\tau}}$$

where  $\omega$  is the angular velocity. Thus the relaxation spectrum of relaxation times between 10<sup>-4</sup> and 10<sup>4</sup> seconds was established. The 23°C spectrum is reproduced in Figure 2.7. The H( $\tau$ ) minimum separates the  $\alpha$  (main chain) relaxation and  $\beta$  (local mode) relaxation processes.

The dependence of M(t) on strain was not investigated by Oberst and Retting. Sternstein and Ho (3) have however shown that



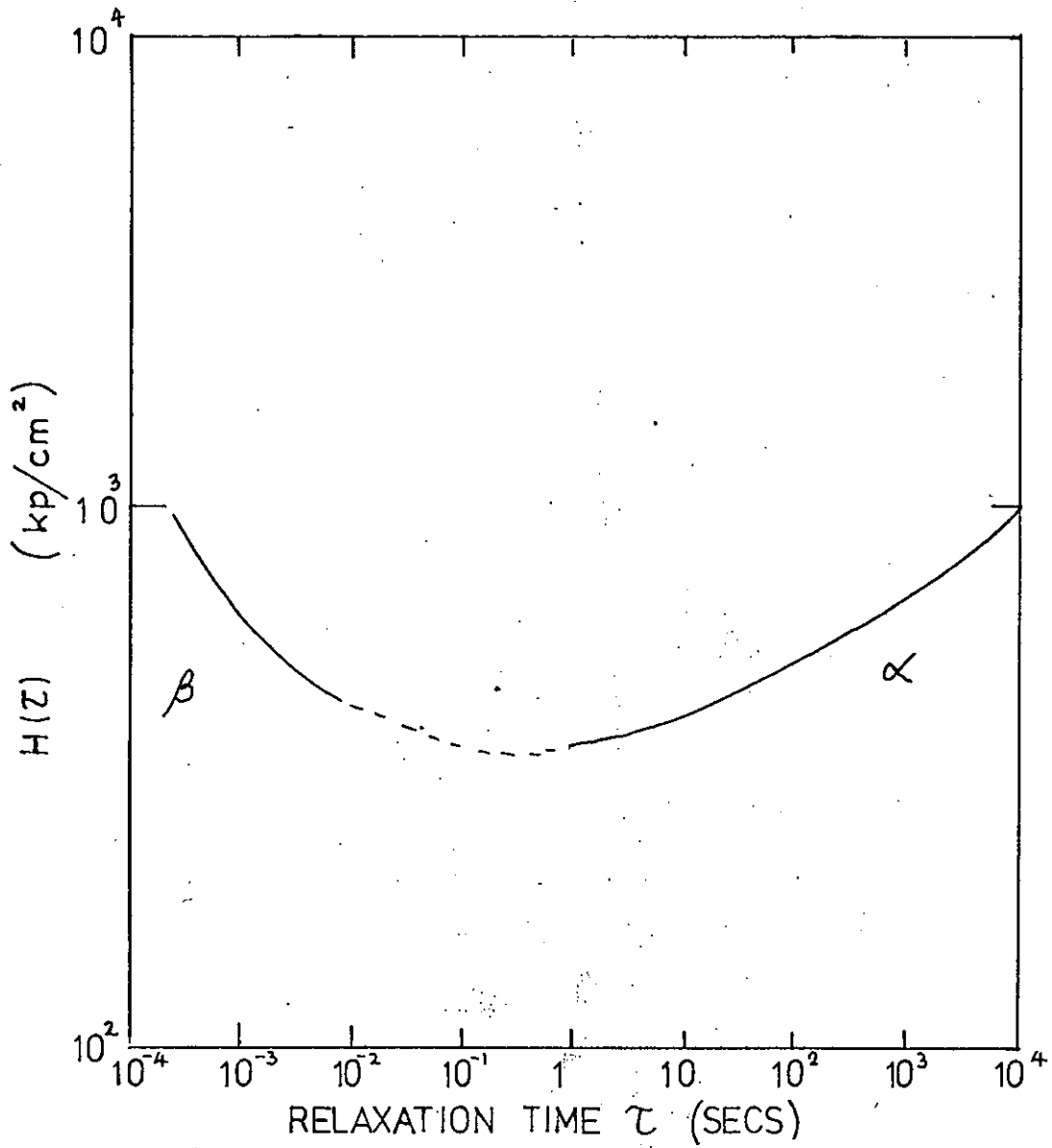


FIGURE 2.7 THE STRESS RELAXATION SPECTRUM OF UPVC. OBERST AND RETTING(37).

PMMA exhibits non-linear tensile stress relaxation above applied tensile strain levels of  $\sim 1.0\%$ . The torsional stress relaxation behaviour of the same material was reasonably linear over the strain range investigated i.e. at strains less than 2%. Sternstein and Ho concluded that the non-linearity is induced by the dilatational stress or strain component associated with uniaxial tensile stress or strain. In combined tension-torsion experiments the dilatational strain due to the tensile stress component increased the rate of torsional (shear) stress relaxation. However shear in a plane transverse to the tensile axis did not effect the tensile relaxation behaviour. Dilatational stress or strain influenced the rate of relaxation and the transition to non-linear behaviour.

Yannas, Sung and Lunn (22) have studied, in detail, the transition to non-linear stress relaxation behaviour in polycarbonate. The transition was observed to be sharp with a well defined strain range for linearity. The critical tensile strain for the transition decreased with increasing temperature and time. Some values are given in Table 2.3.

CRITICAL TENSILE STRAIN %		
$^{\circ}\text{C}$	$t_R = 10\text{s}$	$t_R = 10^3\text{s}$
20	1.30	1.10
40	1.29	1.09
60	1.28	1.08
80	1.25	1.06
100	1.17	0.95
120	1.05	0.78

Table 2.3 - The critical tensile strains for transition from linear to non-linear relaxation modulus  $E(t_R)$  at various temperatures below  $T_g$ . (After Yannas, Sung and Lunn (22) ).

Mercier, Aklonis, Litt and Tobolsky (38) have demonstrated that above its  $T_g$  polycarbonate exhibits a stress relaxation modulus that is independent of strain up to elongations of  $\sim 25\%$ . Yannas and co-workers have proposed that a minimum critical strain for the initiation of non-linear behaviour occurs at a temperature equal to the  $T_g$  of the polymer. In a later paper by Yannas (39) the critical stress/strain coordinates of both tensile creep and tensile relaxation tests were found to be linearly related i.e.

$$\epsilon_c = 0.35 + k\sigma_c$$

where  $\epsilon_c$  (%) and  $\sigma_c$  are the critical strains and stresses for the transition to non-linear viscoelastic behaviour.  $k$  is a constant that is independent of temperature and time. It might be reasonable to conjecture here that at long times or at  $T_g$ :

$$\sigma_c \rightarrow 0$$

and that the minimum critical strain is 0.35%. If non-linearity is connected with irreversible damage initiation then this minimum strain could be a potential rational design limit. Yannas, Lunn and Doyle (40) in fact provided evidence that the non-linear viscoelastic behaviour of polycarbonate is due to the rupture of secondary, inter-chain valence bonds.

#### 2.4 Macroscopic Yielding

Yielding of amorphous glassy polymers below  $T_g$  has been regarded as evidence of a stress or strain induced transition from the visco-elastic to the liquid state. Conceptually the yield process is initiated when the deformation response is no longer completely recoverable - i.e. at the onset of plastic flow. This however is difficult

to determine experimentally. In practice, like other diffuse transitions, yield is characterised by defining a yield point, which is readily identifiable under conditions of constant strain rate. The yield stress at the yield point is commonly defined as:

$$\left(\frac{d\sigma}{d\varepsilon}\right)_{\sigma=\sigma_y} = 0, \text{ for } \dot{\varepsilon} = k(\text{constant}).$$

The yield point together with typical post-yield behaviour are illustrated in Figure 2.8.

From an engineering design aspect the yield stress of a glassy polymer is of limited use. Although it represents the ultimate load-bearing capacity of the polymer, premature brittle failure commonly precludes yield. This is particularly the case at long service lifetimes, or when tensile stresses are involved or if immersed in a non-passive chemical environment. However there is considerable evidence that the phenomenology of macroscopic and microscopic yielding are similar. Therefore a knowledge of gross yielding is useful in understanding craze-phenomena. It is for this reason that this section has been included.

#### 2.4.1. Yield Behaviour

In common with other transitions in the behaviour of a glassy polymer the yield point changes with (strain) rate and temperature. The polymer in its response to shear stress can be classed as a highly non-Newtonian liquid which requires activation before flow can proceed. The Eyring (36) viscosity equation has been adopted by some workers and modified by others to model the measured temperature, and strain rate dependence, of yield. This equation can be expressed conveniently as:

$$\dot{\varepsilon} = A \exp(\Delta U - \sigma V) / KT$$

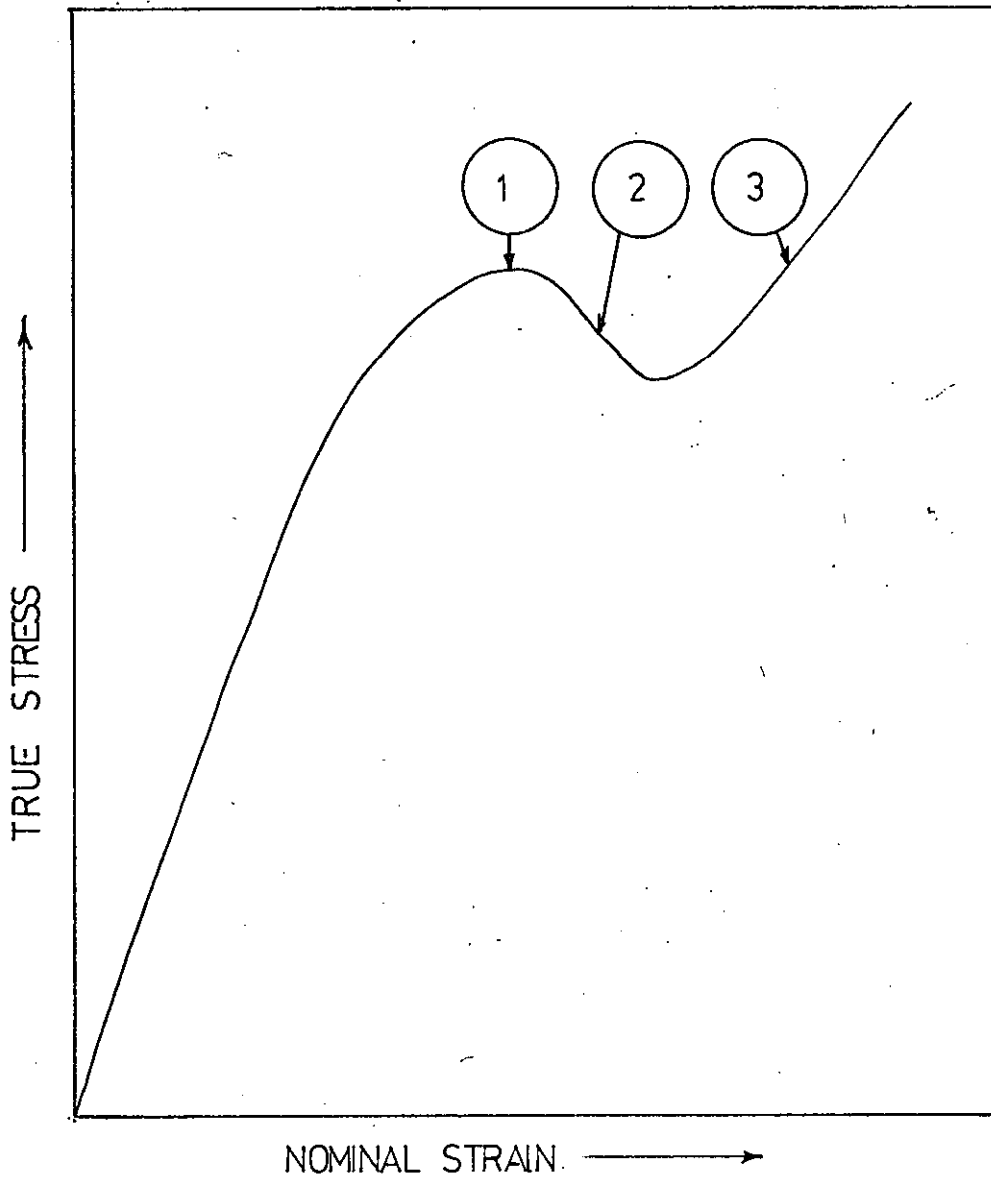


FIGURE 28

TYPICAL STRESS RESPONSE IN A CONSTANT STRAIN RATE TEST.

- 1 YIELD POINT
- 2 STRAIN SOFTENING REGION
- 3 ORIENTATION HARDENING REGION

where  $\sigma$  is the shear stress,  $\Delta U$  the activation energy of the (yield) flow process,  $V$  is the activation or flow volume,  $k$  is Boltzmanns constant, and  $T$  the absolute temperature. The equation predicts that:

$$\frac{d\sigma_y}{d(\ln \dot{\epsilon})} = \frac{2kT}{V}$$

and that

$$\frac{\sigma_y}{T} = \frac{\Delta U}{VT} + \left(\frac{k}{V}\right) \frac{\ln \dot{\epsilon}}{\beta}$$

Thus assuming a constant activation volume  $V$  the relationship between  $\frac{\sigma_y}{T}$  and  $\ln \dot{\epsilon}$  is linear with a gradient that is independent of temperature.

Bauwens-Crowet, Bauwens and Homes (7) have established that the unmodified Eyring equation accurately fits the measured yield stress behaviour of polycarbonate over 5 decades of strain rate, from 21°C to 140°C and down to yield stresses of 10 MN/m<sup>2</sup>. The same authors found that the generalised Ree Eyring (41) equation was required to fit their UPVC yield data. The generalised equation can include several activation modes with different activation energies and volumes. The UPVC data (Figure 2.9) <sup>were</sup> ~~was~~ modelled successfully by using two activation energies, these being 70 and 14 k cal/mol. These energies were identified with the  $\alpha$  and  $\beta$  relaxation processes. Roetling (9) similarly reported for PMMA, activation energies of 81 and 24 k cal/mol, these being close to those of the  $\alpha$  and  $\beta$  transitions (42). The reason given for the comparatively regular behaviour of Polycarbonate was that the  $\alpha$  and  $\beta$  processes of this polymer are widely separated compared with UPVC.

The yield strength of glassy polymers decreases with increasing temperature. At test temperatures that approach  $T_g$  the

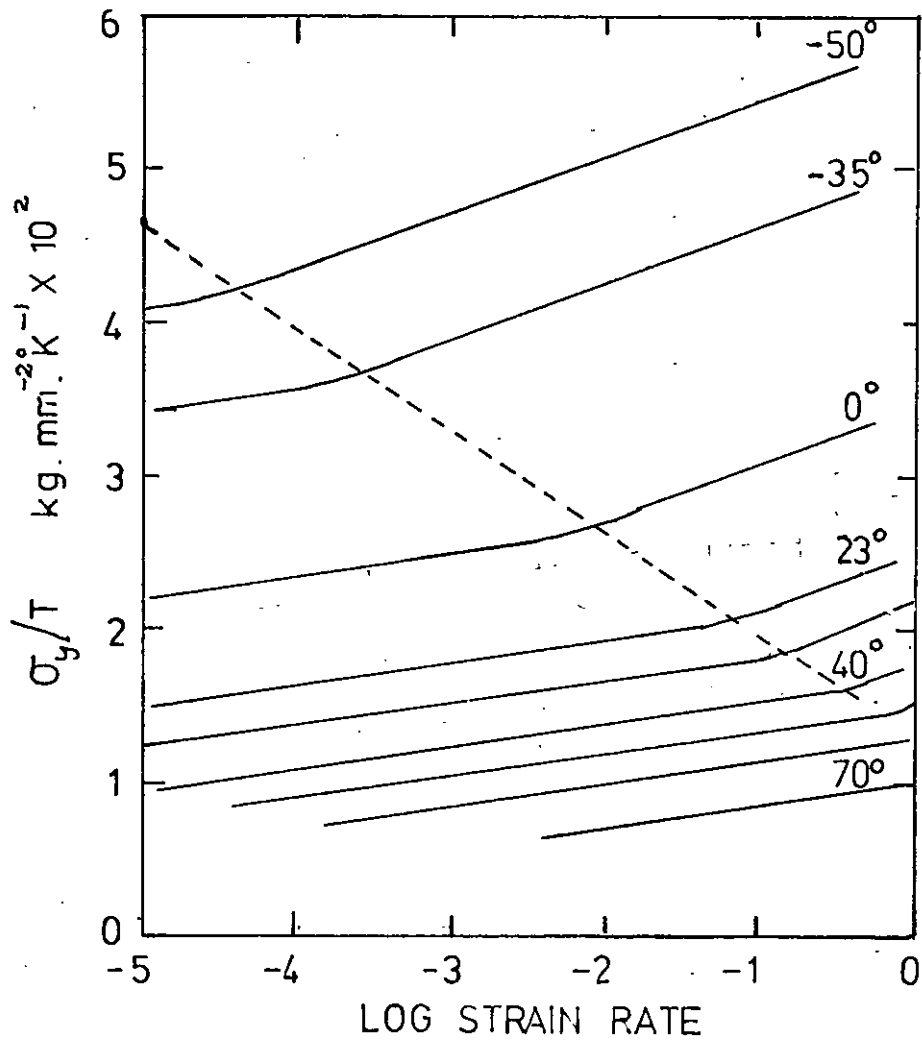


FIGURE 2.9

RELATIONSHIP BETWEEN TENSILE  
YIELD STRESS  $\sigma_y$ , STRAIN RATE,  
AND TEMPERATURE FOR UPVC  
BAUWENS ET AL (7)

yield stress of PVC (7), PMMA (43), PC, and PPO and polysulphone (13) have been shown to approach zero. This feature has promoted the proposition that yield is a stress induced reduction of  $T_g$  (44), or a stress induced increase in free volume (14) (45). The fact that both yield stress and the glass transition temperature increase similarly with hydrostatic pressure lends some support to this hypothesis.

The dependence of yield stress on hydrostatic pressure has been the subject of several studies (46), (47), (48), the main objective of which has been to develop yield stress criteria. Rabinowitz, Ward and Parry (46) have measured the shear yield stress of PMMA up to pressures of 700 MN/m<sup>2</sup>. The yield stress  $\sigma_y$  increased linearly with hydrostatic pressure  $P$  according to the relationship:

$$\sigma_y = 50.3 + 0.204P \quad (\text{MN/m}^2)$$

The shear yield strain was observed to increase with increasing hydrostatic pressure from  $\sim 0.15$  at atmospheric to  $\sim 0.3$  at 300 MN/m<sup>2</sup> and then to decrease with further increases in pressure. The linear dependence of shear yield strength with hydrostatic pressure is similar to the Coloumb yield criterion (49) which states that:

$$\sigma_y = \sigma_y^0 + \mu \sigma_n$$

where  $\sigma_n$  is the compressive stress on the yield plane.

The increase in yield stress with hydrostatic pressure would be expected to lead to the prediction that dilation occurs in advance of, or at, yield. Whitney (50) has demonstrated that this indeed is the case with PS, PMMA and PC under uniaxial compression and tension. Volume increases of up to  $\sim 0.5\%$  were recorded. However other workers have reported a similar decrease in volume at yield under tension (52) and compression (51). The decrease in volume at



yield, presumably due to molecular orientation, has thrown some doubt (53) on free volume explanations for yielding. One possible approach which does not seem to have been considered is to look upon free volume as a vector quantity. Molecular orientation equally implies orientation of free volume. Thus although the total free volume may be reduced (density increased), the effective free volume and its influence on decreasing the resistance to shear yielding is increased.

Dibenedetto and Trachte (13) have proposed a strain criterion for yielding in glassy polymers. The tensile stress/strain behaviour of polycarbonate, PPO, polysulphone, and PMMA up to yield was recorded over a wide temperature range. Dibenedetto et al observed that the 'viscous strain' component at yield was linearly proportional to  $T_T - T_g$ , where  $T_T$  is the test temperature and  $T_g$  the glass transition temperature of the polymer under test. <sup>These<sup>g</sup> are</sup> This data ~~is~~ reproduced in Figure 2.10. The definition of viscous strain  $\epsilon_v$  was given as:

$$\epsilon_v = \epsilon_y - \sigma_y / E_0$$

where  $\epsilon_y$  and  $\sigma_y$  are the tensile strain and stress at yield and  $E_0$  is the initial modulus. This defines the relaxed or time dependent strain component at yield rather than the viscous strain, a distinction not made by the authors. Dibenedetto et al proposed that the increase in free volume  $\Delta V_f$  with dilatation is due only to viscous strain. That is, elastic strain does not involve conformational changes and therefore does not generate free volume.

$$\therefore \Delta V_f = (1 - 2\nu) \epsilon_v$$

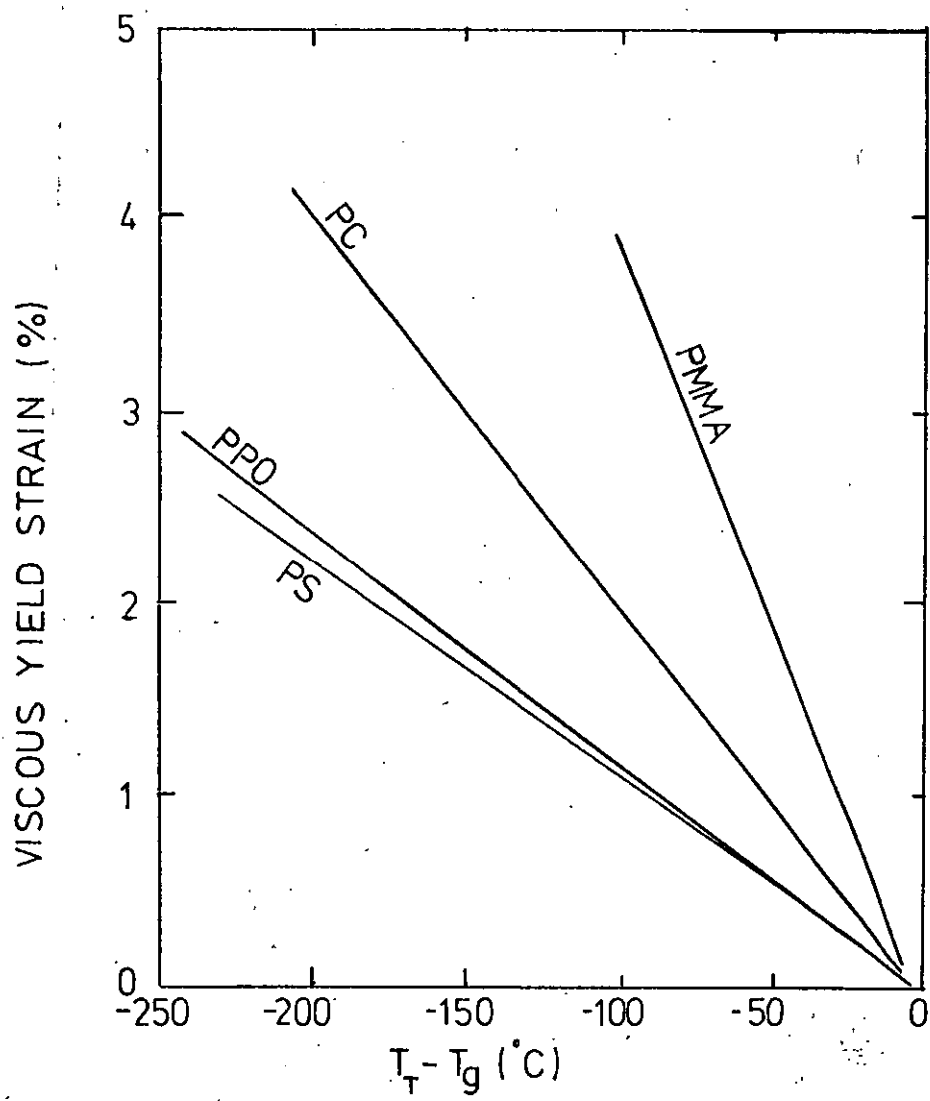


FIGURE 2.10 THE 'VISCIOUS STRAIN' COMPONENT AT THE YIELD POINT FOR VARIOUS AMORPHOUS POLYMERS. DIBENEDETTO AND TRACHTE (13)

where  $\nu$  is Poisson's ratio. Using the definition of free volume change proposed by Litt and Tobolsky (54) together with the above equation, it is stated that:

$$(\epsilon_v)_{\text{yield}} = \left( \alpha_{ga} - \alpha_{gc} \left( \frac{V_c}{V_a} \right) \right) \left( \frac{T_g - T_T}{1 - 2\nu} \right)$$

where  $\alpha_{ga}$  and  $\alpha_{gc}$  are the volumetric coefficients of thermal expansion of the polymer in its amorphous state and close packed (crystalline) state respectively and where  $V_a$  and  $V_c$  are the amorphous and crystalline specific volumes. These are regarded as constants. The data shown in Figure 2.10 all qualitatively agree with this analysis. Furthermore the slope of the Polycarbonate data is in good agreement with that found independently by Litt and Tobolsky (54).

Basically the critical 'viscous' strain theory proposes that yield occurs when the  $T_g$  of the polymer is depressed to the test temperature where this depression is brought about by the 'viscous' dilatational strain. The importance of the viscous, dilatational or anelastic strain in the yield process has been further emphasised by Robertson and Patel (55). They recorded the plastic (non-recoverable), elastic (immediately recoverable), and anelastic (delayed recovery) <sup>strains</sup> of polycarbonate prior to tensile yielding. They calculated that at the yield point the elastic, anelastic and plastic strains were respectively 6.75%, 3.90%, and only 1.35%. Robertson et al deduced from this that the molecular processes responsible for yield were associated with anelastic strains. It was proposed that Robertsons' previous theory of yielding (56) should be modified to account for this evidence. The original theory visualized yield as

the stress induced 'liquifaction' of the polymer due to molecular shape distortion or the formation of 'kink bands'. This was quantified by identifying two molecular segment energy states; the cis (high) and the trans (low). The stress increases the density of cis segments at the expense of trans segments up to the point when yield occurs. The modified theory would now start with the premise that the transition from cis to trans is connected directly with the anelastic strain rather than stress. Conceptually it is more satisfactory to imagine the anelastic strain as being an effect rather than the cause of the energy transition.

#### 2.4.2 Post-Yield Behaviour

The post-yield behaviour shown in Figure 2.8 is typical of a glassy amorphous polymer under uniaxial compressive or shear stress. Similar behaviour can be observed under uniaxial tension, but premature brittle failure and 'necking' make this mode of testing less conclusive. The drop in true stress after the yield point is termed strain softening or simply the 'yield drop'.

Strain softening is always accompanied by some form of strain inhomogeneity in the polymer. This can take the form of a neck, an inclined neck, or a shear band depending on the stress system and the specimen geometry.

The drop in engineering stress that accompanies necking after tensile yield is termed plastic instability. This phenomenon is of interest here because Haward, Murphy and White (57) have proposed that crazing in glassy polymers is a consequence of this instability.

Brittle plastics such as polystyrene exhibit severe plastic instability and also show a propensity to craze. Polymers such as cellulose nitrate, which extend uniformly after yield and therefore do not show plastic instability are strongly resistant to crazing. Furthermore, orientation in the direction of stress is known to both decrease the severity of the instability (58) and the propensity to craze (59). Haward et al point out that the energy required to deform the polymer locally is less than that required to give homogeneous deformation if the polymer exhibits plastic instability.

It is of interest to recall (Section 2.2.4) that Bucknall and Clayton (27) propose that crazing is the cause of plastic instability rather than the reverse.

Orientation hardening, identified by an increase in engineering stress, often follows the yield drop. This tends to stabilise the neck. The orientation on a molecular scale is seen by Bueche (60) as the alignment and extension of chain entanglements. Yield in amorphous glassy polymers does not therefore primarily involve flow but a decrease in configurational entropy. Indeed it has been demonstrated on many occasions that a yielded specimen will return almost exactly to its original shape and size with heating (under zero stress).

## 2.5 Brittle Fracture

Brittle Fracture, or the separation of a material into two or more parts at a strain substantially below that expected for yielding is a catastrophic instability of singular importance in design with plastics. Unlike yield, which can be predicted with some certainty and hence avoided in design, brittle fracture is very sensitive to often quite subtle changes in the service or testing environment, or to small changes in the condition or state of the material.

All glassy amorphous polymers can be made to fail by either yield or fracture by choosing appropriate test conditions. The propensity of a polymer to fracture is increased by an increase in the level of hydrostatic tensile stress. This can be locally increased at the tip of a notch or other stress concentrator when the material as a whole is subjected to uniaxial tensile stress. For this reason the condition of the surfaces of the material is of considerable importance in determining the fracture stress. If the surfaces are chemically attacked this too can decrease the fracture stress.

At high straining rates and/or low temperatures the propensity to fail by brittle fracture increases. Orowan (61) proposes that all polymers have inherent brittle fracture and yield strengths,

both of which are affected by changes in test conditions but to a different degree. The combination of conditions that give equal probabilities of ductile and brittle failure defines the so-called ductile-brittle (d-b) transition. This is not to be confused with the brittle-ductile (b-d) transition which is observed in some plastics after long periods under stress. The b-d transition will be discussed in Section 2.6.

### 2.5.1 Macroscopic Fracture Theories

Although fracture of a polymer must involve the rupture of molecular bonds it is generally agreed that the low brittle strength of glassy polymers, and indeed many elastic materials, is induced by a macroscopic perturbation in the applied stress field. Such perturbations may be existing cracks or inherent flaws. Linear fracture mechanics (62) has been applied with success to linear elastic materials. Basically the theory involves the analysis of the stress distribution in the vicinity of an existing flaw of known geometry. The problem of the stress singularity at the tip of the flaw, which for certain flaw geometries may be infinite is eliminated by proposing that the crack propagates, not at a critical stress, but at a critical stress intensity factor. Without modification linear fracture mechanics can only strictly apply to polymers under infinitesimal strains.

The very relevant condition of a plastic (yielded) zone in advance of a flaw or crack under stress has been considered by Dugdale (63). By extending the approach adopted in linear fracture mechanics Dugdale was able to show that the fracture of an elastic-plastic solid is governed by a critical crack opening displacement  $\delta$

and the yield stress of the material  $\sigma_y$  is governed by the separation of the fracture surfaces at the crack tip. Mills (64) has used the Dugdale model to calculate the critical stress intensity factor and critical yielded zone length for UPVC under plane stress conditions, these being  $2 \text{ MNm}^{-3/2}$  and  $0.5 \text{ mm}$  respectively.

The Dugdale model may prove in the course of time to be very relevant to the fracture of polymers where crazes occur in advance of the crack. However it has been the thermodynamically based fracture theory first proposed by Griffith (65) that has proved in the past to be general enough to accommodate the fracture behaviour of polymers. The theory requires the existence of flaws or cracks which propagate if this is energetically favourable to do so. For slow (isothermal) crack propagation the major energy considerations are the work required to increase the crack surface area and the change in the elastic stored energy that results from such an increase. The criterion for fracture can be expressed as:

$$-\left(\frac{\partial E_n}{\partial A}\right) = \gamma$$

where  $\partial E_n$  is the change in elastic stored energy resulting from an increase in crack surface area  $\partial A$ . The energy per unit area  $\gamma$  was originally associated by Griffith with the surface free energy, indeed the fracture of inorganic glass provides a value of  $\gamma$  that agrees reasonably with independent estimates of surface free energy (66). Estimates of  $\gamma$  via fracture studies on polystyrene and PMMA (67) (68) (69) provide values of  $10^2 - 10^3 \text{ J/m}^2$ . These values are several orders higher than the known surface free energy of these polymers.

For a sheet of infinite area with an edge crack of length  $C$  the Griffith theory would predict a fracture (tensile) stress  $\sigma_c$  of:

$$\sigma_c = \left(2\gamma E / \pi C\right)^{1/2}$$



where  $E$  is Young's Modulus. Berry has verified this prediction by measuring the fracture stress of polystyrene (68) and PMMA (67) containing artificial pre-formed cracks. The fracture stress measured on specimens with no pre-formed cracks indicated a maximum natural flaw length in polystyrene of 1 mm and for PMMA of 0.05 mm. The fact that these flaws are not visible in the unstressed polymer suggests that these are induced during the application of the stress.

### 2.5.2 The Fracture Process

Visible flaws are not observed in unstressed polystyrene, but they are observed under tensile stress in the form of crazes. Berry (68) proposed that the low craze resistance of polystyrene was responsible for its low fracture strength.

The large discrepancy between the theoretical values of surface free energy and the measured values of the fracture surface energy of polymers indicates that fracture involves the dissipation of energy through viscous or inelastic processes. In glassy polymers this process must be very localised as there is no evidence of visible yielding. The fracture surface of PMMA does however reveal interference colours and the high reflectance of craze material. Berry (71) suggested that the interference effects were compatible with a thin surface of polymer with a low refractive index. A craze containing voids would also have a low refractive index. Kambour (73) succeeded in directly observing a craze ahead of a propagating crack in both polystyrene and PMMA. Using an interference technique Kambour was able to establish the size and shape of the craze region ahead of the crack for both polymers. The craze in advance of a propagating crack was

1.2  $\mu$ m maximum thickness and a length of 25  $\mu$ m for PMMA. These craze dimensions in Polystyrene were respectively 6  $\mu$ m and 550  $\mu$ m. The thickness of the polystyrene craze layer is responsible for the high fracture surface energy of this polymer. Kambour estimated the following energy contribution to fracture:

- (1) Surface free energy of craze voids < 3%.
- (2) Plastic work of crazing 11-16%.
- (3) Elastic energy of craze deformation 40%.

The elastic energy would be dissipated as heat on fracture of the craze.

Recent electron microscopy studies of the fracture surface notably by Murray and Hull (74) and Doyle (75) indicate that the 'fracture' of the craze in advance of a crack is not necessarily restricted to its median plane. This can give rise to the characteristic 'mackerel' pattern on the fracture surfaces of polystyrene. It has been proposed that this is due to the crack oscillating from one craze/polymer interface to the other. Doyle suggests that the crack can propagate through the craze by either of three mechanisms.

- (1) viscous flow of the craze layer.
- (2) enlargement and coalescing of craze voids.
- (3) quasi-brittle fracture along the craze/polymer boundary.

These processes tend to predominate at different velocities, with quasi-brittle fracture occurring at high fracture speeds.

## 2.6 Fatigue

The effect of stress history, that is the combination of stress and stress duration, was not considered explicitly in the sections on yield and fracture. Obviously for engineering applications the long term strength of the polymer is of predominant interest.

Long-term laboratory strength tests are necessarily pragmatic in their objectives. Elegant and exhaustive investigations into the mode and mechanism of failure would not be a realistic venture in tests that singly may last for several years. The objective is generally to simulate a service history. Simulations involving static or quasistatic loads are commonly termed static fatigue tests. Those involving intermittent or dynamic loads are termed dynamic fatigue tests.

### 2.6.1 Static Fatigue

The observed attenuation of the strength of a polymer with time under static load is variously termed creep rupture, creep strength or static fatigue. The stress and temperature dependence of the time to failure can often be expressed approximately as:

$$\log t_f = A + (B - C\sigma)/T$$

where A B and C are constants,  $\sigma$  is the applied stress, T the temperature and  $t_f$  the time to fail. This empirical relationship was adopted by Zhurkov (76) as a fit to experimental static fatigue data on PMMA. The equation is analogous to that proposed by Bueche (77) (78) in his molecular theory of time dependent fracture, which can be stated as:

$$\log \frac{t_f}{t_0} = [V_0 - A\sigma]/kT$$

where  $t_0$  is the period of 'atomic vibration',  $V_0$  is the activation energy of the failure mechanism,  $k$  is Boltzmann's constant and  $A$  a constant. Zhurkov's data and <sup>those</sup> that generated by Peschanskaya and Stepanov (79) provide values of  $t_0$  of the order  $10^{-13}$  seconds. The experimentally determined values of  $V_0$  (the activation energy) are very similar to the dissociation energies of the C-C bonds of those glassy polymers under investigation. Peschanskaya et al correlated detailed discrepancies between their static fatigue data and the Bueche theory with secondary relaxation transitions. Discontinuities in the time-dependence of the brittle failure stress coincided with the secondary (side-group) relaxations in terms of temperature and time. Combining this with the proposition (10) that craze initiation is controlled by secondary relaxation processes emphasises the role of inelastic deformation and other entropy based processes in the fracture of glassy amorphous plastics.

The monotonic decrease in strength with the logarithm of time under stress cannot be relied upon, nor unfortunately have the limits been adequately defined. It would indeed be a simple procedure to extrapolate laboratory test data to realistic service lifetimes if this were not so. A so-called ductile-brittle transition (to be distinguished from the brittle-ductile transition) is often observed in the static fatigue characteristics of both glassy and crystalline polymers. The transition is recognised by a sharp increase in the attenuation of strength with time. The onset of the transition is accelerated by:

- (1) hydrostatic tensile stress (80)
- (2) increase in temperature (81)
- (3) solvents and wetting agents (82)
- (4) notches and other stress concentrations (83)
- (5) Reduction of  $M_w$  of the polymer (84)

The 'acceleration' of the transition with increasing temperature is shown diagrammatically in Figure 2.11.

The most comprehensive investigation of the static fatigue of a glassy polymer is available through the work of Andrews and Curran (85) on PMMA. Various specimen surface treatments including sanding and/or polishing always led to a reduction in the static fatigue lifetime. Fatigue failure, at other than the highest stresses (shortest fatigue lifetimes), was preceded by crazing or micro-cracking.

Gotham (86) has presented static fatigue data on PMMA and UPVC in such a way as to include the craze initiation envelope. The crazing stress/logtime curve preceded the static fatigue characteristic by a minimum of 2 decades of time. It might be reasonable to propose that the time to fail under static load  $t_f$  is simply

$$t_f = t_{cr} + t_{crit}$$

where  $t_{cr}$  is the time for craze initiation and  $t_{crit}$  is the time required for the craze or crazes to grow to a critical length for fracture.

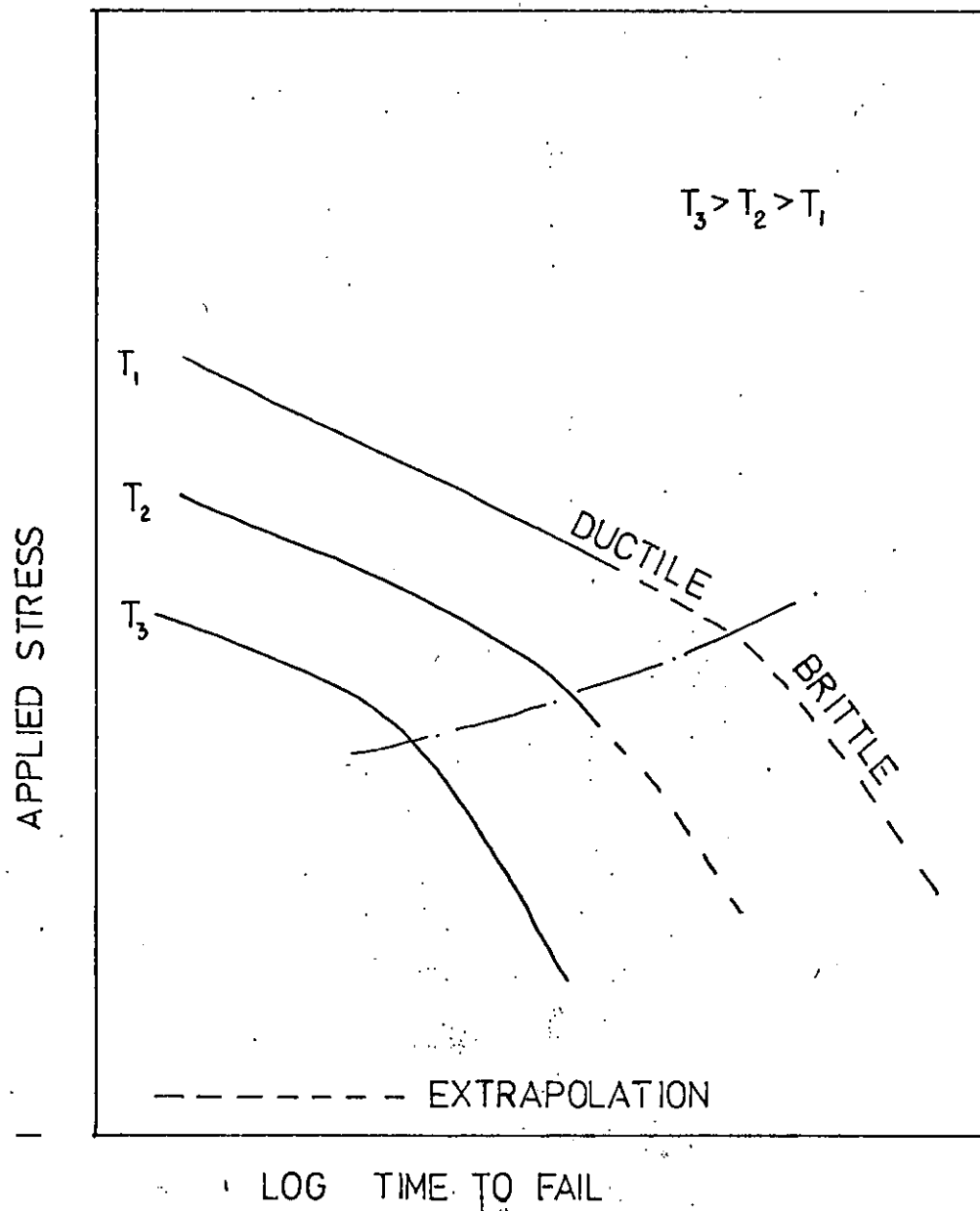


FIGURE 2.11 TYPICAL STATIC FATIGUE CHARACTERISTICS SHOWING THE DUCTILE BRITTLE TRANSITION. — — — — —

### 2.6.2 Dynamic Fatigue

A considerable proportion of published dynamic fatigue data on glassy polymers has concentrated on short-term fatigue lifetimes. The reason for this must be to satisfy experimental expediency rather than to supply data which <sup>are</sup> ~~is~~ of any value in designing to avoid failure.

Failure after short fatigue lifetimes is predominantly due to thermal instability. At high stress amplitudes and/or frequencies, commonly employed in this type of 'accelerated' test, the rate of heat generation in the specimen can exceed the rate of heat loss leading to a runaway increase in temperature. Opp, Skinner and Wiktorck (87) generated dynamic fatigue data up to a maximum of 1000 seconds on several polymers including PMMA, polycarbonate and UPVC. Opp et al proposed two failure criteria. The first is that 'melt fracture' will occur when the temperature of the specimen reaches its T<sub>g</sub>. This derives from the thermal part of the hysteresis energy. The second is that fatigue failure will occur by crack propagation. This, they propose, is derived from non-recoverable mechanical energy (at stress concentrations in the region of microscopic cracks). This (so-called) combined energy model predicts that polymers tested at temperatures below their T<sub>g</sub> will exhibit an endurance limit; that is there will be a stress and strain amplitude below which the fatigue lifetime will be infinite.

The dynamic fatigue in flexure of several glassy polymers including PMMA, PVC and Polycarbonate have been characterised by Gotham (86) at a frequency of 0.5 Hz. Gotham adopted a 'square wave' cyclic

stress or strain input to enable a direct comparison to be made between the static and dynamic fatigue characteristics. Generally for short fatigue lifetimes the dynamic and static characteristics sensibly superpose, but after longer fatigue lifetimes the characteristics diverge with the dynamic fatigue failure occurring earlier than the static. This is illustrated in Figure 2.12. It can be seen from this graph that the long-term dynamic fatigue characteristic tends to superpose with the craze initiation envelope.

An explanation has been proposed by Vincent (88) for the rapid deterioration in the capacity of a glassy polymer to resist crack propagation under intermittent stress or strain. Vincent assessed the size of the plastic zone in advance of a crack under both steady and cyclic loading using polarization microscopy. He observed that the zone size increased with crack propagation under static load, but under cyclic load the zone size stabilised after the first cycle. He concluded that the 'plastic zone' is partially recoverable on removal of stress and that each subsequent loading cycle merely re-equilibrated the zone size. Thus the fracture surface energy of a crack propagating under static load increases with crack growth whilst under cyclic loading the fracture surface energy remains constant. This interpretation has been reinforced by Brown, Harris, and Ward (89) who reported that crack growth under cyclic loading was limited to the on-loading period (during the rise time of the load). Negligible crack growth was observed during the remainder of the loading cycle. It might be reasonable to expect that the growth of craze length is more rapid under cyclic load as compared with that under static load.



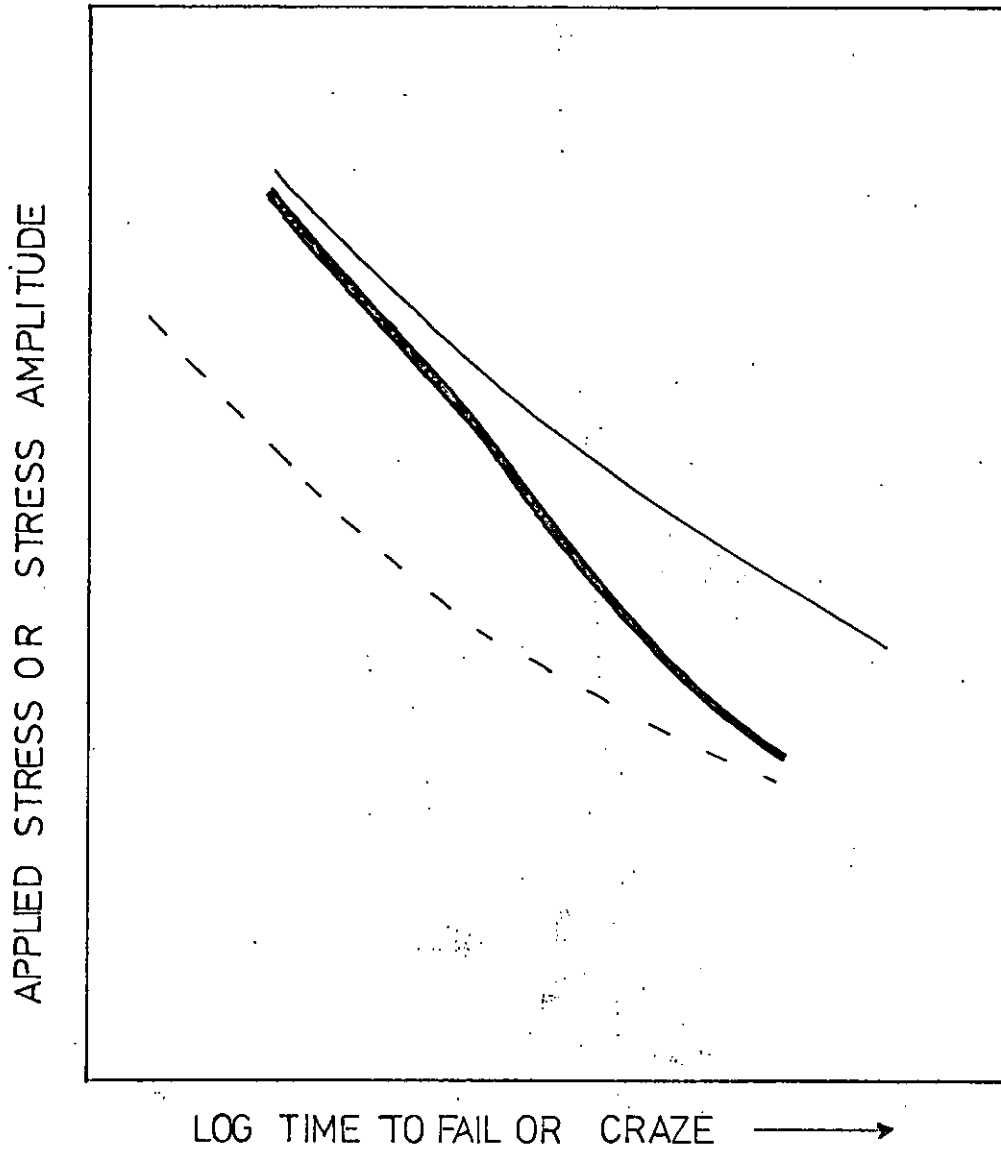


FIGURE 2.12 TIME TO FAIL AND CRAZE AS A FUNCTION OF STRESS LEVEL OR AMPLITUDE

- STATIC FATIGUE FAILURE
- DYNAMIC " "
- CRAZING

Gotham (86), in addition, characterised the dynamic fatigue of UPVC under conditions of controlled strain amplitude. Table 2.4 includes some of his data relating strain amplitude with time to failure. Gotham did not make any attempt to extrapolate ~~this~~<sup>these</sup> data, but obviously if a safe threshold strain is operative this will be less than 0.3%. This value does not support the proposal by Menges (30), namely that fatigue damage (crazing) in UPVC is initiated at tensile strains in excess of 0.85%.

fatigue life secs.	strain amplitudes %
$3 \times 10^3$	1.0
$7 \times 10^3$	0.8
$4 \times 10^4$	0.6
$10^6$	0.4

Table 2.4. Time to fail at various strain amplitudes. Reversed flexural fatigue at 0.5 Hz. After Gotham (86).

Research by Lortsch (90) on polyethylene and UPVC pipes under pulsating hydrostatic pressure reveals clearly the differences in fatigue behaviour between glassy amorphous and crystalline polymers. For any given maximum pressure, the dynamic fatigue lifetime of UPVC pipe is reduced by increasing the pressure amplitude. In the case of polyethylene pipe for any given maximum pressure the dynamic fatigue lifetime is increased by increasing the pressure amplitude. Thus the severest condition for UPVC is:-

$$P_a = P_{max} \text{ or } P_0 = 0$$

and for polyethylene:

$$P_{max} = P_0, \text{ or } P_a = 0$$

where  $P_0$  is the minimum (static) pressure,  $P_{max}$  the peak pressure and  $P_a$  the dynamic pressure amplitude. Therefore glassy polymers are fatigue damaged more readily by a sequence of creep and recovery periods than by static creep. For polythene the situation is reversed which would imply that fatigue in crystalline polymers is controlled by continuum viscoelastic deformation processes. As Benham and Hutchinson (19) have demonstrated, the deformation behaviour of UPVC under intermittent stressing is governed by continuum viscoelastic processes but only below a critical combination of stress amplitude, strain amplitude, (presumably temperature) and time. When these critical conditions are exceeded another deformation process becomes predominant leading to cyclic softening and eventual dynamic fatigue failure. The dynamic fatigue failure of UPVC and the post-critical deformation processes according to Martin and Johnson (91) are both due to craze initiation and growth.

### 3. Craze Geometry, Structure, Initiation and Growth

It is evident from Chapter 2 that crazing has a considerable influence on the mechanical properties of glassy amorphous polymers. It has been established that fracture is often (if not inevitably) initiated by a craze of critical length, and that crack growth is preceded by craze growth. Under conditions that lead to static and dynamic fatigue failure, crazing is observed to precede both ductile and brittle failure. In this chapter the craze phenomenon will be examined in detail. Special emphasis is given to the initiation of crazes, because this condition offers potential as a rational design criterion.

#### 3.1 Craze Geometry and Structure

On a macroscopic scale crazes are distinguishable from cracks in the former's ability to support and transmit a tensile stress. Like cracks they appear to grow in the plane normal to the principal tensile stress or strain direction. However because cracks are planar voids they cannot in themselves transmit or support a tensile stress. Sauer, Marin and Hsiao (92) observed that a craze completely covering the cross-section of a polystyrene specimen had a tensile strength of 50% of that for the bulk polymer. It was generally accepted in view of this and other evidence that crazes are not voids, but are sharply defined regions of oriented polymer.

Spurr and Niegisch (93) succeeded in providing the first electron micrographs of the craze cross-section. The resolution was not sufficient to provide more than a hint of the detailed structure within the craze but it was sufficient to prove that there was material bridging the craze walls. Spurr et al reported a fine structure of 'tiny particles' of diameter  $\sim 50$  nm.

Kambour (94) exploited the optical properties of the craze to calculate the density of craze material. He immersed a polycarbonate specimen in ethanol, applied a tensile stress and succeeded in developing thick crazes. Whilst still under stress and immersed in the liquid, light was reflected from the craze/polymer surface. The angle of incidence was varied until the critical angle for total reflection was determined. From this the refractive index of the craze material and ethanol mixture could be calculated. The Clausius Mosotti (95) equation relating density and refractive index<sup>x</sup> was employed to estimate the density of the craze. Using a simple law of mixtures and assuming a saturation level of ethanol in polycarbonate Kambour estimated a void content of 50-55% in the craze material. Kambour (96) replaced the ethanol with a silver nitrate solution and after exposure to light succeeded in taking electron micrographs of the silver doped craze of sufficient resolution and contrast to reveal its structure in some detail. The craze material consisted of voids (containing silver) some of diameter  $\sim 100$  nm, but the majority were less than 2 nm. The voids were interconnected, this being evident by the rapidity with which liquids penetrated the craze material.

Kambour (96) used the same optical technique to assess the void contents of crazes in polystyrene, styrene acrylonitrile and PMMA. The values obtained were 40%, 60% and 40% respectively. The measurement of the critical angle of reflection for the PMMA craze was particularly difficult. The crazes of PMMA tended to be thinner than those of the other polymers tested. When the craze thickness approaches the wavelength of light it is no longer visible to the naked eye and reflection from the polymer craze boundary is frustrated.

Although there is a minimum craze thickness that can be detected with the naked eye craze thicknesses as low as 30 nm have been detected with electron microscopy (97). The craze thickness is remarkably constant over its area with a taper towards its leading (advancing) perimeter. The taper is generally no more than 1 or 2 degrees. Knight (98) proposed that the tapered craze boundary is 'cusp like'. That is, similar to the craze cross-section observed by Kambour (73) in advance of a propagating crack. This is reproduced in Fig. 3.1.

The internal structure of the craze can be either essentially fibrillar or contain spherical voids. Kambour and Holik (99) observed that in a growing craze the older and thicker parts tend to be fibrillar and the craze tip region can be a single line of spherical voids. The fibrils are assumed to be highly deformed with a high degree of molecular orientation.

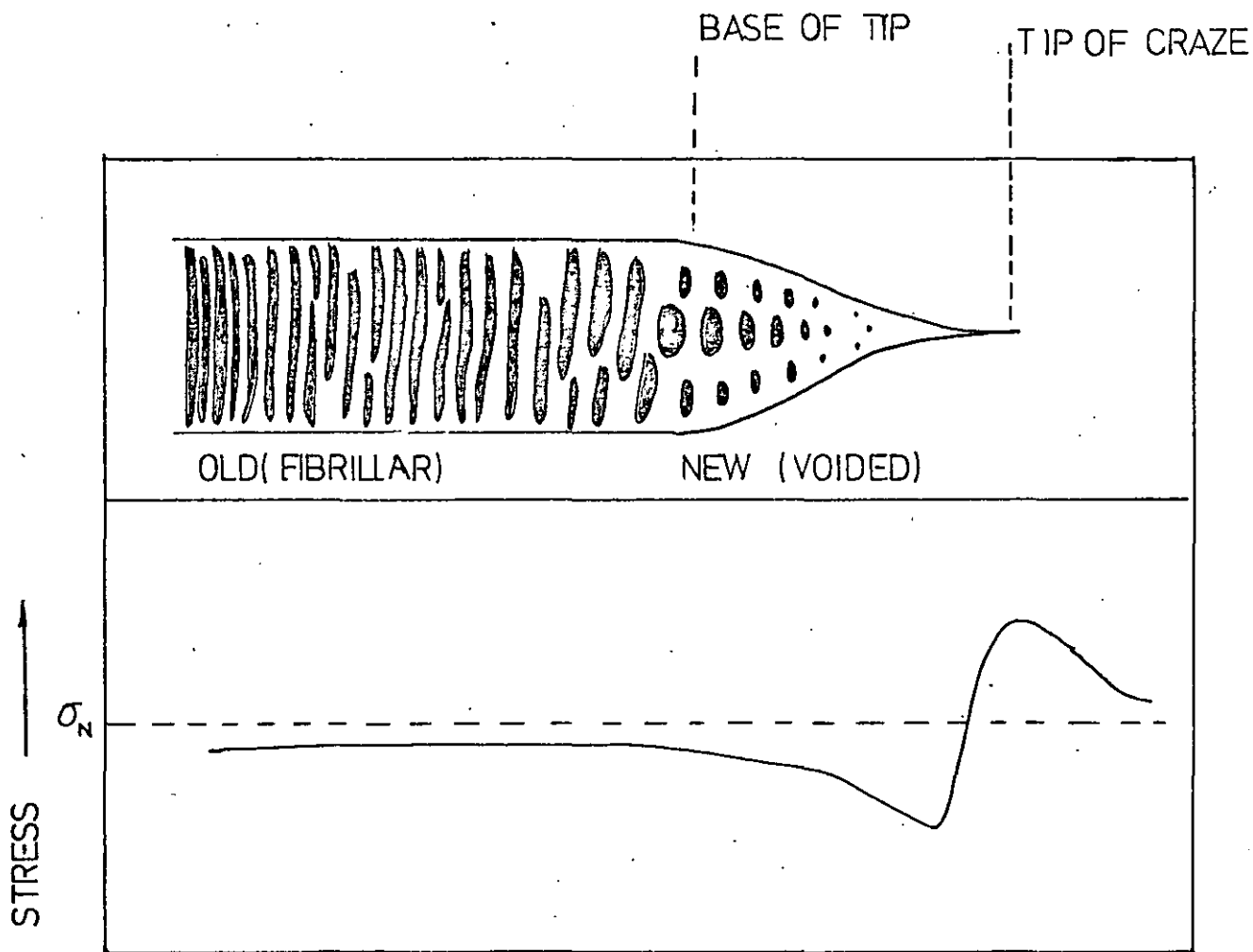


FIGURE 3.1 CRAZE SHAPE AND STRESS DISTRIBUTION ACCORDING TO KNIGHT (98). ALSO SHOWN IS THE CRAZE STRUCTURE ACCORDING TO KAMBOUR AND HOLIK (99)

Baer and Wellinohoff (100) studied the craze structure of polystyrene with varying molecular weights. Stable cavitation by voiding in localised yielded zones was not observed in the low molecular weight polymer ( $M_w = 10,000$ ). The yielded zones propagated by crack growth. Polystyrene of molecular weight 37,500 exhibited stable cavitation by voiding followed by the development of fibrils parallel to the tensile stress axis. The fibril diameters were in the region of 20 nm, but this could be reduced to 10 nm by increasing the stress. Baer et al suggested that the difference in the ability of high and low molecular weight polymers to form stable crazes is connected with their capacity to form 'entanglement networks'.



## 3.2 The Initiation of Crazes

### 3.2.1 Sites for Craze Initiation

Stress induced crazes are generally initiated on the free surfaces of the polymer if the polymer is homogeneous and the specimen isotropic. Crazes can be induced to initiate internally in a homogeneous polymer if the internal molecular orientation is transverse to the tensile stress direction and the surface molecular orientation is parallel to this direction. This has been demonstrated by White, Murphy and Haward (101) on injection moulded polystyrene.

The explanation proposed by Knight (102), Gent (103) and others for the propensity of crazes to initiate on free surfaces is that:

- (i) The free surface is more likely to be damaged by stress concentrating flaws and scratches and by chemical contamination.
- (ii) The stress concentrating capacity of a flaw on the surface is twice that of the same flaw internally.

The belief that crazes are initiated by chance imperfections on the surfaces of test specimens is probably the main reason for the dearth of serious experimental studies into initiation behaviour. The surface topography cannot be controlled or known in detail, and if the phenomenon is expected to be so sensitive to fabrication it would be futile to attempt to establish materials based initiation criteria.

There exists however considerable evidence that the polymer itself has an important role, perhaps even the predominant role in determining the conditions for craze initiation. This evidence can be summarised as follows:

(i) The number of crazes initiated per unit area of surface is very sensitive to the temperature and stress level at initiation (104). This so-called craze density is apparently also very dependent on the polymer type. Craze densities in polycarbonate are almost inevitably higher than those observed in polystyrene or PMMA specimens.

(ii) The mechanics of craze initiation and of craze growth are thought to be very similar. Indeed Bucknall and Clayton (27) have established identical activation energies for both processes. Electron micrographs (99) of long crazes have shown that crazes grow without deviation along a defined plane (if the polymer is homogeneous and isotropic). Perturbations in the preferred direction of growth might be expected if craze growth (and implicitly craze initiation) is sensitive to macroscopic discontinuities in the material.

(iii) Craze initiation is often observed to occur at sites with no macroscopic flaw (105). In addition it is not inevitable that crazes are initiated at even quite severe surface scratches or stress concentrations (93).

(iv) The inter-specimen variability of the critical stress and strain for craze initiation is smaller than would be expected if surface stress concentrations played a predominant role.

Obviously the craze site must differ from the bulk polymer. On a micro-scale this need not imply the presence of inclusions, flaws, or other chance features, as there are various molecular models of the glassy amorphous state that provide for a short-range variation in molecular order, free volume, conformational entropy and yield strength. The sites for craze initiation and hence the criteria that control the process might therefore be regarded as characteristic of the material.

Baer and Wellinghoff (100) have recently reported on an investigation into the micro-yield mechanism prior to craze formation. Their observations provide convincing evidence that craze initiation is not a chance event. Ultra-thin sheets of polystyrene were subjected to tensile strain and examined under an electron microscope. Highly strained regions of approximately 20 nm were initiated, which moved on increasing the strain to <sup>a</sup>coalesce into lines perpendicular to the tensile strain direction. On further straining the linear yielded zone cavitated at a critical strain. It is of interest to note that the minimum craze thickness observed by Kambour (Section 3.1) is very similar to the diameter of these pre-craze yielded zones.

### 3.2.2 Craze Initiation Criteria

Gent (103) has proposed that crazing in glassy amorphous plastics can be attributed to 'stress-activated devitrification of polymer at the tip of a chance flaw' or stress concentration. Under the action of the hydrostatic tensile stress the polymer, which at the tip of the flaw is in the rubbery state, (above its glass transition temperature) cavitates. Knight (102) gave a similar emphasis to the role of chance flaws in the surface of the polymer but did not include

the influence of dilation in reducing  $T_g$ . Knight proposed that the hydrostatic tensile stress at the tip of the flaw results in a 'splitting action' and the formation of fibrils, the axes of which are parallel to the direction of the principal tensile strain. The electron micrographs of nascent and developed crazes published by Kambour (99) would tend to support Gent's cavitation hypothesis rather than that of fibrillation.

Gent computed that the stress concentration factor  $K$  due to machining marks will be in the range 10-50. By involving a relationship for the increase of  $T_g$  with pressure Gent calculated that the critical stress  $\sigma_c$  required to develop a thin band of softened polymer in advance of a flaw is:

$$\sigma_c = [\beta (T_g - T) + P] / K$$

where  $T$  is the test temperature,  $P$  the hydrostatic pressure and  $\beta$  is the linear coefficient of the pressure dependence of  $T_g$ . The cavitation behaviour of soft rubbery solids (106) was used to predict that profuse cavitation would occur within the thin band of softened polymer when the hydrostatic tensile stress is sufficient to depress the  $T_g$  about  $20^\circ\text{C}$  below the test temperature. The Gent hypothesis accounts qualitatively for:

- (i) The suppression of crazing under hydrostatic pressure.
- (ii) The reduction in crazing stress with the polymer immersed in solvent (due to solvent induced reduction in  $T_g$  (plasticization) ).
- (iii) The dependence of crazing stress on temperature.

The qualitative predictions of the hypothesis are apparently satisfactory but this depends critically on the value of K. It could be argued, for instance, that the effect of surface plasticization by solvent action would be to eliminate macroscopic surface flaws. Similarly although the stress concentration factor of a typical surface may be high, the surface stress might be expected to be only a fraction of the applied nominal stress.

An alternative approach that does not rely upon stress concentrations as such is to assume that the craze initiation process is controlled by void 'initiation' and growth. The hydrostatic tensile stress  $\sigma$  required to expand an existing void of radius r has been derived by Hill (107) for a classical elastic-plastic solid:

$$\sigma = \frac{2}{3} \sigma_y \left\{ \ln \frac{E}{3\sigma_y(1-\nu)} + 1 \right\} + \frac{2S}{r}$$

where  $\sigma_y$  is the yield strength, E is Young's modulus,  $\nu$  is Poisson's Ratio and S is the surface tension. Obviously the approach does require the existence of inherent voids. Drabble, Haward and Johnson (108) have calculated the value of the first term in the equation for polystyrene. This value was reported to be:

$$\sigma = 2.5 \sigma_y$$

and therefore even without the surface tension term Hill's unmodified equation is quite inadequate for predicting the crazing stress. Drabble et al proposed that 'overlapping proliferation of voids' could reduce the above value considerably. They calculated that for a craze of 40% void volume, the critical hydrostatic stress could be as low as:

$$\sigma \sim 0.07 \sigma_y$$

The hydrostatic tensile stress required to increase the surface area of an existing void of radius  $r$  is significant when  $r < 1$  nm. This is comparable with some of the partially developed voids detected on Kambour's (96) micrographs. An approach adopted by Haward (109) using Irwin's (110) model for the 'tensile strength' of liquids does not involve the value of the inherent void radius. The hydrostatic tensile stress to form a void in a liquid is given by:

$$\sigma = k \left[ \frac{s^3}{T} \right]^{1/2}$$

where  $T$  is the absolute temperature and  $k$  a dimensionless constant that is characteristic of the liquid. Haward estimates that the void nucleation stress for polystyrene at room temperature is about 30% of the stress required for void growth.

The limitations of the void nucleation and growth, and yield in advance of a stress concentration approaches is that they are derived through the application of continuum mechanics which ignores microscopic variations in the state of the material. On the evidence published of short-range macro-molecular features in glassy amorphous polymers (111) (112), it would not be justified to assume homogeneity at dimensions on a nanometer scale.

Sternstein and Ongchin (113) have developed a phenomenological model for 'normal stress yielding' (craze initiation) under a biaxial tensile stress system. Tubes of PMMA were internally pressurised to give a hoop stress  $\sigma_1$ . In addition a tensile stress  $\sigma_2$  was generated in the axial direction. Sternstein et al observed the combinations of  $\sigma_1$  and  $\sigma_2$  required to initiate crazing. A stress criterion was proposed:

$$\sigma_b = A(T) + \frac{B(T)}{I_1}$$

where  $\sigma_b$  is the 'stress bias' and equal to  $|\sigma_1 - \sigma_2|$  and  $I_1$  is the first stress invariant  $\sigma_1 + \sigma_2$ . A(T) and B(T) are temperature dependent material parameters. For  $\sigma_b = 0$  the above equation defines a critical first stress invariant. Sternstein et al proposes that this is sufficient to increase the molecular mobility to the point of normal stress yielding. The limitation of this and any criterion based on stress is that in common with other viscoelastic processes craze initiation is time dependent, with the initiation stress reducing with time under load.

Experimental observations aimed specifically at separating the stress and deformation components have tended to support the thesis that it is the tensile strain and not the stress that is critical for craze initiation. Theoretical research has to an extent ignored this evidence and concentrated on stress criteria. The reasons for this could be:

- (i) Stress rather than strain is historically the primary descriptive variable in continuum mechanics - particularly for shear and fracture.
- (ii) Most data on initiation in air have been published in terms of stress. This is understandable for short term tests involving Instron type machinery.
- (iii) Associated phenomena, for example the increase of yield strength under pressure, and the lowering of Tg under hydrostatic tension are invariably discussed in terms of stress.

Early experimental investigations (114) provided some evidence that the tensile strain played a primary role in craze initiation. However the large proportion of effort made in this direction is due to Menges and co-workers (30) (104) (115) (116) (117) (118) at the Institut Für Kunststoffverarbeitung (IKV) Aachen. Menges et al employ uniaxial tensile creep over comparatively extended periods of time. With transparent specimens the onset of crazing is established visually. With translucent specimens sudden clouding or increase in opacity is detected by means of a photo-electric cell (118). The stress, time, strain and temperature conditions that are critical for craze initiation (or micro-crack initiation in the case of partially crystalline thermoplastics) are thus established.

Figure 3.2 is typical of the data generated by Menges et al. By performing tensile creep tests for a number of stress levels a craze initiation envelope superimposed onto a family of creep curves is developed. The features observed were:

- (1) At any given stress level an induction time is required before craze initiation.
- (2) The induction time increases as the creep stress decreases.
- (3) The critical tensile strain for crazing decreases with decreasing creep stress.
- (4) The stress dependence of the critical strain appears to become insignificant after long creep periods. This defines an asymptotic tensile strain value  $\epsilon_{\infty}$  below which crazing will never occur.
- (5) Although the induction time for craze initiation decreases with increasing temperature, the minimum critical strain  $\epsilon'_{\infty}$  is independent of temperature below the 'softening point' of the polymer (104).



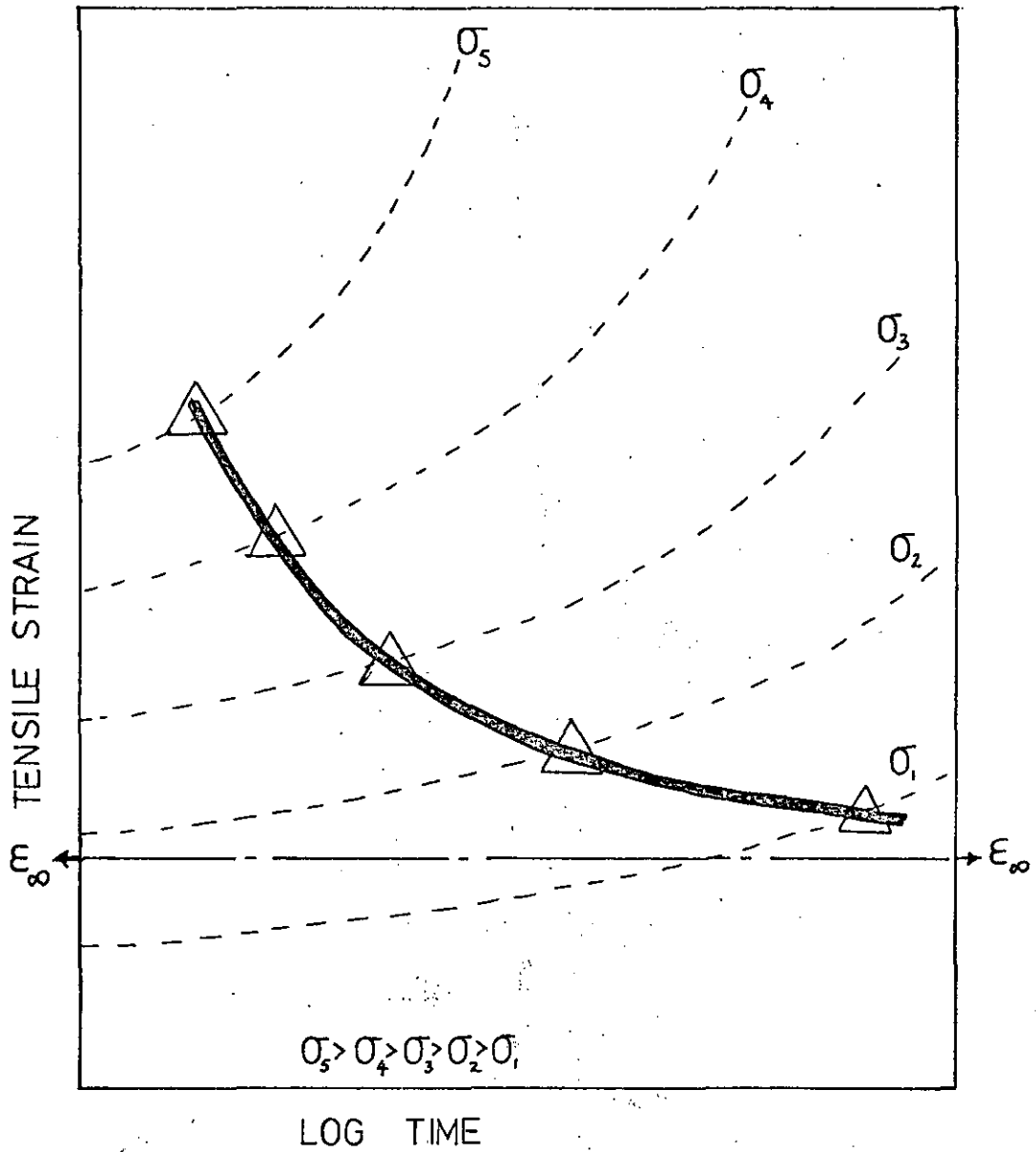

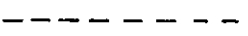


FIGURE 3.2 TYPICAL RELATIONSHIP BETWEEN THE CRITICAL STRESS  $\sigma_c$ , STRAIN, AND INDUCTION PERIOD FOR CRAZE INITIATION ACCORDING TO MENGES(30).  $\epsilon_\infty$  IS THE MINIMUM CRITICAL STRAIN.

-  CRAZE INITIATION
-  CREEP CHARACTERISTICS

(6) Under biaxial tension,  $\epsilon_{\infty}$  (principal tensile strain) is the same as under uniaxial tension (30). The only specific effect of the hydrostatic tensile component is to reduce the induction period for crazing.

(7)  $\epsilon_{\infty}$  is independent of the action of wetting agents\* (30).

(8) The initiation of non-linear viscoelastic behaviour coincides with the initiation of crazes,

Menges (104) proposes that critical tensile strains above  $\epsilon_{\infty}$  ascertained when the induction period is short and the creep stress is high are not valid initiation strains. He argues that  $\epsilon_{\infty}$  is singular for all stress levels and creep times, but the growth of a craze to a size that can be detected takes a finite time. Menges suggests that 'particle boundaries that are normal to the tensile stress axis suffer 'adhesive failure''. Using a fracture mechanics approach he developed a relationship for the critical strain:

$$\epsilon_{\infty} = \frac{C}{\sqrt{L}} \sqrt{\frac{\gamma}{E}}$$

where L is the length of the boundary,  $\gamma$  the surface tension, E is Young's Modulus and C is a constant. L is primarily dependent on the granulated raw material and the quality of its processing. It is therefore surprising that different polymers processed in different laboratories should display similar critical strains. Additionally at elevated temperatures  $(\gamma/E)^{1/2}$  will be increased (119) leading to a temperature dependent value for  $\epsilon_{\infty}$ . If, as Menges suggests, the value of  $(\gamma/E)^{1/2}$  is sensibly constant at temperatures up to the softening point then this removes the opportunity of explaining the increase in craze site density with temperature.

\*This was later found not to be valid (117).

The proposition that  $\epsilon_0$  is independent of stress level is suspect if considered in conjunction with the work of Bucknall and Clayton (27) (see Section 2.2.4). In this work craze initiation was detected non-visually and therefore the artefact referred to by Menges to explain the apparent stress dependence of the critical strain did not apply. Bucknall et al reported a regular dependence of craze induction time  $\tau$  on stress level  $\sigma$  :

$$\tau^{-1} = k e^{b\sigma}$$

Thus for finite stress levels  $\tau$  is always greater than zero. However, Menges would propose that  $\tau = 0$  when the stress is sufficient to generate an initial elastic strain in excess of  $\epsilon_0$

The proposition that non-linear behaviour is an effect of damage initiation and growth is a reasonable concept. However, the very comprehensive study of non linear 'initiation' by Yannas (39) does not support this quantitatively. Yannas estimates that the transition from linear to non-linear viscoelastic behaviour in polycarbonate occurs at a minimum tensile strain of  $\sim 0.35\%$  whilst Menges (30) estimates a minimum craze initiation strain of  $\sim 0.9\%$  for the same polymer.

A limitation of the experimental techniques so far discussed is that they are not designed to isolate conclusively the influence of the variables. Many criteria have been suggested including critical principal tensile stress (102), stress bias (113), tensile strain (114) (30), dilation (121) shear strain energy (122) and total strain energy (123) (124). However because these variables operate simultaneously, a special experimental approach is required to delineate between them. Kwei, Matsuo and Wang (125) developed such an approach.

Matsuo et al prepared specimens of polystyrene containing embedded steel balls of diameter  $\sim 3$  mm. The specimens were loaded in tension at a constant cross-head speed. Photographs revealed that crazes were initiated at the interface between the steel ball and the polymer matrix at a polar angle of  $\theta = 37.2^\circ$ . This is shown diagrammatically in Figure 3.3\*. According to the Goodier (126) solution, the maxima of the relevant stress, strain, and energy variables are as shown in Table 3.1.

Variable	$\theta$
Tensile Strain	$37^\circ$
Dilatational strain	$0^\circ$
Shear stress	$44^\circ$
Tensile stress	$24^\circ$
Shear energy	$39^\circ$
Total strain energy	$44^\circ$

Table 3.1. The Polar angle  $\theta$  (w.r.t. the tensile strain axis) for the maxima of variables. Spherical inclusion of greater rigidity than the matrix after Goodier (126).

The result therefore strongly supports the critical tensile strain hypothesis proposed by Menges. Wang et al extended the study to rubber inclusions in polystyrene to investigate the stress bias criterion of Sternstein and Ongchin (113). On the data obtained, Wang et al concluded that the predictions of the stress bias criterion were physically inadmissible.

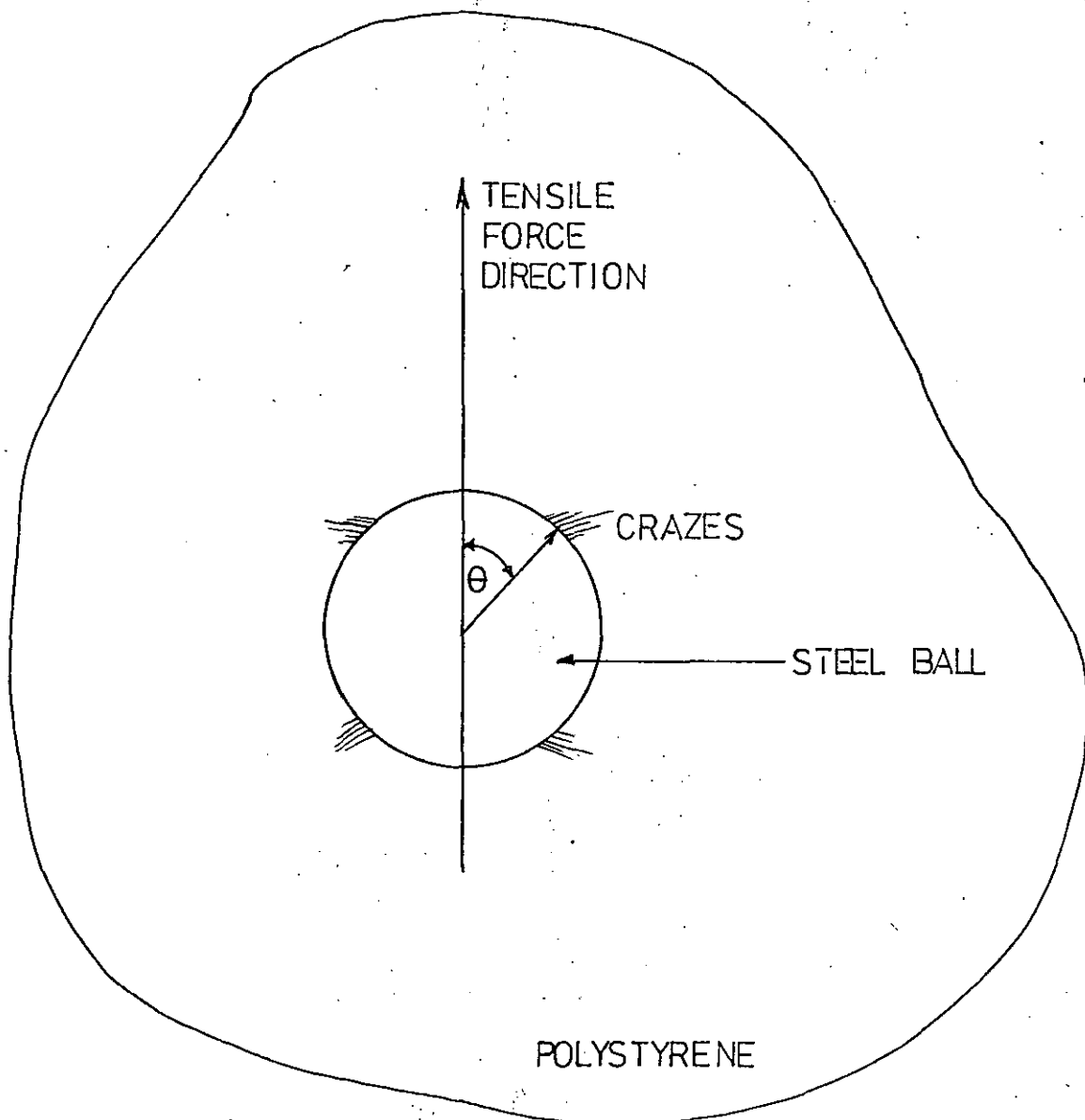


FIGURE 33\*

INITIATION OF CRAZES AT THE INTERFACE BETWEEN AN EMBEDDED STEEL BALL AND A POLYSTYRENE MATRIX.  $\theta = 37^\circ$  WHICH COINCIDES WITH THE POSITION OF MAX. TENSILE STRAIN. MATSUO ET AL(125)

### 3.3 Craze Growth and Recovery

#### 3.3.1 Growth under static tensile stress

The growth of a craze, which is essentially restricted to a plane normal to the principle tensile stress, differs fundamentally from that of a true crack. Under axial tension the stress concentration at a crack tip increases with the growth of the crack leading inevitably to a catastrophic instability. Such an instability is not observed in the growth of a craze unless the craze itself ruptures. The many reports of crazes completely covering the cross-section of tensile specimens is ample evidence that the growth can be completely stable.

The stability and hence the growth characteristics of a craze is generally assumed to derive from the load bearing ability of craze matter. Knight (98) calculated the 'probable' stress distribution around a craze under uniaxial tensile stress  $\sigma$  using classical elasticity equations together with certain geometrical assumptions. The craze was considered to be parallel sided with a 'craze opening displacement of  $2D$  except in the region of the craze tip where the thickness decreased to zero over a length  $k$ . The peak stress  $\sigma_{max}$  at the craze tip was calculated as:

$$\sigma_{max} = \sigma + \frac{bD}{k}$$

where  $b = 1.8 (1 - \nu^2) E / \pi$ , and can thus be considered as a constant at constant temperature. According to Knight, therefore, the peak stress is not influenced directly by the total length of the craze. Knight proposed that  $\sigma_{max}$  must exceed a critical stress before the point will propagate. Provided the base of the craze does not advance, the propagation rate of the point will decrease with time because  $k$  will increase and eventually reduce  $\sigma_{max}$  to the critical

stress. (The base is the perimeter of the parallel-sided part of the craze). However if  $\sigma_{\text{max}}$  exceeds both the critical stress for propagation of the point and the base, as might be expected when the applied tensile stress is high, then the craze will propagate linearly with time.

Regal (123) [PMMA], and Sato (124) [polycarbonate] both reported that under constant tensile stress the length of crazes  $l(t)$  increased as:

$$l(t) = a_c \log(t/t_0)$$

where  $a_c$  and  $t_0$  are constants. Sauer and Hsaio (127) reported a linear rate of craze propagation in polystyrene, (after the initiation stage).

$$\frac{dl(t)}{dt} = k_c (\sigma - \sigma_0)$$

where  $\sigma_0$  is the initiating stress. Knight (128) combined both growth characteristics which in fact applied to different parts of the total growth characteristic. Craze growth begins rapidly followed by a decreasing growth rate, and if the applied stress is sufficient, a final period of constant growth rate.

The constant growth rate of crazes under static tensile stress has been observed by Bucknall and Clayton (27) for rubber modified glassy polymers.

At high levels of tensile stress and/or temperature, the length of craze marks appears to be restricted by the high density of craze sites. Thus although they grow at a faster rate after initiation than at lower temperatures or stresses they reach a stable length very rapidly. Cohen and Haslett (129) have suggested that this is due to the attenuation of the stress concentration on individual crazes by their near neighbours.

### 3.3.2 Growth and Recovery under Intermittent Stress

It was observed in the earliest studies of crazing phenomena that when the stress was removed from a crazed specimen the craze marks slowly disappeared. Spurr and Niegisch (93) found that crazes in polystyrene and PMMA could be 'healed' within 5 minutes at a temperature of 100°C. In retrospect it is possible to argue that the crazes did not heal but merely contracted in thickness to less than the wavelength of light. However, Spurr et al noted that when the stress was re-applied, crazes were not observed immediately and when they were initiated these did not always correspond with the original craze sites. (This may be regarded as additional evidence to support the argument that crazes are not inevitably initiated at surface flaws or other stress concentrators).

There are several mechanisms that can be identified that would aid the recovery of a craze. It is probable that each contributes to the process. Spurr and Niegisch point out that the 'contraction' of the craze on heating is similar to the recovery of yielded specimens above the softening point. The craze contains yielded material which is oriented. At high temperatures the oriented polymer undergoes reversion to the random state. At lower temperatures the process would continue but at a lower rate. Basically therefore this is an entropic process. Kambour (130) has calculated the surface area of voids in craze matter. This is extremely high, being of the order of 100 m<sup>2</sup>/cm<sup>3</sup>. Kambour and Kopp (131) have in addition calculated the 'retractive stress' in a polycarbonate craze due solely to surface energy. Using a value of surface energy of 40 ergs/cm<sup>2</sup>, the estimate was ~ 5-8 MN/m<sup>2</sup>. The entropy contribution was calculated to be a similar quantity. A third factor which



does not appear to have been considered is the effect of the stress distribution in the vicinity of the craze. On the removal of the applied stress a residual stress would remain due to distortion of material particularly in advance of the craze tip. This would encourage the rapid collapse of the craze.

In Kambour and Kopp's measurements of craze recovery in polycarbonate this third factor was absent because the craze completely covered the cross-section of the tensile specimen. The strain in the craze material  $\epsilon_c$  was calculated from measurements of craze thickness. It was reported that over a period of 105 days the craze strain recovered under zero load at ambient temperatures according to the relationship:

$$\epsilon_c(t) = \epsilon_c(0) e^{-kt}$$

where  $t$  is the recovery period. Corresponding measurements with the craze under tensile stress revealed a craze modulus of  $\sim 560 \text{ MN/m}^2$  which is approximately one fifth of the tensile modulus of the parent material.

Takahashi (132) succeeded in indirectly measuring the rate of the initial elastic craze recovery in an ABS/MMA copolymer. A notched specimen was subjected to an impact tensile load and the light transmissability of the material in the vicinity of the propagating crack was monitored. A rapid elastic recovery was followed by a slow viscous recovery. The first phase accounted for about 50% of the total craze recovery and was completed within 30  $\mu$  secs. This short period corresponded to the time required for the propagation of a stress wave through the affected zone.

The recovery behaviour of craze material may be responsible for the relatively high rate of crack propagation under intermittent stressing as compared with static stress, and indeed may be responsible for the difference between the static and dynamic fatigue characteristics as discussed previously in section 2.6.2. Vincent's (88) explanation for this would seem appropriate. The partial recovery of the 'plastic zone' in advance of the crack tip when under zero or compressive stress is sensible if the plastic zone is identified with craze material. Partial recovery of the craze during the recovery period would lead to a temporary increase in stress intensity at the crack tip on re-application of tensile stress.

The mechanism of craze recovery could account for various features observed in the dynamic fatigue behaviour of glassy amorphous polymers. These include:

(a) The dynamic fatigue lifetime at the same frequency and stress amplitude is longer for sinusoidal cycling than for 'square wave' cycling (133). For square wave cycling the craze in advance of a propagating crack is not completely re-established during the rise time of the stress. Thus for a short period the full stress amplitude is applied to the specimen whilst the stress intensity at the crack tip is high. For sinusoidal stress cycling the 'rise time' is considerably longer which allows the craze(s) to be completely re-established.

(b) The same argument can be extended to explain the rapid growth rate of cracks during the rise time and the very slow growth rate during the actual stress period reported by Brown et al (89) for

'square wave' cycling.

(c) Cyclic softening of UPVC (see section 2.2.3) occurs earlier and is more severe for tension/compression cycling, than for tension only cycling (19). Craze recovery is more rapid under compressive stress (131) and it could therefore be expected that the stress intensity associated with a collapsed craze during the rise time (increasing tensile stress) of the stress will be higher if this is preceded by a period of compression. This leads to the speculation that cyclic strain softening, the pre-cursor to dynamic fatigue in UPVC, is due to craze initiation and growth.

#### 3.4 Crazing and Solvent Plasticization

The critical tensile stress and strain for craze initiation in glassy polymers can be severely reduced by contact with organic liquids and vapours. Earlier studies, notably by Wieser (134), tended to concentrate on the fracture stress in contact with liquids and to correlate, quite successfully, the reduction of brittle strength with the surface tension of the liquid. It was argued that crack initiation and growth essentially involves the creation of new surfaces. Liquid with a low surface tension would assist the cracking process. However with the increased knowledge of the role of crazing in brittle fracture, and in addition the fact that crazing is essentially a micro-yield process, attention became directed to the role of solvent plasticization in this phenomenon.

Bernier and Kambour (135) designed an experimental programme aimed directly at isolating the roles of surface tension and solvent

plasticization. The degree of plasticization increases directly with the concentration of solvent in the polymer. The solubility of a solvent and polymer combination increases as the difference between the solubility parameters of the liquid  $\delta_l$  and polymer  $\delta_p$  decreases. The surface tension of the liquid solvent increases monotonically with  $\delta_l$ .

Bernier et al carefully prepared thin strips of rubber modified PPO. Each strip was pre-equilibrated by soaking in one of thirty organic liquids. The solubility parameter  $\delta_l$  of the liquid ranged from 5.85 to 19 (cal/cm<sup>3</sup>)<sup>1/2</sup>. The solubility parameter  $\delta_p$  of PPO was estimated as 8.9 (cal/cm<sup>3</sup>)<sup>1/2</sup>. The strips were bent over an elliptical former and the critical strain for crazing measured 3 hours after the application of strain. The minimum critical strain of value 0.1% coincided with the condition that  $|\delta_p - \delta_l| = 0$ . It was therefore concluded that solvent plasticization and not surface energy is the predominant causative mechanism in solvent stress crazing.

In a later paper Kambour (136) extended the study to polystyrene, SAN, and polysulfone. The results supported the conclusions of the previous study on PPO. The polysulfone critical crazing strain data <sup>are</sup> reproduced in Figure 3.3 where <sup>they are</sup> ~~it is~~ plotted against the T<sub>g</sub> of the swollen polymer. The critical strain reduces with decreasing T<sub>g</sub> until this equals or falls below the test temperature T<sub>T</sub>. When T<sub>T</sub> ≥ T<sub>g</sub>, the minimum critical strain is ~ 0.1%. It would be reasonable to suppose that, as the stress (or strain) to initiate macroscopic yielding tends to zero when T<sub>T</sub> → T<sub>g</sub> (13), (17), this would also apply to the initiation of microscopic yielding

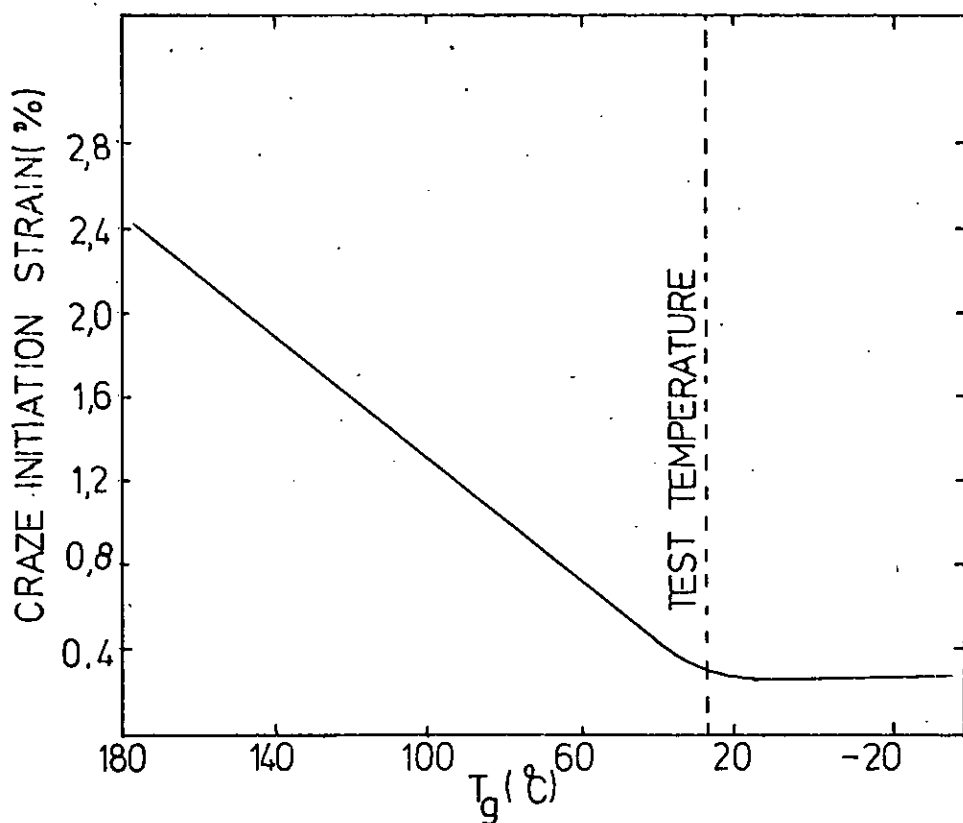


FIGURE 33 RELATIONSHIP BETWEEN CRAZING STRAIN AND THE  $T_g$  OF SOLVENT PLASTICIZED POLYSULFONE. [KAMBOUR (136)]

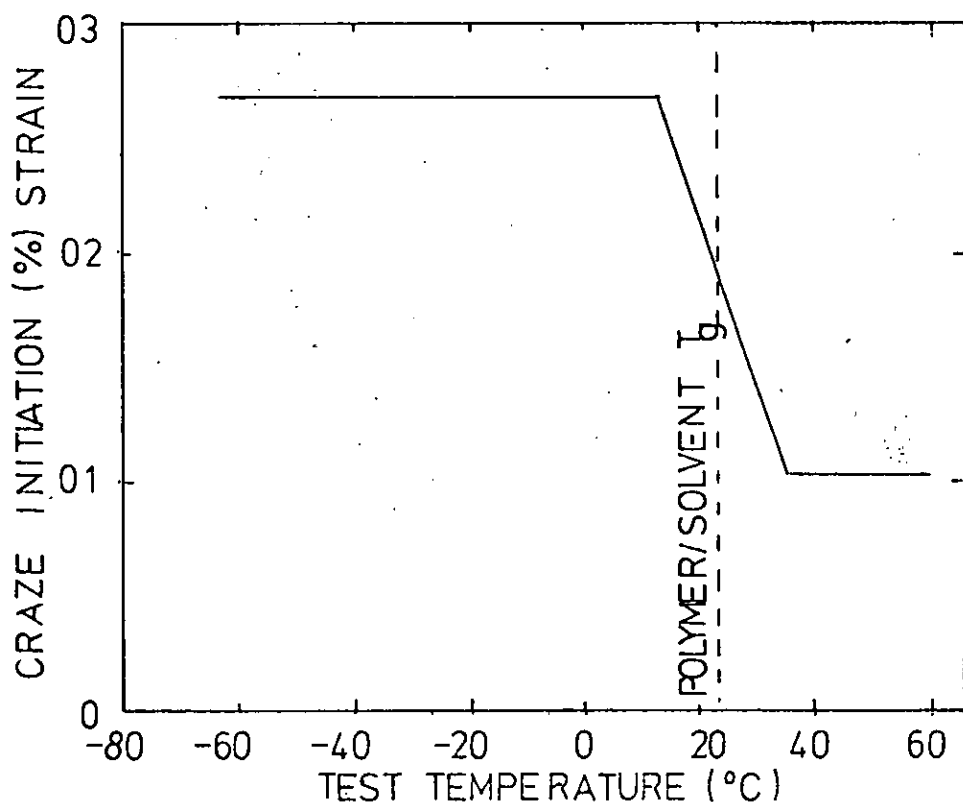


FIGURE 34 RELATIONSHIP BETWEEN CRAZING STRAIN AND TEST TEMPERATURE, AMORPHOUS POLYMER IN ALCOHOL (138).

or crazing. Kambour suggests that the surface tension of the liquid does have a secondary role in promoting the stabilization of localised yielded zones and hence suppressing homogeneous (shear) yielding

Kambour and Bernier chose organic liquids which were known not to interact with the polymers via hydrogen bonding. Vincent and Raha (137) used a similar 'bent strip' test technique to measure the critical tensile strain for craze or crack initiation of UPVC, PMMA and polysulphone in contact with 72 organic liquids. They concluded that hydrogen bonding is an important factor in determining whether a combination of liquid and polymer will result in swelling (and shear yielding), cracking, or crazing. However, although hydrogen bonding is an important factor in determining the solubility of the solvent in the polymer, this does not detract from Kambour's general conclusion that plasticization is the major influence in solvent stress crazing or cracking. The results of Vincent et al do however show that the quantity  $|\delta_e - \delta_p|$  is not sufficient in itself to predict the deterioration in mechanical properties by organic chemicals. The critical strains for crazing or cracking of UPVC in contact with a selection of liquids are included in Table 3.2.

Liquid	Critical tensile crazing strain
Diethyl ether	0.23%
Toluene	0.15%
Acetic acid	0.31%
Ethanol	0.72%
Methanol	0.68%
n-Pentane	1.23%
Glycerol	1.36%
Water	1.90%

Table 3.2. The minimum critical tensile strain for craze initiation of UPVC in various liquids. Vincent and Raha (137).

A study by Crook, Earl, Johns and Loneragan (138) has also emphasised the role of plasticization in solvent stress crazing. The procedure adopted differs from that of Bernier and Kambour in that the quantity  $(T_g - T_T)$  was varied over a range by varying the test temperature  $T_T$ . Polystyrene and PMMA in the form of bent strips were immersed in various alcohols and the critical crazing strain measured over the temperature range  $-40^{\circ}\text{C}$  to  $+60^{\circ}\text{C}$ . The data obtained in each case included the features shown in Figure 3.4. These are:

1. A significant discontinuity on the crazing strain data at a characteristic temperature. This temperature was found to be related directly to the  $T_g$  of the polymer/solvent mixture.
2. At temperatures above the discontinuity i.e.  $(T_g - T_T) \leq 0$ , the craze initiation strain is a minimum and independent of a further increase in  $T_T$ . In this respect the data fully supports <sup>those</sup> that published by Bernier and Kambour (135). The minimum critical strains are included in Table 3.3.

Polymer	Liquid	Initiation Strain
Polystyrene	Methanol	0.2%
	Ethanol	0.15%
	n-Propanol	0.10%
	n-heptane	0.05%
PMMA	Methanol	0.4%
	n-butanol	0.1%

Table 3.3. The minimum critical strain for craze initiation of PMMA and polystyrene in various alcohols, Crook, Earl, Johns and Loneragan (138).

3. At temperature such that  $(T_g - T_T) > 0$  the critical strain is above the minimum but independent of further decrease in  $T_T$ . In this respect the behaviour differs from that observed by Bernier et al. In their case the critical strain increased with increasing value of  $(T_g - T_T)$ .

Crook et al commented that craze initiation and stress relaxation would appear to be intimately (cause and effect ?) connected. An increase in temperature or decrease in  $T_g$  reduced the period for craze initiation and increased the rate of the relaxation process by the same degree. This they claim might offer an explanation for the observed independence of critical strain with temperature. No explanation was offered for the disparity between their own data and <sup>those</sup> ~~that~~ published by Bernier and Kambour (compare Figures 3.3 and 3.4).

The low tensile strains for craze initiation in contact with solvents (invariably  $\sim 0.1\%$ ) cannot be accounted for rationally by the critical tensile strain criteria approach championed by Menges and co-workers (see 3.2.2). It is implicit that earlier, Menges (30) had assumed that the surface energy effect was responsible for environmental stress crazing. He concentrated on wetting agents which tended to support his hypothesis, and totally excluded solvent interaction as such. In a recent paper Menges and Riess (117) have finally included a study on solvent stress crazing, the results of which generally support the view that  $\epsilon_{\infty}$  is not singular. The paper is confusing in some respects. They report that the minimum critical strain for crazing of UPVC in air (0.8%)



is reduced to 0.1% by immersion in water and reduced to 0.2% by immersion in wetting agent. Water is not generally regarded as a stress cracking or crazing agent for UPVC, and indeed the polymer is used extensively in water distribution. Also Vincent and Raha (137) measured a critical strain of 1.9% for UPVC in water. The severe effect of the wetting agent is quite at variance with the earlier publications by Menges (30). No attempt was made to explain this reversal in their conclusions.

#### 4. Experimental Model and Equipment

Craze initiation, on the evidence presented in Chapters 2 and 3, would appear to be an attractive prospective design criterion for amorphous glassy polymers. For this to be a practical criterion however, craze initiation must be detected unambiguously and precisely, if the combination of service conditions such as stress, strain, time, temperature, and chemical environment, are to be established as operational design limits. The visual detection of craze initiation used extensively by Menges (see 3.2.2) in combination with tensile creep, and also used by others in conjunction with solvent stress crazing (see 3.2.3) is limited. The most serious limitation is that only transparent polymers can be studied. Additionally the method is highly subjective, particularly when the craze density is low. Crazes of thickness less than the wavelength of light cannot be detected visually (see 3.1). Additionally it is often not possible to monitor visually the surface condition of a specimen under stress; for instance under dynamic load and when immersed in an opaque environment.

Many of the limitations of the visual detection techniques do not apply when crazes are detected mechanically. Craze initiation and growth contribute to the creep strain. The perturbation in the characteristic is however small, unless crazing is very severe. Bergen (34), for instance, detected solvent crazing by comparing the

creep response in air with that for the polymer immersed in solvent.

Apart from the fact that crazing in air introduces only a minor perturbation, it is obvious that no reference characteristic (uncrazed) can be developed to compare the air-crazed creep response with.

Therefore it is not possible to resolve the initiation criterion for crazing in air simply by the examination of creep characteristics.

The technique developed by Bucknall and Clayton (27) (see 2.2.4) again is only adequate when crazing is a major deformation process; hence its exclusive use with rubber modified polymers.

The mechanical technique for craze detection discussed here has been developed specifically for homogeneous glassy polymers where crazing is a minor contributor to deformation but nevertheless a major factor in determining the mechanical integrity of the material. The technique is based on a concept which is conveniently embodied by the term 'Core Stress Model'.

#### 4.1 The Core Stress Model

The crazes contribute to the creep deformation because each craze represents an incremental extension of the material. The craze also has a low tensile modulus (131) which combines to effect a reduction in the apparent modulus of the craze damaged skin. The undamaged core of the specimen therefore has a higher tensile modulus than the crazed skin. Thus in addition to the increased rate of creep, surface craze initiation and growth leads to a modification of the stress distribution across the cross-sectional area of the specimen.

Consider the case of a linear viscoelastic material subjected to a step input of uniaxial tensile stress  $\sigma_N$ . Crazeing is initiated on the free surfaces of the specimen after a time  $t_c$ . The undamaged core area  $A_c$ , the total cross-sectional area  $A$ , and the area of craze damaged skin  $A^*$ , are simply related if lateral contraction is neglected:

$$A = A^* + A_c \quad [2]$$

From compatibility considerations:

$$\sigma_c E^* = \sigma_s E_c \quad [3]$$

where  $\sigma_c$  and  $\sigma_s$  are the core stress and skin stress respectively.  $E^*$  and  $E_c$  are the moduli of the craze damaged skin and undamaged core respectively.

From equilibrium considerations:

$$\sigma_N A = \sigma_c A_c + \sigma_s A^* \quad [4]$$

Combining equations [2], [3] and [4] give:

$$\sigma_c = \sigma_N \left[ 1 - \frac{A^*}{A} \left( 1 - \frac{E^*}{E_c} \right) \right]^{-1} \quad [5]$$

Therefore provided  $A > A^* > 0$ , and  $E^* < E_c$ , the mean core stress will exceed the applied (nominal) stress  $\sigma_N$ . The effect of this re-distribution of stress might be detectable by an appropriate creep and recovery experiment (see 2.2.2).

For simplicity assume that due to surface craze initiation the core stress increases from  $\sigma_N$  to  $\sigma_c$  at time  $t_c$  after load application, as shown in Figure 4.1. In practice of course this will not be a step increase but will increase in accordance with craze growth and the further nucleation of craze sites. However the assumption is reasonable in that it will be used only as an aid to the definition of physically measurable

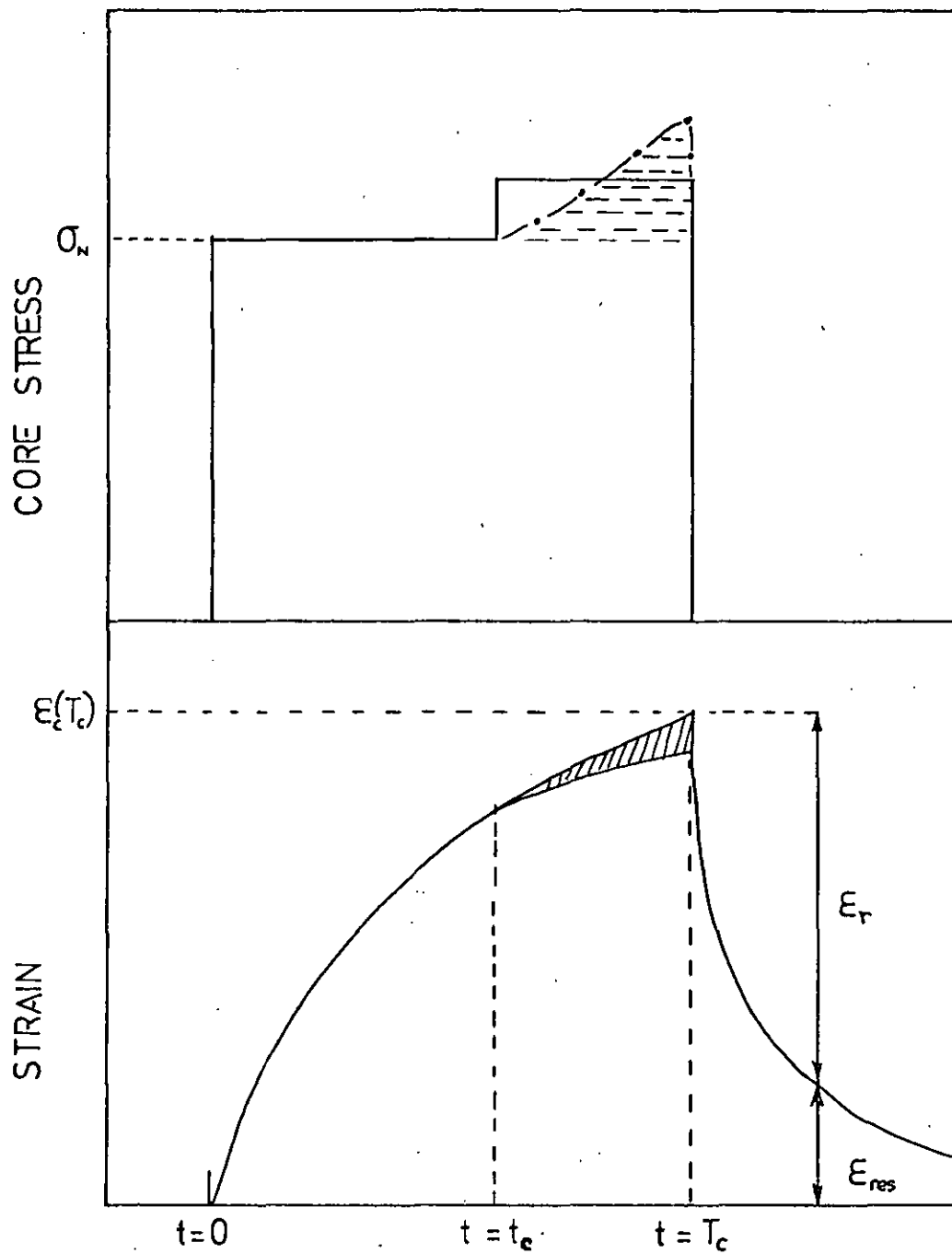


FIGURE 4.1 THE EFFECT OF CRAZE INITIATION ON THE SPECIMEN CORE STRESS  $\sigma_0$  AND CREEP STRAIN  $\epsilon(t)$ .

parameters.

The damaged specimen is unloaded after a total creep period  $T_c$  and allowed to recover. Linear superposition theory (29) would predict a maximum creep strain (just prior to load removal) of:

$$\epsilon_c(T_c) = C(T_c)\sigma_N + C(T_c - t_c)(\sigma_c - \sigma_N) \quad [6]$$

Similarly the creep strain at time  $\theta$  after load application is given by:

$$\epsilon_c(\theta) = C(\theta)\sigma_N \quad \text{provided } \theta < t_c \quad [7]$$

The residual strain at time  $\theta$  after the removal of stress is:

$$\epsilon_{res}(T_c + \theta) = C(T_c + \theta)\sigma_N + C(T_c + \theta - t_c)(\sigma_c - \sigma_N) - C(\theta)\sigma_c \quad [8]$$

The recovered strain  $\epsilon_r(\theta)$ , at time  $\theta$  after the removal of stress is defined as:

$$\epsilon_r(\theta) = \epsilon_c(T_c) - \epsilon_{res}(T_c + \theta) \quad [9]$$

If  $\theta \ll T_c$ , then  $C(T_c + \theta) \approx C(T_c)$  and equations [6], [8] and [9] give:

$$\epsilon_r(\theta) \approx C(\theta)\sigma_c \quad [10]$$

Comparing equations [7] and [10] reveal that if surface crazing is initiated during the creep period then provided  $\theta \ll T_c$ ,

$$\epsilon_r(\theta) > \epsilon_c(\theta)$$

i.e. the initial recovered strain exceeds the initial creep strain. The

damage parameter  $\Delta R_{CR}$  is defined here as:

$$\Delta R_{CR} = \epsilon_r(\theta) - \epsilon_c(\theta) \quad [11]$$

$$\text{or } \Delta R_{CR} = \epsilon_c(T_c) - \epsilon_{res}(T_c + \theta) - \epsilon_c(\theta) \quad [12]$$

where the subscript CR denotes sequence of strain comparison. The core stress model would predict that if crazing occurs during the creep period then:

$$\Delta R_{CR} > 0$$

and for no surface crazing,  $\sigma_c = \sigma_N$  and:

$$\Delta R_{CR} \approx 0$$

In practice  $\theta$  is not infinitesimal, and therefore slightly negative values of  $\Delta R_{cr}$  would be expected for an undamaged linear viscoelastic material.

The rapid initial recovery of the core of a surface crazed specimen would be resisted by the comparatively sluggish recovery response of the damaged skin. However, the resistance offered by the craze to compressive collapse, must by the nature of their structure be small compared with the tensile stresses that caused their initiation and growth (131). It is proposed therefore that the 'energetic' recovery of the core is the major factor in determining, at least initially, the recovery of the specimen as a whole. The core stress model therefore predicts that the recovered strain of a surface crazed specimen of linear viscoelastic material at a short time after the removal of load, exceeds the creep strain at the same time after load application.

Alternative definitions of the damage parameter can be derived to suit the experimental conditions. Consider the stress input and strain response for intermittent creep and recovery cycling shown in Figure 4.2. If the effect of recovery time is to be studied, a one and a half cycle stress history namely creep, recovery, and creep, would be appropriate. Obviously  $\Delta R_{cr}$  is not sufficiently flexible to apply in this situation. However, the core stress model would predict that if surface damage is initiated during the first creep cycle, and if this damage is not completely healed during the recovery period then:

$$\epsilon_c (T_c + T_R + \theta) - \epsilon_{res} (T_c + T_R) > \epsilon_c(\theta)$$

i.e. the additional strain response to the second stress cycle exceeds that of the first. This leads to the definition of the damage parameter  $\Delta R_{cc}^n$ ,

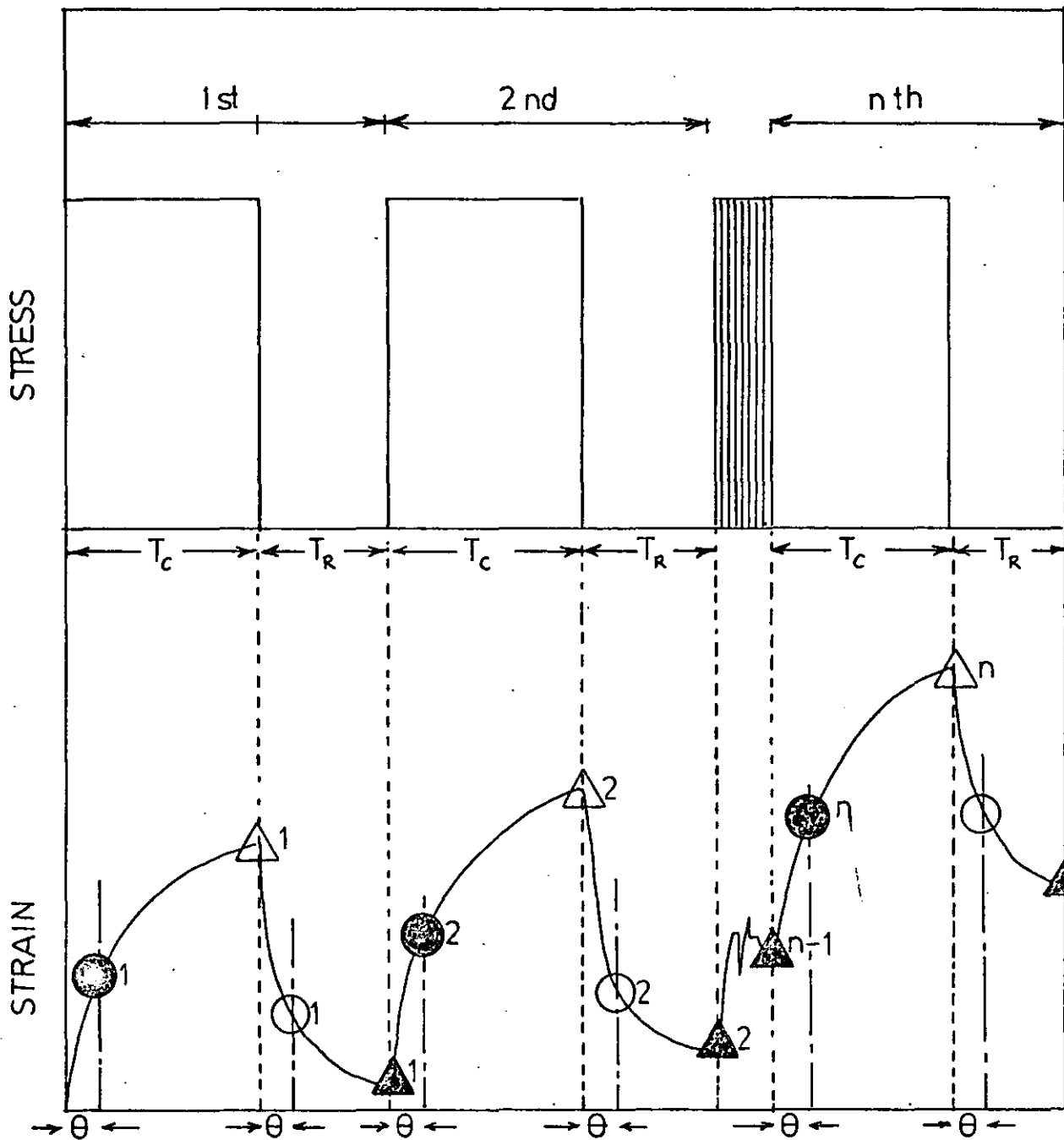


FIGURE 42 STRESS INPUT AND STRAIN RESPONSE FOR CYCLIC CREEP AND RECOVERY PROGRAMME.  
COORDINATES:

$$\bullet_n, E_c [(n-1)(T_R + T_c) + \theta]$$

$$\triangle_n E [(n-1)T_R + nT_c]$$

$$\circ_n E_{res} [(n-1)T_R + nT_c + \theta]$$

$$\blacktriangle_n E_{res} [n(T_c + T_R)]$$



where n is the cycle number:

$$\Delta R_{cc}^n = \epsilon_c [(n-1)(T_c + T_R) + \theta] - \epsilon_{res} [(n-1)(T_c + T_R)] - \epsilon_c(\theta) \quad [13]$$

Similarly, and again with reference to Figure 4.2, if no damage is initiated in the first cycle (which must be considered the usual case in practice) then:

$$\Delta R_{RR}^n = \epsilon_c [nT_c + (n-1)T_R] - \epsilon_{res} [nT_c + (n-1)T_R + \theta] - \epsilon_c(T_c) + \epsilon_{res}(T_c + \theta) \quad [14]$$

Although the three definitions of damage parameter  $\Delta R_{CR}$ ,  $\Delta R_{cc}^n$ , and  $\Delta R_{RR}^n$  given above differ, it would be expected that the transition from zero to positive values would all coincide with craze initiation.

Various workers have reported positive values of  $\Delta R_{CR}$  on both semi-crystalline and glassy amorphous polymers. Hadley and Ward (139) reported that, for polypropylene fibres after a constant creep period under tensile creep stress, :

$$\Delta R_{CR} = A\sigma_N + B\sigma_N^2 + C\sigma_N^3$$

Thus  $\Delta R_{CR}$  is always positive and increases with stress level. Hadley et al used this as evidence to support a multiple integral superposition technique for non-linear viscoelastic materials. It is therefore implicit that a positive  $\Delta R_{CR}$  is compatible with the predictions of continuum mechanics. This is supported by the smooth continuous functional relationship between  $\Delta R_{CR}$  and stress level. However Hadley and Ward pre-conditioned their creep specimens very severely. The specimens were cycled at a strain amplitude of 3-4% prior to creep and recovery testing to ensure 'repeatability'. Menges and Alf (118) reported the initiation of micro-cracking in polypropylene at tensile strains in excess of 2.5%. It is therefore probable that the non-virgin specimens tested by Hadley

et al were damaged. It is therefore not surprising that  $\Delta R_{CR}(\sigma)$  is a continuous function under these conditions.

Turner (31) observed that for PMMA, PVC, polypropylene, and acetal,  $\Delta R_{CR}$  was positive for short recovery periods and negative for long recovery periods.  $\Delta R_{CR}$ , as measured after a short recovery period ( $t = 5$  seconds), as a function of tensile strain proved to be a common characteristic for all the plastics studied. ~~This data is~~ <sup>These are</sup> reproduced in Figure 4.3. It would also appear from ~~this~~ <sup>these</sup> data that  $\Delta R_{CR}$  values for UPVC are only significantly positive at tensile strains in excess of  $\sim 1.0\%$ . This feature, which was not commented on by Turner, is interesting because the strain limit almost coincides with that for craze initiation (117).

Positive values of  $\Delta R_{CC}^n$  and  $\Delta R_{RR}^n$  have not been reported explicitly. However the paper by Jaksch (33), discussed in Section 2.2.2, does indicate that positive values are exhibited by polyethylene.

Recently a considerable interest has focused on the phenomenon. The interest appears to be exclusively one of mathematical curiosity. Brereton (140) has developed an analytical approach for non-linear viscoelastic materials which predicts positive values of  $\Delta R_{CR}$ . Lockett (141) has developed a modified 'spring and dash pot' model which gives the same (retrospective) predictions. Without exception the explanations offered by Hadley and Ward, Turner, Brereton, and Lockett all invoke the continuum deformation properties of the polymer. They predict, therefore, values of  $\Delta R_{CR}$  that are

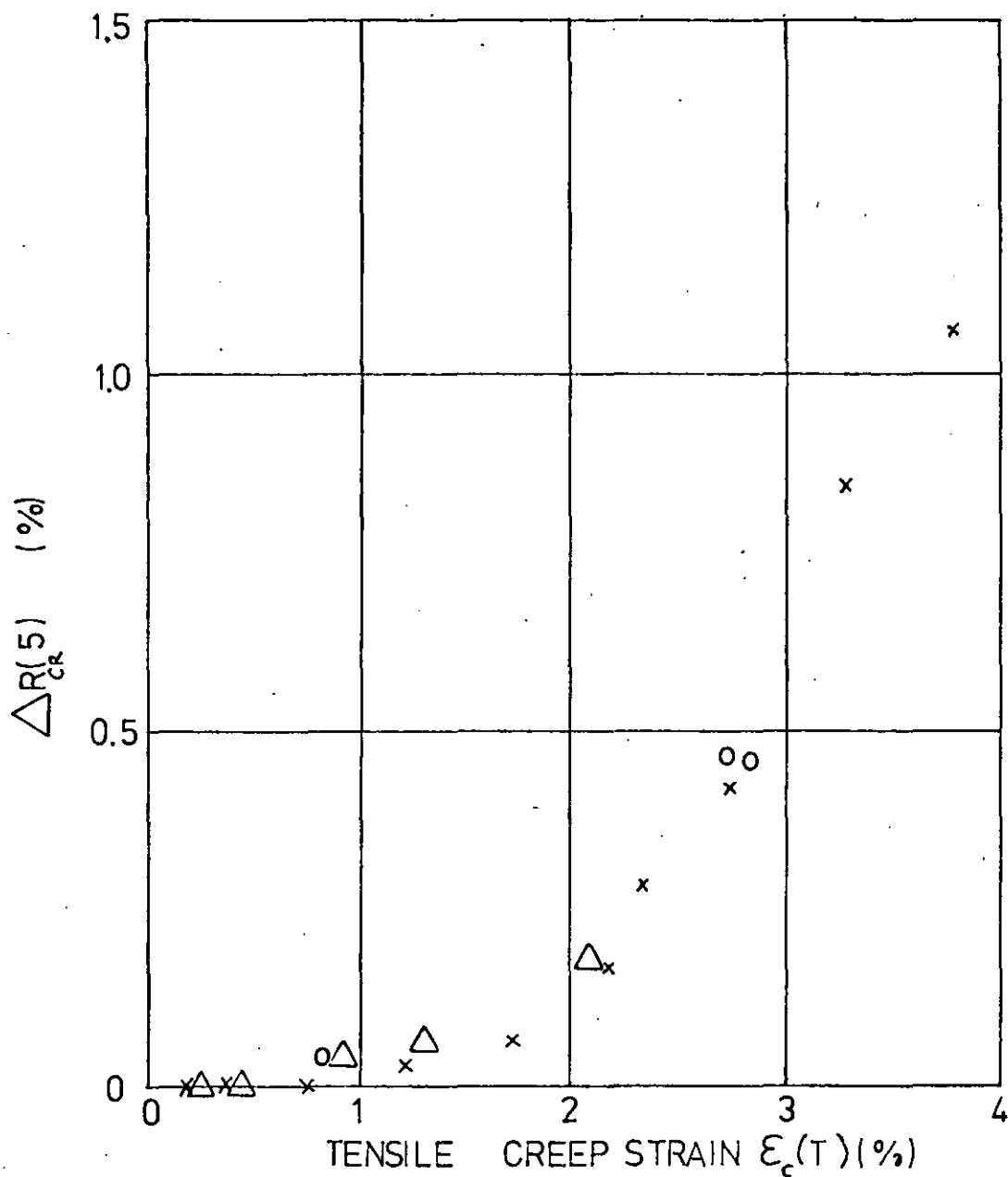


FIGURE 4.3 THE GROWTH OF THE FUNCTION  $\Delta R_{CR}(5)$  WITH FINAL CREEP STRAIN ACCORDING TO (TURNER (31))

- x UPVC
- $\Delta$  ACETAL COPOLYMER
- o POLYPROPYLENE

continuous and positive. The core stress model on the other hand, is essentially mechanistic and predicts a  $\Delta R$  function that is positive but discontinuous. The continuity or otherwise of the  $\Delta R$  function can be ascertained by a comprehensive experimental programme involving strain measurements of high resolution. The next section includes a detailed description of the high strain resolution tensile creep machine and extensometry, developed as an integral and necessary part of this study.

## 4.2 The RAPRA Tensile Creep Machine

### 4.2.1 Design Considerations

At the time of the initial design phase only one commercially available tensile creep machine warranted serious consideration, this being the Macklow Smith/ICI machine described by Turner and Mills (142.) This equipment satisfies the recommendations of BS4618 and indeed is often recognised as the example used in the preparation of this advanced British Standards document. The specimen geometry and the principles of the extensometer used in this equipment are shown in Figure 4.4. The widespread use of this specimen geometry in the UK was sufficient reason to adopt the same for this work.

The modified Lamb extensometer shown diagrammatically in Figure 4.4 incorporates an optical lever system which essentially transforms linear displacement into angular displacement. In the standard model with rollers of 12.5 mm diameter and an 80 mm gauge length the angular displacement of the light spot reflected from mirrors on both rollers combines to give 0.256 radians per 1% extension or contraction of the specimen gauge length. The light

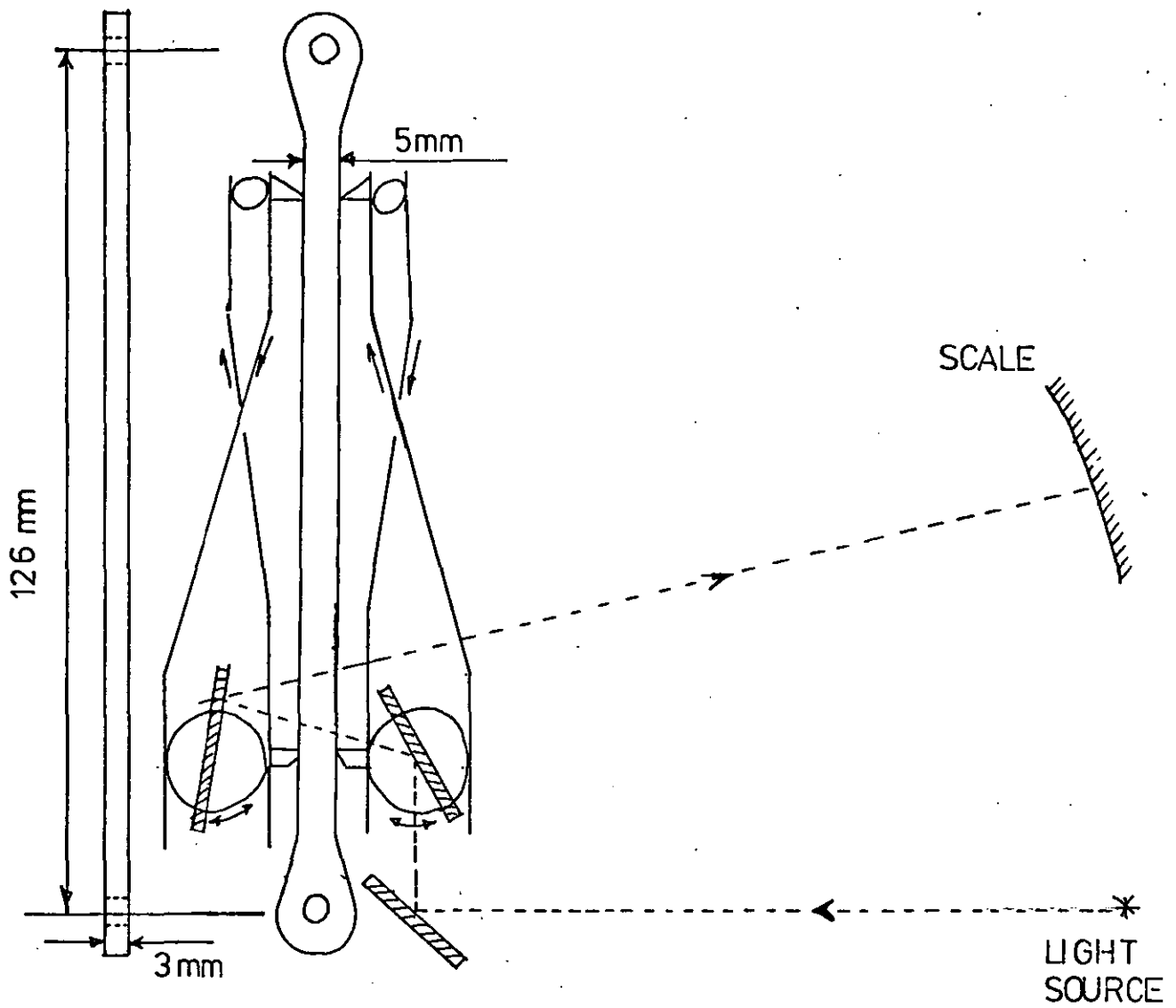


FIGURE 4,4 PRINCIPLES OF THE ICI EXTENSOMETER.  
ALSO SPECIMEN GEOMETRY AND DIMENSIONS

spot is focused on a curved graduated scale of radius 50 cm with the mirrors at its centre. Thus a specimen strain of 1% displaces the light spot (and fine hair-line image) a distance of 128 mm on the scale. It is argued by the manufacturers that the position of the hair-line can be determined to within  $\pm 0.1$  mm, which is a strain resolution of better than 0.002%. This is within the requirements of Class A (BS4618) extensometry. The strain resolution can be increased easily by decreasing the diameter of the rollers, however this reduces the maximum strain that can be recorded. Unfortunately difficulties arise in determining the hair-line position accurately when this is moving appreciably; as will be the case a short time after the application or removal of load. The operator must record the scale reading at a specified time.

The uniaxial tensile load is applied to, and removed from, the specimen via a lever arm and a slide-guide alignment system. The alignment of the load axis with the central axis of the specimen is an important design feature. The flexibility of plastics and difficulty in preparing planar specimens combine to create a considerable alignment problem. 'Passive' alignment mechanisms such as the universal couplings, used in the testing of metals, are not appropriate in this case because friction in the bearings must be overcome by the misalignment torque developed in the specimen itself. The slide-guide system adopted in the ICI machine is 'active' but contact between sliding surfaces and therefore friction cannot be avoided with this mechanism.

To ensure that the load is applied to the specimen rapidly and without transient overloading a critically damped 'dash pot' is

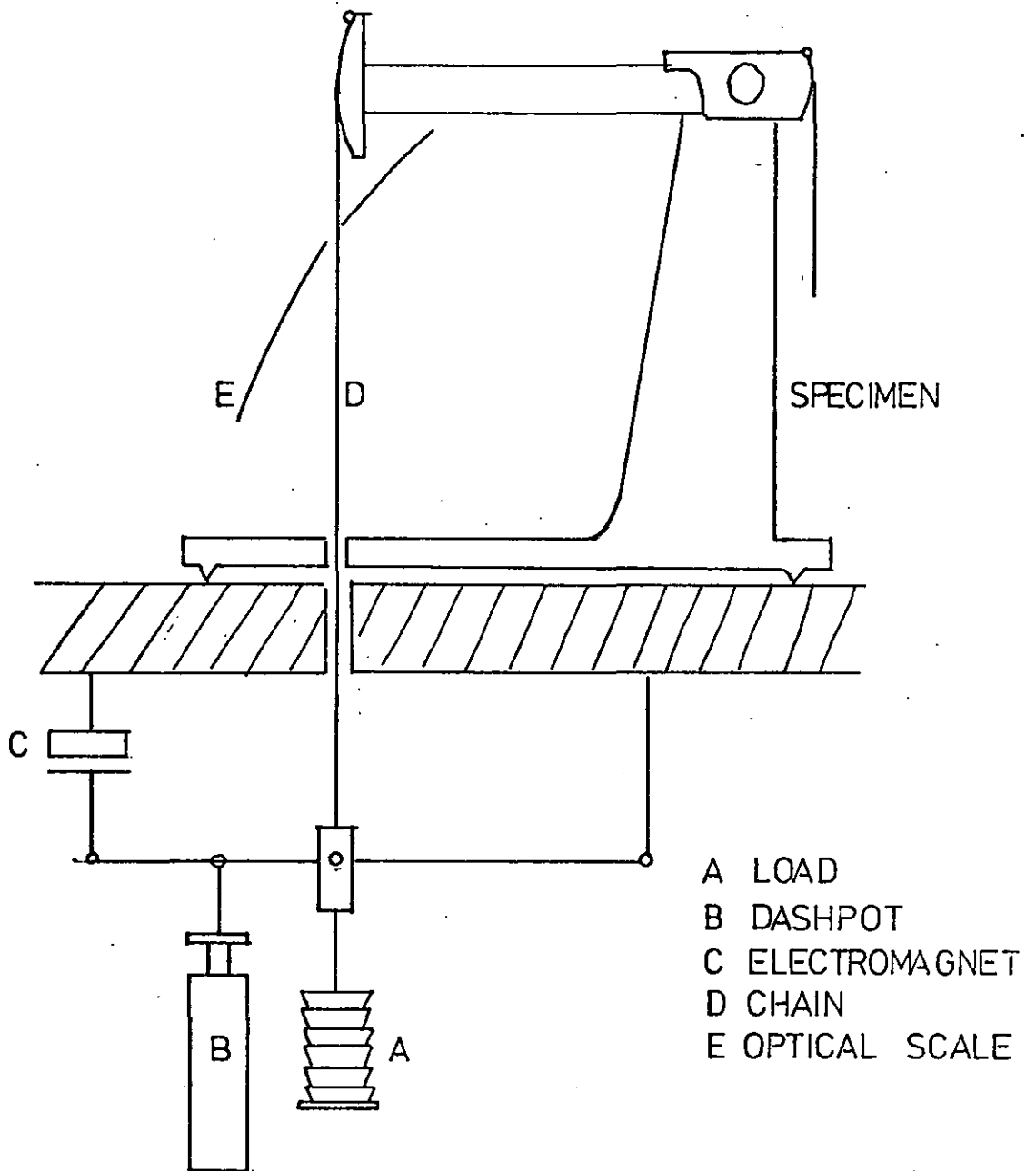


FIGURE 4,5 ICI CREEP MACHINE SHOWING LOADING MECHANISM

incorporated as shown in Figure 4.5. The dash pot is not activated when the load is removed. The problem with the arrangement, as shown in Figure 4.5, is that when the load is removed the specimen recovery is resisted by the substantial inertia of the lever arm. This was considered as a possible source of error in measured recovery strains after short recovery periods.

A second machine justifying serious consideration at the design stage was that developed at the Cranfield Institute of Technology and described by Darlington and Saunders (143). The equipment was not available commercially, but certain features of the design were attractive. A linear displacement capacitive differential transducer is employed as the basis of automatic strain monitoring. The transducer offers an excellent potential strain resolution of  $\pm 0.002\%$  with a specimen gauge length of only 1.2 cm. It can be argued of course that the resolution of an analogue device is meaningless without reference to its stability and the stability of the energising and recording equipment. The limitation on the practical resolution of such a device is invariably dominated by stability. The Cranfield system adopts sophisticated electronics to improve stability - particularly of the energising voltage. The system is costly. However the equipment was designed specifically for small specimens to study the effect of orientation in polymers and sections of moulded parts. It is also capable, by addition of further instrumentation, of measuring strains developed orthogonally to the principal tensile strain. Lateral contraction and dilatational strains are thus capable of being measured (see Section 2.2.4).



In a later development of the Cranfield machine the slide guide alignment mechanism was replaced with a single cantilever spring system. For the small displacements, the loading axis is constrained to coincide with the specimen axis without friction. This was considered as an important design feature.

#### 4.2.2 Design Details

Patents have been applied for the <sup>in</sup> UK, Australia, Germany and Japan for the extensometer described in 4.2.2.1. below. Patents have been granted in the USA (3802781), France (72030293) and South Africa (72/524444). The extensometer and creep machine is licensed to, and manufactured by, Hampden Test Equipment Ltd., Rothersthorpe Avenue, Northampton. A copy of the UK Patent Specification is included in Appendix I. A copy of the manufacturer's specification is included in Appendix II.

##### 4.2.2.1. The Moiré Fringe Extensometer

It was considered that an intrinsically digital strain monitoring device based on the phenomenon of Moiré Fringes would satisfy both the stability and resolution requirements of this research programme.

Moiré fringes are produced when light is passed through two similar gratings aligned so that their rulings are sensibly parallel to one another. For coarse 'line and space' (photogrid) gratings the modulation of light intensity can be understood by reference to Figure 4.6. The transmitted light intensity varies approximately sinusoidally in the direction at right angles to the direction of the rulings and in the plane of the gratings. For a

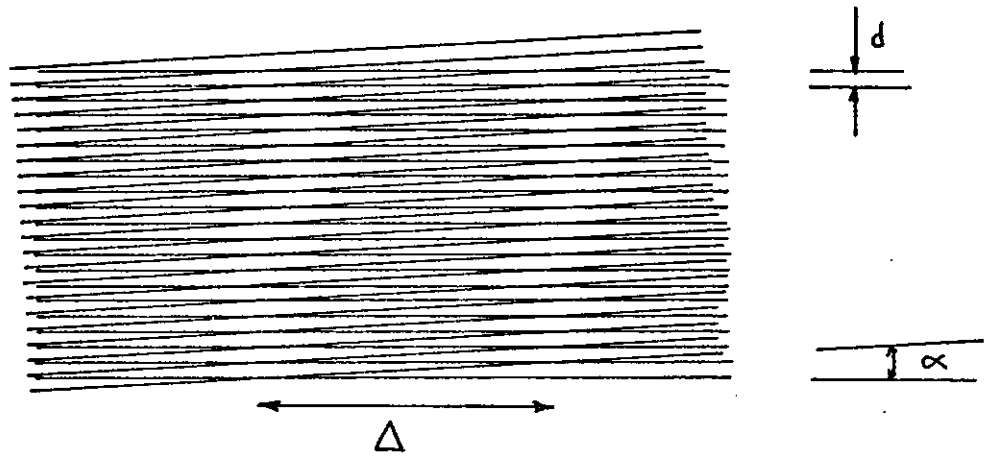


FIGURE 4,6 'LINE AND SPACE' MOIRÉ FRINGES

$\Delta$  FRINGE SPACING

$d$  GRATING PITCH

$\alpha$  ANGLE BETWEEN GRATINGS

parallel transmitted beam of light incident normal to the plane of the gratings, the fringe separation  $\Delta$  is given simply as:

$$\Delta \approx \left( \frac{d}{\alpha} \right)$$

where  $d$  is the grating pitch and  $\alpha$  is the (small) relative angle between the rulings. If one grating is fixed and the other displaced a distance  $x$  in the plane at right angles to its rulings then an individual Moiré fringe will be displaced by an amount  $Y$ , where

$$Y = \left( \frac{\Delta}{d} \right) x \quad \text{or} \quad Y = \left( \frac{1}{\alpha} \right) x$$

The periodic change in intensity at any point with displacement of the gratings can be represented as:

$$I = I_{\min} + I_0 \sin \left( \frac{2\pi x}{d} - \beta \right) \quad [15]$$

where  $I_{\min}$  is the background illumination,  $2I_0$  is a measure of the fringe contrast and  $x$  is the grating displacement. The inclusion of  $\beta$  simply normalises the intensity at  $x = 0$ , at all points in the image. Thus at any point within the image the light intensity changes through one complete 'cycle' for each incremental grating displacement of  $d$  (the grating pitch). This 'periodicity' is independent of the angle between the grating pair provided the relative grating movement is at right angles to the rulings on one grating. The periodic change in light intensity (one cycle per grating pitch of relative grating displacement) can be easily monitored using photocells or photodiodes in the fringe image. The electrical current or voltage output from such devices is sensibly proportional to the incident light intensity.

Line and space gratings with a grating pitch less than about 0.025 mm are not commercially available. The optical interference

effects rather than simple shadowing become predominant with gratings of 40 lines per mm or more. For high incremental displacement resolution, diffraction gratings are used with the profile as shown in Figure 4.7. The blaze angle of such gratings is chosen to match the spectral sensitivity of silicon photodiodes (peak sensitivity 0.85  $\mu$ m). This ensures that the maximum potential fringe contrast will occur in the infra-red region of the diffraction image. This image includes a central undiffracted image with symmetrical diffraction patterns on either side as shown in Figure 4.8. A full analysis of the interference pattern generated by a pair of diffraction gratings has been published by Guild (144).

Commercially available transparent diffraction gratings can contain up to 400 rulings per mm. A thin plastic replica of a master grating is adhesively bonded to a flat glass plate. The contrast of the Moiré fringes which determines the photodiode signal response decreases with an increasing gap between the grating pair. The rate of attenuation of contrast with increasing distance between the gratings depends to a significant degree on the grating pitch. Shepherd (145) suggests that gratings of pitch 0.01 mm should have an inter-grating gap of no greater than 0.12 mm. The first mechanical requirement therefore for a high resolution Moiré fringe extensometer is that the inter-grating gap must not change significantly during relative displacement. The second stringent mechanical requirement is that the grating pair must not rotate relatively during displacement. Such rotation will change the fringe spacing with a resultant loss of photodiode signal stability. It is important however to emphasize that neither rotation or changes in grating separation would alter the

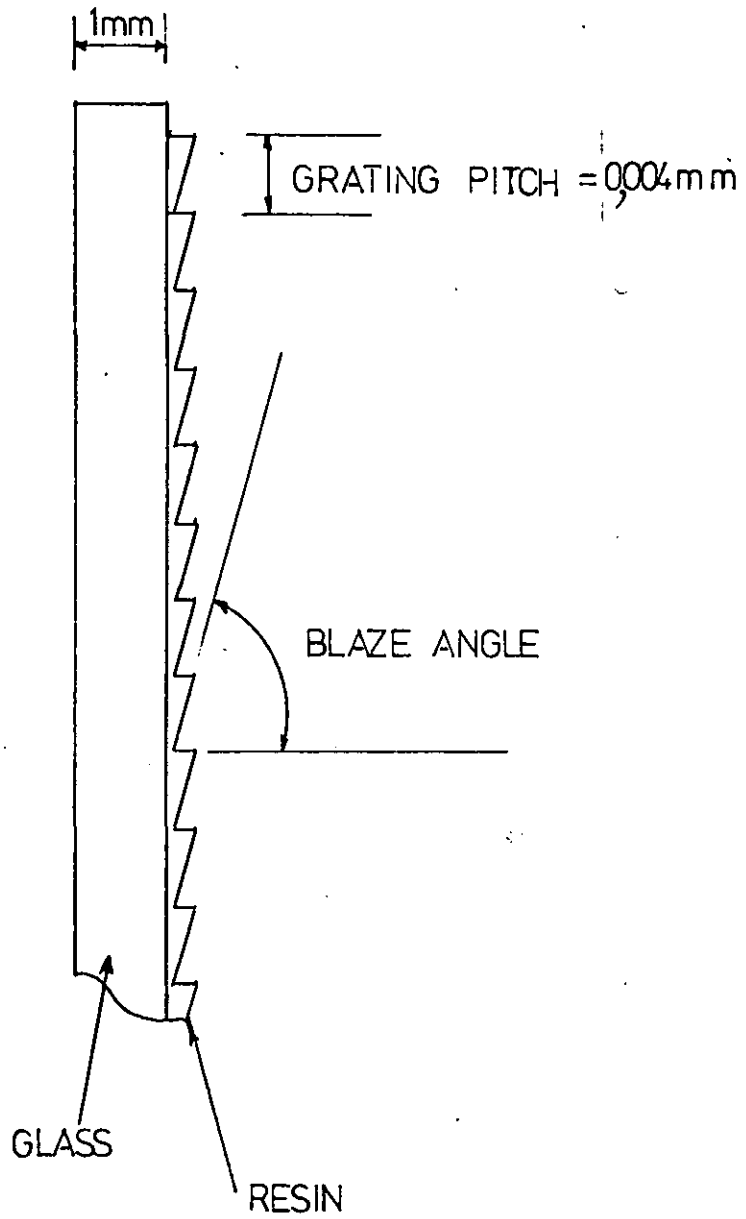


FIGURE 4,7 CROSS-SECTION ( SCHEMATIC) OF A DIFFRACTION GRATING.

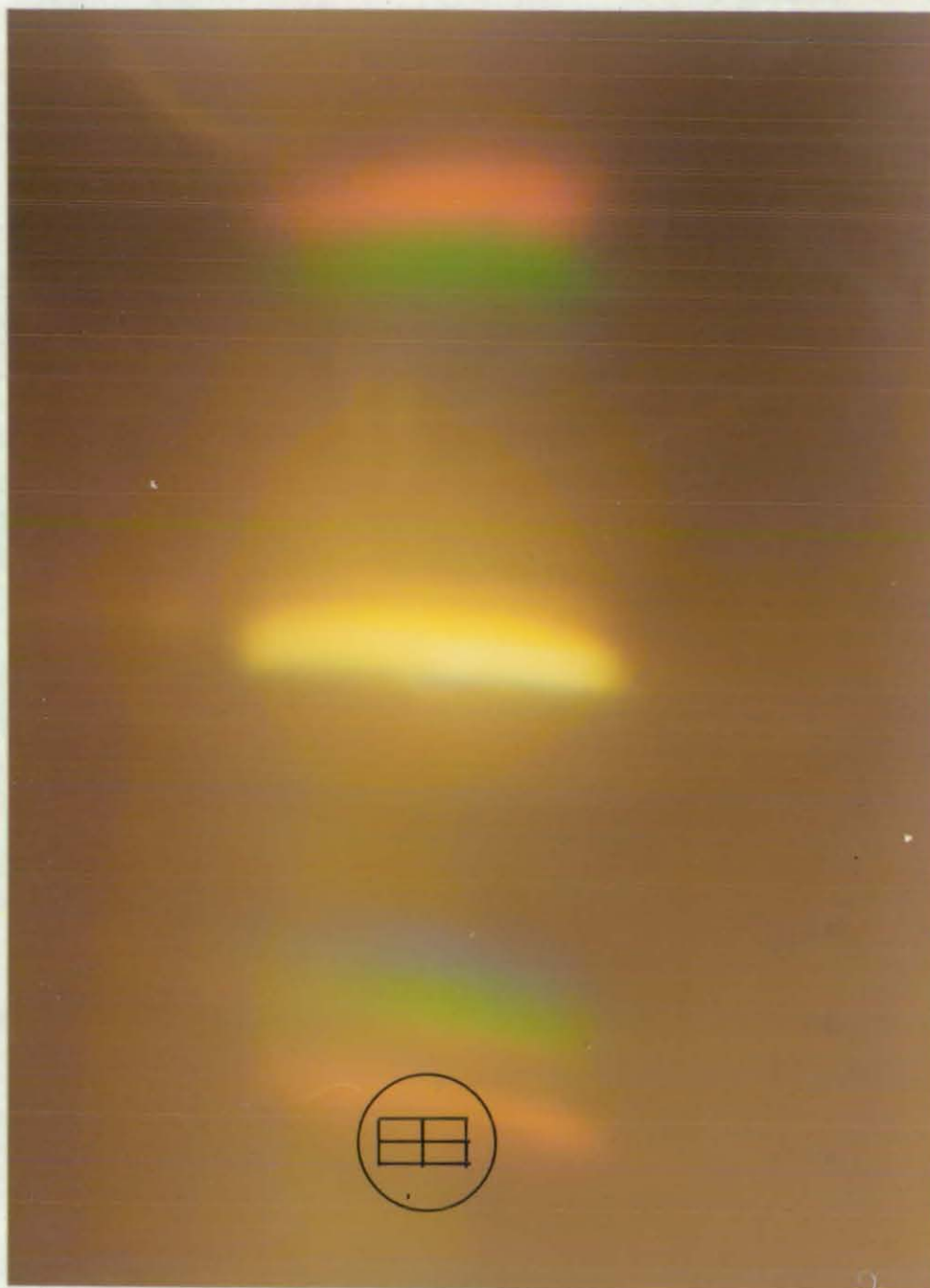


Fig. 4.8 The Moire Fringe Diffraction Image Showing The Optimum Position of the Photo-diode Assembly.

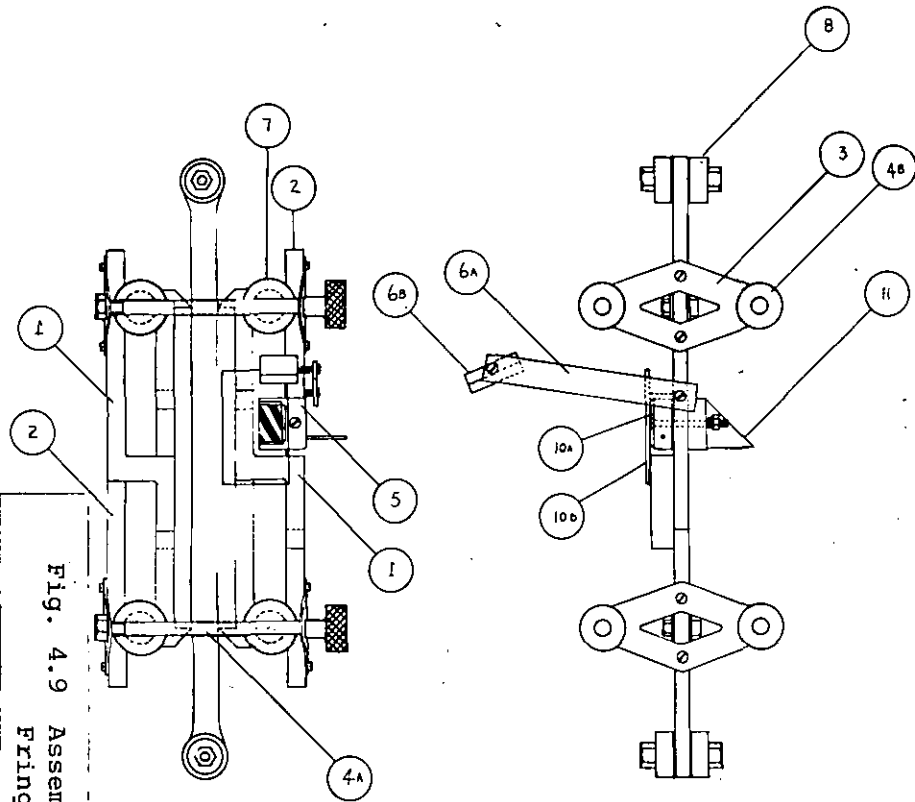
inherent digital resolution of the grating pair.

An assembly drawing of the Moiré fringe extensometer is shown in Figure 4.9. With reference to this diagram the following parts can be identified.

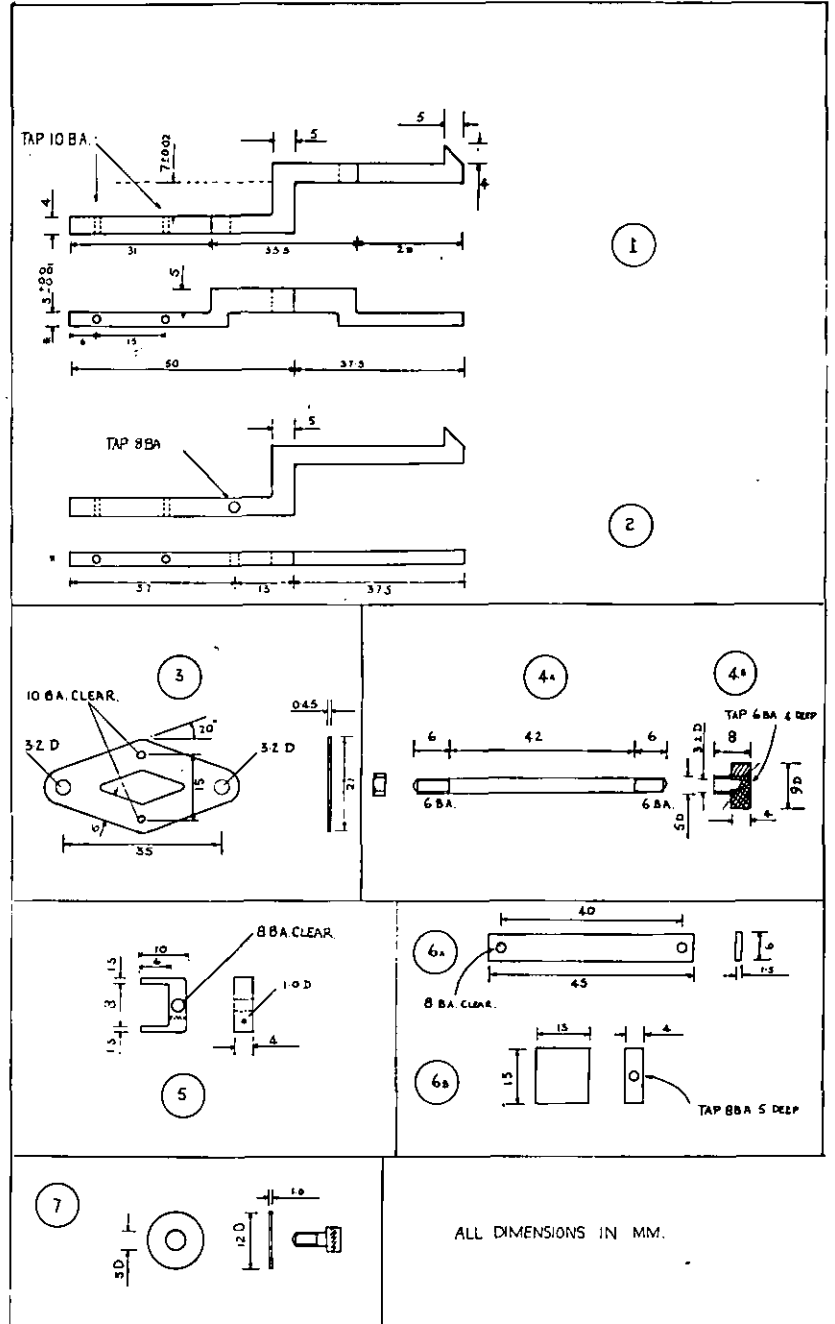
- (1) Stepped cross-members with integral knife edge - two off.
- (2) Flat cross-members with integral knife edge - two off.
- (3) Leaf springs - 4 off.
- (4a) and (4b) Tensioning rods and nuts respectively - 4 off each.
- (5) Rotatable index grating yoke.
- (6) Rotatable 'output' mirror.
- (7) Miniature precision roller bearings with side washers - 4 off.
- (11) Reflecting Prism.

The extensometer is supported by the specimen at the four knife edges with contact pressure supplied by the four leaf springs. The specimen dimensions (see Fig. 4.4) are identical to those used in the ICI - Macklow Smith machine. The gauge length of the specimen (66.66 mm) is defined by the axial distance between the knife edges. The four roller bearings have flanges in the form of accurately ground washers which ensure that relative movement of the cross-members is constrained to move parallel with the specimen axis. The accurate concentricity of the bearings together with the fact that the cross-members are machine ground to be accurately parallel ensures that no significant relative rotation of the cross-members can occur. Thus the only degree of freedom available for relative cross-member movement is parallel to the axis of the specimen.

Fig. 4.9 Assembly drawings of the Moiré Fringe Extensometer



PART NO.	UNIT QTY.	DESCRIPTION	COMMENTS
1+2	2 EACH	X-MEMBERS	Cr PLATED GROUND FLAT STOCK, SLIDING FIT TO ⑦
3	4	LEAF SPRINGS	BLUED SPRING STEEL
4A	4	STAYS	Cr PLATED M.S.
6B	4	TENSIONING NUTS	Cr PLATED, KNURLED M.S.
5	2	GEARING, PESH HOLDER	BLUED M.S.
6A	2	MIRROR SUPPORT	BRASS
6B	1	MIRROR HOLDER	ALUMINIUM
7	8	BEARING WASHERS	GROUND Cr PLATED + 4 OFF BEARINGS R.H.B. UL 3071
8	4	SPECIMEN BEARINGS	10. O.D. 5 KF EL 3
10A	1	INDEX GEARING	10x5x1 250 LINES/MM. ROTATABLE
10B	1	REFERENCE GEARING	15x15x1 250 LINES/MM. INTER GEARING GAP = 0.05
11	1	REFLECTING PRISM	HYDROGENOUS SILVERED (1x1x1)





Part (5) is critically dimensioned because this determines the inter-grating gap. The diffraction gratings - the larger being termed the reference grating, and the smaller the index grating, are mounted on glass plate of 1 mm thickness (nominal). The reference grating is bonded to the stepped cross-member and the index grating is bonded to the yoke, using adhesive. It was found necessary to carefully reduce the thickness of each yoke individually, because of variations in glass thickness, to ensure an optimum inter-grating gap of 0.05 mm. A detail of this region is shown in Figure 4.10.

The extensometer is difficult to attach onto the specimen without a jig. The device shown in Figure 4.11 is designed to allow rapid exchange of specimens and also serves to accurately fix the gauge length at 66.66 mm.

The total weight of this extensometer carriage plus mirrors and gratings is 90 grams.

#### 4.2.2.2. The optical system

The light source and fringe detection devices are too heavy to be supported by the extensometer. In addition the heat from the light source adjacent to the specimen was considered to be unacceptable. Light guides were tried but these absorbed a significant proportion of the infra-red part of the spectrum. Also some twisting of the specimen due to the weight and stiffness of the light guides could not be avoided.

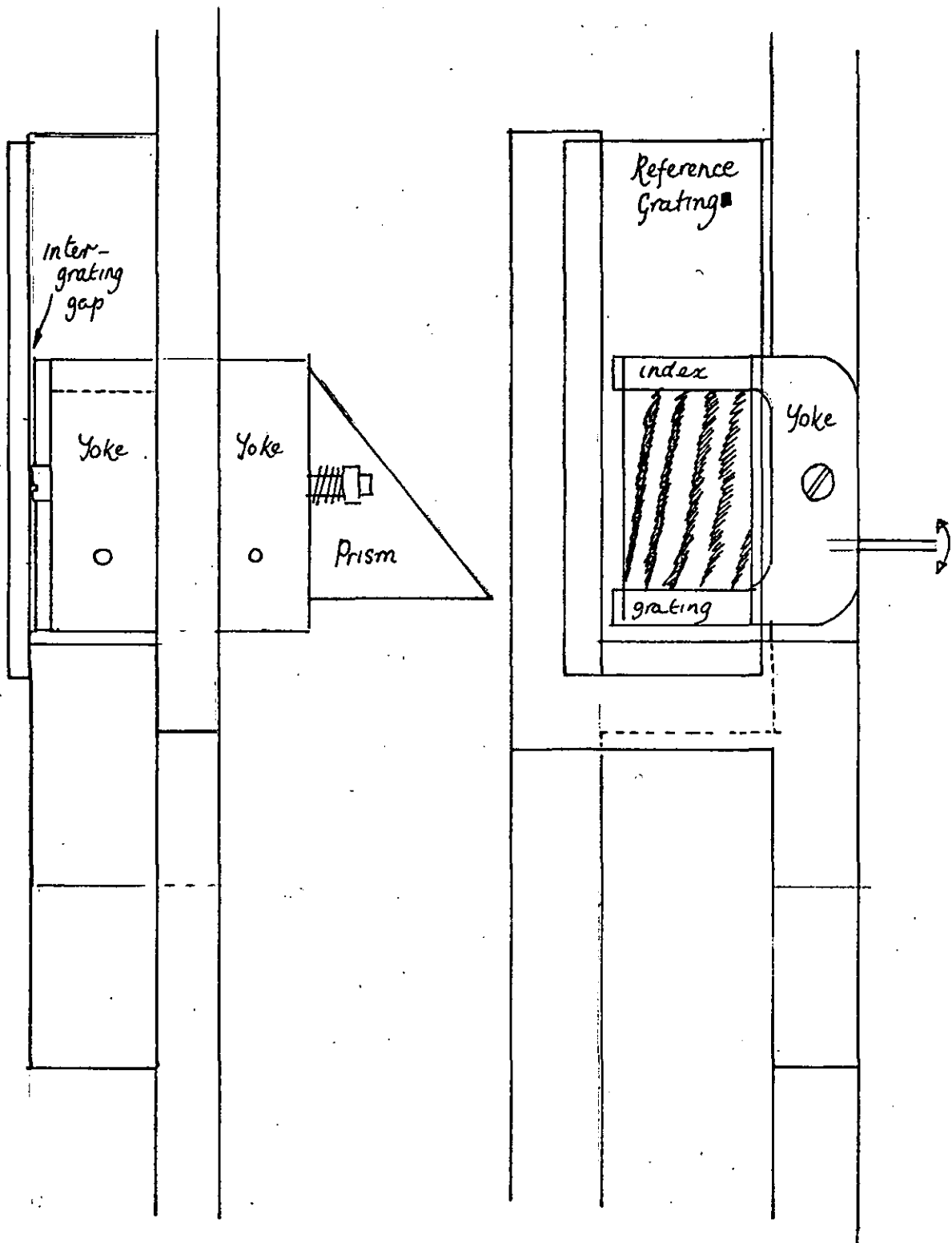


FIGURE 4,10 INDEX AND REFERENCE GRATING POSITION

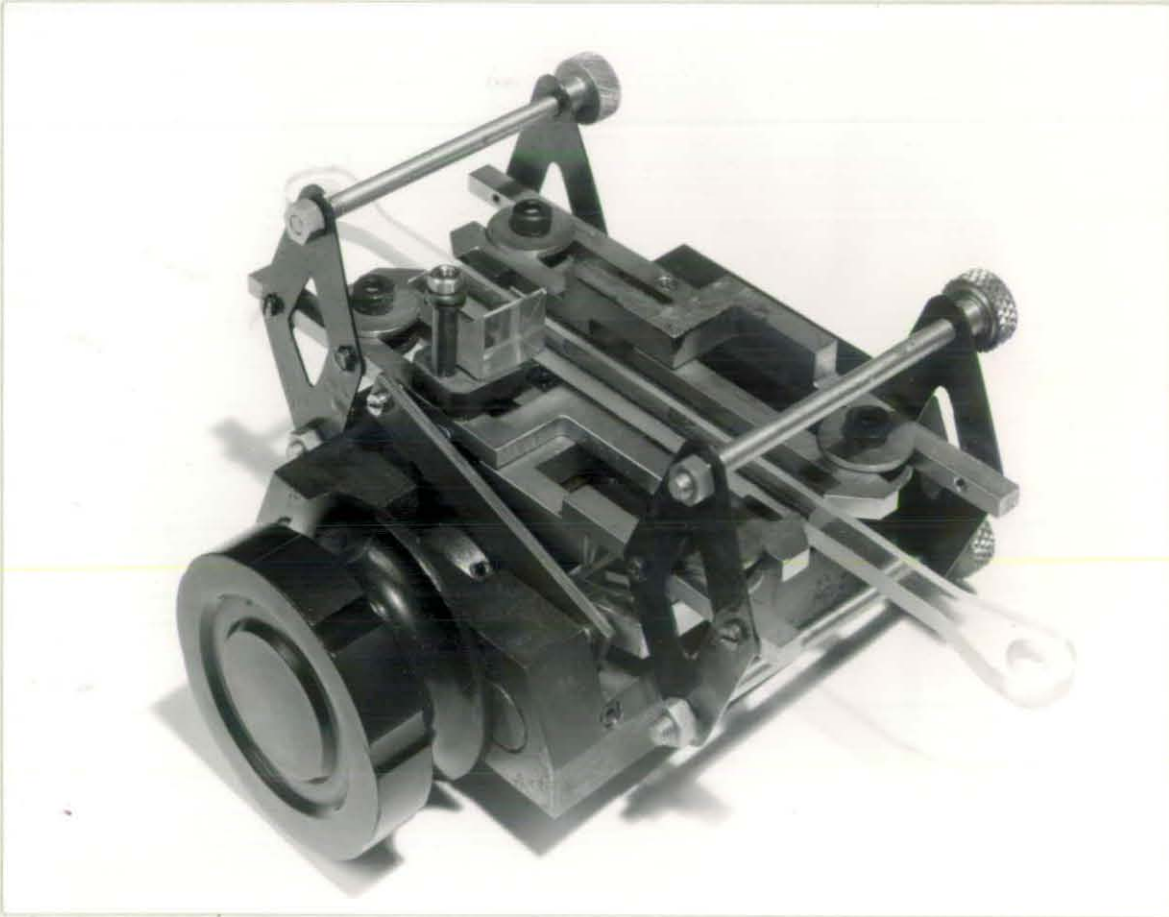


Fig. 4.11 Extensometer setting-up jig for changing test specimens

The problem with an optical system supported other than by the extensometer is that, as the specimen deforms, the gratings are themselves displaced with reference to any external reference point. Therefore a simple linear system of light source - gratings - detectors would not be adequate. The system adopted is shown in Figure 4.12. The light source is a Mazda F.10. which is operated at only 9 volts to extend the lifetime of the filament. The light beam is collimated with the aid of a moveable lens of focal length 5 cm. The optical axis is horizontal at this stage. The collimated light beam is reflected vertically (approximately) by a rotatable mirror which, in common with the light source and lens, is fixed to the machine base. The light beam is directed through the grating pair by a right angular reflecting prism supported on a rotatable yoke which in turn is attached to the extensometer cross-member which makes contact with the specimen at the lower knife-edge.

Attached to the same cross-member via a second rotatable yoke is an index grating of dimensions 6 mm x 8 mm x 1 mm (nominal thickness). The reference grating (8 mm x 20 mm x 1 mm) is attached to the other cross-member. Both gratings have 250 rulings per mm. Finally the appropriate portion of the Moiré fringe image is selected by a rotatable mirror and directed almost vertically downwards onto a photodiode assembly. Thus, axial strain of the specimen changes only the optical path-length and not the position of the image.

The spectroscopic arrangement shown schematically in Figure 4.13 is generally regarded as the optimum for fringe contrast, with good tolerance to variation of the inter-grating gap (145). In this

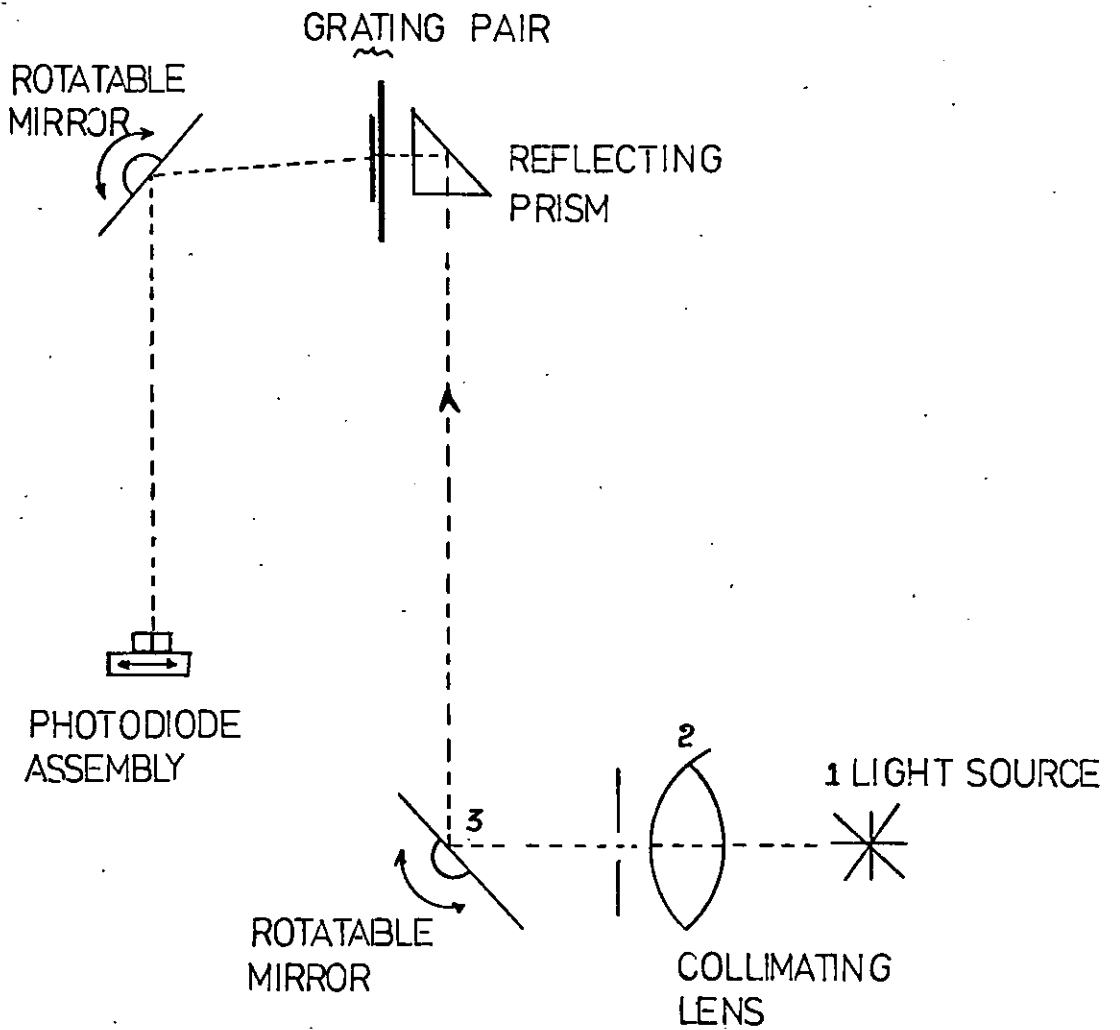


FIGURE 4.12

THE ELEMENTS OF THE MOIRÉ FRINGE OPTICAL SYSTEM.

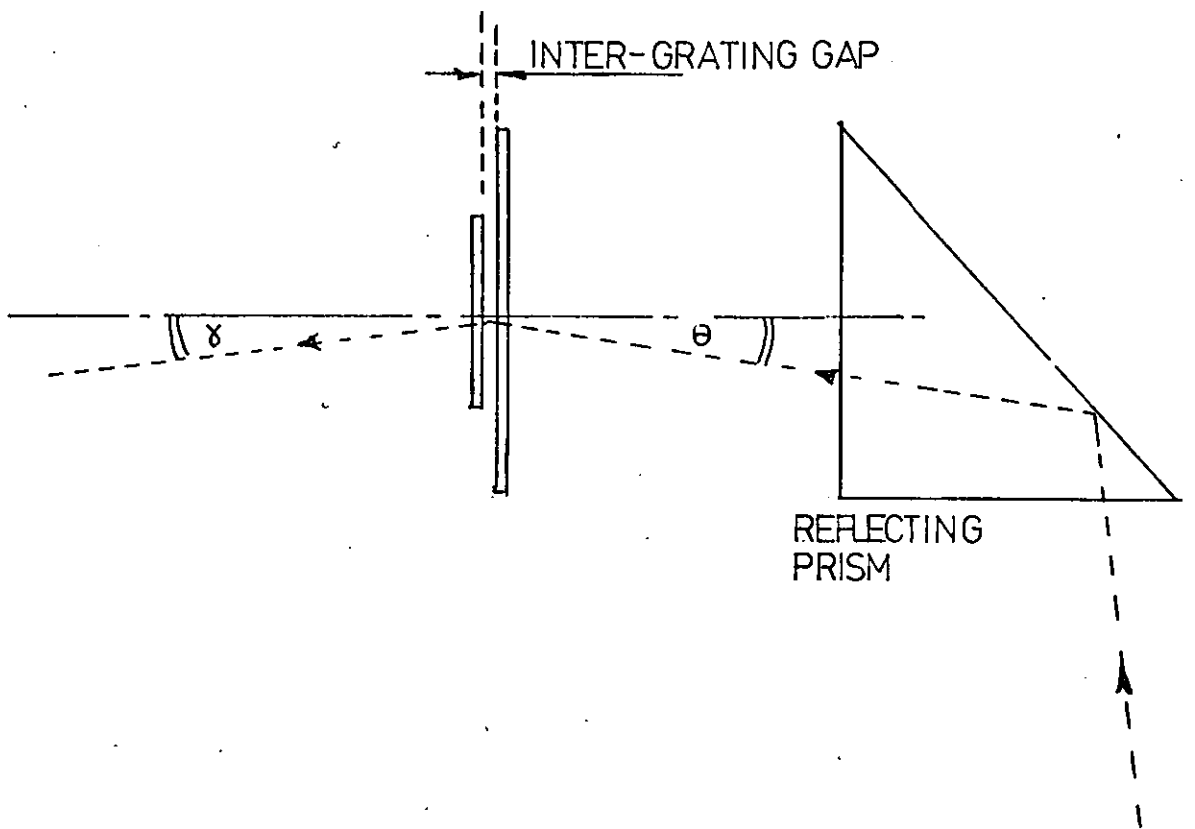


FIGURE 4.13 THE 'SPECTROSCOPIC ARRANGEMENT' WITH  $\theta$  (INCIDENT ANGLE) EQUAL TO  $\gamma$  (ANGLE OF DIFFRACTION FOR THE 1st ORDER DIFFRACTION IMAGE).

arrangement the incident angle at the gratings should be equal to the emergent angle of the part of the diffraction image most appropriate for the detectors. As seen from figure 4.8 the best position for the detection is in the brighter of the two 1st order diffraction images. With silicon photodiodes, with a peak spectral sensitivity at wavelengths of  $\sim 0.85 \mu\text{m}$ , the optimum position is as shown, just beyond the visible red region. This corresponds to an emergent diffraction angle of  $7^\circ$ . The first rotatable mirror (part 3 in Fig. 4.12) is used, in practice, to optimise the grating incidence angle and hence the fringe contrast. This of course means that the optical path is no longer unaffected by specimen strain. However, in practice the incidence angle required for the spectroscopic arrangement is relatively small and the movement of the image with strain is tolerable (certainly up to tensile strains of  $\sim 10\%$ ).

The final stage of the optical system is a rotatable assembly of 4 MS9AE Ferranti silicon photodiodes. The assembly is arranged as shown in Figure 4.14 and positioned within the image as shown in Fig. 4.8. The assembly is designed to provide a means of not only monitoring the light intensity, but also the direction of fringe movement and hence whether the gauge length is increasing or decreasing. The fringe spacing is set equal to the width of the photodiode assembly by rotation of the index grating. Therefore  $\Delta \approx 4 \text{ mm}$ . The voltage

output  $V_{AB}$  from the parallel pair of photodiodes A and B according to equation [15] is:

$$V_{AB} = k \left[ I_{\min} - I_{\min} + I_0 \sin\left(\frac{2\pi x}{a} - \beta\right) - I_0 \sin\left(\frac{2\pi x}{a} - \beta - \pi\right) \right]$$

$$\therefore V_{AB} = 2kI_0 \sin\left(\frac{2\pi x}{a} - \beta\right)$$

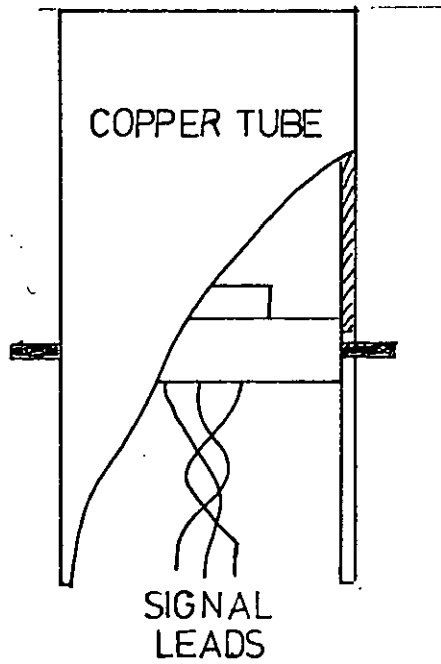
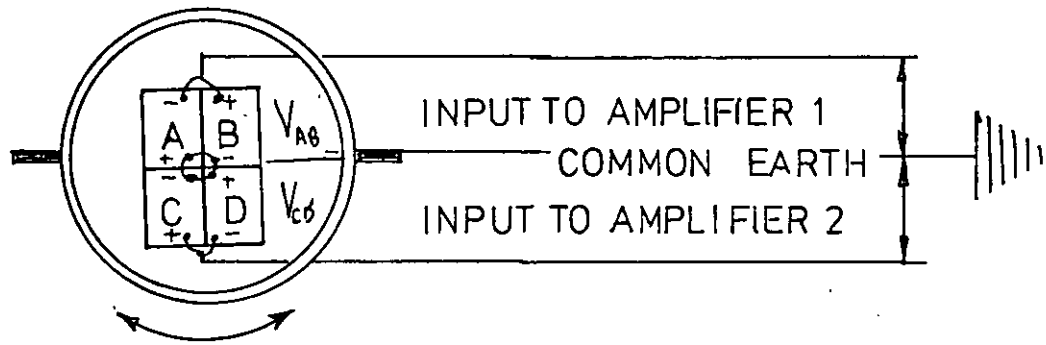


FIGURE 4,14 PHOTODIODE ASSEMBLY



where  $k$  is a constant. If the photodiode assembly axis is parallel to the Moiré fringes  $V_{CD} = V_{AB}$ . In practice the assembly is rotated so that  $V_{CD}$  leads or lags  $V_{AB}$  by a phase angle of  $\sim \frac{\pi}{2}$

$$\text{Thus: } V_{CD} = 2kI_0 \cos\left(\frac{2\pi x}{d} - \beta\right)$$

If the amplified outputs  $V_{AB}$  and  $V_{CD}$  are connected respectively to the X and Y plates of an oscilloscope then the coordinates (X,Y) are given by:

$$\begin{aligned} X^2 &= \left[2kI_0 A \sin \theta\right]^2 \\ Y^2 &= \left[2kI_0 A \cos \theta\right]^2 \\ \theta &= \left[\frac{2\pi x}{d} - \beta\right] \text{ and } A \text{ is the amplification factor.} \end{aligned}$$

$$\therefore X^2 + Y^2 = 4k^2 I_0^2 A^2$$

Therefore the oscilloscope trace describes a circle of radius  $2kI_0 A$ . This is shown in Figure 4.18. One circle is completed for each extension or contraction of the gauge length equal to the diffraction grating pitch ( $4 \mu\text{m}$ ). The direction of rotation of the displayed signal is reversed when the direction of specimen strain is reversed. Therefore this arrangement of photodiodes:

- (a) Doubles the signal amplitude.
- (b) Reduces or eliminates variations in background light level  $I_{\text{min}}$ .
- (c) Provides the basis of directional discrimination.

#### 4.2.2.3 Electronics and Recording Equipment

The voltage amplitudes from the photodiode assembly normally do not exceed  $\sim 20$  mv. The current amplitude is normally in the

region of only  $2 \mu\text{a}$ . The photodiode signals are amplified and processed by specially designed electronics. In Fig. 4.16 the first stage is a pair of D.C. operational amplifiers, (one for  $V_{AB}$  and one for  $V_{CD}$ ) with variable gain and offset level control. The final stage shown in Figure 4.16. is a power switch with variable hysteresis control. The function of each stage can be appreciated by reference to Fig. 4.17. The low voltage amplitude input includes electrical noise and inevitably a D.C. level. The signal is amplified and the D.C. level removed by operation of the offset level control. The amplified signal is used to switch to a level of + or - 10 volts when the signal amplitude exceeds  $\pm \frac{1}{2} H$  volts where H is the hysteresis (variable) voltage. Thus two noise-free, out of phase, square wave voltage outputs are generated. Obviously the noise level should not exceed the hysteresis level, otherwise multiple switching would occur.

The photographs in Figure 4.18 show:

- (a) Amplified signals  $V_{AB}$  and  $V_{CD}$  (taken at monitor 1 of amplifier 1 and 2 (Figure 4.16) applied to the X and Y amplifiers of an oscilloscope. The specimen is undergoing rapid creep.
- (b) Amplified signal  $V_{AB}$  from monitor 1 applied to the X axis and the switched output from monitor 2 applied to the Y axis. Rapid creep rate.
- (c) The switched outputs from monitor 2 of both amplifiers applied to the X and Y amplifiers of an oscilloscope. The spot changes position for each extension or contraction in the gauge length of  $1 \mu\text{m}$ .

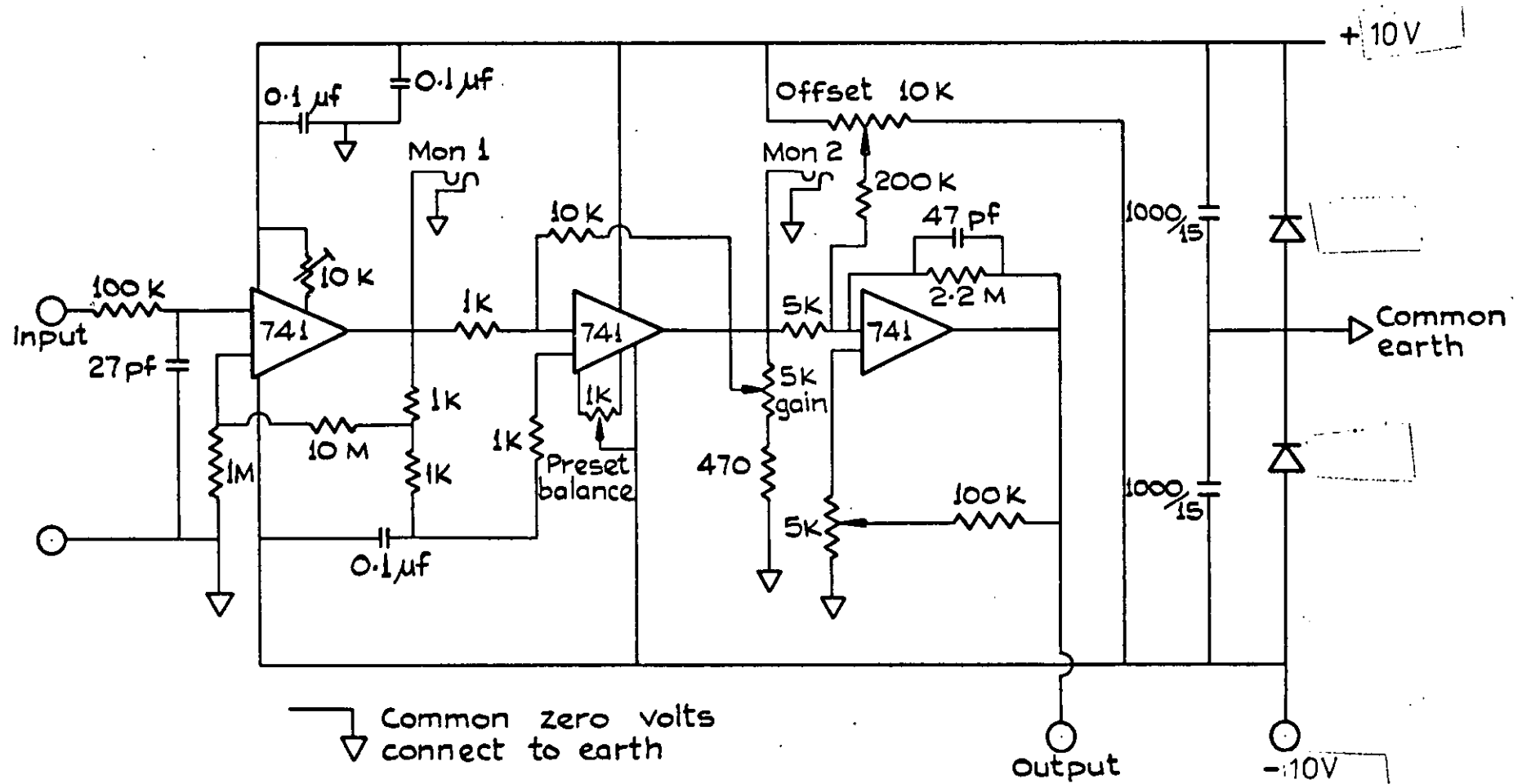


FIGURE 4,16  
PHOTODIODE AMPLIFIER AND PULSE SHAPER

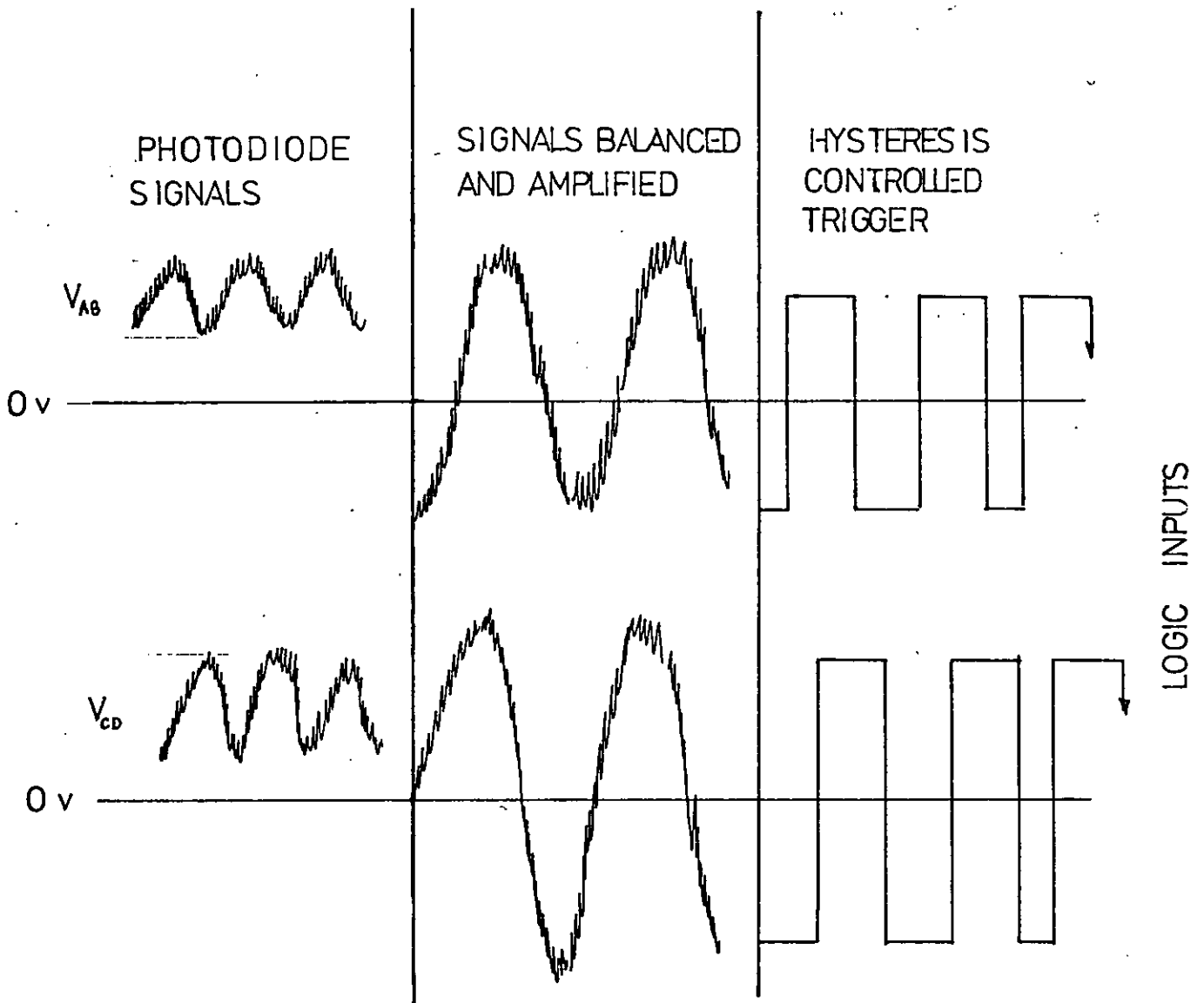


FIGURE 4,17 PHOTODIODE SIGNAL PROCESSING.  
UNIFORM STRAIN RATE INPUT.

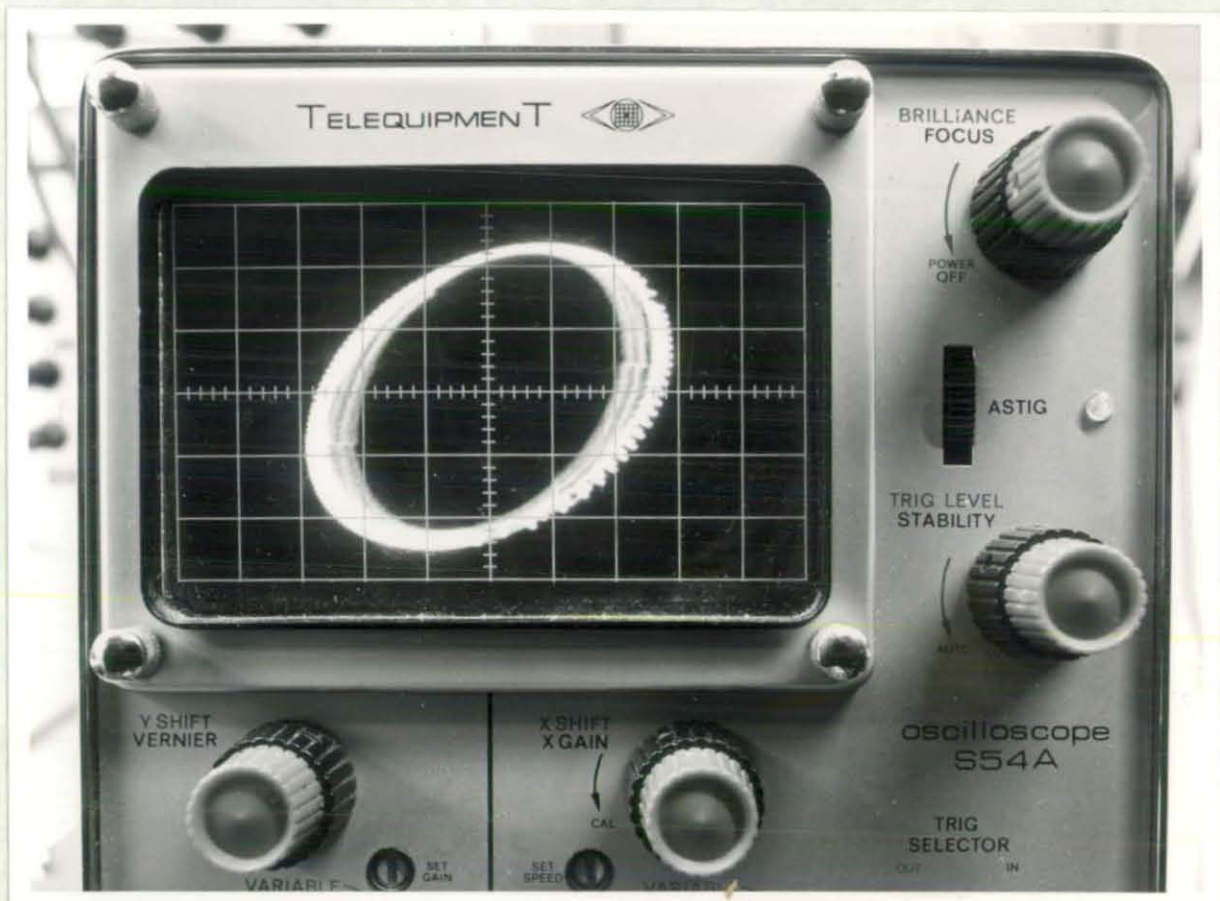


Fig. 4.18(a) Amplifier signals displayed on an oscilloscope

X - plates,  $V_{AB}$  from Monitor 1

Y - plates,  $V_{CD}$  from Monitor 1

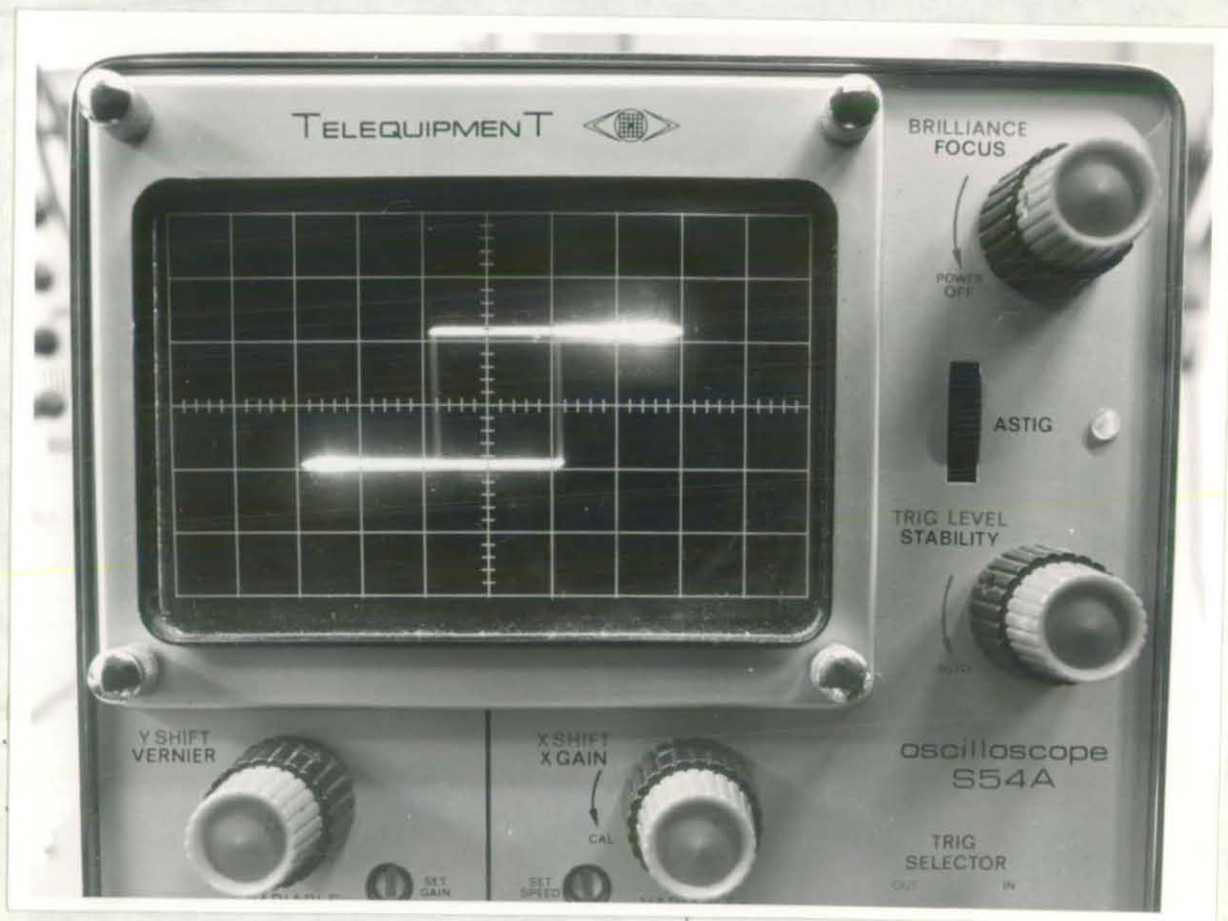


Fig. 4.18 (b) Amplifier signals displayed on an oscilloscope

X - plates,  $V_{AB}$  from Monitor 1

Y - plates,  $V_{AB}$  from Monitor 2



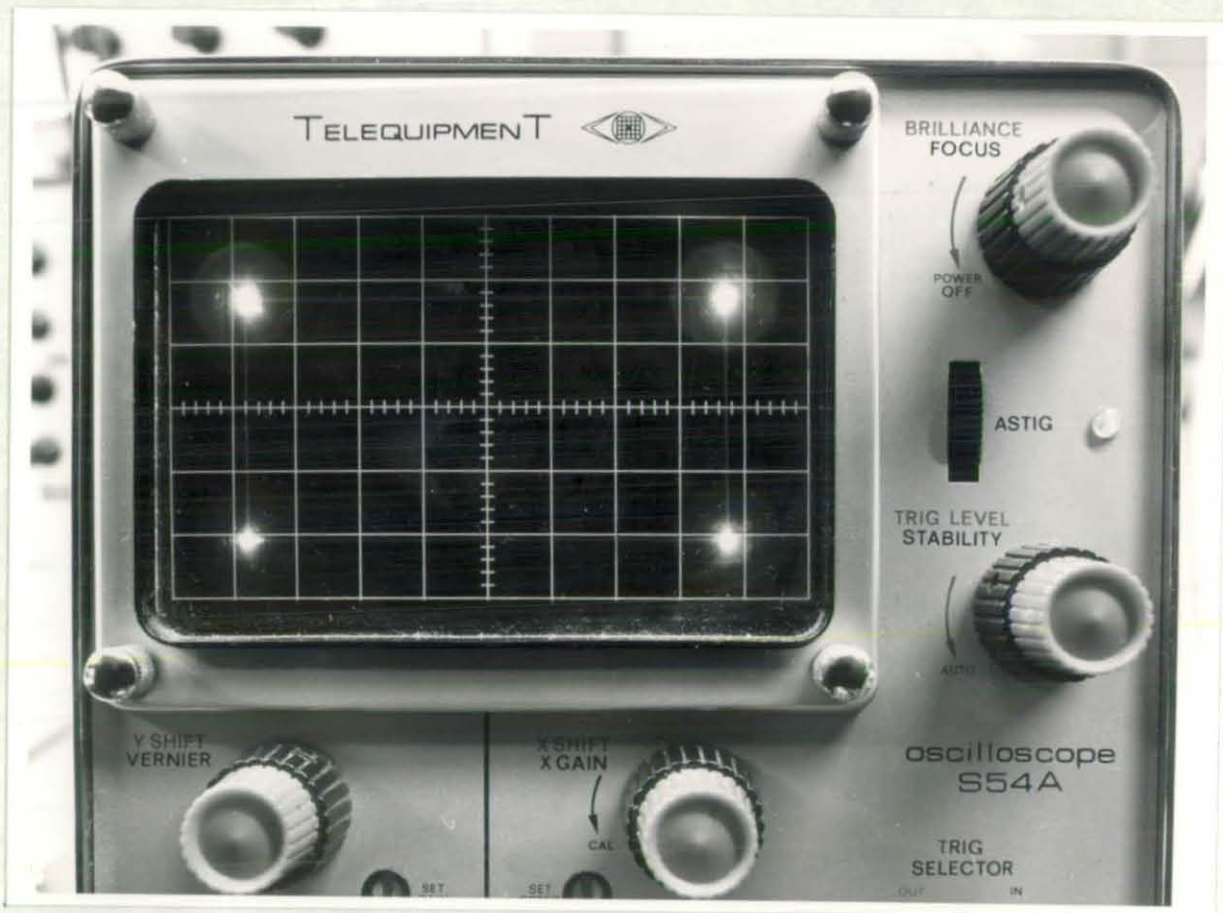


Fig. 4.18(c) Amplifier signals displayed on an oscilloscope

X - plates,  $V_{AB}$  from Monitor 2

Y - plates,  $V_{CD}$  from Monitor 2

The logic circuit shown diagrammatically in Figure 4.19 is designed to sense the direction of specimen strain using the output (C) in Fig.4.18. The amplifier pair connected to one creep machine generates a sequence of rapid changes in voltage level from negative (say off) and positive (say on) levels. The logic circuit is designed to separate changes in level that signify a positive and negative increment of strain. One square wave input is differentiated and provides the counter pulse. The other input to the logic is used as a gate. Two logic outputs are provided:

Logic output 1. Positive counts, from gates 1 and 4. Gate 1 is gated by an inverted input 2, with counts provided by the inverted differential of input 1. These account for the level changes identified as ① in Fig.4.20. Gate 4 is gated directly by input 2 with the counts provided by the differential of input 1. These account for the level changes identified as ② in Fig. 4.20.

Logic output 2. Negative counts from gates 2 and 3. Gate 2 is gated directly from input 2 with counts provided by the inverted differential of input 1. These accounts for the level changes identified as ③ in Figure 4.20. Gate 3 provides a pulse at level changes identified as ④ in Figure 4.20.

The logic circuit therefore provides two pulse outputs; representing increments of positive and negative strain. These increments represent a gauge length extension or contraction equivalent to one half of a grating pitch, i.e.  $2 \mu\text{m}$ , or for a gauge length of 66.66mm, a tensile strain increment of  $\pm 0.00003$ . Double this sensitivity can easily be achieved by suitable modification of the



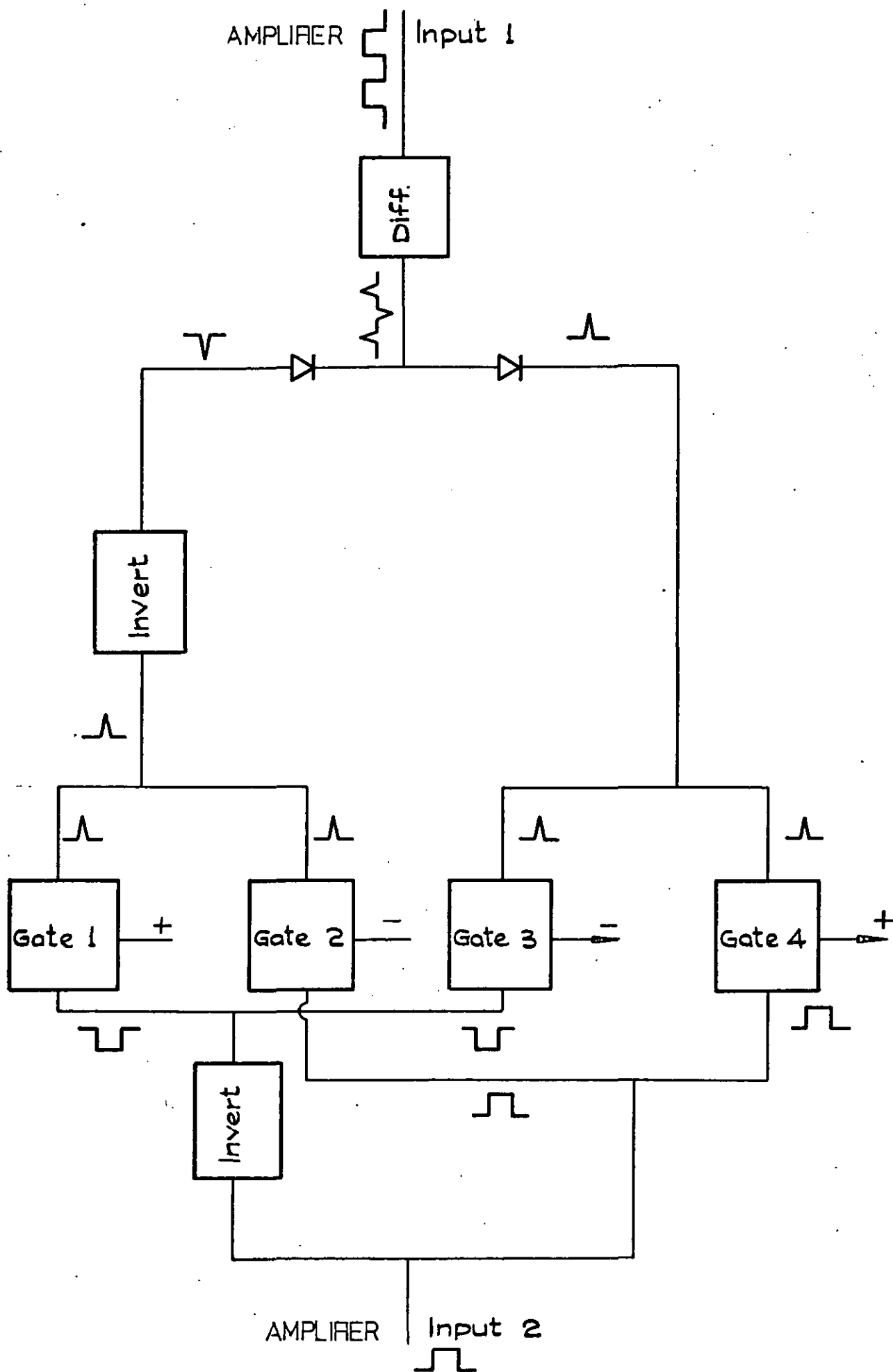


FIGURE 4,19 LOGIC FOR  $\mp$  DISCRIMINATION



logic circuit. It is proposed however that for Class A (BS4618) requirements the digital resolution of 0.003% is more than satisfactory. It is noted that the Class A extensometry requires a minimum detectable strain change 0.002%. It would be incorrect to compare these figures directly and to conclude that the Moiré fringe extensometer does not satisfy Class A requirements. By simply displaying the signal on a scope a 'subjective strain resolution' of  $\pm 0.0001\%$  can be readily achieved.

Finally the pulses are recorded either by totalising on a bi-directional decade counter, or on a digital event recorder. The bi-directional counter is used when the count rate (strain rate) is high, for instance at the start of the creep test. The amplifiers and counter can accept frequencies up to 5 kHz. This is equivalent to a strain rate of  $\sim 0.15 \text{ sec}^{-1}$  which exceeds the maximum envisaged in practice. The counter is manufactured by Orbit Ltd. When the count rate is below  $\sim 0.5 \text{ Hz}$ , the logic outputs are transferred to a twenty four channel digital event recorder type WX504 marketed by Environmental Equipment Ltd. This records the time of an event (a positive or negative increment of strain) and identifies, by means of a letter, the source and polarity of the increment. Figure 4.21 is a reproduction of a typical event recorder print-out. Positive and negative strain increments from machines 1, 2, 3, etc., are identified by the letters AB, CD, EF, etc. Thus the creep data from 12 machines can be recorded simultaneously and automatically.

#### 4.2.2.4 Machinery hard-ware and Environmental control

Design drawings of the creep machine base are included in Fig. 4.22. These were cast integrally in aluminium alloy and although

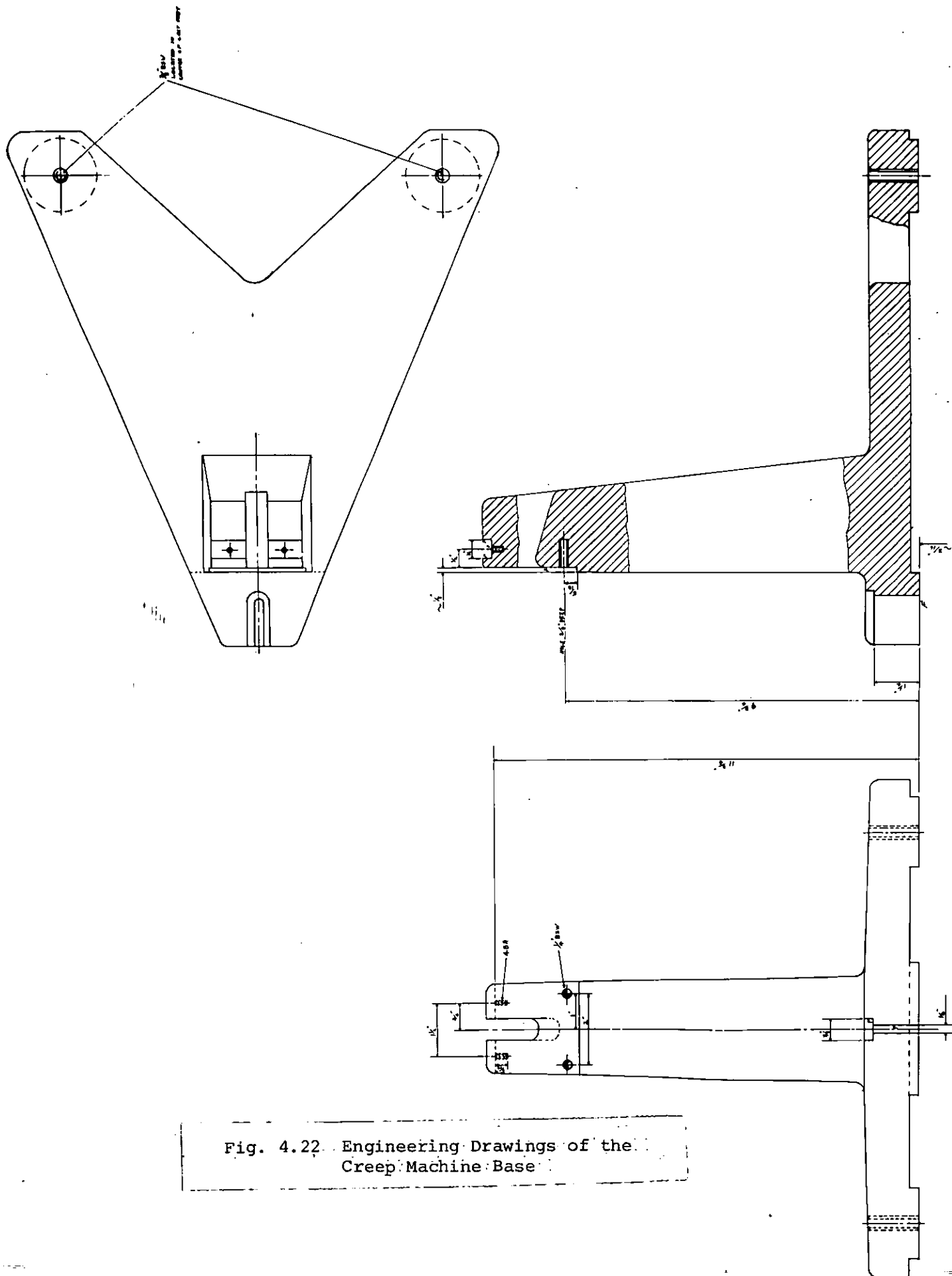


Fig. 4.22 Engineering Drawings of the Creep Machine Base

the specimen dimensions are the same as used by I.C.I. Ltd., the casting is considerably smaller than those used in the construction of the Macklow-Smith creep machine. Basically the casting consists of a solid rectangular column and a solid 'triangular' base. The base is designed to stand on a table top via three adjustable screw supports.

The main machining operations are all performed with the casting bolted in one position to ensure correct alignment. Only five basic machining operations are required. These are:

- (a) An area on the front face of the support column is faced vertical. This provides the mating surface for the alignment system.
- (b) A slot is machined on the top surface of the column with the base of the slot horizontal and the sides of the slot parallel with the machined surface described in (a). This locates the knife edge supports.
- (c) A slot is machined on the top surface of the front of the base. This locates the lower specimen hook.
- (d) A small area on the upper surface of the base is machined to be horizontal. This is the location point for a small spirit level.
- (e) A pair of holes are drilled and tapped in the machined surface of the support column. These are positioned about a central line passing vertically through the centre of the lower hook location slot. The alignment mechanism is bolted to the casting via these holes.

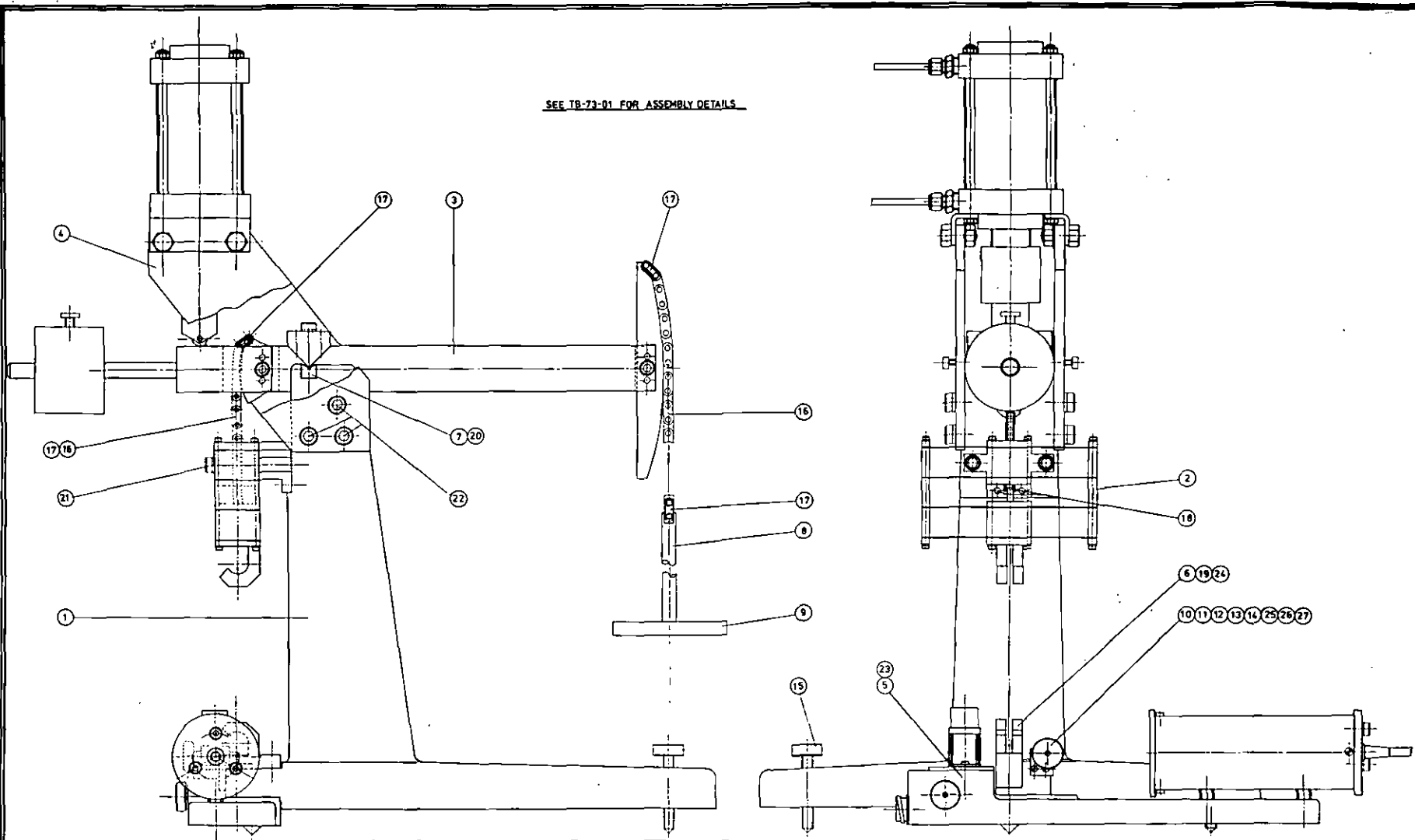
Special attention was aimed at designing a specimen alignment mechanism which would not introduce stick-slip friction. This was

achieved by the use of a particular arrangement of spring steel cantilevers and floating supports. The assembled arrangement is shown in position on a creep machine in Fig. 4.23. The spring geometry is such that the stiffness in the direction of specimen strain is very low compared with stiffness in all other directions. The mechanism is located on the casting such that the effective hook separation is 0.5 mm greater than the effective length of the specimen (for specimen dimensions see Fig. 4.4). The springs thus supply the specimen pre-load. With springs of thickness 0.38 mm the pre-load is  $\sim 2.5\text{N}$ . With increasing specimen strain the pre-load decreases and becomes zero at  $\sim 0.5\%$  tensile strain, and  $-2.5\text{N}$  (i.e. compressive load) at  $\sim 1.0\%$  strain. The load required to generate an elastic tensile strain of  $1.0\%$  in a typical glassy polymer specimen of the dimensions shown in Figure 4.4, is  $500\text{N}$ . The spring restoring force is therefore typically only  $0.5\%$  of the applied force.

A 5:1 (25 cm: 5 cm) lever arm amplifies and transmits the load from the weight pan to the specimen via segment and chain couplings. The rear and forward segments have radii of 25 cm and 5 cm respectively. The purpose of the segments is to ensure that the lever arm ratio is independent of lever arm rotation over the practical range of interest. In fact a specimen strain of  $20\%$  can be tolerated before the lever ratio is affected by arm rotation.

The lever arm fulcrum is normally either a pair of roller bearings or knife edge supports. Both arrangements have advantages and disadvantages but on balance the heavy duty bearings were considered to be a source of excessive friction. The knife arrangements chosen

Fig. 4.23 Assembly Drawing of the Creep Machine



SEE TB-73-01 FOR ASSEMBLY DETAILS

Cr Pin	SCREW DOWEL 6g x M3	27	BRASS	1	FOOT	73-07-5	15		2
--	-- 10g x M3	25	--	2	MAIN MIRROR	73-07-7	14		1
--	-- 15g x M3	25	--	2	KNOB	73-07-8	13		1
--	SOCKET CAP 20g x M6	24	H.T. STEEL	1	MIRROR SPINDLE	73-07-9	12		1
--	-- 25g x M6	23	--	2	INNER MIRROR BRACKET	73-07-9	11		1
--	-- 16g x M6	22	--	6	OUTER	73-07-10	10		1
--	-- 65g x M6	21	--	2	BASE LOAD PIN	73-07-11	9		1
DOWEL	10g x 3g	20	SILVER STEEL	2	ROD	73-07-13	8		1
--	25g x 6g	19	--	1	VEE BLOCK	73-07-12	7		2
--	15g x 4g	18	--	2	BOTTOM HOOD	73-04-15	6		1
SPLIT LINK	5/8 BS	17	--	4					
CHAIN	--	16	--	15					
		15		1					

OPTICAL SYSTEM	73-09	5		1
LOADING SYSTEM	73-07	4		1
LEVER ARM ASSY	73-03	3		1
ALIGNMENT SYSTEM	73-04	2		1
BASE	73-02	1		1

ALL VIEWS ARE ENGLISH PROJECTION  
ALL DIMENSIONS IN MM

here suffers from not being positively located. However, the spring alignment system, unlike the slide guide system adopted for the ICI/Macklow-Smith machine, can tolerate a loading axis which is not exactly co-linear with the central axis of the alignment system.

It was considered important that the problem of lever arm inertia discussed in Section 4.2.1 should be eliminated by the appropriate design of loading system. This was achieved by locating an hydraulic actuator at the front end of the lever arm, i.e. ahead of the fulcrum, as shown in Figure 4.23. Thus the lever arm chains and weight pan can be balanced by adjusting the position of the jockey weight at the front end of the lever arm. On recovery with the actuator in the 'down' position, the specimen is effectively disconnected from the lever arm and resistance to recovery due to lever arm inertia is eliminated.

The loading and unloading system is shown diagrammatically in Figure 4.24. Air at a pressure of between 0.4 and 0.8 MN/m<sup>2</sup> is used to pressurise oil in either one of two air/hydraulic reservoirs. With air switched via reservoir A the actuator piston extends and removes the load from the specimen. With air switched via reservoir B the piston detracts and the load is applied to the specimen. The rate of movement of the piston can be controlled by adjustment of the flow restrictor valves. It <sup>was</sup> found necessary to use 2 mm thick rubber sheet between the actuator piston and the lever arm when high loads were applied to the specimen to prevent oscillatory over-load.



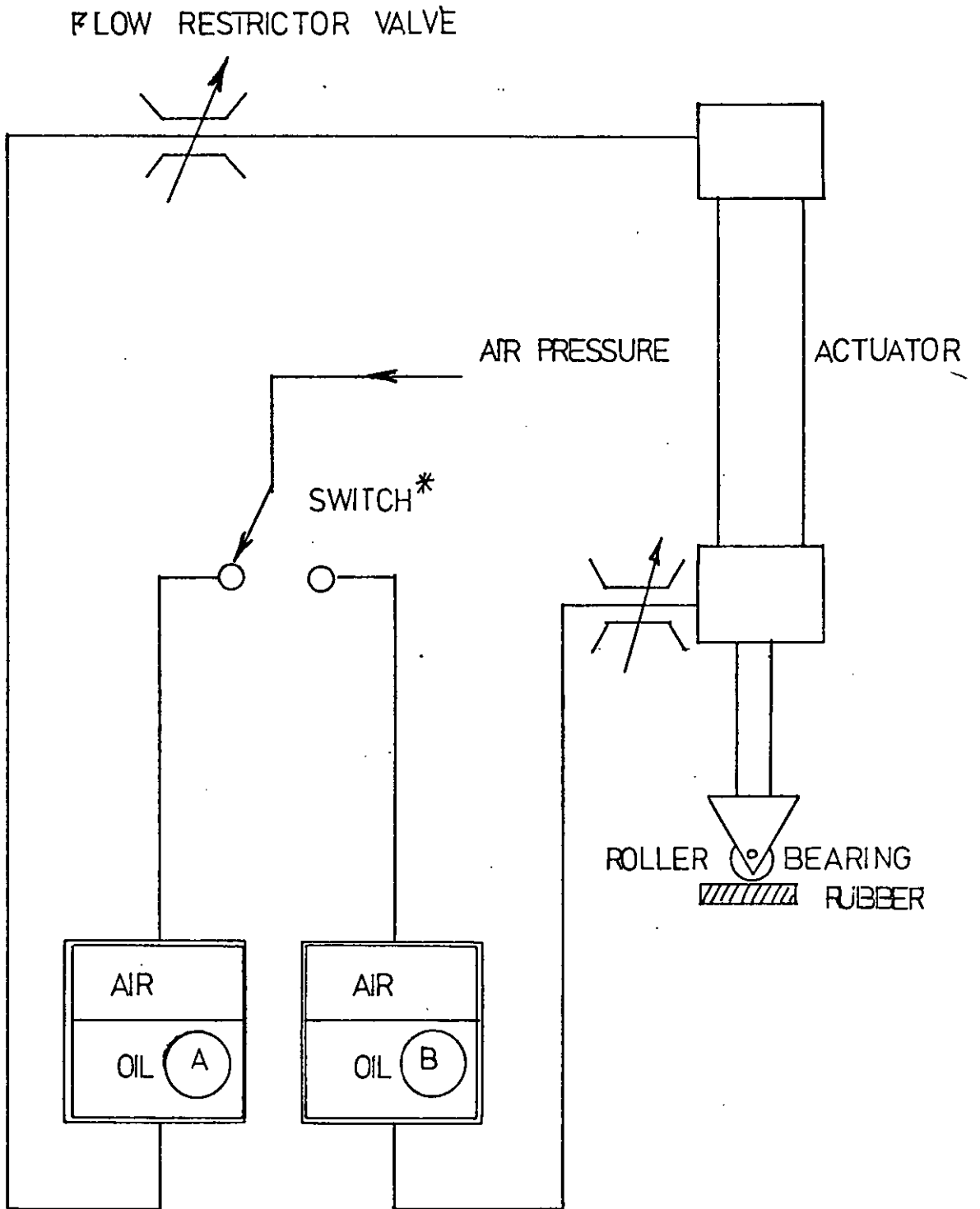


FIGURE 4,24 PNEUMO-HYDRAULIC LOAD ACTUATOR SYSTEM. FOR INTERMITTENT LOADING THE MANUAL SWITCH\* IS REPLACED BY A SOLENOID SWITCH.

The pneumatic switch used to direct the pressurised air from reservoir A to reservoir B and vice versa is manually controlled for normal creep and recovery tests. For low frequency cycling the manual switch is replaced by a solenoid switch powered by a low frequency square wave generator. The generator built for this purpose has a minimum cyclic period of 4 mins and a maximum period of 1000 minutes. The creep to recovery ratio for any selected period within this range can be 11:1, 5:1, 3:1, 2:1, 1:1, 1:2, 1:3, 1:5 or 1:11.

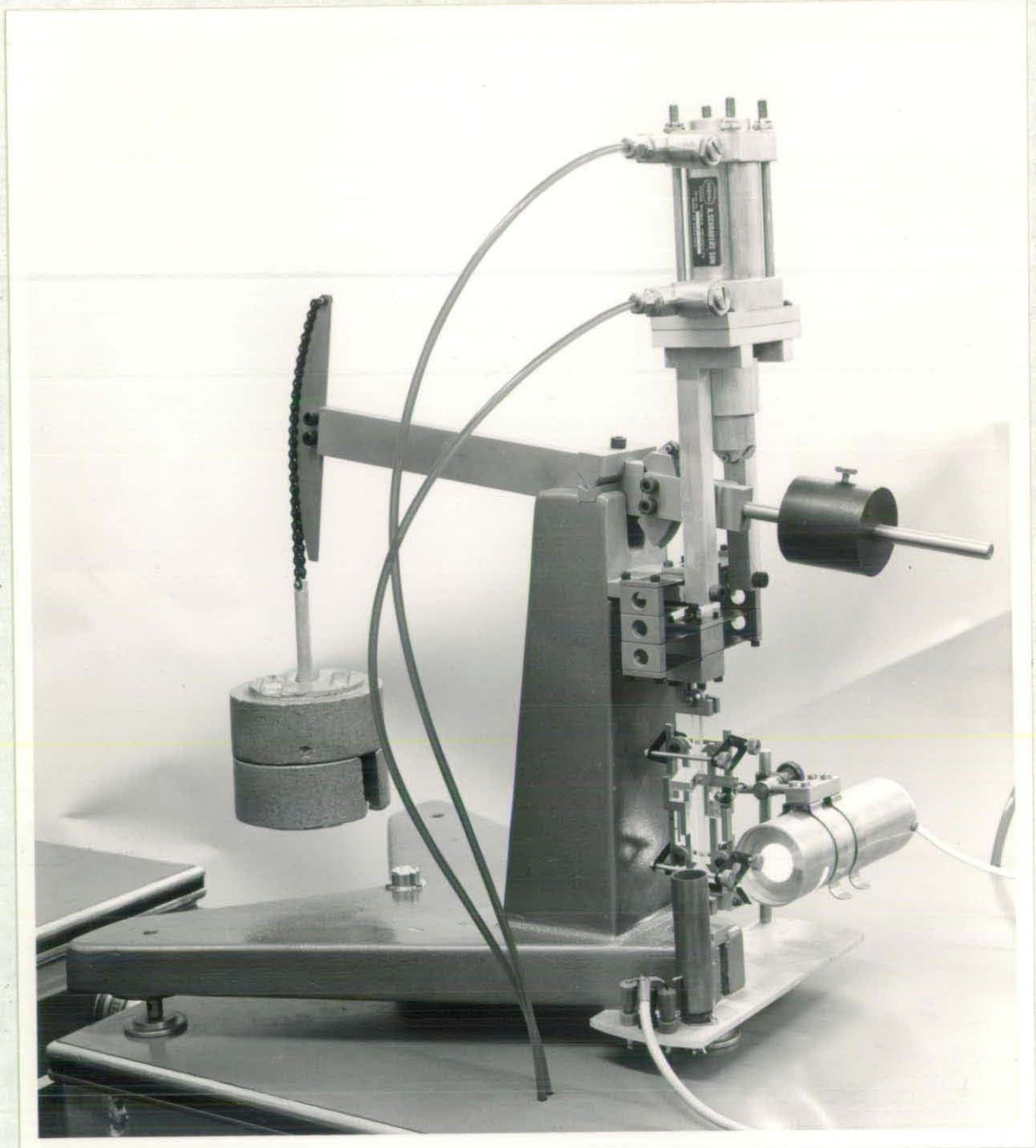
For elevated temperature testing it was considered preferable that the whole machine be placed in a large oven rather than just enclosing the specimen. This reduces the temperature gradient in the region of the specimen. It also eliminates the rapid cycling between two temperature limits that is common with ovens of low thermal capacity. Hutchinson and McCrum (146) have recently published results that indicate anomalous creep behaviour when the temperature of a specimen is rapidly changed.

The oven used for the work reported in this thesis uses an air blower to circulate air over heating elements within the oven. The volume rate of air flow and the voltage of the heating coils is controlled by a proportional temperature controller type TH2 supplied by AEI Ltd. A Cu/Con thermocouple positioned near to the specimen is used to 'drive' the temperature controller. A similar thermocouple is used to monitor the temperature using a digital thermometer type 3000 supplied by Comark Ltd. Although several hours were sometimes required for the temperature in the oven to stabilize, the temperature was controlled when stabilized to within  $\pm 0.25^{\circ}\text{C}$ . The humidity in the oven is not controlled. The

oven temperature control is therefore superior to that of the creep laboratory which was controlled to within  $20 \pm 1^{\circ}\text{C}$  and  $50\% \pm 2\% \text{ RH}$  by an installation manufactured by Spencer and Halstead.

Photographs of one creep machine and part of the creep testing facility (including the signal processing and recording installation) are included in Figures 4.25 and 4.26 respectively.

Detailed setting-up and operating instructions for the machinery described in this section are included in Appendix III.



4.25 The Tensile Creep Machine





4.26 The Creep Facility

## 5. Experimental Procedures and Results

The major experimental effort has been directed at establishing the value of  $\Delta R$  (defined in section 4.1) for unplasticised PVC over a range of combinations of service variables. These variables include, time, temperature, tensile stress and tensile strain. Both static and intermittent stress histories have been employed. In addition  $\Delta R$  has been measured with the UPVC immersed in an organic solvent (N-hexane). To complete the experimental programme the  $\Delta R$  function was established over a limited range for rubber modified polyphenylene oxide (Noryl).

### 5.1 Thermal Conditioning of UPVC

Calendered sheets of UPVC (Cobex 018 Grade supplied by BXL Ltd) of nominal thickness 3 mm were stored in the creep laboratory for 2 years at 20°C, 50% rh prior to any mechanical testing. The purpose of this storage (which in fact coincided with the period required to construct and install the creep facility) was to attempt to eliminate or reduce the inter-sheet variability. Following this, an attempt was made to reduce this variability further by annealing sheets at temperatures below  $T_g$ . This small programme also served as an adequate commissioning exercise for the newly installed creep machinery.

A full description of the test procedure and results (147) is given in Appendix IV. Although the consequence of the annealing programme was negative in the sense that it was not adopted as a specimen conditioning procedure, the results did influence the procedure and conclusion of the major experimental programme. It is for these reasons that the following brief discussion is considered

relevant:

(a) The unannealed (room temperature conditioned) UPVC was more stable than annealed UPVC. A stable state here refers to one which exhibits no perceptible change in mechanical properties with delay in testing. It was for this reason that the annealing procedure was not adopted. Classically the annealing of a glassy amorphous polymer below the  $T_g$  should lead to a more stable state (148).

(b) Annealing would be expected to result in an increase in density and tensile modulus (148). The increase in modulus would be expected to be greater the longer the annealing period. However the results of the annealing programme show that for annealing temperatures in excess of  $45^\circ\text{C}$  the modulus is decreased and that this effect is greater the shorter the annealing period.

(c) For annealing temperatures below  $\sim 45^\circ\text{C}$ , rapid 'softening' is not observed.

(d) It is proposed that the  $45^\circ\text{C}$  transition in the response of UPVC to annealing is due to the change from one form of volume relaxation to another. Below  $45^\circ\text{C}$  small crystallites or regions of zero configurational entropy (149) are formed by the local expulsion of free volume. These are rapidly disrupted on heating above  $45^\circ\text{C}$ . Volume relaxation above  $45^\circ\text{C}$  proceeds by the (classical) homogeneous diffusion of free volume.

(e) Pictorially the proposed state below  $45^\circ\text{C}$  is similar to the fringed micellar grain model of the glassy state

adopted by Yeh (150). The regions of high molecular disorder would be expected to exhibit high molecular mobility, reduced Tg, and a reduced resistance to yield deformation.

Thus a high density of microscopic yield sites (craze sites) would be predicted prior to macroscopic yielding with unannealed specimens. Yeh has proposed that the density of the yield sites has a considerable influence on the ductility of the polymer. The site density in polystyrene - which tends to be brittle is low, whilst that for polycarbonate - which is tough, is high. Also it is generally agreed that annealing of glassy polymers results in a decreased brittle strength (151). The explanation proposed here would be that annealing homogenises the free volume distribution and thereby reduces the density of potential microscopic yield sites.

As a direct result of these observations it was decided not to anneal the UPVC sheet prior to the evaluation of  $\Delta R$ . In addition it was decided to limit any elevated temperature investigations to below 45°C. Obviously if any change in the material state occurs during the creep period then any comparison between the creep and recovery response would be difficult to interpret.



## 5.2. The Damage Parameter in Response to Static Stress Histories

The 20°C creep characteristics of UPVC at tensile stress levels of 20, 25, 30, 35, 40, 45, and 50 MN/m<sup>2</sup> are displayed graphically in Figure 5.1. The tabulated data for one stress level (35 MN/m<sup>2</sup>) <sup>are</sup> ~~is~~ given in Table 5.1 as an example. The isochronous stress strain cross-plots for creep times of 10, 10<sup>2</sup>, 10<sup>3</sup>, 10<sup>4</sup>, 10<sup>5</sup> and 10<sup>6</sup> seconds have been extracted from Figure 5.1 and plotted in Figure 5.2. An estimated one second isochronous characteristic has also been included. This was achieved by the simple expedient of extrapolating the creep curves in Figure 5.1 to shorter times. It is observed that the compliance  $C(t)$  is not singular over the entire stress and strain range for  $t > 10$  s seconds. For  $t = 1$  second a linear region (stress <sup>i</sup> independent compliance) is observed below stress levels of  $\sim 45$  MN/m<sup>2</sup>

Similar creep and isochronous data generated at a temperature of 35°C are shown in Figures 5.3 and 5.4. <sup>These</sup> ~~This~~ creep data <sup>are</sup> ~~is~~ of a significantly higher quality than <sup>those</sup> ~~that~~ generated at 20°C. The 20°C data exhibit a perceptible oscillation which follows the periodic fluctuations in laboratory temperature; this having an amplitude of  $\pm 1^\circ\text{C}$  and a period of approximately 20 minutes. This feature was not observed in the elevated temperature characteristics because the oven temperature fluctuations were only  $\pm 0.25^\circ\text{C}$ , with a period of less than 5 minutes.

On completion of the creep period the removal of stress was delayed or advanced to ensure that the laboratory or oven temperature was within  $0.1^\circ\text{C}$  of the temperature prevailing when the stress was originally applied. The purpose of this was to reduce errors in  $\Delta R_{CR}$  due to temperature variations.

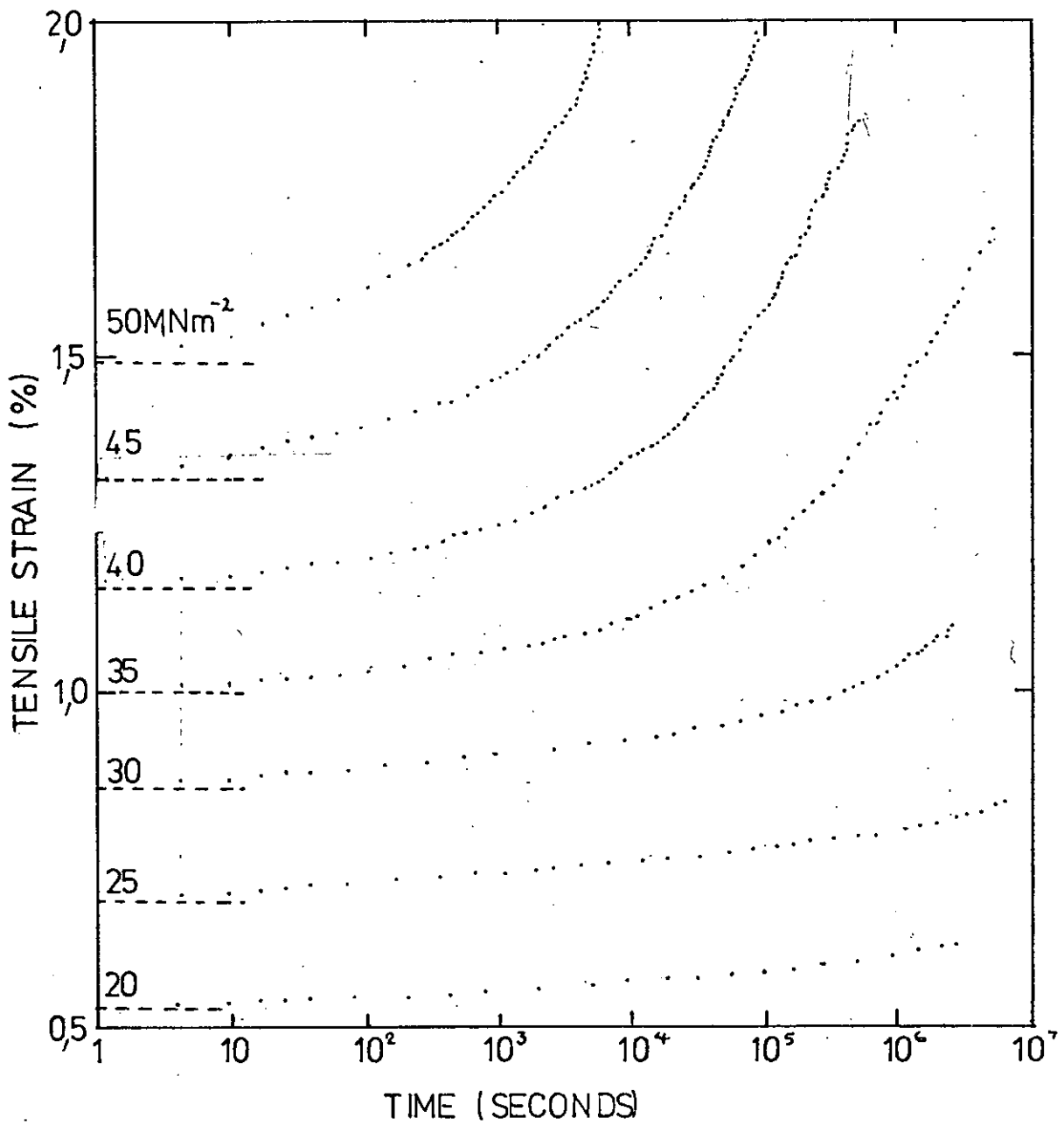


FIGURE 5.1 TENSILE CREEP CHARACTERISTICS OF UPVC AT 20°C

----- ESTIMATED STRAIN AT 1 SECOND

Time (S)	Strain Increments	Strain %	Time (S)	Strain Increments	Strain %
5	339	1.017	89,880	402	1.206
10	340	1.020	103,900	406	1.218
20	342	1.026	138,600	410	1.230
35	343	1.029	161,700	414	1.242
56	344	1.032	183,300	418	1.254
82	345	1.035	210,200	422	1.266
110	346	1.038	220,600	426	1.278
152	347	1.041	255,800	430	1.290
181	348	1.044	321,000	438	1.314
222	349	1.047	422,700	446	1.338
295	350	1.050	680,800	454	1.362
998	354	1.062	742,000	462	1.386
2,472	358	1.074	963,700	470	1.410
4,128	362	1.086	1,110,000	478	1.434
5,822	366	1.098	1,222,000	486	1.548
9,243	370	1.110	1,556,000	494	1.482
13,179	374	1.122	1,937,000	502	1.506
20,020	378	1.134	2,525,000	510	1.530
30,160	382	1.146	3,152,000	518	1.554
39,270	386	1.158	3,902,000	526	1.578
47,980	390	1.170	4,777,000	534	1.602
58,230	394	1.182	5,200,000	542	1.626
71,110	398	1.194	5,908,000	550	1.650

Table 5.1. Tensile creep data for UPVC at 20°C and 35 MN/m<sup>2</sup>.

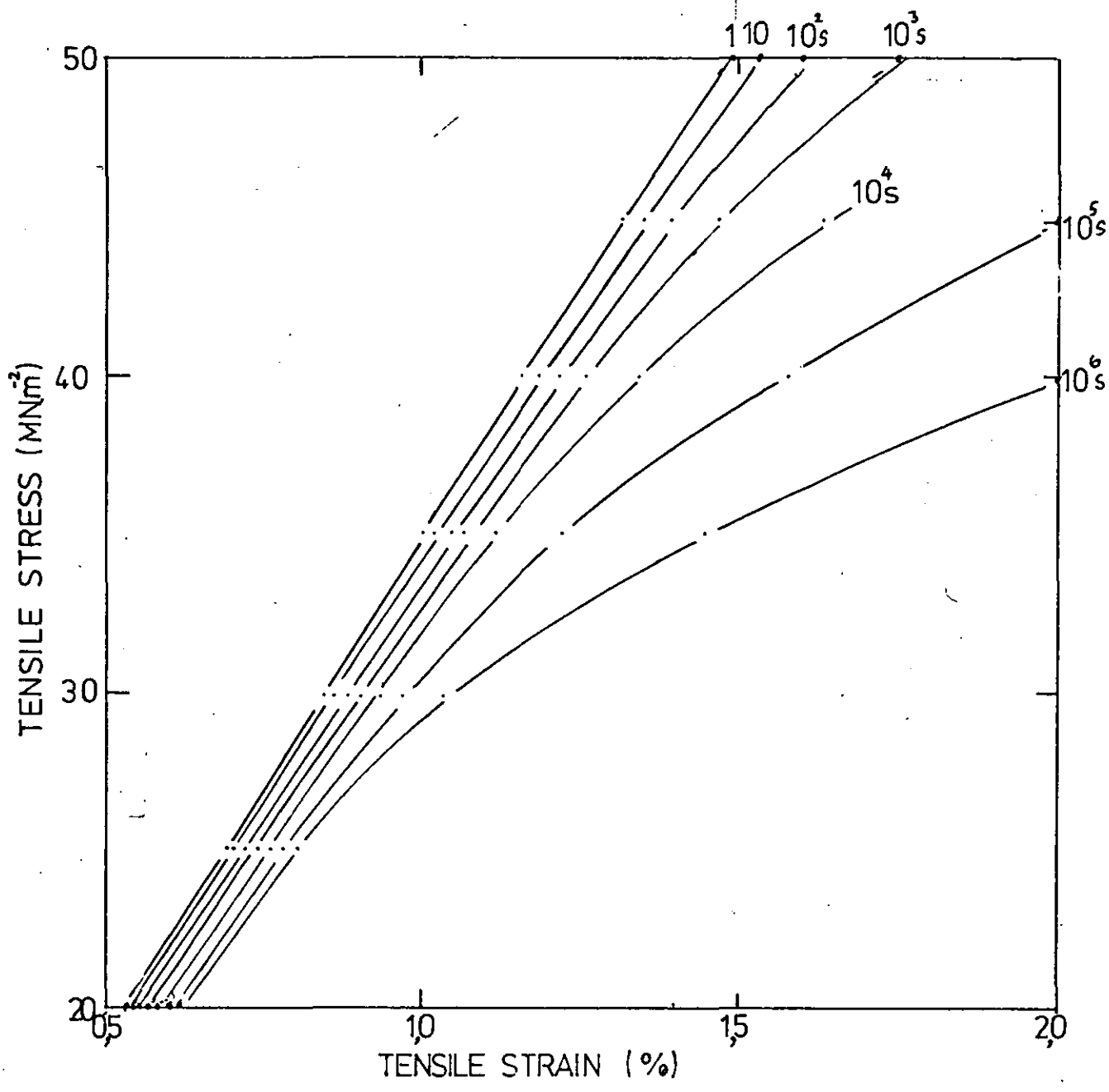


FIGURE 5.2 ISOCHRONOUS STRESS STRAIN DATA FOR UPVC AT 20°C

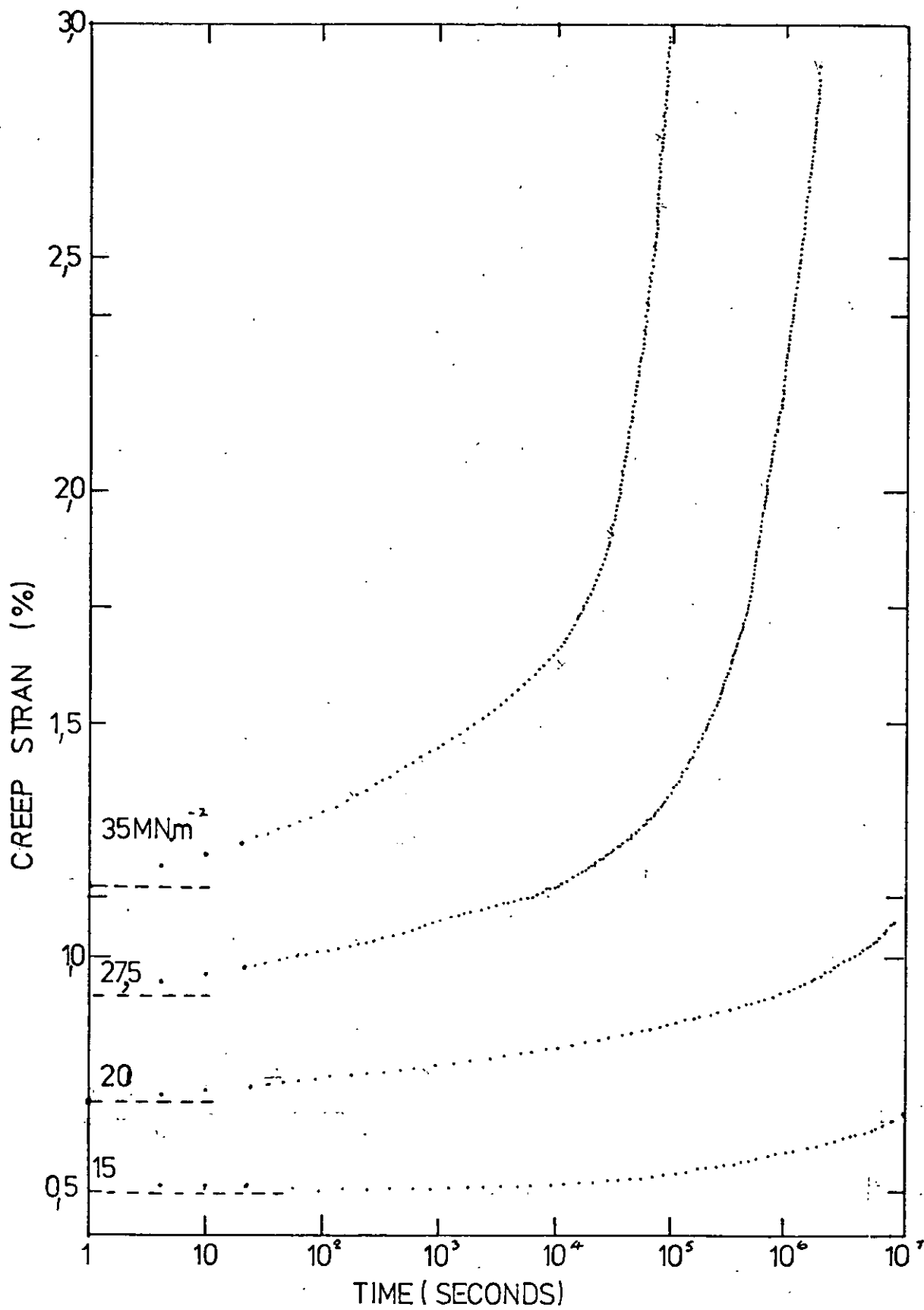


FIGURE 53 TENSILE CREEP CHARACTERISTICS OF UPVC AT 35°C  
 ----- ESTIMATED STRAIN AT 1 SECOND

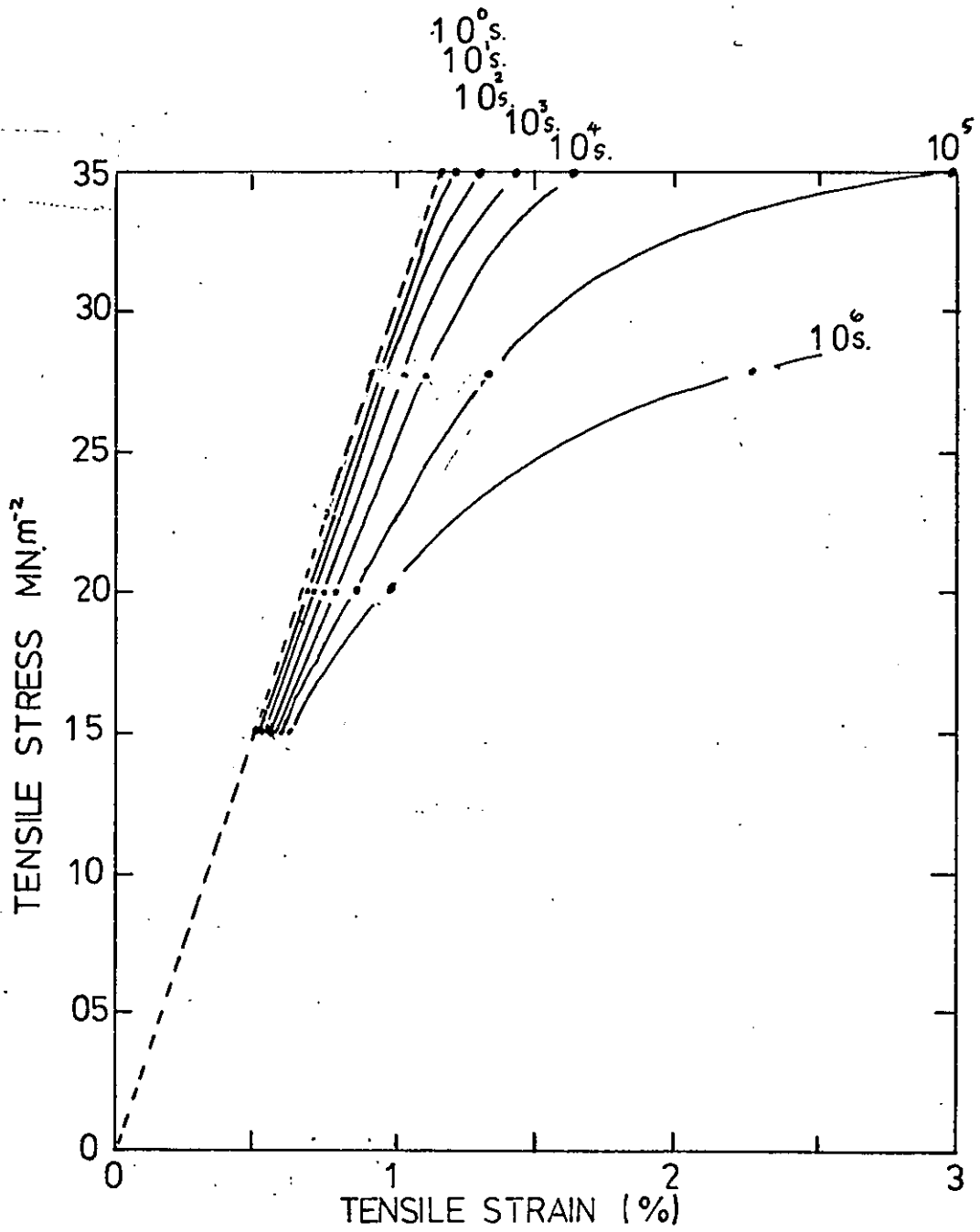


FIGURE 54 ISOCHRONOUS STRESS STRAIN DATA FOR UPVC AT 35°C

The recovery periods for these initial tests were generally ten times longer than the creep period preceding them. Two recovery characteristics are included in Figure 5.5 together with the respective creep characteristics. It is observed that  $\Delta R_{CR}$  is positive for short recovery times ( $\theta$ ) and negative at long recovery times. Values of  $\Delta R_{CR}(\theta)$  are given in Table 5.2 for the 12 creep and recovery tests performed at 20°C and 35°C. On the evidence provided by these initial tests it was concluded that  $\Delta R_{CR}(\theta)$  is reasonably independent of  $\theta$  when  $\theta$  is less than  $\sim 50s$ . Timing errors would be unacceptable for  $\theta < 15s$ . It was decided therefore that an optimum 'monitor time' would be 20s. Therefore the experimental definition of  $\Delta R_{CR}$  is:

$$\Delta R_{CR}(20) = \epsilon_r(20) - \epsilon_c(20)$$

Where  $\epsilon_r(20)$  and  $\epsilon_c(20)$  are the recovered strain and creep strain as measured 20 seconds after load removal, or load application. Thus for all additional creep and recovery tests only three strains were recorded for each test, these being  $\epsilon_r(20)$ ,  $\epsilon_c(T)$  and  $\epsilon_{res}(20)$ .  $\epsilon_c(T)$  is the final creep strain as measured just prior to the removal of stress (after a creep period T) and  $\epsilon_{res}(20)$  is the residual strain 20 seconds after stress removal.  $\epsilon_r(20)$  is simply:

$$\epsilon_r(20) = \epsilon_c(T) - \epsilon_{res}(20)$$

Virgin specimens of UPVC were creep tested at selected tensile stress levels at 20°C and 35°C over a range of creep periods (T). The strain measurements  $\epsilon_c(20)$  and  $\epsilon_c(T)$  were recorded. On recovery, the residual

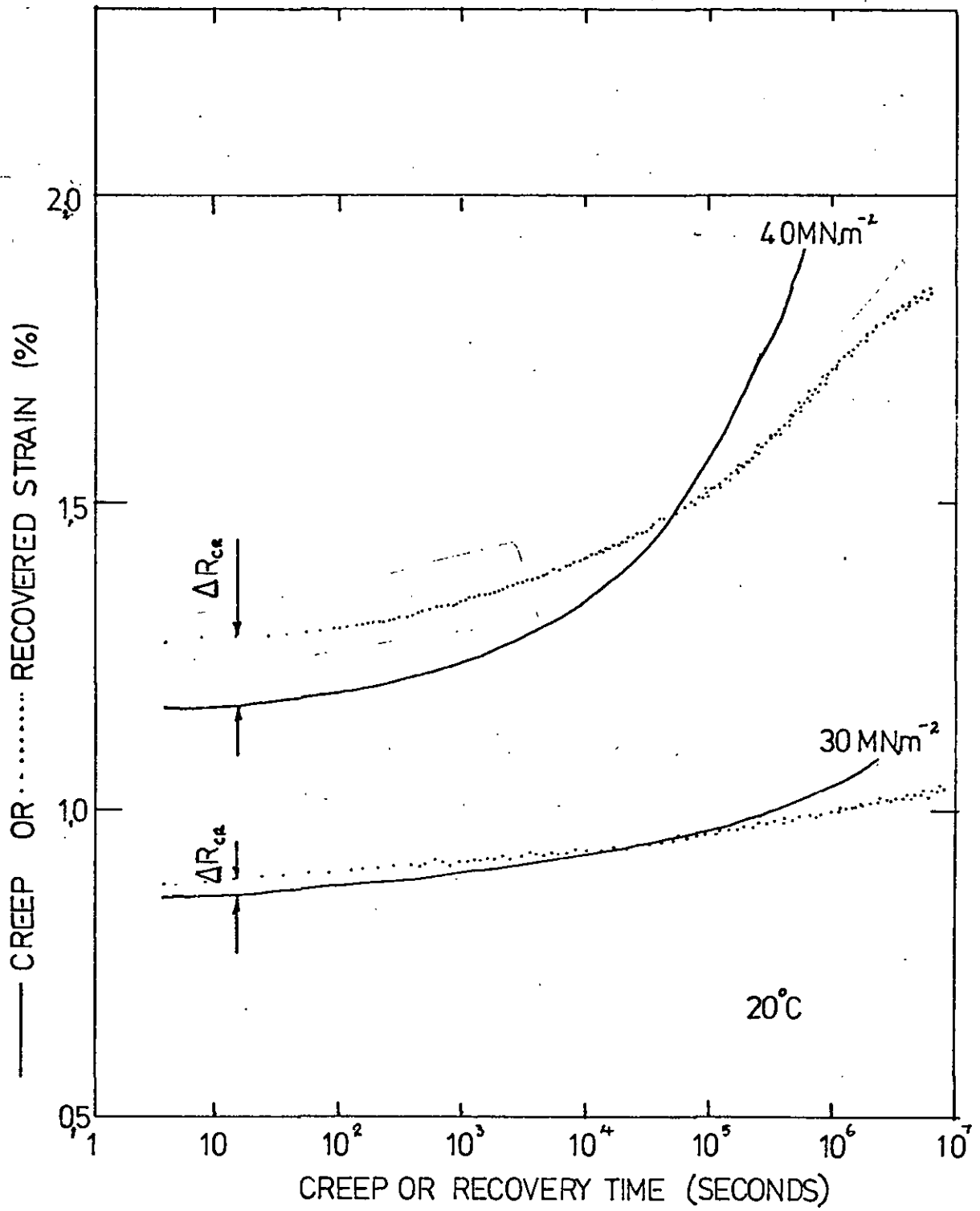


FIGURE 55 COMPARISON OF CREEP AND RECOVERY DATA.



Temp. °C	Creep Stress MN/m <sup>2</sup>	Creep time (T) secs	$\Delta R_{CR} (\theta) \quad (\%)$						
			$\theta = 5s$	$\theta = 10\%s$	$\theta = \frac{15}{10}s$	$\theta = 20s$	$\theta = 50s$	$\theta = 100s$	$\theta = T$
20	50	$8.5 \times 10^4$	+0.660	+0.666	+0.666	+0.663	+0.663	+0.654	-0.321
20	45	$1.6 \times 10^5$	+0.291	+0.285	+0.288	+0.288	+0.288	+0.282	-0.153
20	40	$9.2 \times 10^5$	+0.111	+0.114	+0.111	+0.111	+0.111	+0.105	-0.267
20	40	$2.0 \times 10^4$	+0.069	+0.066	+0.066	+0.069	+0.066	+0.060	-0.006
20	35	$6.2 \times 10^6$	+0.079	+0.079	+0.079	+0.079	+0.072	+0.066	-0.057
20	35	$4 \times 10^4$	+0.048	+0.048	+0.048	+0.048	+0.048	+0.042	-0.003
20	30	$2.1 \times 10^6$	+0.027	+0.030	+0.030	+0.027	+0.027	+0.027	-0.066
20	25	$7.5 \times 10^6$	+0.006	+0.006	+0.006	+0.006	+0.006	+0.006	-0.006
35	35	$9.5 \times 10^4$	+0.495	+0.492	+0.498	+0.498	+0.495	+0.480	-0.210
35	27.5	$1.8 \times 10^6$	+0.273	+0.270	+0.270	+0.270	+0.273	+0.264	-0.189
35	20	$9 \times 10^6$	+0.051	+0.051	+0.048	+0.048	+0.048	+0.048	-0.0126
35	15	$10^7$	+0.030	+0.030	+0.033	+0.033	+0.033	+0.033	-0.090

TABLE 5.2 The Damage Factor  $\Delta R_{CR} (\theta)$  at various values of  $\theta$  for UPVC after various creep histories.

strain  $\epsilon_{res}$  (20) was recorded. The computed  $\Delta R_{CR}$  (20) data <sup>are</sup> ~~is~~ presented graphically in Figures 5.6 (20°C) and 5.7 (35°C) as a function of creep time with stress as the parameter. In addition the  $\Delta R_{CR}$  (20) data <sup>are</sup> ~~is~~ plotted as a function of maximum creep strain  $\epsilon_c(T)$  in Figures 5.8 (20°C) and 5.9 (35°C), again with stress level as the parameter. Data from the 40 MN/m<sup>2</sup> (20°C) tests are tabulated in Table 5.3 as an example.

Micro-damage was observed in all specimens which, as a result of their stress and strain history, had provided significantly positive values of  $\Delta R_c(20)$ . The two photographs shown in Figure 5.10 (a) and (b) are of the damaged surfaces of specimens with a severe (a) and moderate (b) stress history. The increase in micro-damage site density with stress level is similar to that observed with crazing (129). To confirm that the surface micro-damage was in fact crazing, the technique suggested by Kambour (96) and discussed in section 3.1 was adopted. The minimum incidence angle for the total reflection of light from the crack/polymer, craze/polymer boundary was in all cases in the range 56° - 68°. This suggests that the void content of the micro-damage regions in recovered or partially recovered specimens was in the range 20% to 30%. Similar measurements on selected specimens under load provided values of void content in the range 40% to 45%. It was therefore concluded that the damage observed in UPVC during, and/or after, creep tests of sufficient severity was predominantly crazing.

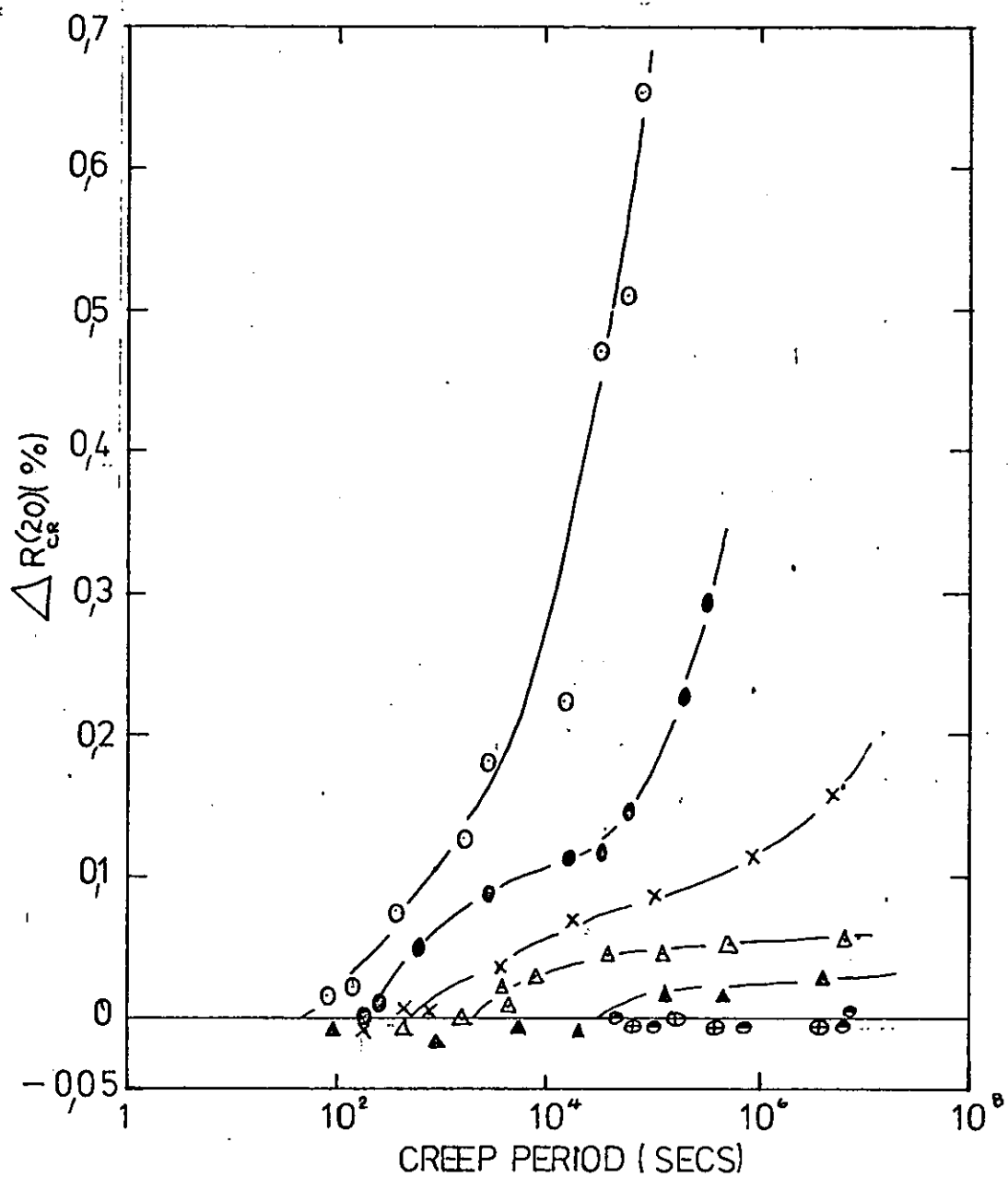


FIGURE 56  $\Delta R_{CR}(20)$  AS A FUNCTION OF STRESS HISTORY FOR UPVC AT 20°C. TENSILE STRESS IN MN,m<sup>-2</sup>:  
 o 50, ● 45, x 40, Δ 35, ▲ 30, ⊙ 25, ⊕ 20,

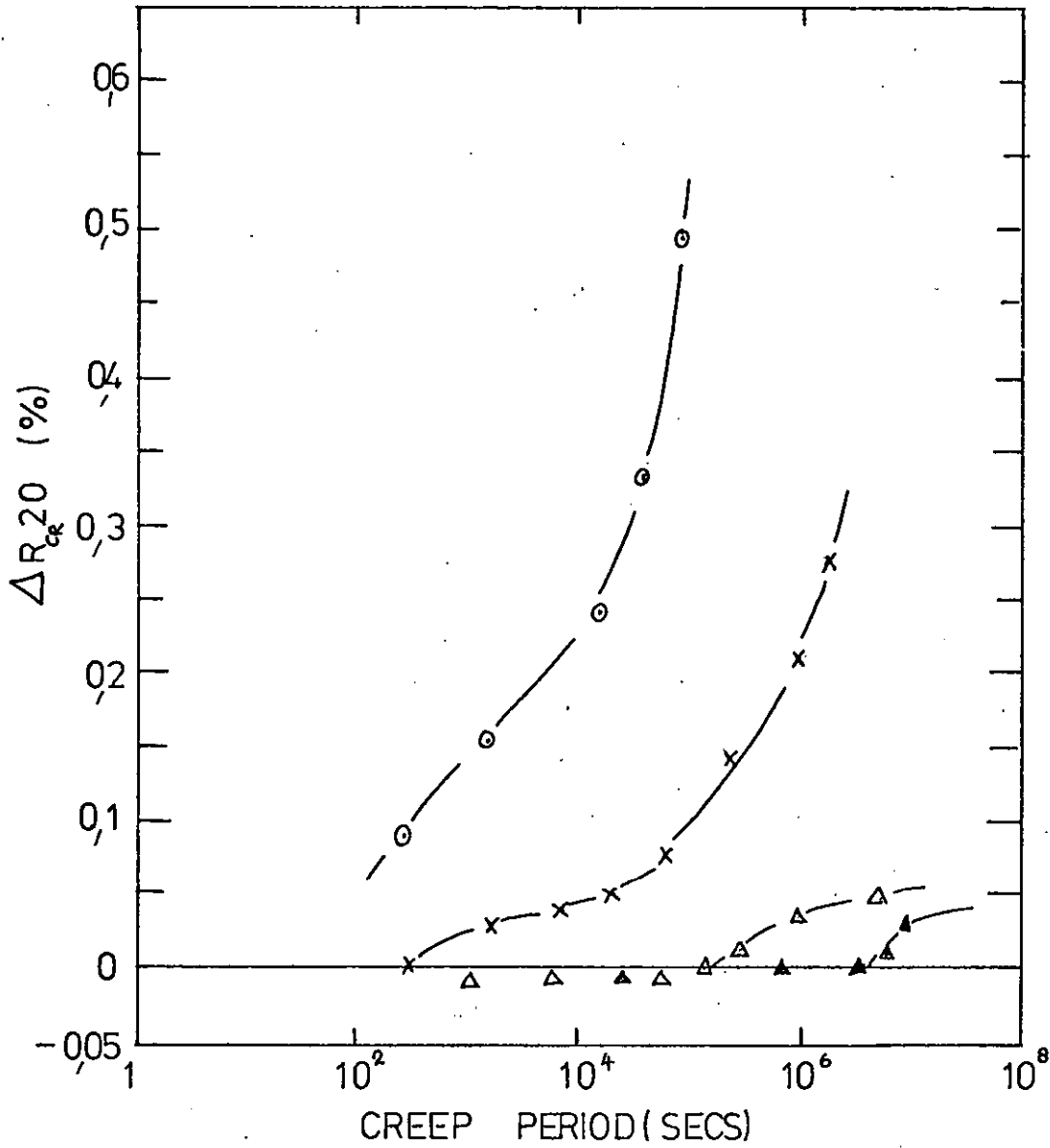


FIGURE 5,7

$\Delta R_{cr}(20)$  AS A FUNCTION OF STRESS HISTORY FOR UPVC AT 35°C. TENSILE STRESS IN MN.m<sup>-2</sup>  
 ○ 35, x 27.5, Δ 20, ▲ 15,

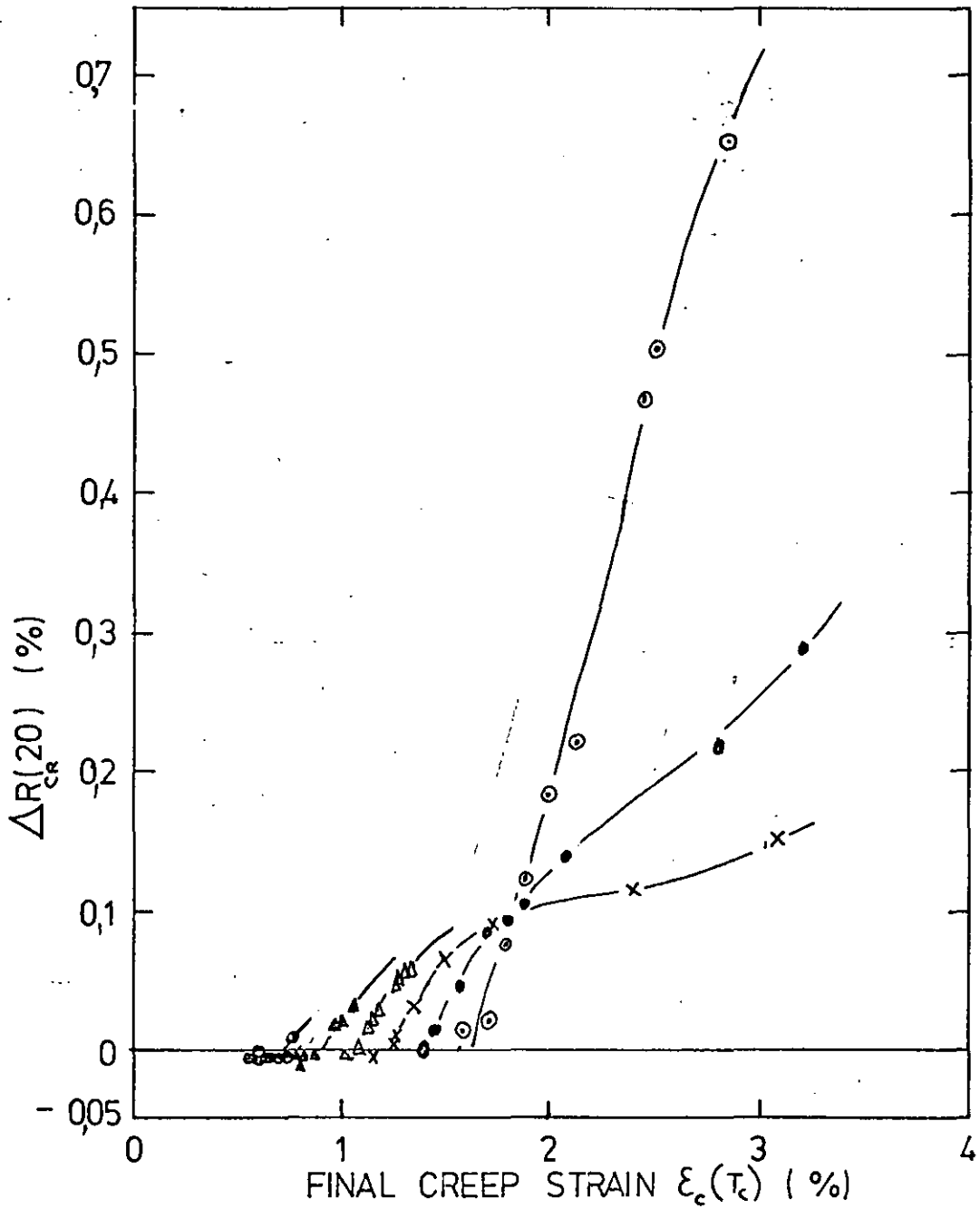


FIGURE 5,8

$\Delta R_{cr}(20)$  AS A FUNCTION OF TENSILE STRAIN FOR UPVC AT 20°C. STRESS IN  $\text{MN.m}^{-2}$ :

○50, ●45, ×40, △35, ▲30, ⊙25, ⊖20,

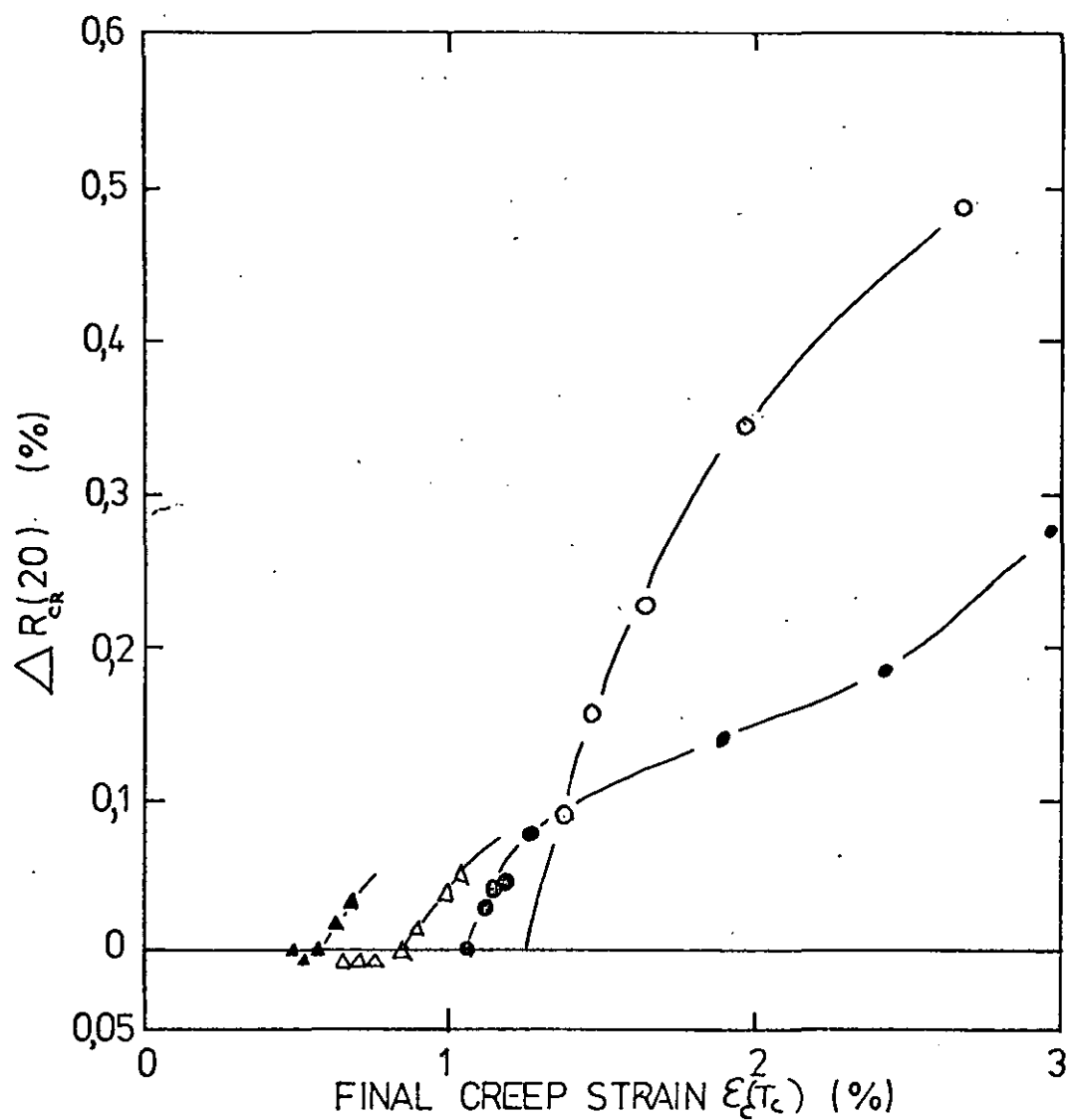


FIGURE 59

$\Delta R_{cr}(20)$  AS A FUNCTION OF TENSILE STRAIN FOR UPVC AT 35°C. STRESS IN MN m<sup>-2</sup>:

○ 35, ● 27.5, △ 20, ▲ 15,

Creep time (T) secs	20 second Creep strain $\epsilon_c(20)$ %	Final creep strain $\epsilon_c(T)$ %	20s residual strain $\epsilon_{res}(20)$ %	20s recovered strain $\epsilon_r(20)$ %	$\Delta R_{CR}(20)$ = $\epsilon_r(20) - \epsilon_c(20)$ %
180	1.140	1.203	0.072	1.131	- 0.009
590	1.149	1.254	0.096	1.158	+ 0.009
810	1.131	1.245	0.108	1.137	+ 0.006
3240	1.137	1.275	0.096	1.179	+ 0.042
20,000	1.140	1.374	0.165	1.209	+ 0.069
93,000	1.143	1.587	0.351	1.236	+ 0.093
920,000	1.149	1.986	0.726	1.260	+ 0.111
8,100,000	1.143	2.610	1.305	1.305	+ 0.162

TABLE 5.3 Measured values of  $\epsilon_c(20)$ ,  $\epsilon_c(T)$  and  $\epsilon_{res}(20)$ , and calculated values of  $\epsilon_r(20)$  and  $\Delta R_{CR}(20)$  for the 40 MN/m<sup>2</sup>, 20°C Tests.



Fig. 5.10(a) UPVC Surface Crazing (X150).  
After recovery from a tensile stress  
of  $40 \text{ MN/m}^2$  at  $20^\circ\text{C}$



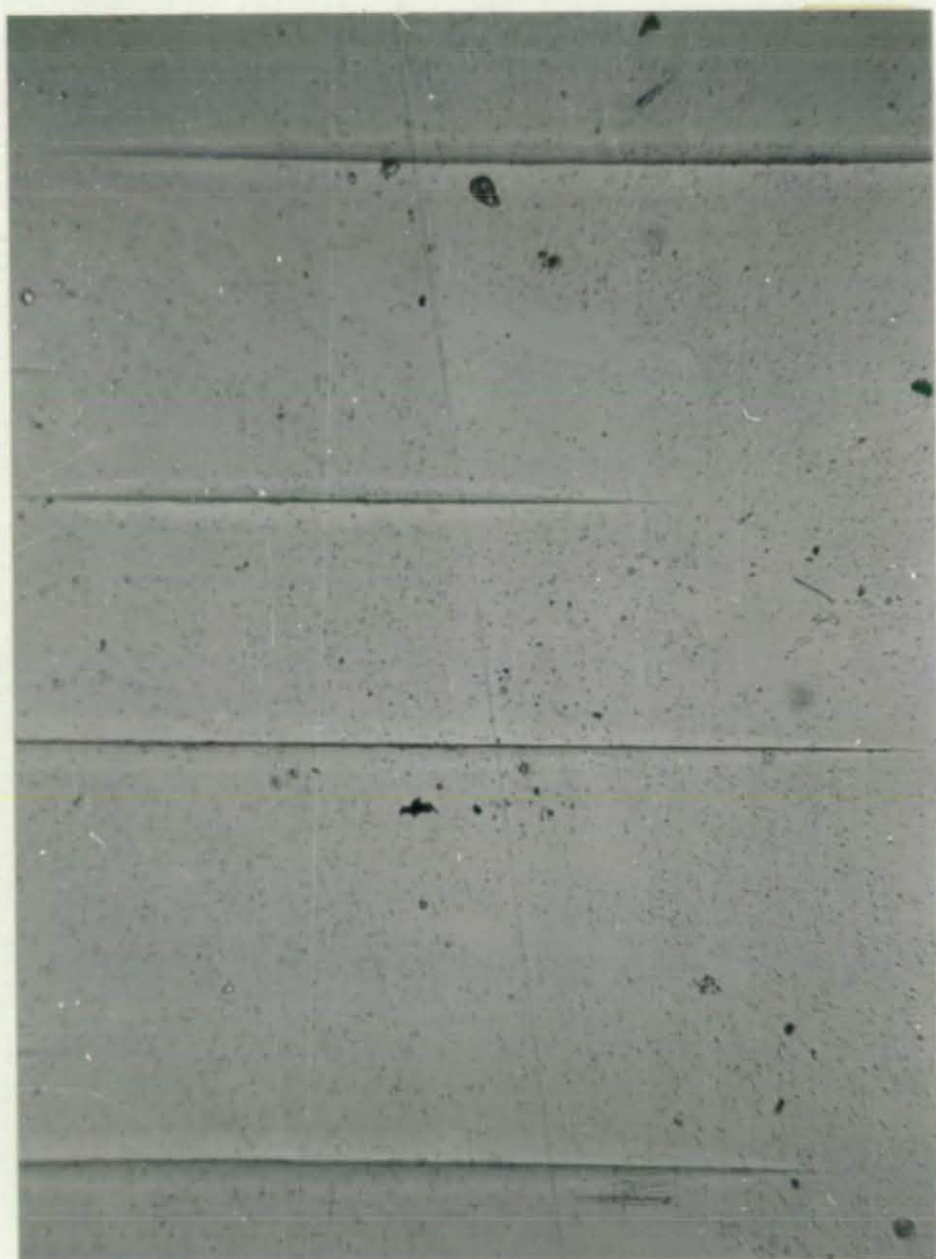


Fig. 5.10(b) UPVC Surface Crazing (X150).  
After recovery from a tensile stress  
of  $25 \text{ MN/m}^2$  at  $20^\circ\text{C}$ .

Specimens which had provided near zero or negative values of  $\Delta R_{CR}(20)$  were generally observed to be undamaged although this was not conclusive. On some occasions several craze like events were observed at the routed edge of the specimen but detection and identification of these events was so subjective that a confident visual assessment of the critical craze initiation condition cannot be offered.

### 5.3. The Damage Parameter after a Variable Rest Period

Approximately one half of those specimens used for the measurement of  $\Delta R_{CR}(20)$  were not removed after recording  $\epsilon_{RS}(20)$  but were left under zero load for a selected period of time  $T_R$ .

Just prior to the re-application of stress the residual strain  $\epsilon_{RS}(T_R)$  was recorded. In addition the creep strain twenty seconds after the start of the second creep period was measured. This is denoted as  $\epsilon_c^2(20)$ . The damage parameter  $\Delta R_{CC}(20)$  as defined in Section 4.1 equation (13) is:

$$\Delta R_{CC}(20) = \epsilon_c^2(20) - \epsilon_{RS}(T_R) - \epsilon_c^1(20)$$

where  $\epsilon_c^1(20)$  is the creep strain 20 seconds after the start of the first creep period.

The ratio:

$$\frac{\Delta R_{CC}(20)}{\Delta R_{CR}(20)}$$

is plotted against rest period  $T_R$  in Figure 5.11 (20°C) and 5.12 (35°C).

It is evident that for long rest periods:

$$\Delta R_{CC}(20) < \Delta R_{CR}(20)$$

and for short rest periods:

$$\Delta R_{CC}(20) > \Delta R_{CR}(20)$$

#### 5.4 The Damage Parameter in Response to Dynamic Stress Histories

The stressing sequence shown schematically in Figure 4.2 was adopted. Automatic control of stress application and removal was achieved using a low frequency square wave generator to energise and de-energise the loading system. The total period, that is  $T_C + T_R$ , could be selected together with an independent selection of the ratio  $T_C : T_R$ . All tests were performed at 20°C and at stress amplitudes which were estimated would provide craze initiation within 5 days of continuous cycling.

The strain response to cyclic stressing could not be recorded automatically because of the rapidly changing frequency of the extensometer output. Consequently the strain response to each cycle could not be monitored. However, for the measurement of the

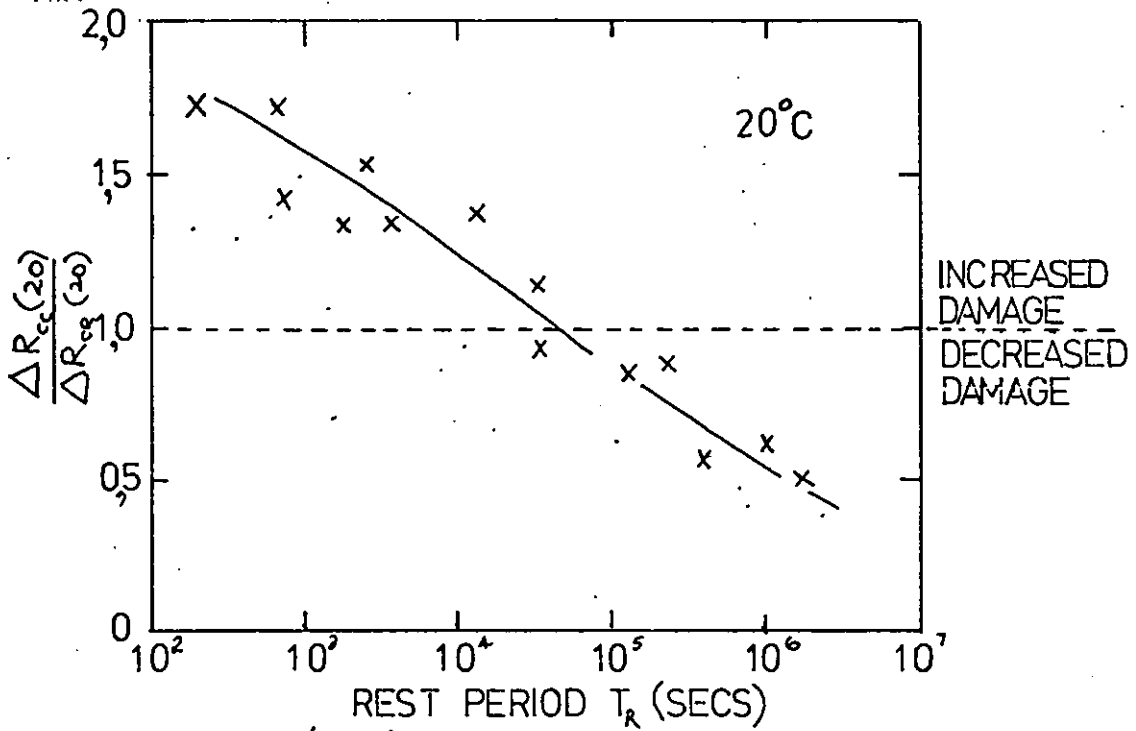


FIGURE 5,11  $\left(\frac{\Delta R_{cc}}{\Delta R_{cg}}\right)$  V.  $T_R$  AT 20°C.

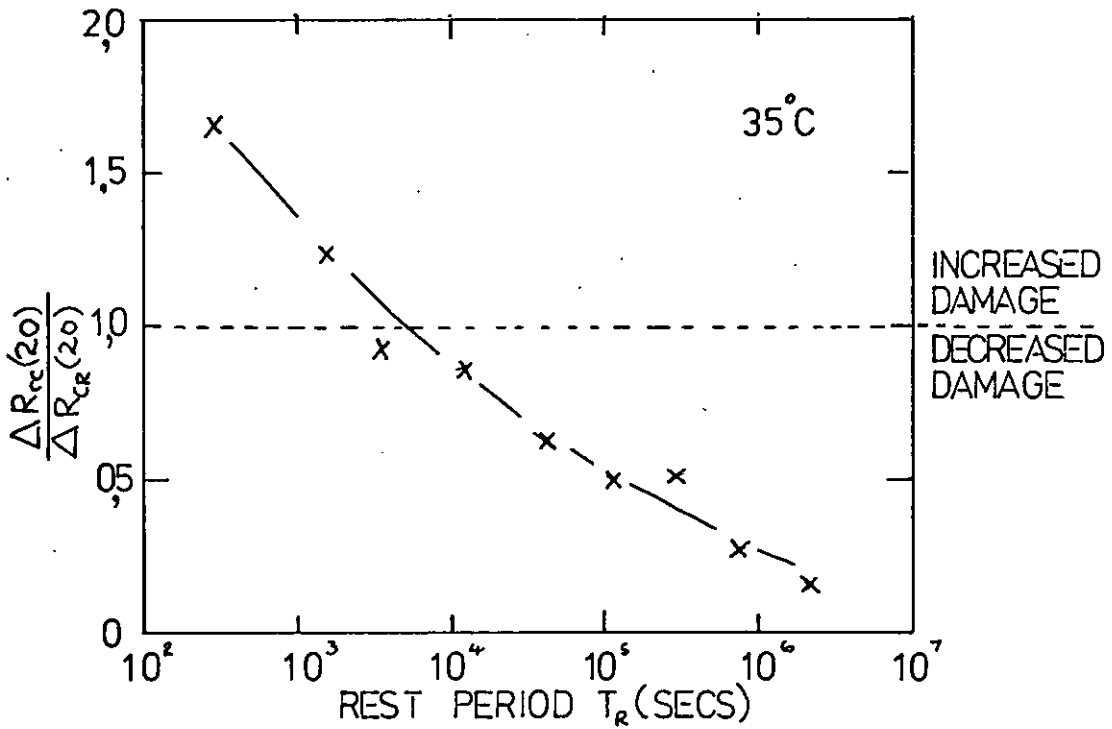


FIGURE 5,12  $\left(\frac{\Delta R_{cc}}{\Delta R_{cg}}\right)$  V.  $T_R$  AT 35°C

growth of the function  $\Delta R_{RR}^N(20)$ , it was necessary to monitor the strain response at selected cycles only. Generally, monitoring involved 2 strain recordings per cycle these being  $\epsilon_c^N(T_c)$  and  $\epsilon_{rs}^N(20)$  where N is the cycle number. In addition some cycles were monitored by recording the strain response during the recovery period.

The strain response  $\epsilon_c^N(T_c)$  with time under load ( $N T_c$ ) is displayed graphically in Figures 5.13, 5.14 and 5.15 for stress amplitudes of 30, 35, and 40 MN/m<sup>2</sup> respectively. The creep to recovery periods investigated were 1320S: 120S (11:1), 900S : 300S (3:1), and 120S : 120S (1:1). Each graph also includes for comparison, the strain response to static stress (∞:1).

The strain responses of individual recovery cycles are given in Figures 5.16-5.24. These present the recovered strain  $\epsilon_r^N(\theta)$  as a function of recovery time  $\theta$ , where:

$$\epsilon_r^N(\theta) = \epsilon_c^N(T_c) - \epsilon_{rs}^N(\theta)$$

It is observed, on inspection of <sup>these</sup> ~~this~~ data that the initial ('unrelaxed') recovered strain increases significantly with cycle number whilst the time-dependent ('relaxed') component of individual recovery cycles changes only slowly with progressive cycling. The increase in the initial recovered strain response with progressive cycling is interpreted as the growth of  $\Delta R_{RR}$ . If it is assumed that damage initiated in the first cycle is negligible then from equation (14) (section 4.1) :

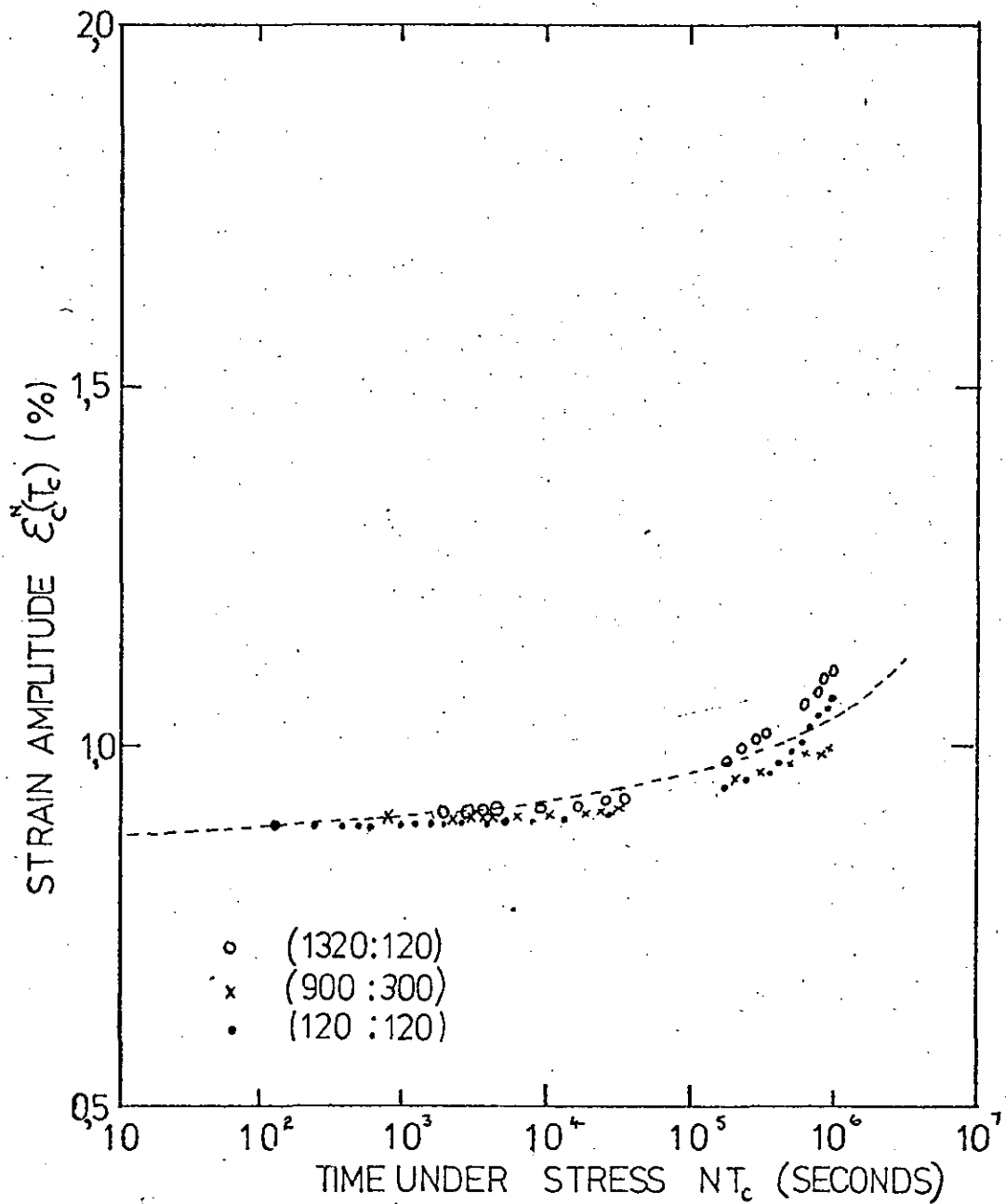


FIGURE 5.13 TENSILE CREEP IN RESPONSE TO  
 INTERMITTENT CREEP AND RECOVERY  
 CYCLING AT A STRESS AMPLITUDE OF  
 $30 \text{ MNm}^{-2}$ .

----- RESPONSE TO STATIC STRESS

( ; ) CREEP : RECOVERY PERIOD IN SECONDS

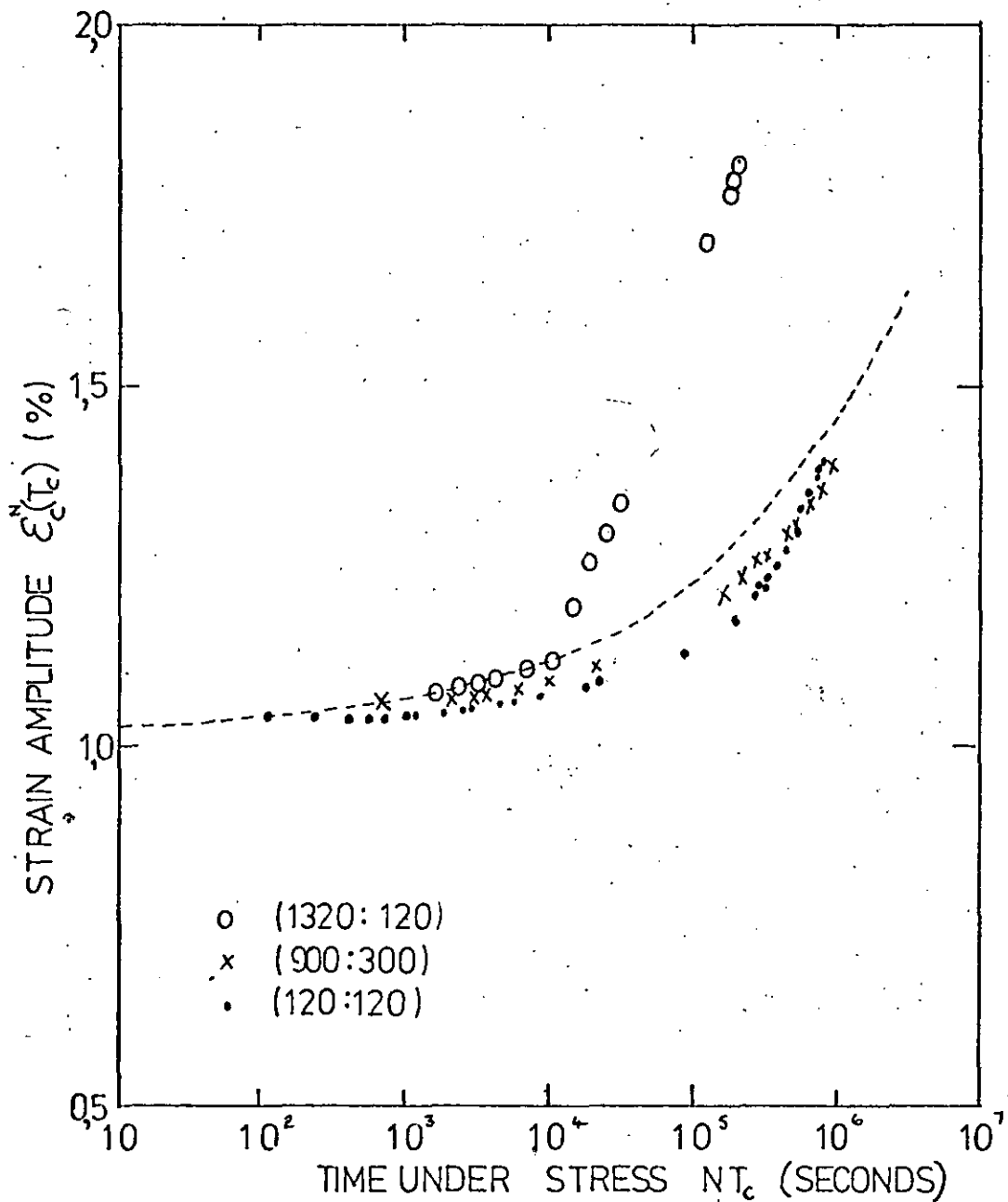


FIGURE 5,14 TENSILE CREEP IN RESPONSE TO  
 INTERMITTENT CREEP AND RECOVERY  
 CYCLING AT A STRESS AMPLITUDE OF  
 $35 \text{ MNm}^{-2}$

----- RESPONSE TO STATIC STRESS

( ; ) CREEP : RECOVERY PERIOD IN SECONDS

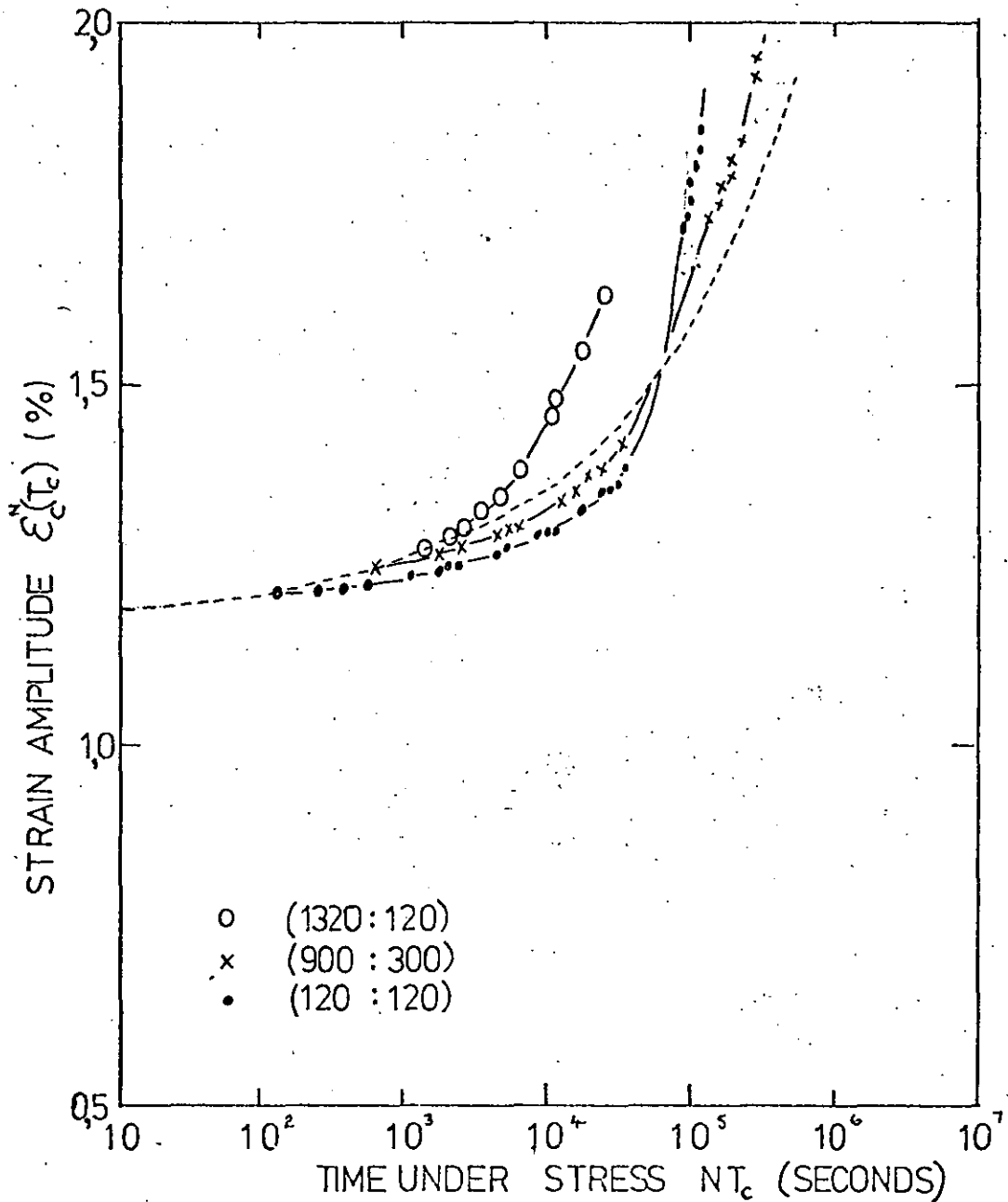


FIGURE 5,15 TENSILE CREEP IN RESPONSE TO INTERMITTENT CREEP AND RECOVERY CYCLING AT A STRESS AMPLITUDE OF  $40 \text{ MNm}^{-2}$ .

----- RESPONSE TO STATIC STRESS

( ; ) CREEP : RECOVERY PERIOD IN SECONDS



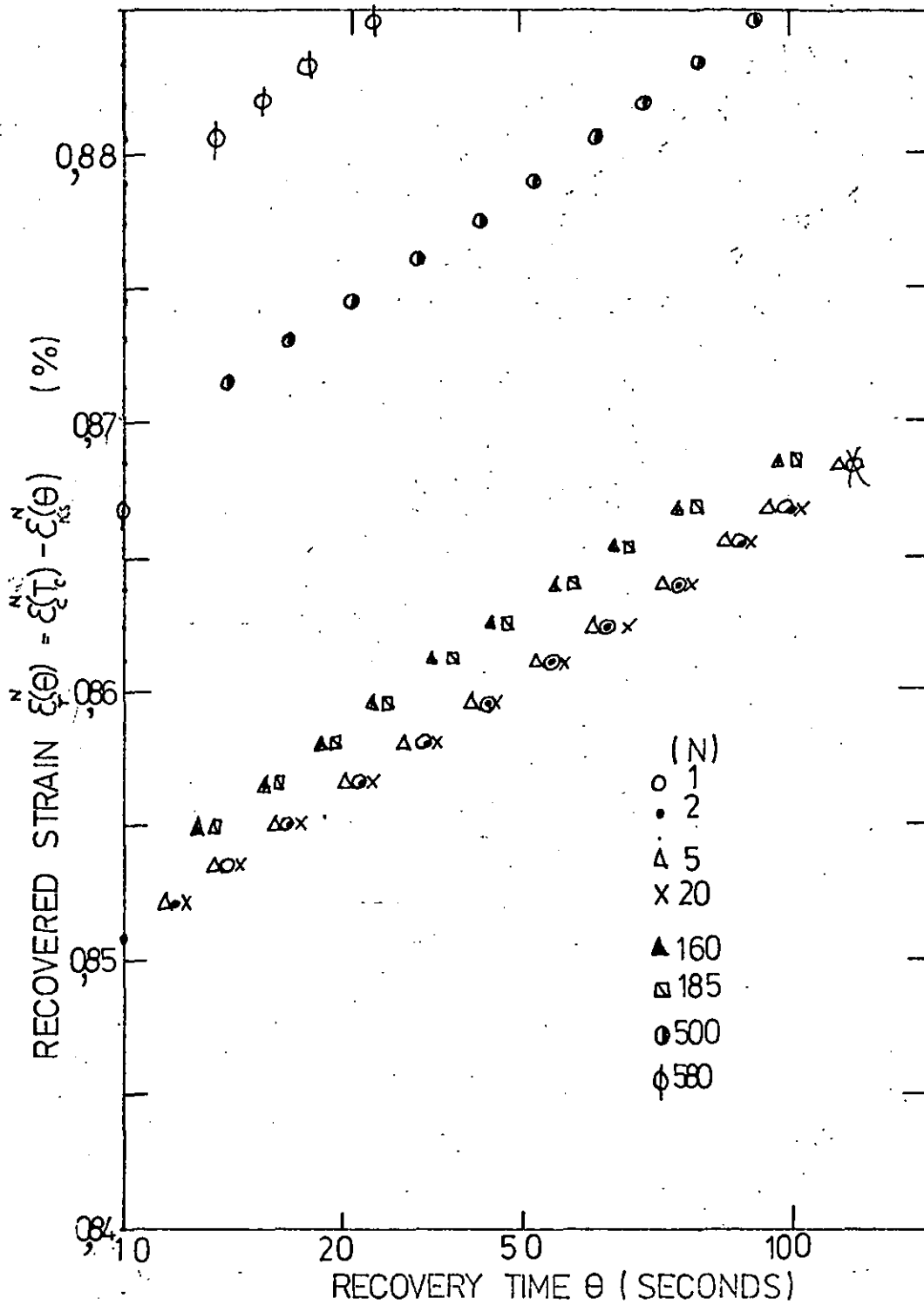


FIGURE 5,16 INDIVIDUAL RECOVERY CHARACTERISTICS AFTER VARIOUS CYCLES (N).  
 STRESS AMPLITUDE = 30 MN.m<sup>-2</sup>  
 CREEP : RECOVERY PERIOD IN SECONDS ( 1320 : 120 )

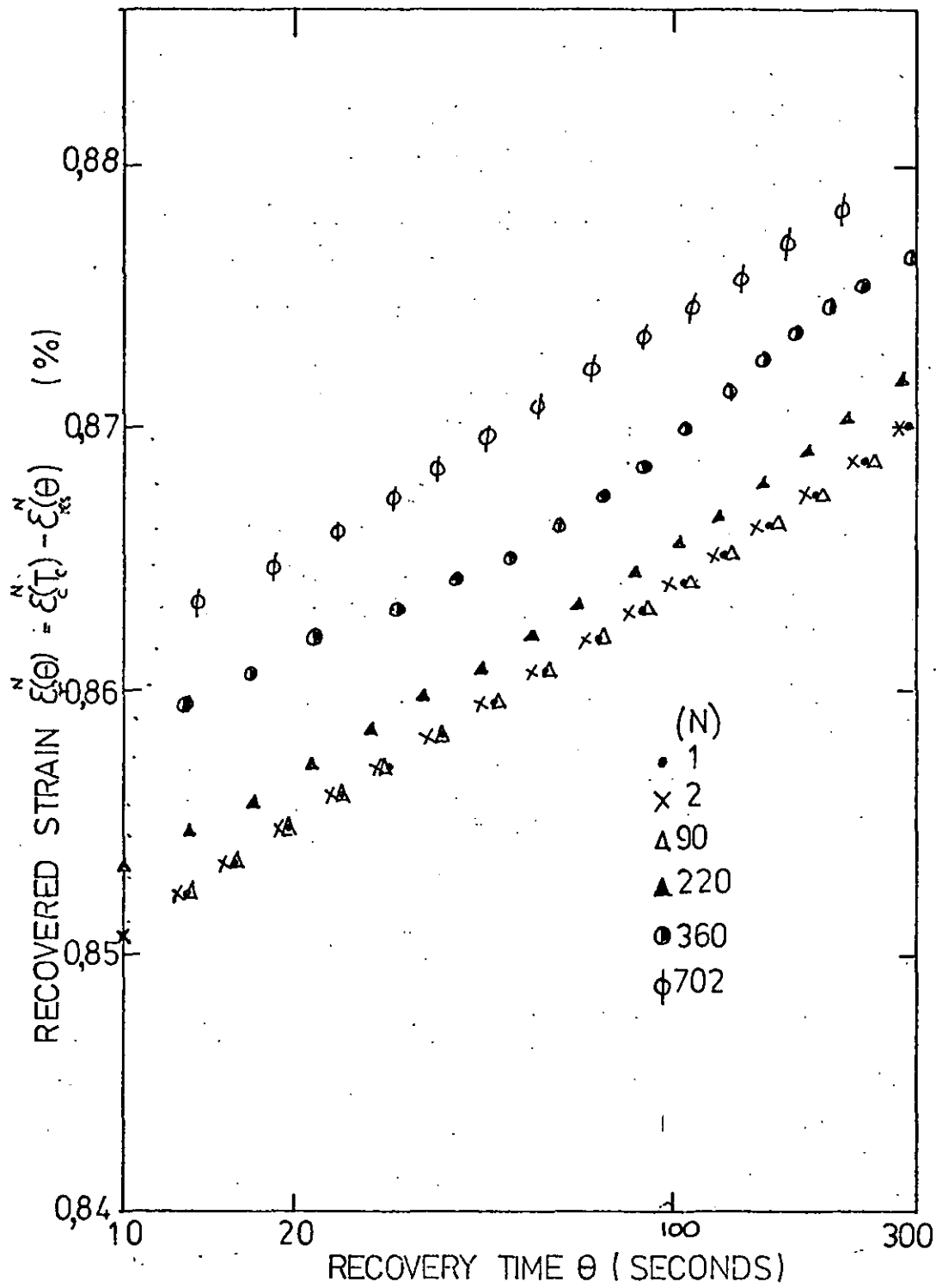


FIGURE 5,17 INDIVIDUAL RECOVERY CHARACTERISTICS AFTER VARIOUS CYCLES (N).  
 STRESS AMPLITUDE = 30 MN.m<sup>-2</sup>  
 CREEP : RECOVERY PERIOD IN SECONDS ( 900 : 300 )

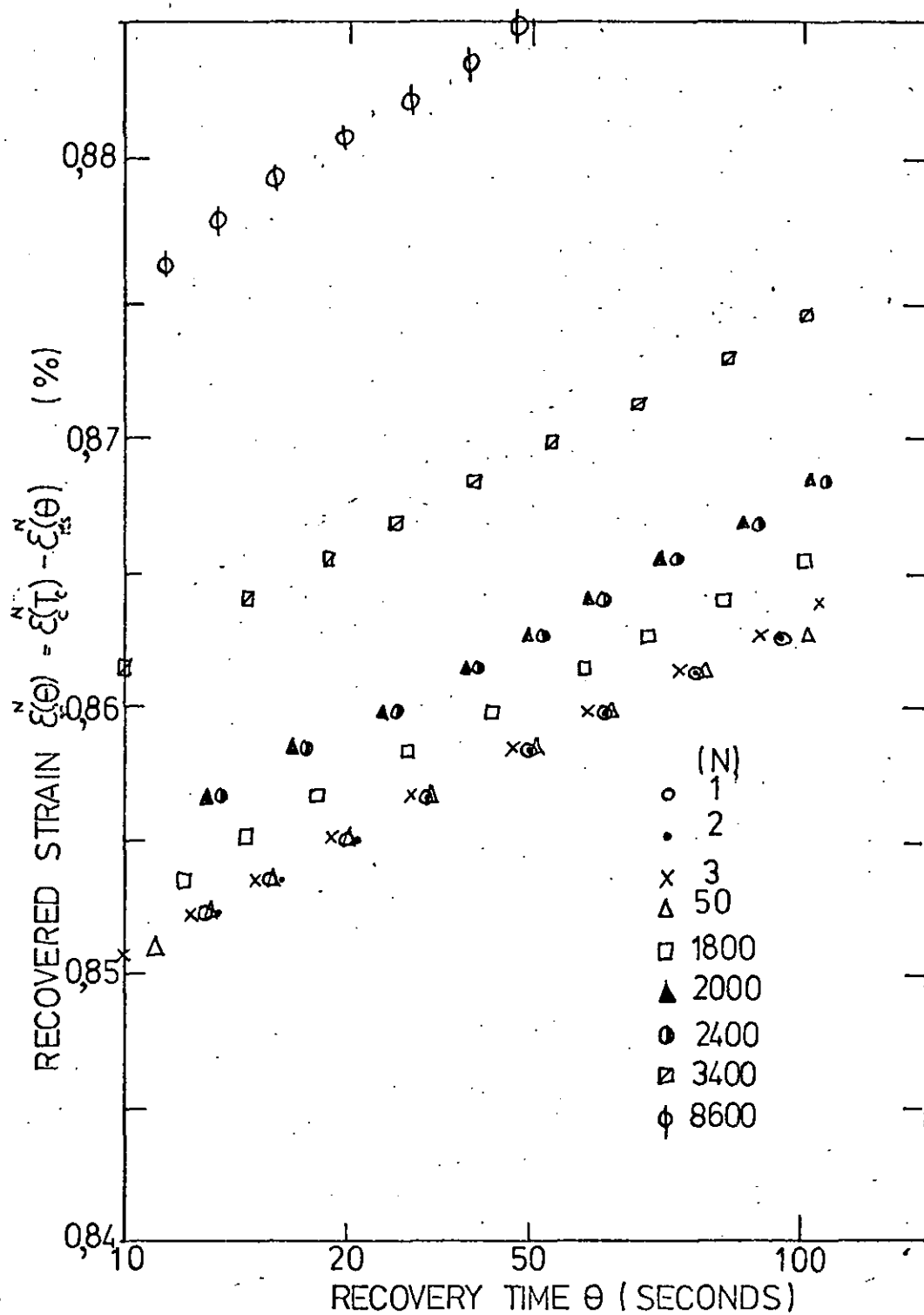


FIGURE 5, 18 INDIVIDUAL RECOVERY CHARACTERISTICS  
 AFTER VARIOUS CYCLES (N).  
 STRESS AMPLITUDE =  $30 \text{ MNm}^{-2}$   
 CREEP : RECOVERY PERIOD IN SECONDS (120 : 120)

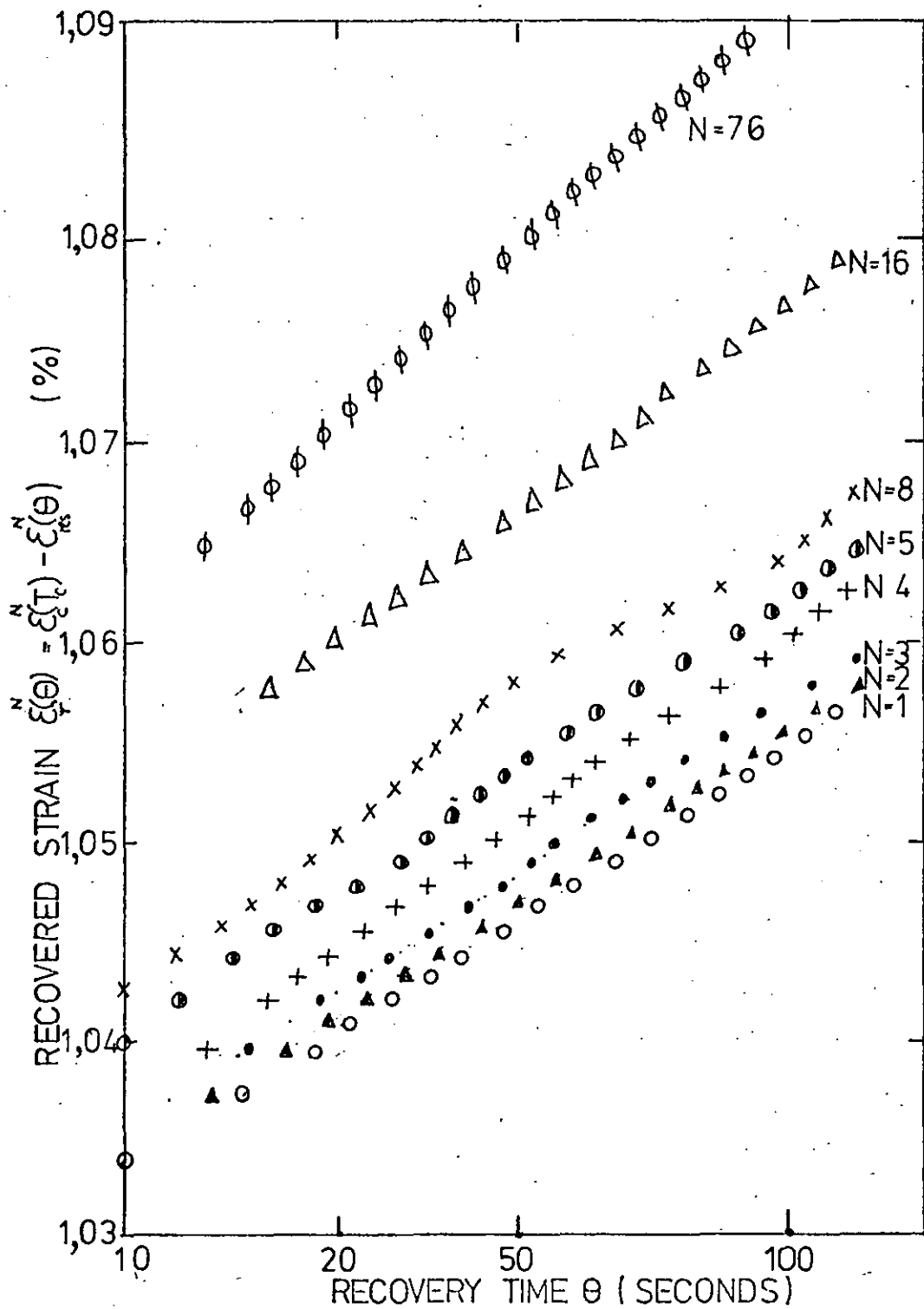


FIGURE 5,19 INDIVIDUAL RECOVERY CHARACTERISTICS AFTER VARIOUS CYCLES (N).  
 STRESS AMPLITUDE =  $35 \text{ MN.m}^{-2}$   
 CREEP : RECOVERY PERIOD IN SECONDS (1320 : 120)

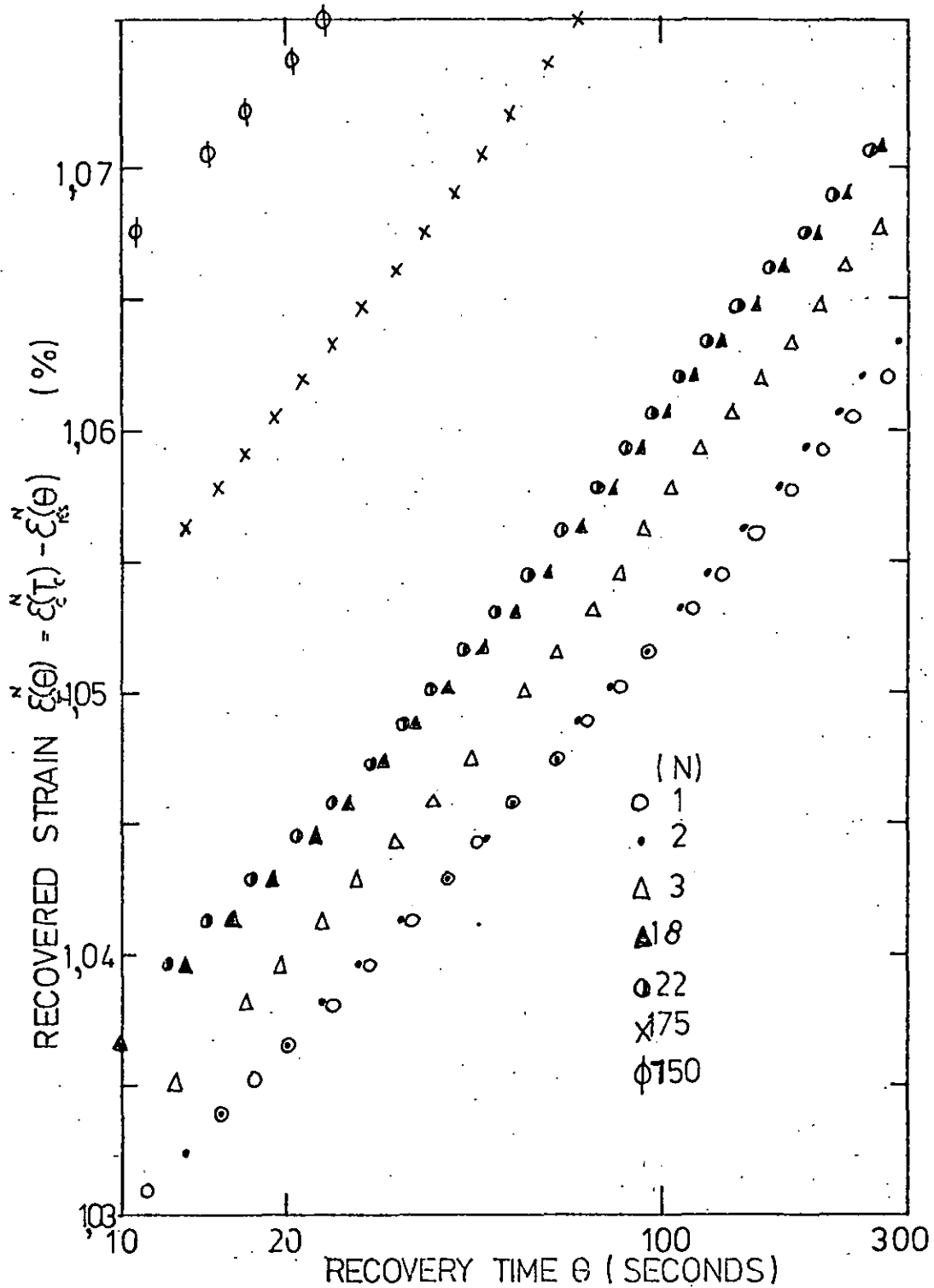


FIGURE 5,20 INDIVIDUAL RECOVERY CHARACTERISTICS  
 AFTER VARIOUS CYCLES (N).  
 STRESS AMPLITUDE =  $35 \text{ MN/m}^2$   
 CREEP : RECOVERY PERIOD IN SECONDS ( 900 : 300 )

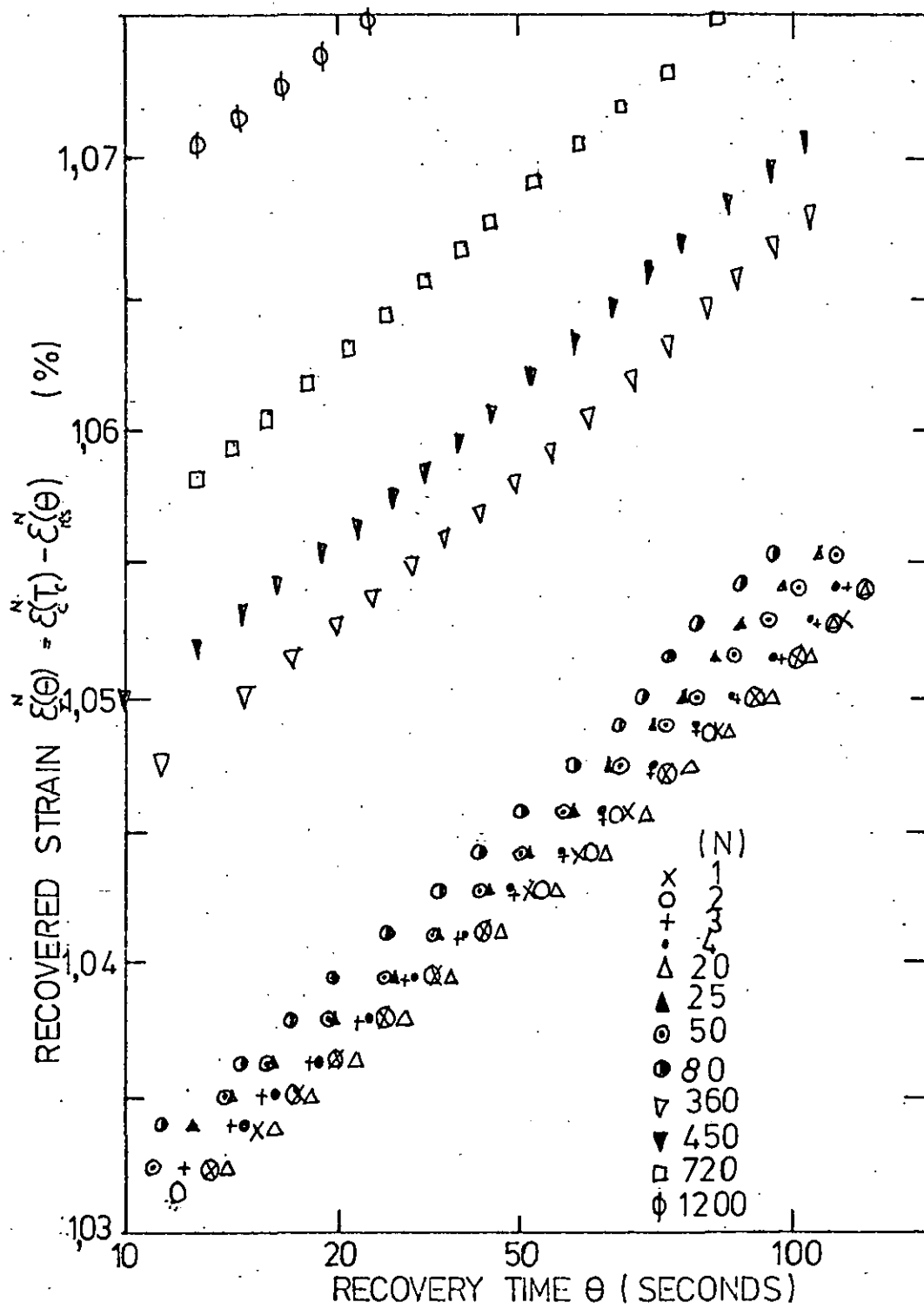


FIGURE 5.21 INDIVIDUAL RECOVERY CHARACTERISTICS AFTER VARIOUS CYCLES (N).  
 STRESS AMPLITUDE =  $35 \text{ MN.m}^{-2}$   
 CREEP : RECOVERY PERIOD IN SECONDS (120 : 120 )

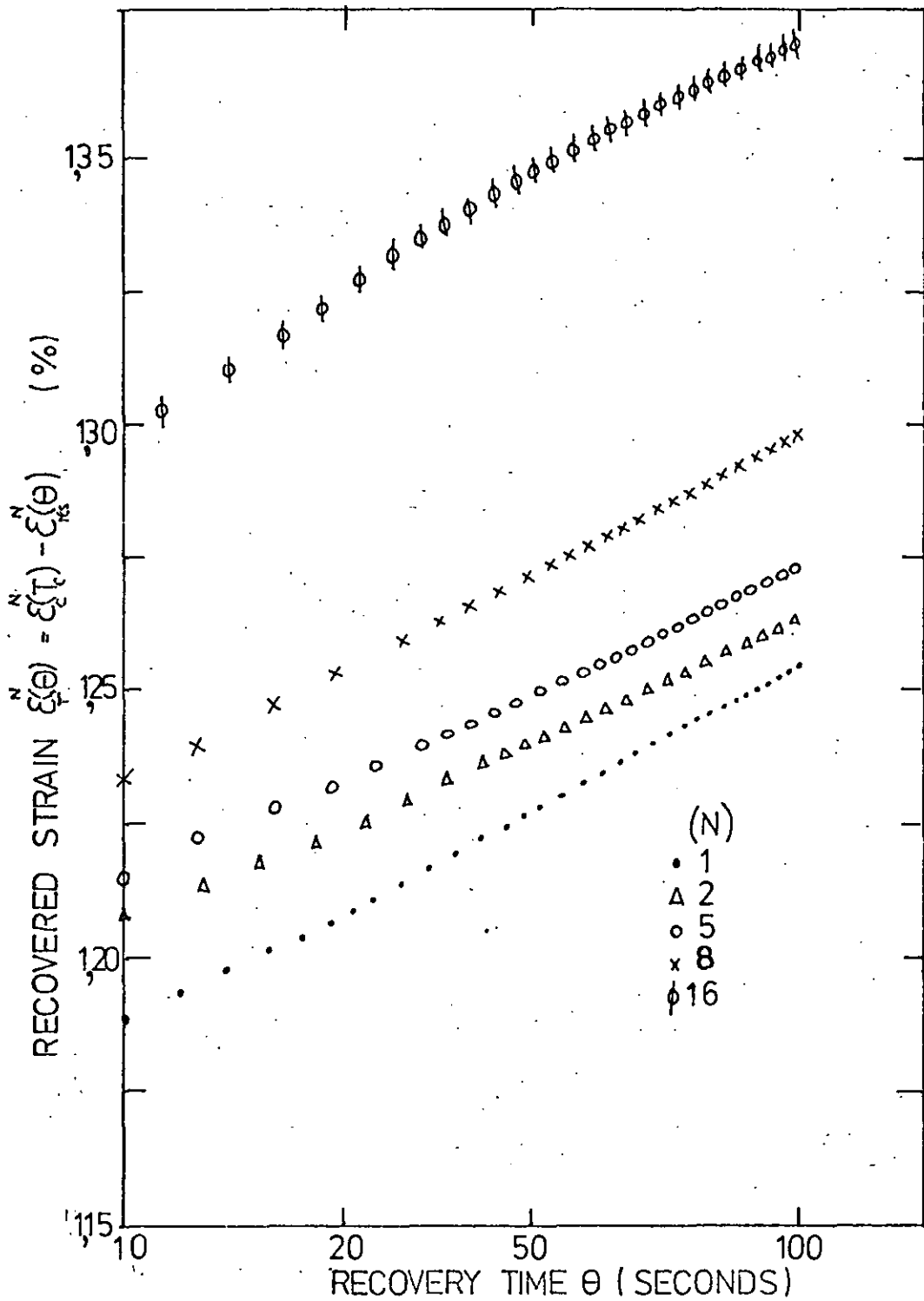


FIGURE 5,22 INDIVIDUAL RECOVERY CHARACTERISTICS AFTER VARIOUS CYCLES (N).  
 STRESS AMPLITUDE =  $40 \text{ MNm}^{-2}$   
 CREEP : RECOVERY PERIOD IN SECONDS (1320 : 120 )

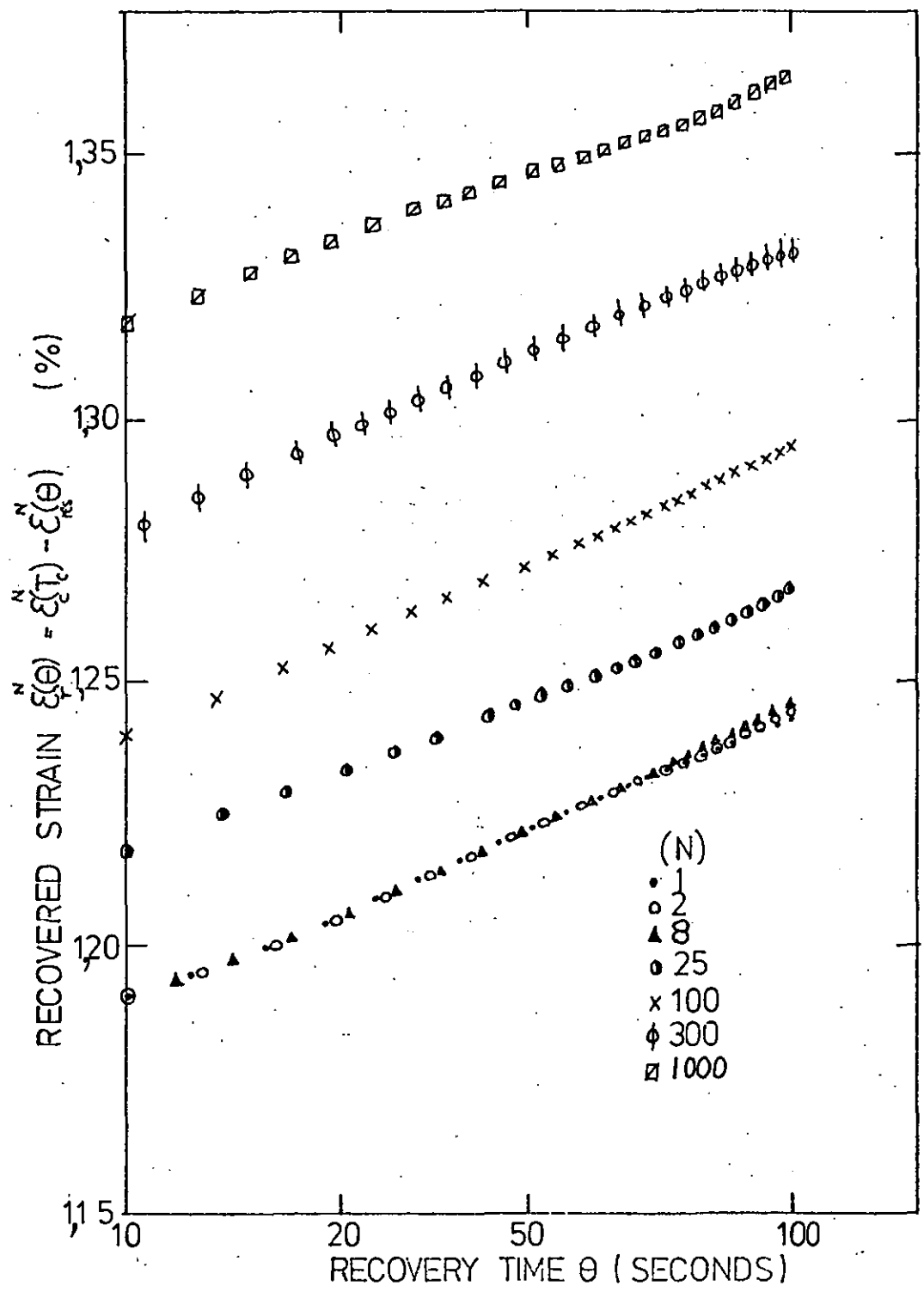


FIGURE 5,23 INDIVIDUAL RECOVERY CHARACTERISTICS AFTER VARIOUS CYCLES (N).  
 STRESS AMPLITUDE =  $40 \text{ MN.m}^{-2}$   
 CREEP : RECOVERY PERIOD IN SECONDS (120 : 120 )



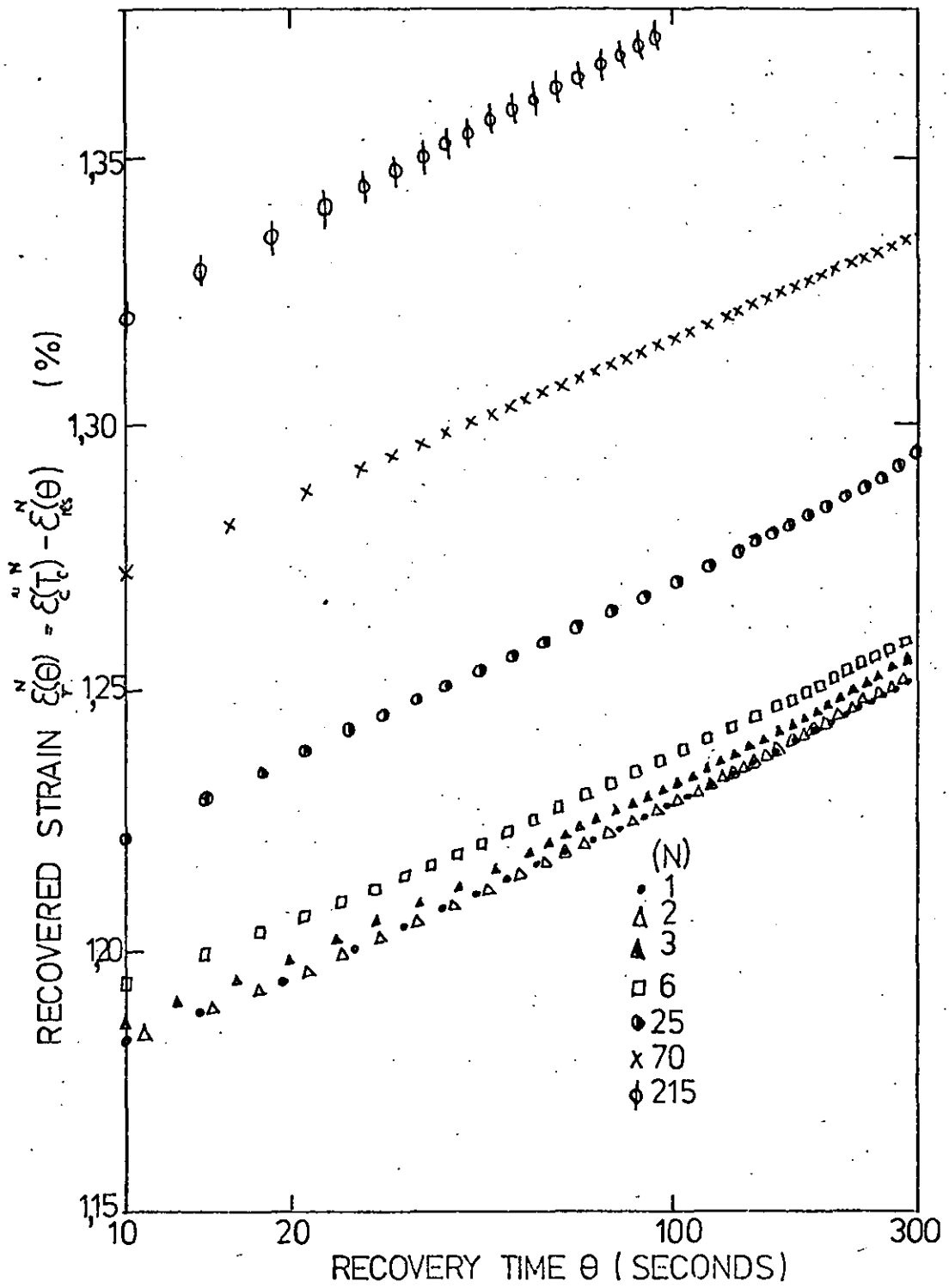


FIGURE 5,24. INDIVIDUAL RECOVERY CHARACTERISTICS AFTER VARIOUS CYCLES (N).  
 STRESS AMPLITUDE =  $40 \text{ MNm}^{-2}$   
 CREEP : RECOVERY PERIOD IN SECONDS (900 : 300)

$$\Delta R_{RR}^N(20) = (\epsilon_c^N(T_c) - \epsilon_{rs}^N(20)) - (\epsilon_c^I(T_c) - \epsilon_{rs}^I(20))$$

$$\therefore \Delta R_{RR}^N(20) = \epsilon_r^N(20) - \epsilon_r^I(20)$$

Thus the monitored values of  $\epsilon_c^N(T_c)$  and  $\epsilon_{rs}^N(20)$  and the values estimated from Figures 5.16-5.24 provide calculated values of  $\Delta R_{RR}^N(20)$ . These are plotted as a function of maximum cyclic creep strain  $\epsilon_c^N(T_c)$  in Figures 5.25, 5.26 and 5.27 for the stress amplitudes of 30, 35 and 40 MN/m<sup>2</sup> respectively.

#### 5.5. The Effect of n-Hexane Immersion

90% of the specimen gauge length was immersed in n-Hexane by means of a copper tube attachment as shown in Figure 5.28. The specimen was in contact with the solvent for 1 hour before the application of stress. The 20°C creep response at various stress levels is shown in Figure 5.29. The creep response of UPVC immersed in n-Hexane is initially identical to that generated in air. A very rapid acceleration of creep rate is observed after a period that increases with decreasing tensile stress, and at a strain that decreases with decreasing stress. This severe discontinuity is also evident in the 100-second isochronous plot shown in Figure 5.30. According to Bergen (34) this sudden increase in tensile compliance is due to craze initiation and growth. This was confirmed by replacing the copper tube by a glass tube. Visual detection of craze initiation coincided with the discontinuity.

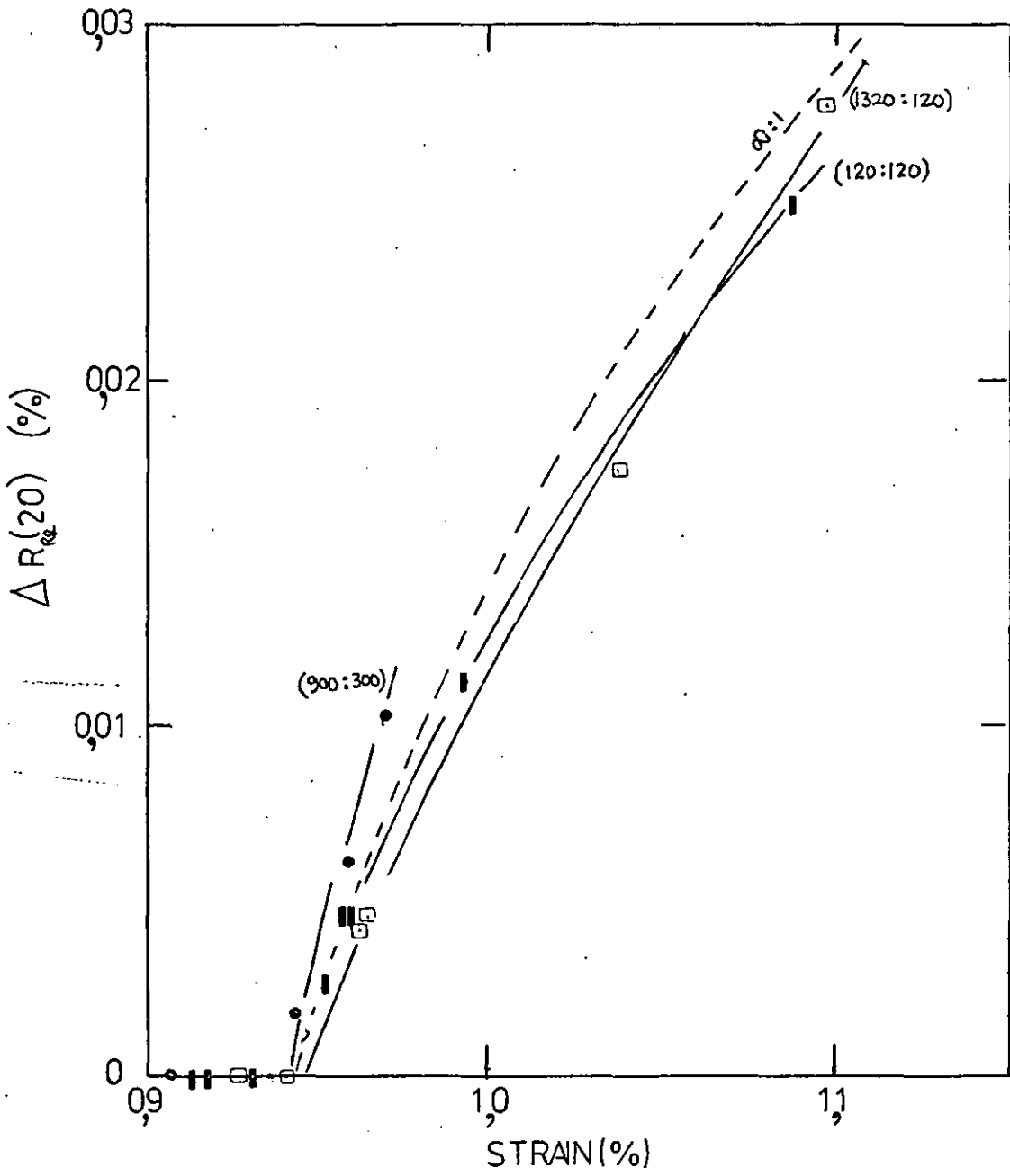


Fig. 5.25 The damage parameter as a function of tensile creep strain under static and intermittent stress of 30 MN/m<sup>2</sup>

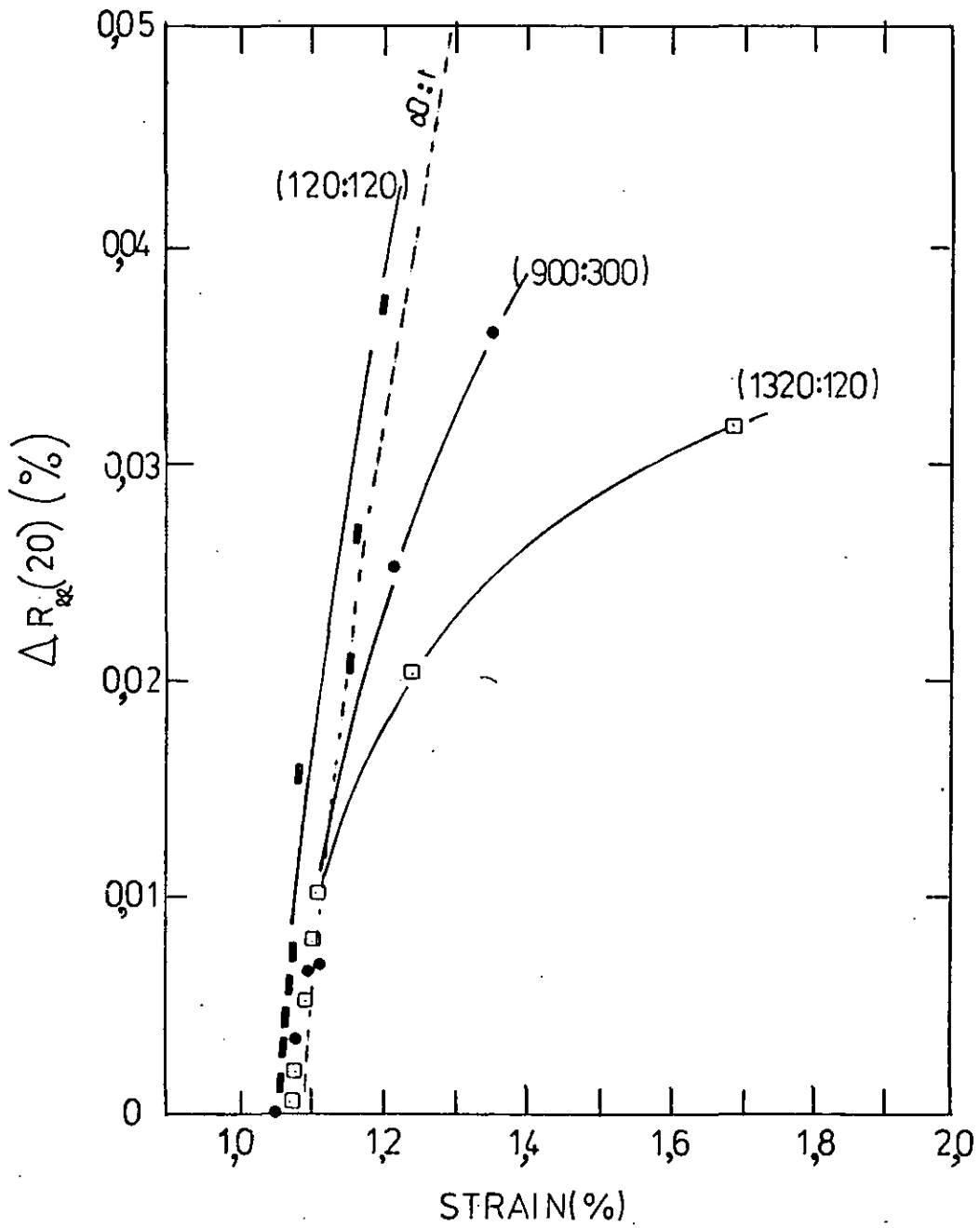


Fig. 5.26 The damage parameter as a function of tensile creep strain under static and intermittent stress of  $35 \text{ MN/m}^2$

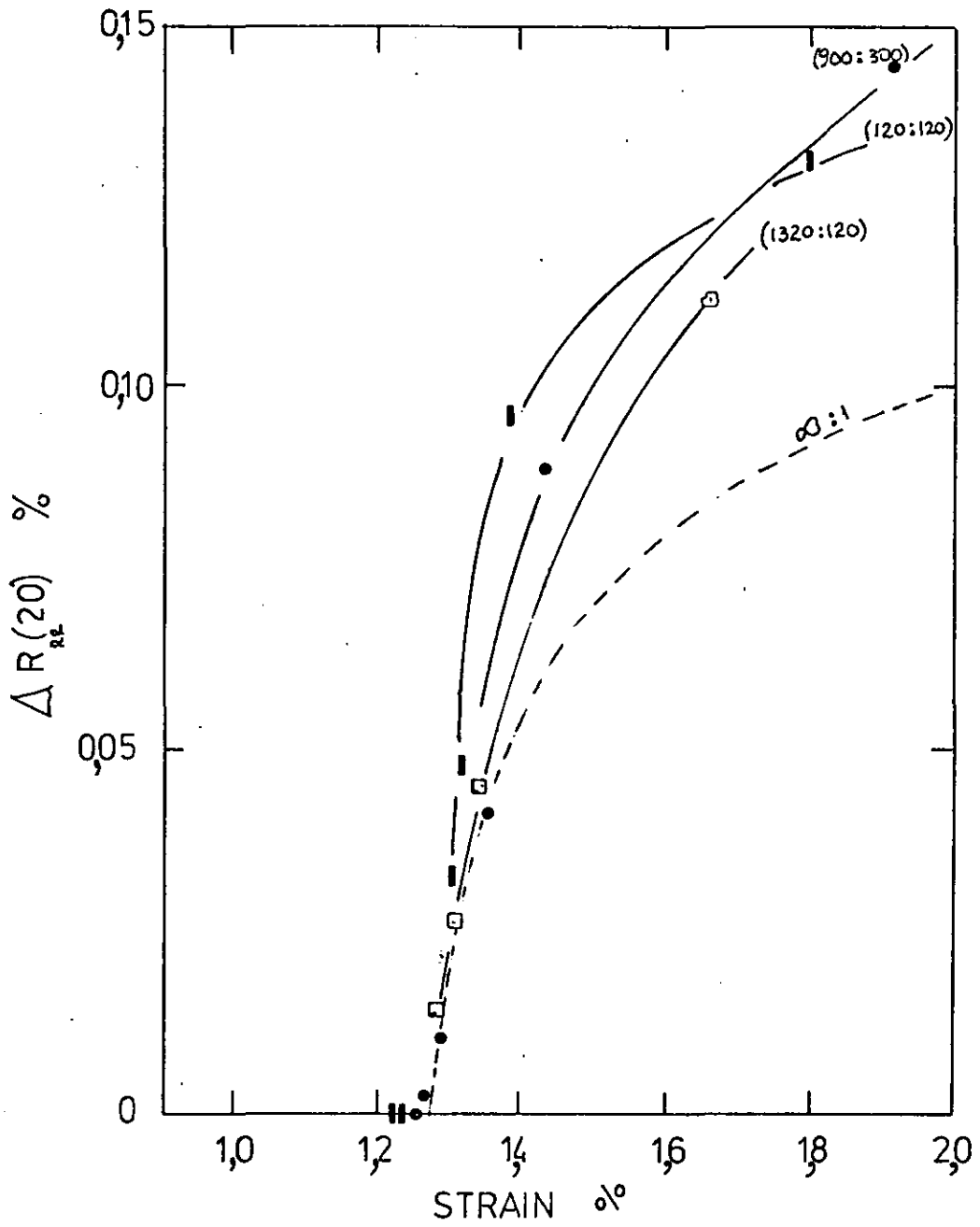


Fig. 5.27 The damage parameter as a function of tensile creep strain under static and intermittent stress of  $40 \text{ MN/m}^2$

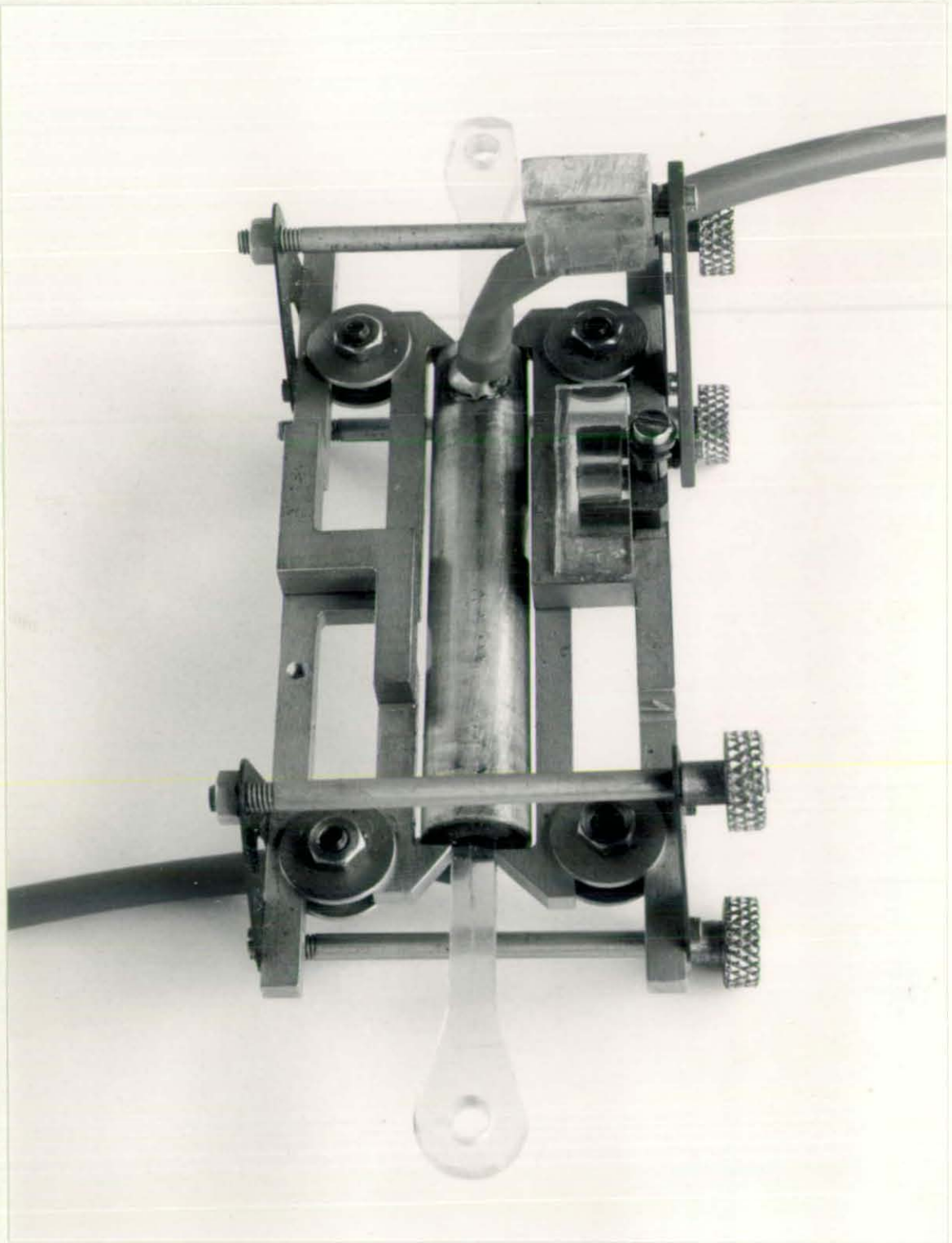


Fig. 5.28 Extensometer attachment for creep in liquid environments.

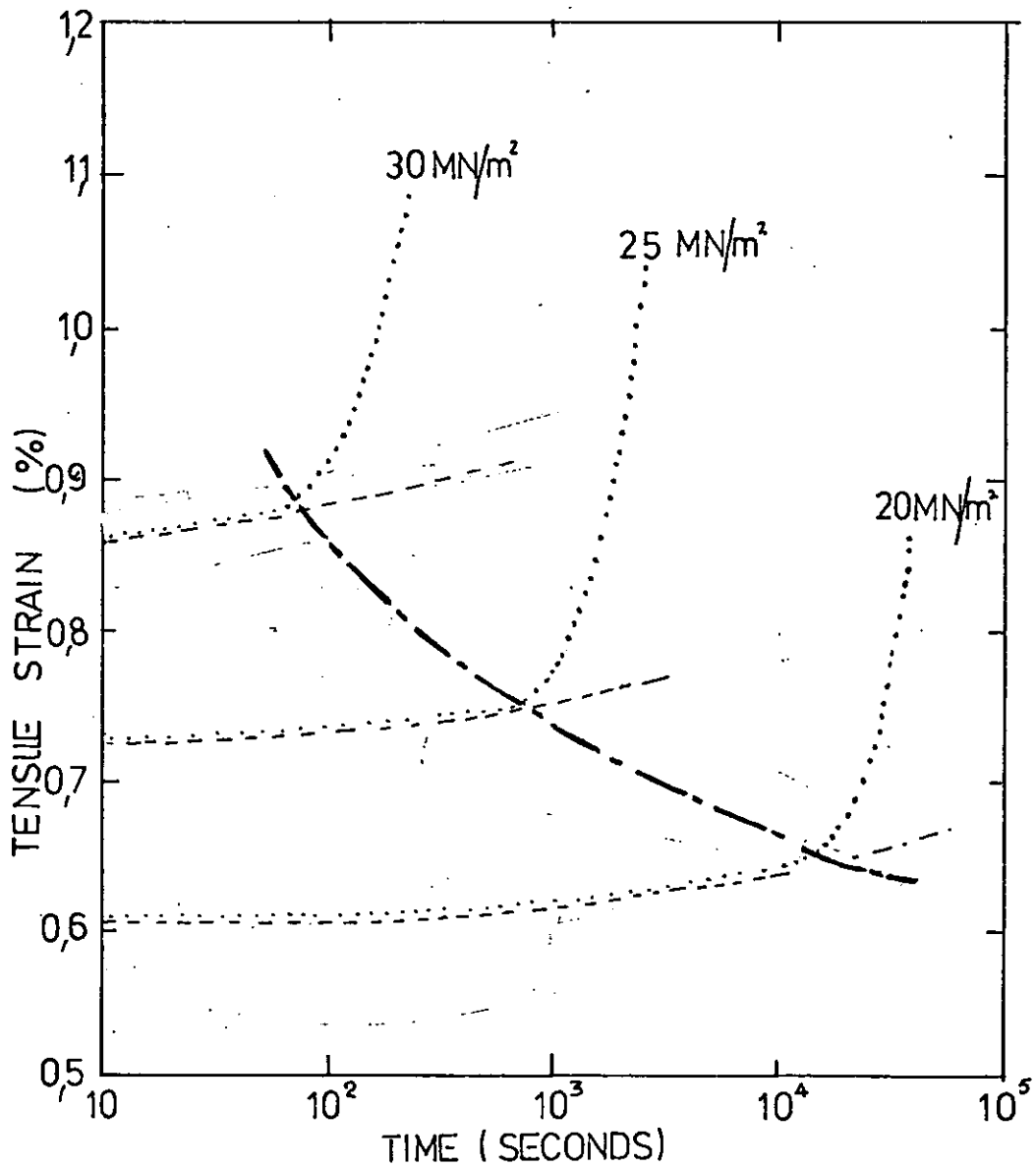


FIGURE 5.29 20°C CREEP RESPONSE OF UPVC.

- ..... IN N-HEXANE
- IN AIR
- . - . CRAZE INITIATION

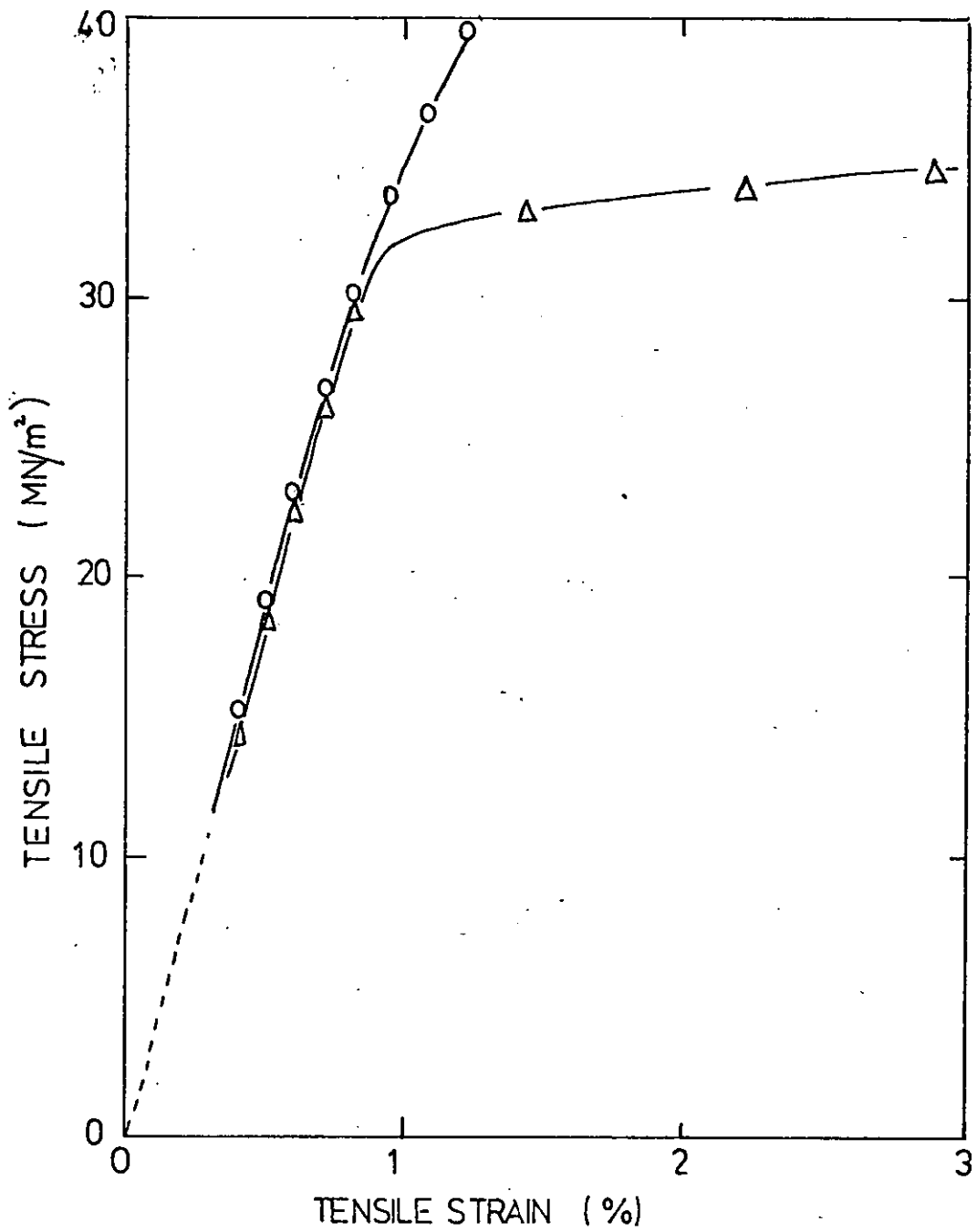


FIGURE 5,30 100 SECOND ISOCHRONOUS DATA

— o — IN AIR  
 — Δ — IN N-HEXANE



Further creep and recovery tests on UPVC immersed in n-Hexane were performed at stress levels and creep periods selected to investigate the value of  $\Delta R_{CR}^{(20)}$  in the region of the transition in creep rate.  $\Delta R_{CR}^{(20)}$  exhibited a transition from near zero values to positive values which coincided with the transition to rapid creep rates and crazing. This is shown graphically in Figure 5.31. Although this zero-positive transition was stable, the  $\Delta R_{CR}^{(20)}$  data above the transition proved to be very erratic and large negative values were often obtained.

Casual inspection of the specimens revealed that deeply craze damaged skins generally were connected with large negative values of  $\Delta R_{CR}^{(20)}$ . This was followed by a more exact measurement of craze depth. The edge of the specimen was polished and viewed through a travelling microscope. Both craze 'fronts' were regular and parallel to the sides of the specimen. Ten readings of craze depth were taken, five from each side within the gauge length. This provided the values of mean craze depth: specimen thickness ratio given in Table 5.4. The relationship between  $\Delta R_{CR}^{(20)}$  and this ratio shown in Figure 5.32 reveals a transition from positive to negative values of  $\Delta R_{CR}^{(20)}$  when the ratio exceeds 0.5. Thus two transitions can be observed:

- 1  $\Delta R_{CR}^{(20)} \Big|_{0 \rightarrow (+)}$  at craze initiation ( $A^* > 0$ )
- 2  $\Delta R_{CR}^{(20)} \Big|_{(+ \rightarrow (-)}$  when the undamaged core area vanishes. ( $A_c = 0$ )

Where  $A^*$  and  $A_c$  are defined in section 4.1.

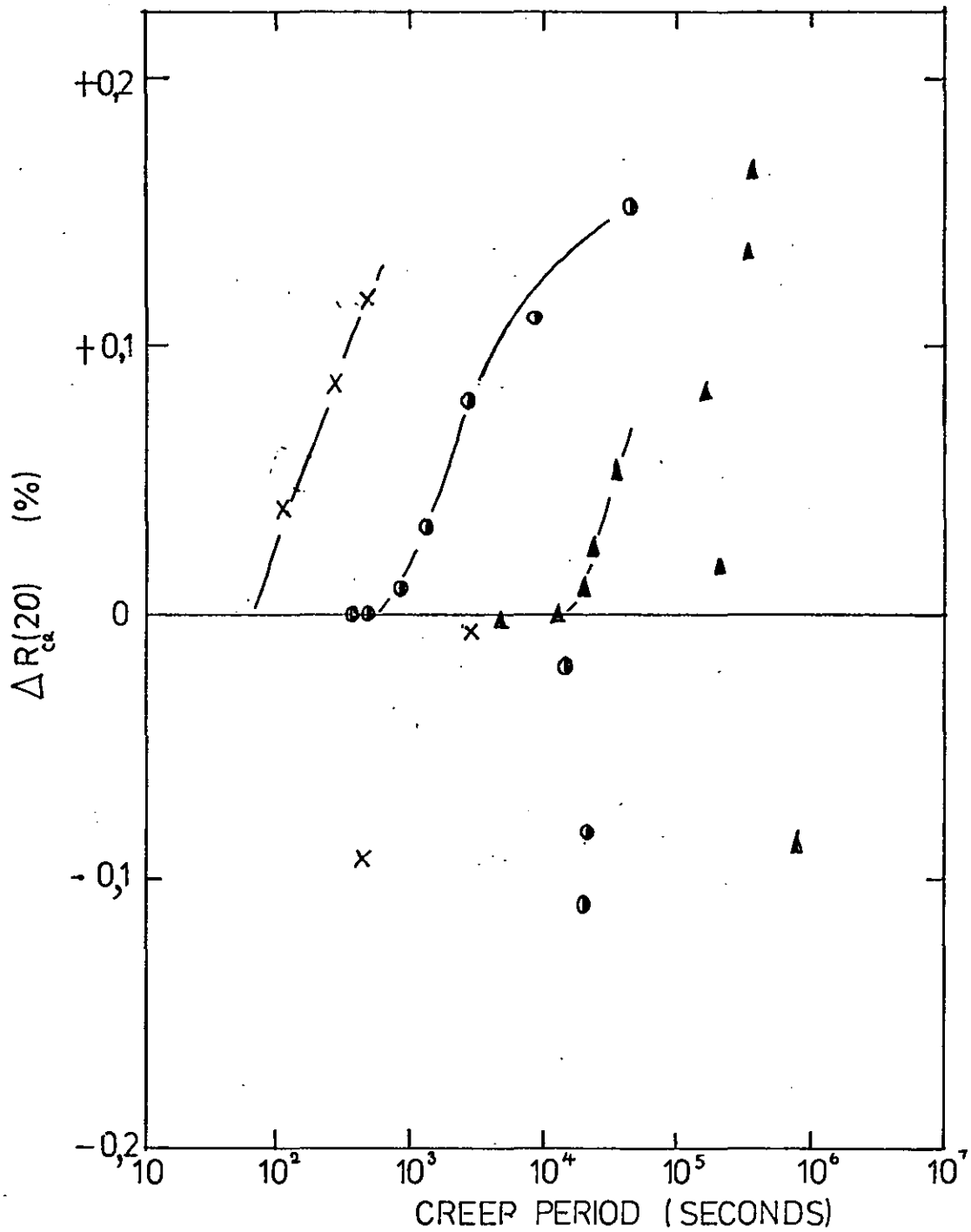


FIGURE 5.31 THE VALUE OF  $\Delta R_c(20)$  AFTER VARIOUS TENSILE CREEP PERIODS AT  $\times$  30,  $\circ$  25, AND  $\blacktriangle$  20 MN.m<sup>-2</sup>. UPVC IN N-HEXANE.

Stress Level MN/m <sup>2</sup>	Creep Period (secs.)	$\Delta R_{CR}(20)$ (%)	Craze Depth (mm)		Mean Craze Depth (mm) $\bar{d}$	Mean Specimen Thickness (mm) $\bar{b}$	$\frac{\bar{d}}{\bar{b}}$
			Side 1	Side 2			
25	$5 \times 10^2$	0.0	0.0	0.0	0.0	3.32	0.0
20	$10^4$	0.0	0.0	0.0	0.0	3.37	0.0
30	$10^2$	+0.03	0.38	0.36	0.37	3.37	0.11
30	$2.5 \times 10^2$	+0.096	0.796	0.81	0.803	3.34	0.24
25	$4.5 \times 10^3$	+0.120	1.22	1.22	1.22	3.40	0.36
25	$5.5 \times 10^4$	+0.174	1.52	1.52	1.52	3.31	0.46
20	$4 \times 10^5$	+0.162	1.80	1.84	1.82	3.32	0.55
30	$5 \times 10^2$	+0.114	1.90	1.90	1.90	3.34	0.51
25	$10^4$	+0.108	1.75	1.73	1.74	3.34	0.52
30	$6 \times 10^3$	-0.08	2.04	2.04	2.04	3.33	0.62
30	$4.5 \times 10^2$	-0.093	3.08	3.00	3.04	3.30	0.92
20	$9 \times 10^5$	-0.090	3.32	3.32	3.32	3.32	1.00
25	$2 \times 10^4$	-0.114	3.31	3.31	3.31	3.31	1.00
25	$2 \times 10^4$	-0.08	3.33	3.33	3.33	3.33	1.00

Table 5.4  $\Delta R_{CR}(20)$  for a range of Stress Histories and

$\frac{\text{mean craze depth}}{\text{specimen thickness}}$  ratios  $\left( \frac{\bar{d}}{\bar{b}} \right)$

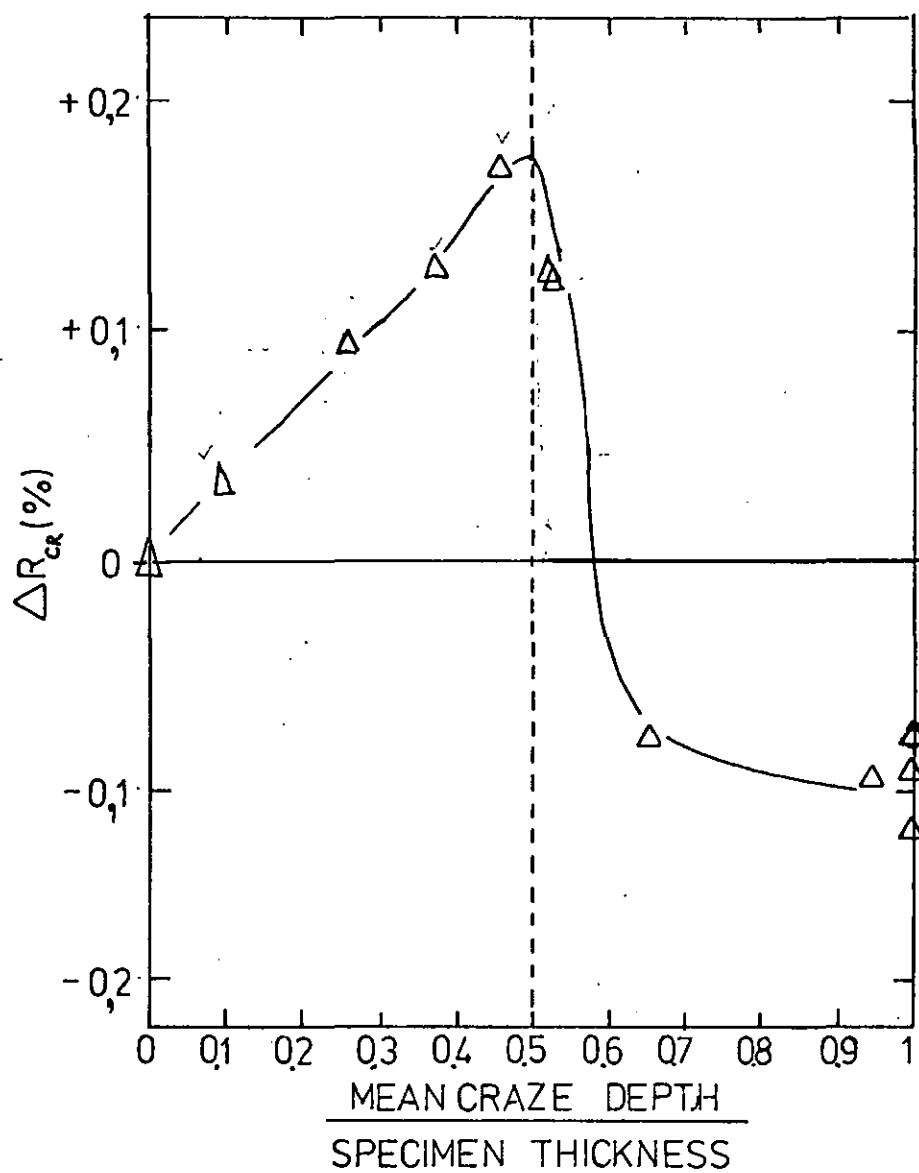


FIGURE 5.32 THE TRANSITION FROM POSITIVE TO NEGATIVE  $\Delta R_{cr}$  AS THE AREA OF UNDAAGED CORE APPROACHES ZERO. UPVC IMMERSED IN N-HEXANE,

## 5.6. Additional Test Results on Rubber Modified PPO (Noryl)

It has been established (152) that rubber modified glassy polymers suffer internally initiated craze damage in addition to surface crazing. It has never been explicitly stated that internal and surface crazing are initiated simultaneously, or whether external crazing precedes internal crazing. It would however be reasonable to assume that, because crazing is initiated at the boundary between the soft inclusions and the hard matrix, that the delay between surface and internal crazing is short. It is therefore of interest to check the validity of the core stress model by measuring  $\Delta R_{cr}^{(20)}$  for a rubber modified polymer.

A rubber modified polyphenylene Oxide (NORYL, General Electric Company Incorporated) was tested for creep and recovery at creep stresses of 25, 27.5 and 30 MN/m<sup>2</sup> at 20°C. The creep period was varied to cover a range of maximum creep strain  $\epsilon_c(T)$ .  $\Delta R_{cr}^{(20)}$  was measured in the manner previously described, and is plotted against  $\epsilon_c(T)$  in Figure 5.33.

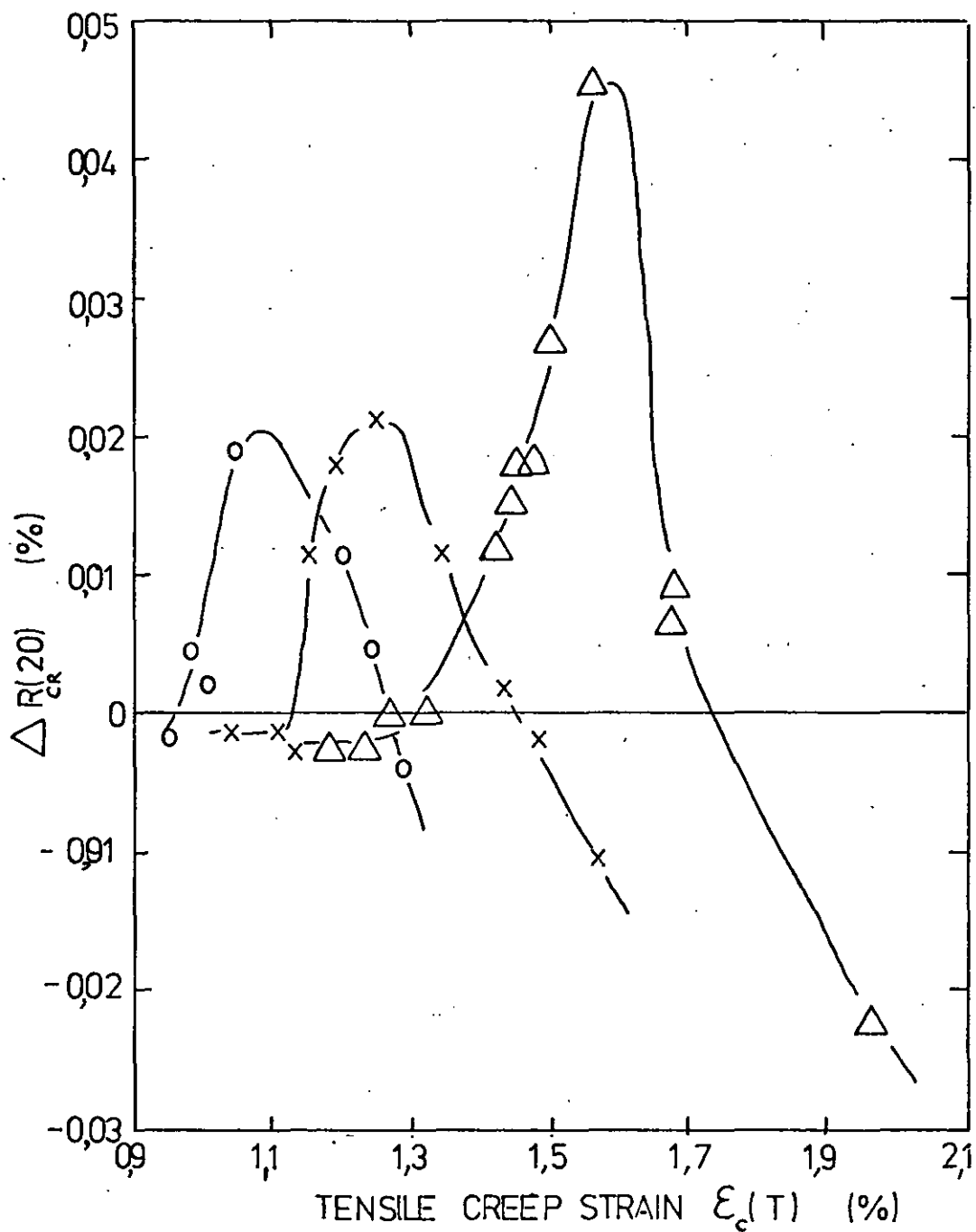


FIGURE 5.33 THE GROWTH OF  $\Delta R(20)$  WITH TENSILE STRAIN FOR RUBBER MODIFIED PPO.

- o 25 MN/m<sup>2</sup>
- x 27,5 "
- $\Delta$  30 "

## 6 Discussion of Results

The discussion will be developed, and sectionalised in accordance with the 'flow diagram' shown in Figure 6.1. This diagram includes the main elements for discussion, these being identified as (sections) 6.1 - 6.6. Three sections 6.1, 6.3, and 6.5, discuss the correlation between the established phenomenology of glassy polymers, (eg. craze initiation and growth, yield, fracture, and fatigue) and data or concepts presented in this thesis. The concepts are discussed in sections 6.2, 6.4, and 6.6. An abbreviated form of this discussion, and indeed of other parts of the thesis is included in reference (153).

### 6.1. The Damage Parameter and its Transitions

The damage parameter  $\Delta R$  is a strain based function which, according to the core stress model, (section 4.1), will exhibit two gross features. The first feature is a transition from zero to positive values, which if the model is valid, should coincide with the initiation of surface micro-damage. The second feature, according to the model, should be a 'sharp' reduction in  $\Delta R$  as the undamaged core area approaches zero. As the micro-damage is in the form of crazes the 'growth' of  $\Delta R$  during the period between the first and second transitions (features) should be qualitatively similar to the (known) growth characteristics of crazes.

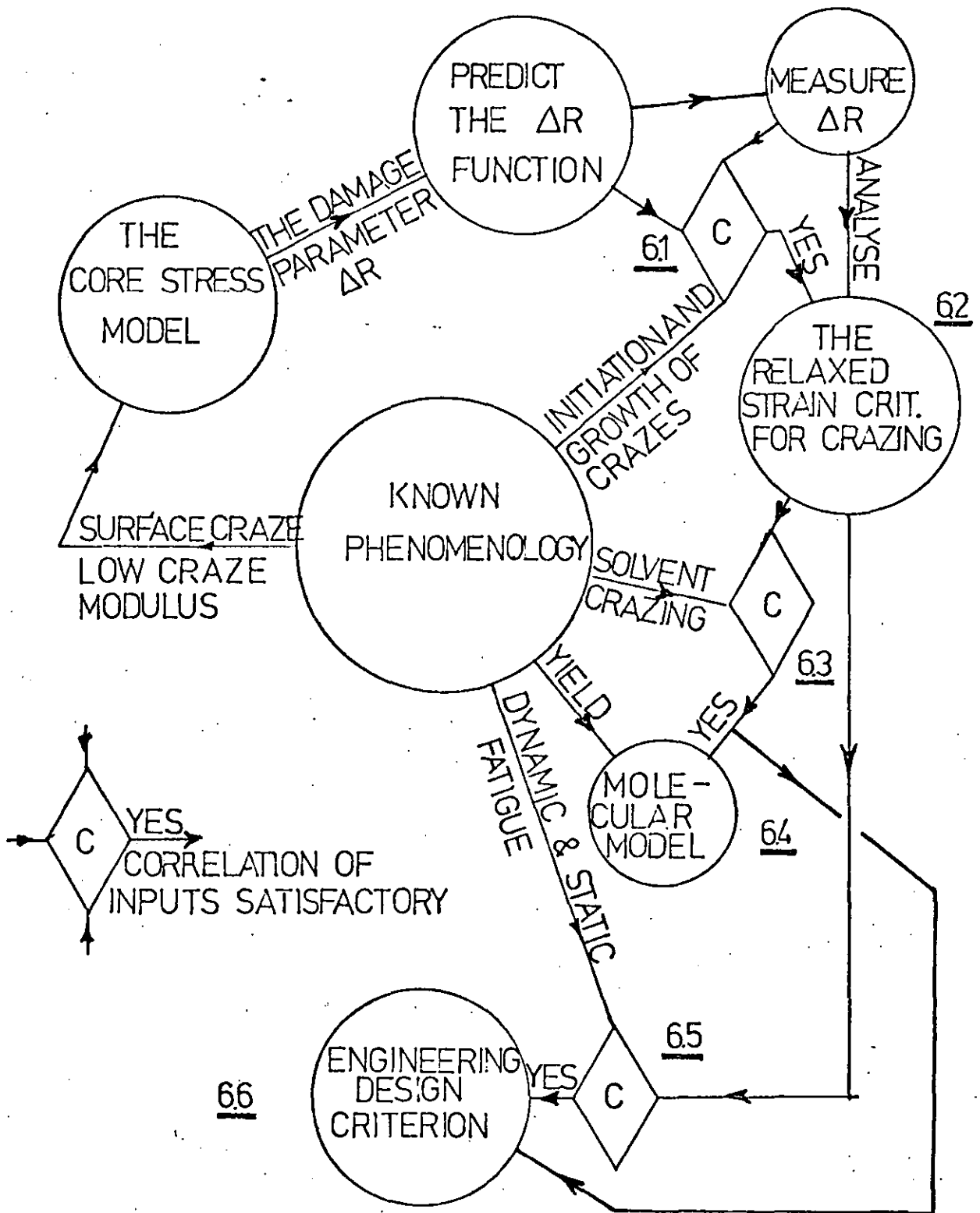


FIGURE 6.1 A FLOW DIAGRAM SHOWING THE PRINCIPAL ELEMENTS FOR DISCUSSION 6.1 - 6.6



### 6.1.1. The First Transition

It is evident from Figures 5.6 and 5.7 that for creep times below a critical time (induction period),  $\Delta R_{CR}(20)$  is near zero and negative, with typical values of between 0 and -0.009%. Negative values of  $\Delta R_{CR}(20)$  are in agreement with the predicted response of a classical linear viscoelastic solid (29), this being

$$\Delta R_{CR}(20) = \epsilon_c(\tau) - \epsilon_c(\tau + 20)$$

where  $\epsilon_c(\tau)$  is the creep strain at the end of the creep period  $\tau$ . It can therefore be stated with some justification that the strain response to a gate input of stress is linearly superposable. Thus as regards interaction, it is responding as a linear viscoelastic material during the induction period.

The induction period for the first transition increases with decreasing tensile stress and decreasing temperature. This is qualitatively similar to the effect of these variables on the induction period for craze initiation (27) (30) (102).

From Figures 5.8 and 5.9 it is apparent that the critical tensile strain for the first  $\Delta R_{CR}(20)$  transition decreases with decreasing tensile creep stress. Again this is qualitatively similar to the effect of this variable on the critical tensile strain for craze initiation. Figure 6.2 combines the stress, strain and time co-ordinates of the first  $\Delta R_{CR}(20)$  transition.

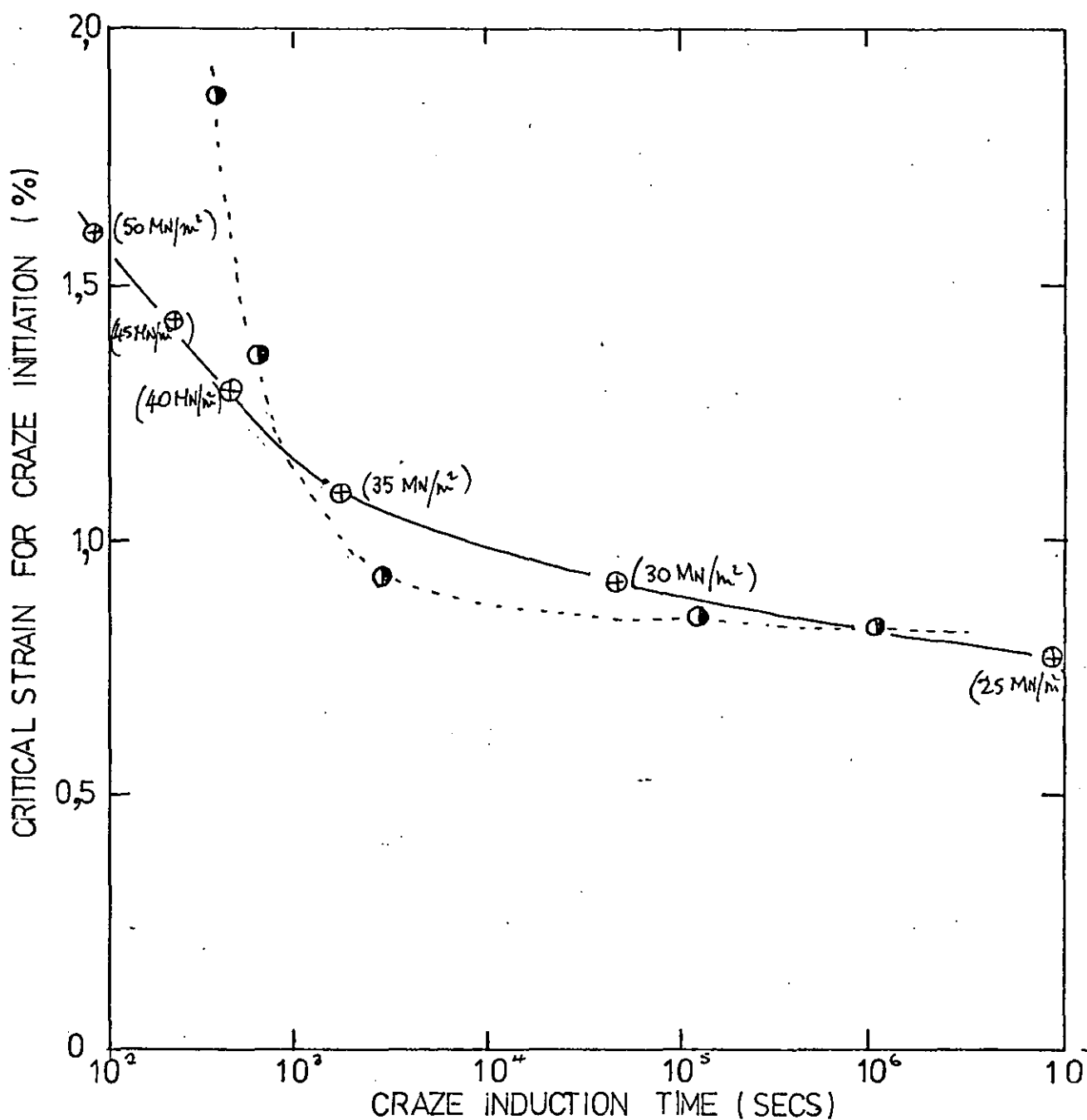


FIGURE 6,2 THE CRITICAL STRESS (IN BRACKETS), STRAIN, TIME COORDINATES FOR CRAZE INITIATION ● (116) AND THE 1st TRANSITION IN  $\Delta R_{c_2}(20)$  ⊕ FOR UPVC AT 20°C

Included in Figure 6.2 is the stress, strain, and time co-ordinates for craze initiation in UPVC as detected visually by Menges et al (116). The correlation between the two curves is good considering that the grades of UPVC are different.

The existence of the first transition in the strain function  $\Delta R_{cr}^{(20)}$ , its mode (near zero to positive) and the stress and temperature dependence of the critical tensile strain, and induction period of the transition closely resembles and coincides with the known phenomenology of craze initiation. This therefore supports the hypothesis that the transition to positive  $\Delta R_{cr}^{(20)}$  is a direct effect of craze initiation. Furthermore the first transition in  $\Delta R_{cr}$  is so localised that it would not be satisfactorily accounted for by the application of continuum mechanics.

The critical strain for the first transition of  $\Delta R_{cr}^{(20)}$  coincides with that of  $\Delta R_{RR}^N(20)$  under equivalent stress or stress amplitude conditions. This is shown in Figures 5.25, 5.26 and 5.27. It has previously been reported (30) that the critical strain for craze initiation under static and dynamic loading (applied static stress = dynamic stress amplitude) are identical. The coincidence of the  $\Delta R_{cr}$  and  $\Delta R_{RR}$  transitions is thus further evidence in support of the core stress model. In addition, of course, the coincidence promotes the concept of a strain based design criterion.

### 6.1.2. The Growth of $\Delta R_{cR}^{(20)}$

The rate of growth of  $\Delta R_{cR}^{(20)}$  increases with the level of applied tensile stress. This is in agreement with the dependence of craze growth rate observed by Regal (123) Sato (124) and Sauer et al (127).

Knight (102) in a review of the subject of craze initiation and growth identifies three separate phases in the growth of crazes. The first phase is one of initial rapid growth rate followed by a second phase of slow growth, and finally a tertiary phase of high and constant growth rate. At high temperatures or stress levels, or in the presence of crazing agents, the primary and secondary phases are not readily discernible. The growth characteristics of crazes are therefore qualitatively similar to  $\Delta R_{cR}^{(20)}$  as shown in Figures 5.6 and 5.7.

An interesting feature observed during the growth of  $\Delta R_{cR}^{(20)}$  is its apparently singular value at a strain of 1.6% (Figure 5.8) and 1.4% (Figure 5.9). At 200C the value of  $\Delta R_{cR}^{(20)}$  is 0.1% for a tensile strain of 1.6%, this being independent of the stress level (and by implication also of the induction period). At 350C the feature is observed at  $\Delta R_{cR}^{(20)} = 0.08\%$  and  $\epsilon(\eta) = 1.4\%$ . If it is assumed that, at stress levels above those used to generate the data in Figures 5.8 and 5.9, the singularity is still operative then this would predict an infinite growth rate for  $\Delta R_{cR}^{(20)}$  and therefore, by association, an infinite rate of craze growth, at stress levels of  $\sim 60 \text{ MN/m}^2$  and  $42.5 \text{ MN/m}^2$

at temperatures of 20°C and 35°C respectively. An infinite rate of craze growth or craze nucleation would imply macroscopic yielding. The tensile yield stress of UPVC at a strain rate of 50%/minute and at 20°C and 35°C is recorded (154) as 57 and 46 MN/m<sup>2</sup>, respectively.

### 6.1.3. The Second Transition

The second transition was not observed in the  $\Delta R_{cr}(20)$  function with UPVC tested in an air environment. However the second transition is exhibited unambiguously in the data for UPVC immersed in n-Hexane. This is shown in Figure 5.32. The transition coincides with the extinction of the undamaged core by the advancing craze fronts. This is predicted by the core stress model and must be regarded as singly the most convincing evidence for the validity of the model.

The absence of the second transition in  $\Delta R_{cr}(20)$  for UPVC tested in air could be due to the irregular craze front observed in these specimens. By comparison the craze fronts observed in n-Hexane immersed specimens were regular. This regularity was noted by Crook et al (138) who proposed that the advance of the craze front was strongly controlled by the diffusion characteristics of the solvent. The diffusion proceeds by case II transport (155).

The second transition is also clearly present in the  $\Delta R_{cr}(20)$  function for rubber modified PPO. This is shown in Figure 5.33. The maximum positive value of  $\Delta R_{cr}(20)$  is small compared with the UPVC data. The core stress model is strictly

not applicable to inhomogeneous polymers where internal and surface craze initiation is simultaneous. The model does however appear to be valid at very low levels of damage. This could be because:

- (a) Surface crazing just precedes internal crazing.
- (b) The crazes collapse rapidly (132).
- (c) Although surface crazing and internal crazing is initiated simultaneously, at low levels of damage small undamaged cores are still present in the specimen gauge length. This is shown (2-dimensionally) in Figure 6.3.

## 6.2. The Relaxed Strain Criterion for Craze Initiation

The various criteria previously proposed for craze initiation in glassy amorphous polymers have all failed to account satisfactorily for many aspects of the phenomenon. Simple stress and strain criteria cannot explain the time-dependence of craze initiation. The adoption of these criteria and their further development into design limits (30), even though they have been proved on many occasions not to be singular, is justified only because of the lack of comprehensive and accurate craze initiation data. The major objective of the experimental programme reported in Chapter 5 was to generate by an objective mechanical method, initiation data to a high degree of resolution. Evidence was presented in section 6.1 which indicated that there is a direct coincidence between the initiation of positive values in the strain based functions  $\Delta R_{cc}$ ,  $\Delta R_{cl}$  and  $\Delta R_{RR}$  and craze initiation. The

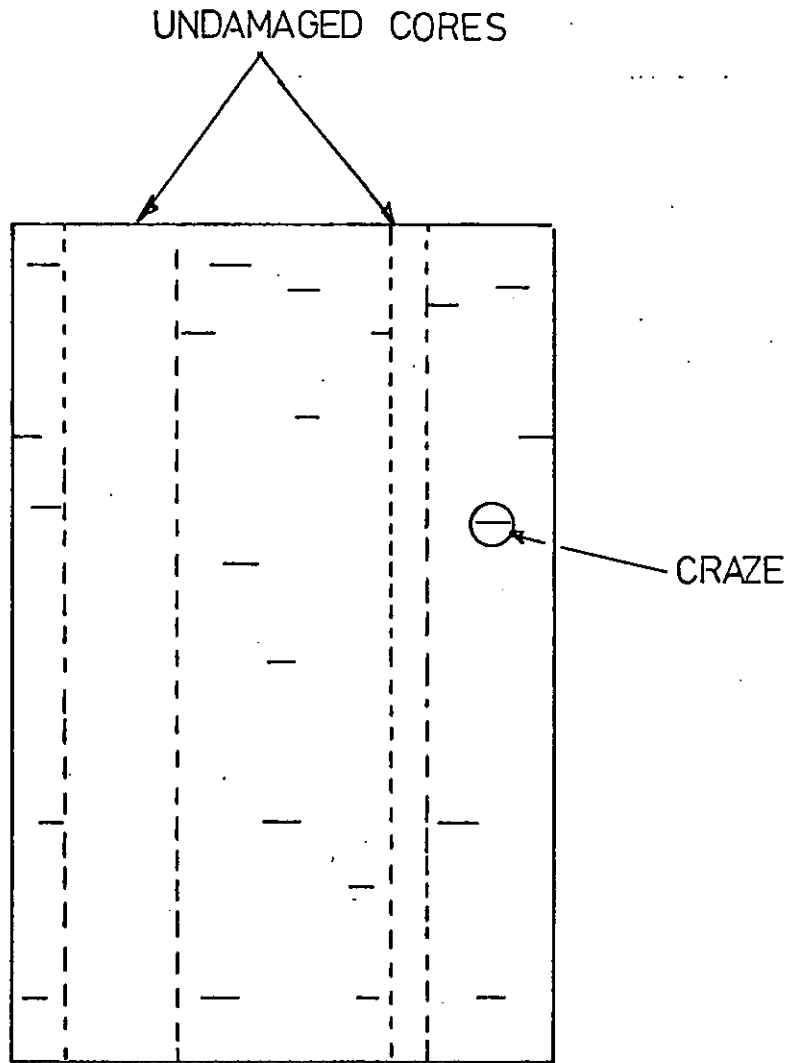


FIGURE 63 POSSIBLE LOW DENSITY DISTRIBUTION OF CRAZE SITES IN A RUBBER MODIFIED POLYMER

service variables that operate at craze initiation cover a range that should offer the possibility of delineating a criterion that is singular and therefore identifiable as the cause of initiation.

If the data in Figure 6.2 <sup>are</sup> ~~is~~ examined in isolation it could be concluded that after long induction periods the 'critical strain' for craze initiation is approaching an asymptotic minimum. This conclusion has been reached by Menges et al (30), (115), (116), (117), (118) who termed this minimum  $\epsilon_{\infty}$ . However if Figures 5.8 and 5.9 are also examined, this conclusion would no longer appear to be justified. The critical strain  $\epsilon_{cr}$  for craze initiation decreases linearly with decreasing tensile stress. There is no evidence in Figures 5.8 and 5.9 to suggest that on further decreasing the tensile stress the value of  $\epsilon_{cr}$  would not fall below  $\epsilon_{\infty}$  ( $\sim 0.85\%$ ). The linearity between  $\epsilon_{cr}$  and  $\sigma_N$  can be appreciated by reference to Figure 6.4 (20°C) and 6.5 (35°C). The co-ordinates  $(\epsilon_{cr}, \sigma_N)$  have been estimated from the intercepts ( $\Delta R_{cr}(\infty) = 0$ ) in Figures 5.8 and 5.9.

Included in Figures 6.4 and 6.5 are the respective values of  $\epsilon_c^{(1)}$  versus  $\sigma_N$  estimated by extrapolation of the creep data in Figures 5.1 and 5.3.  $\epsilon_c^{(1)}$  is the creep strain 1 second after the application of tensile stress  $\sigma_N$ . By definition:

$$\epsilon_c^{(1)} = J^{(1)} \sigma_N$$

Where  $J^{(1)}$  is the 1 second creep compliance. At 20°C and 35°C, the critical strain for craze initiation  $\epsilon_{cr}$ , versus  $\sigma_N$  characteristic is parallel to the  $\epsilon_c^{(1)}$  versus  $\sigma_N$  characteristic.



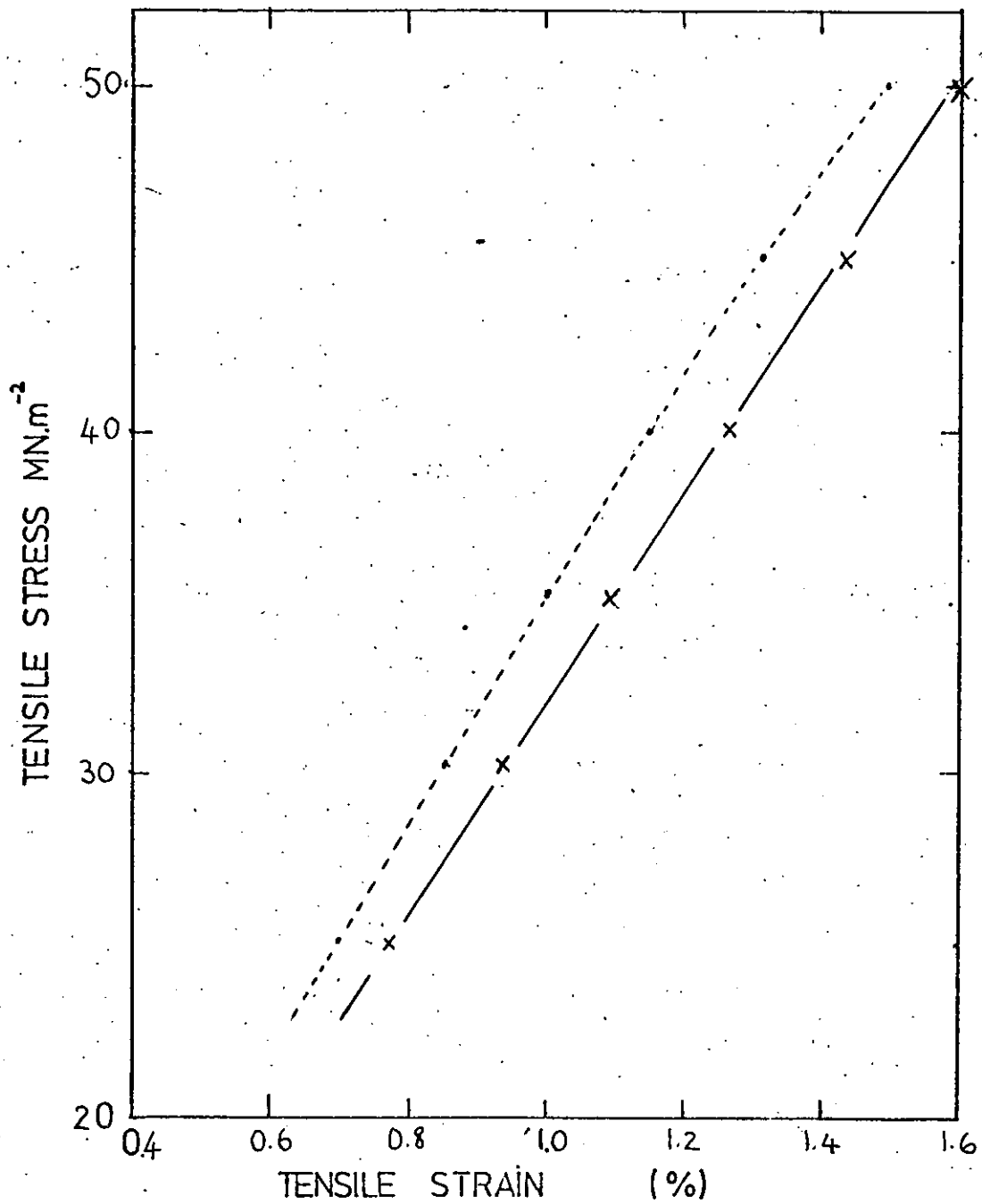


FIGURE 6, 4. THE CRITICAL STRESS STRAIN COORDINATES FOR CRAZE INITIATION IN UPVC AT 20 °C. ALSO INCLUDED IS THE 1 SECOND ISOCHRONOUS STRESS STRAIN DATA -----•-----

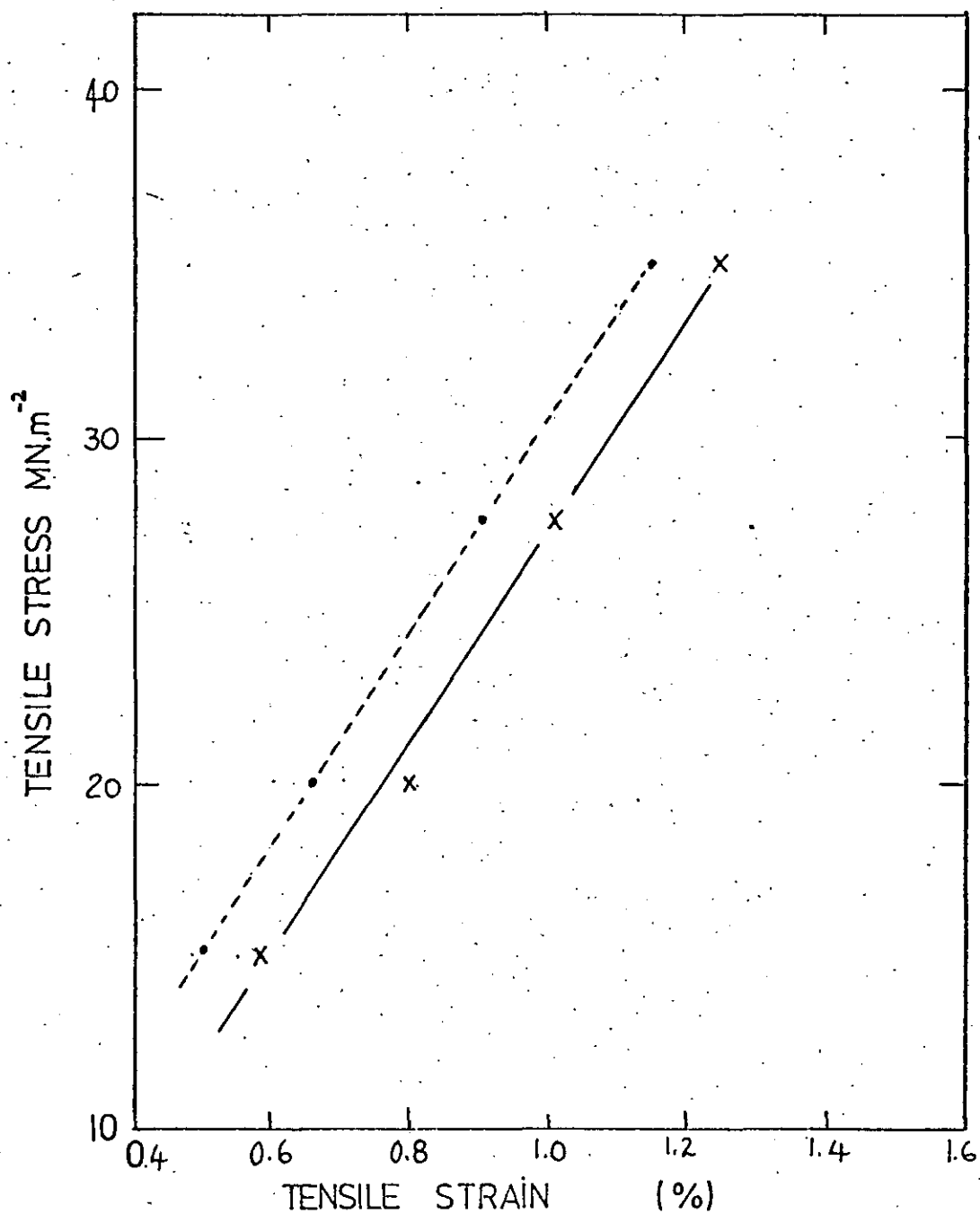


FIGURE 6, 5 THE CRITICAL STRESS STRAIN COORDINATES FOR CRAZE INITIATION IN UPVC AT 35°C. ALSO INCLUDED IS THE 1 SECOND ISOCHRONOUS STRESS STRAIN DATA

Thus:

$$\epsilon_{cr} = J(t) \sigma_N + K \quad [16]$$

Where K is a strain based constant. From Figures 6.4 and 6.5 it can be seen that K has a value in the region of 0.1%. From Figures 5.1 and 5.3 it would appear that the creep curves are approaching an asymptote at short creep times. Therefore it is assumed that:

$$J(t) - J(0) \ll K$$

and equation [16] can be simplified (conceptually) to:

$$\epsilon_{cr} = J(0) \sigma_N + K \quad [17]$$

The term  $J(0) \sigma_N$  can be identified as the initial, elastic, or unrelaxed strain component  $\epsilon(0)$ . All strains can be conveniently separated into two components  $\epsilon(0)$  and  $\epsilon_{rel}$ , where  $\epsilon_{rel}$  is the time dependent, inelastic, or relaxed strain component. Thus equation [17] becomes:

$$\epsilon_{cr} = \epsilon(0) + (\epsilon_{rel})_{cr} \quad [18]$$

The experimental values of  $\epsilon_{cr}$ , and the estimated values of  $(\epsilon_{rel})_{cr}$  and  $\epsilon(0)$  are given in Table 6.1 for various stress levels at 20°C and 35°C. It is evident that:

$$(1) \quad (\epsilon_{rel})_{cr} \sim 0.1\%$$

and (2) That the 0.1% relaxed strain criterion is singular, being independent of  $\sigma_N, \epsilon_{cr}$ , time and temperature over the range studied.

Temp. (°C)	Stress (MN/m <sup>2</sup> )	$\epsilon(0)$ (%)	$\epsilon_{cr}$ (%)	$(\epsilon_{rel})_{cr}$ $= \epsilon_{cr} - \epsilon(0)$ (%)
20	25	0.69	0.77	0.08
	30	0.85	0.94	0.09
	35	1.00	1.10	0.10
	40	1.16	1.28	0.12
	45	1.32	1.43	0.11
	50	1.49	1.60	0.11
35	15	0.50	0.59	0.09
	20	0.67	0.80	0.13
	27.5	0.90	1.01	0.11
	35	1.16	1.26	0.10

Table 6.1. The critical relaxed strain  $(\epsilon_{rel})_{cr}$  for various stress levels at 20 and 30° C.

The implication is, therefore, that crazing is initiated when the relaxed tensile strain component equals or exceeds 0.1%. Although the service variables of stress and temperature combine to <sup>a/</sup> effect the total tensile strain and induction time for craze initiation these variables do not apparently affect the singularity of the critical relaxed strain.

The minimum total tensile strain for craze initiation in UPVC is therefore proposed not to be  $\sim 0.85\%$  as suggested by Menges et al (30), but 0.1%. This condition is satisfied when:

- (3) The induction time for crazing approaches infinity and the stress approaches zero.
- or
- (4) The temperature is such that all strains generated are fully relaxed within the considered time scale  $t$ . This occurs when  $J(t)$  approaches zero.

### 6.3 The Relaxed Tensile Strain Criterion and Solvent Crazing

The substantial reduction in crazing stress and strain by immersion in organic solvents (discussed in section 3.2.3) is considered to be the basis of the most severe test for any craze initiation criterion.

Solvent crazing has been studied using stress relaxation (135), (136), (137), (138), and tensile creep (34), (156). Bergen

(34) concluded from his data (see Figure 2.5) that solvent crazing is initiated at a critical level of tensile strain, which is independent of stress level. This conclusion has considerably strengthened the critical strain hypothesis of Menges et al. However, independent examination of Bergen's data does not support this conclusion because a significant decrease in critical strain with decreasing stress level can be discerned. The opinion that Bergen's conclusion was unjustified has also been expressed recently by McCammond and Ward (156). They repeated Bergen's experiments on the creep of ABS and UPVC in isopropanol and observed a linear relationship between craze initiation strain (as detected by the transition to high creep rates) and tensile stress. Critical stress/strain data on ABS <sup>are</sup> given in Table 6.2

$\epsilon_{cr}(\%)$	$\sigma_N \text{ MN.m}^{-2}$
0.275	7.0
0.33	8.75
0.36	10.5

Table 6.2. The critical strain  $\epsilon_{cr}$  at various stress levels  $\sigma_N$  for craze initiation in ABS immersed in isopropanol. McCammond and Ward (156)

Although the data in Table 6.2 <sup>are</sup> insufficient for curve fitting it is of interest to note that the 'best straight line' through these points is:

$$\epsilon_{cr} = 0.115 + 0.0228 \sigma_N \quad (\%)$$

This implies a critical relaxed strain of 0.115%.

The craze initiation in UPVC immersed in N-Hexane as shown in Figure 5.29 supports the relaxed strain criterion. The stress/strain co-ordinates for solvent crazing are shown in Figure 6.6. Again it is evident that the critical strain for craze initiation is linearly related to the creep stress. Also the predicted minimum critical strain at near zero levels of stress is in the region of 0.14%

Solvent crazing under conditions of stress relaxation is by far the more common test method. Conventionally, a strip of polymer with a rectangular cross-section is bent over a rigid frame. The tensile skin strain  $\epsilon_s(\lambda)$  is known and determined only by the geometry of the test apparatus and the specimen dimensions. The specimen is immersed in the solvent and the position of the craze front  $x_0$  after a time  $t_R$  defines the critical strain for craze initiation  $\epsilon_s(x_0, t_R)_{cr}$ . Alternatively the specimen can be pre-soaked in the solvent (to achieve equilibrium solvent/polymer mixtures) prior to the imposition of flexural deformation. This has the advantage of eliminating additional stresses due to solvent induced swelling.

The solvent crazing strain data published by Kambour (136), Kambour and Bernier (135), and Crook, Earl, Johns, and Loneragon (138) have been discussed previously in section 3.2.3. This <sup>see</sup> data <sup>are</sup> is of particular interest because the degree of solvent plasticization was quantified in terms of the effective Tg of the polymer/solvent mixture. With reference to Figures 3.3 and 3.4 and Table 3.3, two features are identified:

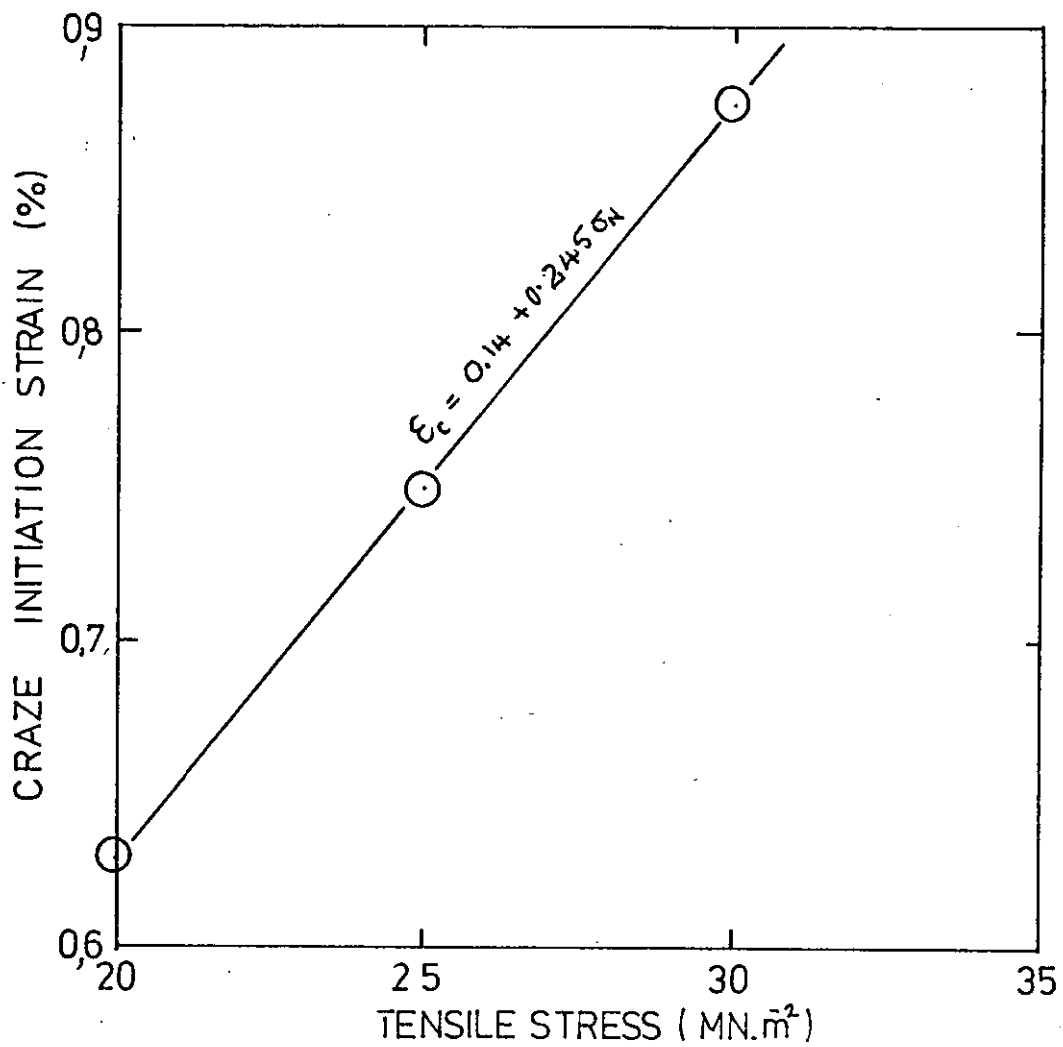


FIGURE 66 THE LINEAR DEPENDENCE OF CRAZING STRAIN ON CREEP STRESS FOR UPVC IN N HEXANE AT 20°C



- (1) When the solvent/polymer mixture and test temperature  $T_T$  is such that  $(T_g - T_T) \leq 0$ , the critical strain for solvent crazing is a minimum and independent of the value of  $(T_g - T_T)$ . The minimum tensile strains in Kambour's (136) measurements were invariably  $\sim 0.1\%$ . Crook et al reported values between 0.05% and 0.4%.
- (2) When  $(T_g - T_T) > 0$  Kambour's data (Figure 3.3) reveals an increasing critical strain with increasing  $(T_g - T_T)$ . The critical strains reported by Crook et al however, are independent of  $(T_g - T_T)$  in this range.

Both features can be predicted satisfactorily by the relaxed strain hypothesis. Equation [18] can be presented in terms of compliance loss. According to the relaxed strain hypothesis, crazing in UPVC is initiated when:

$$\sigma_N (\bar{J}(t) - \bar{J}(0)) \geq 0.001 \quad [19]$$

Where  $\sigma_N$  is the tensile stress and  $\bar{J}(t)$  and  $\bar{J}(0)$  the tensile creep compliances as measured  $t$  and 0 seconds after the application of stress. Equation [19] can be generalised to:

$$\sigma_N (\bar{J}(t) - \bar{J}(0)) \geq (\epsilon_{rel})_{cr} \quad [20]$$

where  $(\epsilon_{rel})_{cr}$  is the characteristic critical relaxed strain for craze initiation. For a bent strip test with an applied tensile skin strain  $\epsilon_s$ , equation [20] can be modified for the stress relaxation mode. This assumes that  $\bar{E}(t) = \bar{J}(t)^{-1}$ :

$$\epsilon_s \left( 1 - \frac{\bar{E}(t)}{\bar{E}(0)} \right) \geq (\epsilon_{rel})_{cr} \quad [21]$$

where  $E(0)$  and  $E(t)$  are the instantaneous and time dependent relaxation moduli. It would be reasonable to assume that at temperatures above  $T_g$  and for finite test periods  $t_R$ :

$$E(t_R) \ll E(0)$$

Therefore the relaxed strain hypothesis via equation (21) would predict that for  $T_T > T_g$ , the critical total strain for craze initiation is:

$$(\epsilon_s)_{cr} = (\epsilon_{rel})_{cr}$$

This is in agreement with the published data (135), (136), and (138). The difference in the minimum value of  $(\epsilon_s)_{cr}$  observed by Crook et al (138) (see Table 3.3) for different solvents could be due to the effect of swelling on the stress/strain distribution. Indeed the authors suggested that, because of the correlation between solvent molecule size and  $(\epsilon_s)_{cr}$ , the solvent swelling was responsible for this variation. Kambour's (135) (136) data revealed a value of  $(\epsilon_s)_{cr}$  for  $T_T > T_g$  which invariably was in the range 0.1-0.2%. Kambour pre-equilibrated the solvent/polymer mixture prior to bending and therefore minimised the effect of swelling.

When the test temperature is below the  $T_g$  of the polymer solvent mixture ( $T_g > T_T$ ), then the relaxed strain hypothesis would indicate the importance of the test period  $t_R$ . Bernier and Kambour (135) used a constant test period of  $t_R = 3$  hours.

If the polymer is assumed to be a linear viscoelastic material in terms of its stress relaxation behaviour, then the

Maxwell (157) 'spring and dashpot' model would predict that:

$$E(t) = E(0) \exp\left(\frac{-t_R}{\tau}\right) \quad [22]$$

Where  $\tau$  is the temperature dependent relaxation time. Combining equations [21] and [22] gives:

$$\epsilon_s \left(1 - \exp\left(\frac{-t_R}{\tau}\right)\right) \geq (\epsilon_{rel})_{cr}$$

or at the limit:

$$(\epsilon_s)_{cr} = \frac{(\epsilon_{rel})_{cr}}{\left[1 - \exp\left(\frac{-t_R}{\tau}\right)\right]} \quad [23]$$

As  $\tau$  increases with decreasing temperature, equation [23] predicts that when  $t_R = \text{constant}$ , the critical strain for craze initiation  $(\epsilon_s)_{cr}$  will increase with decreasing temperature. This is qualitatively in agreement with experimental observations (136) (see Figure 3.3).

Crook et al (138) did not adopt a constant test period. The crazing strain  $(\epsilon_s)_{cr}$  was measured at a time  $t_R$  such that there was no apparent reduction in the crazing strain (no perceptible movement of the craze front) over a further period of  $3 t_R$ . Thus if the strain resolution of their equipment is  $\Delta$ , then the test period is such that:

$$(\epsilon_s)_{cr} \Big|_{t_R} - (\epsilon_s)_{cr} \Big|_{4t_R} \leq \Delta \quad [24]$$

$$\frac{(\epsilon_{rel})_{cr}}{\left[1 - \exp\left(\frac{-t_R}{\tau}\right)\right]} - \frac{(\epsilon_{rel})_{cr}}{\left[1 - \exp\left(\frac{-4t_R}{\tau}\right)\right]} = \text{constant.}$$

$$t_R \propto \tau$$

Therefore according to the relaxed strain hypothesis, via equation (23), the critical strain for craze initiation should be independent of the test temperature or  $T_g$  when  $(T_g - T_r) > 0$ , and when the test period  $t_R$  is chosen according to equation (24). This is in good agreement with the solvent crazing data (Figure 3.4), published by Crook et al (138). The discontinuity at  $T_g = T_r$  shown in Figure 3.4, should be an artifact of the experimental technique only. That is, its magnitude should be a constant function of  $\Delta$ . For a hypothetical test where the resolution is infinite ( $\Delta = 0$ ) the discontinuity, according to the relaxed strain hypothesis, would vanish and the critical strain for craze initiation would equal  $(\epsilon_{rel})_{cr}$  at all test temperatures and degrees of solvent plasticization (including the condition of zero plasticization).

The implications of the relaxed strain hypothesis as regards standard test methods for assessing solvent crazing are considerable. Various stress relaxation techniques are in use which do not specify adequately the test duration or if they do, this is far too short a period for the behaviour to be correctly quantified. For instance, Vincent and Raha (137) (see Table 3.2) used a test duration of only 1 hour to generate their comprehensive data on solvent stress cracking and crazing. The published critical strains are therefore probably higher than would apply at reasonable service lifetimes. Indeed the craze initiation strain of UPVC immersed in water, reported by Vincent et al to be 1.9%, is twice the value reported by Menges et al (30) for long test periods.

Free volume in an amorphous polymer is a concept, it is not a quantity that can be measured. Various attempts have been made to measure free volume indirectly and to define it quantitatively (16) (158) (159). These have resulted in large differences which give the impression that such attempts are invariably inappropriate. The concept as such is comparatively undeveloped and insufficiently defined to account for many aspects of the yield phenomena. For instance it is often debated that cold flow of polymers below  $T_g$  is connected with stress induced generation of free volume. It is argued (14) (160) (161) that under the action of hydrostatic tensile stress components, the volume of the polymer is increased, leading to an increase in free volume and a depression in  $T_g$ . When the free volume increase is sufficient to depress  $T_g$  to the test temperature, cold flow occurs. It is generally assumed (14) (45) (156) that the increase in volume of the polymer is due entirely to the increase in free volume - which implies that the occupied volume is unaffected by the imposition of stress and strain. Under uniaxial tensile strain  $\epsilon$  this approach assumes that the increase in free volume  $\Delta V_f$  is approximately:

$$\Delta V_f = V(1 - 2\nu)\epsilon \quad [25]$$

where  $V$  is the volume of the unstressed polymer and  $\nu$  is the lateral contraction ratio. Although this approach is compatible with the observations of an increase in  $T_g$  (2), and yield stress (46) with hydrostatic pressure it is incompatible with the observations that yield occurs in shear and compression below  $T_g$ , where according to equation (25), the free volume content is unchanged or reduced.

If, as has been proposed previously (57), macroscopic yielding and craze initiation involve similar molecular (segmental) processes, then the relaxed strain hypothesis would indicate a severe modification of equation [25] and refinement of the free volume concept. The elastic volume increase does not influence the initiation of crazes and therefore possibly does not influence the yield process. Therefore, as the free volume is best defined to accommodate known phenomenology, equation (25) could become:

$$\Delta V_f = V(1 - 2\nu_{rel}) \epsilon_{rel} \quad [26]$$

where  $\nu_{rel}$  and  $\epsilon_{rel}$  are the relaxed lateral contraction ratio and relaxed tensile strain respectively.  $\Delta V_f$  is the effective increase in free volume in terms of its influence on yielding and crazing.

Equation [26] implies that elastic dilation is due entirely to an increase in the effective occupied volume. This is not altogether unreasonable. The elastic volume increase must derive from an extension of, or rotation of, segmental bonds which increases the occupied volume of the molecules. The molecular conformation of the polymer under elastic dilatational strain is only negligibly affected because conformational changes require co-operative molecular movement and above all, they require time. Thus it might be imagined that under an elastic tensile strain the molecular dimensions and the dimensions of individual packets of free volume are distorted by the same amount. Thus for elastic strains, the percentage increase in physical free volume is the same as the percentage increase in occupied volume. The effective free volume

change, which rationally must take account of the exchangeability of occupied and unoccupied regions, could therefore be zero.

Evidence to support the relaxed strain approach to macroscopic and microscopic yielding is available through the work of Dibenedetto and Trachte (13). They concluded that the tensile yield strength of various glassy polymers as a function of temperature was determined by the free volume induced by 'viscous' dilatational strain. The definition of viscous strain was similar to that used here for a relaxed strain. In addition Robertson et al (55), who measured the increase in the elastic, time dependent, and plastic strain components observed that the time dependent strain component was the primary influence at the yield point. One attraction of the relaxed strain criterion, as regards macroscopic yielding, is that free volume within the polymer can be envisaged to increase even when the polymer volume remains constant (shear), or even decreases (uniaxial compression). Of course it would be necessary to predict that under uniaxial compressive stress the free volume increased whilst the total volume exhibits a nett decrease. In conjunction with the relaxed strain hypothesis this would be possible physically if:

- (1) The lateral expansion ratio under elastic uniaxial compressive strain is less than 0.5 (giving, according to equation (25), a nett decrease in volume because  $\gamma < 0.5$  ).

and (2) The lateral expansion ratio  $\nu_{kl}$  under relaxed uniaxial compressive strain is greater than 0.5 (giving according to equation (26), an increase in free volume).

Alksne, Ainbinder, and Slonimskii (162) observed that the density of UPVC increased when the uniaxial compressive strain was increasing (constant strain rate test) and predominantly elastic. However at higher strains and longer times, when it is assumed that the relaxed strain component predominates, the density decreased. It is conceivable therefore that although there is a net decrease in the volume of the polymer, the free volume is increased because the relaxed dilatational strain  $((1-2\nu_{kl}) \epsilon_{kl})$  is positive ( $\nu_{kl} > 0.5$ ).

Brady and Yeh (163) have recently proposed that yielding under tensile and uniaxial compressive stress (and presumably also in shear) is controlled by a common process. This is the generation of localised dilatational yielded zones. These yielded zones are similar to those observed by Baer and Wellinghoff (100) in polystyrene and by Klement and Giel (164) in polycarbonate, Baer et al commented that the site density of the yielded zones, being lower in polystyrene than in polycarbonate, was in agreement with the predictions of Yeh's (150) fringed micellar grain model of the glassy amorphous state.

The fringed micellar grain model is a concept of the molecular structure which is based on experimental evidence of molecular order in glassy polymers (164) (165). The model differs from others in that it concentrates not on the regions of aligned segments (grain), but on the disordered (inter-grain) regions interspersed between them. According to Yeh, these regions contain

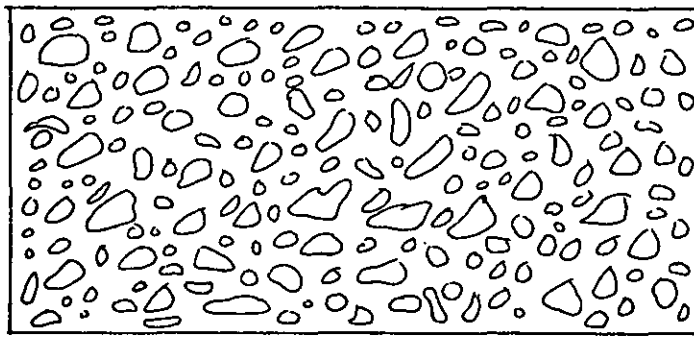


excess free volume and therefore can be expected to act as localised yield nucleation sites. Yeh calculated the free volume content of the disordered regions for various glassy polymers and found a good correlation between excess free volume and the 'ductility' of the polymer. The comment made by Baer et al. (100), as to the density of micro-yield sites in ductile and brittle polymers, and the observation that these sites diffused and coalesced to give crazes, supports the view that craze initiation is controlled by the inter-grain amorphous regions.

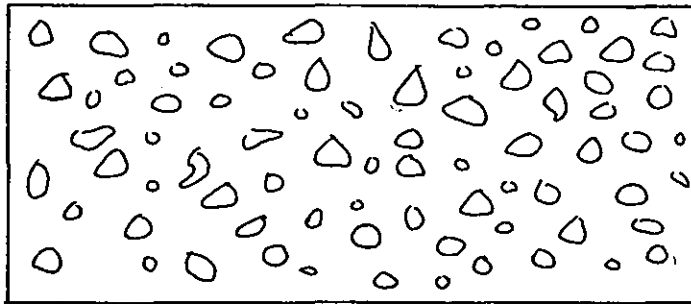
It is proposed here that the relaxed dilatational strain generates additional free volume within the inter-grain regions. When the free volume concentration of the inter-grain region reaches the level that is characteristic of the unstressed polymer in thermal equilibrium at  $T_g$ , dilatational yielding is initiated. The localised yielded zones diffuse and coalesce to form crazes, and/or shear bands (macroscopic yielding). This concept requires that the inter-grain regions have a characteristic maximum free volume concentration which is less than that of the unstressed polymer at  $T_g$ . Furthermore, the concept requires that this maximum concentration is not affected (in UPVC) by changes in temperature in the range 20-35°C, because the relaxed strain and hence the additional free volume for craze initiation is independent of temperature within this range. This is incompatible with classical concepts of the glassy amorphous state, but it is not incompatible with the conclusions (see Appendix IV) of the UPVC annealing programme. These conclusions are that in UPVC:

- (1) Classical free volume contraction, by homogenous diffusion only operates at temperatures above  $45^{\circ}\text{C}$  ( $T_2$ ) and below  $T_g$ .
- (2) Below  $T_2$  free volume contraction proceeds by the nucleation and growth of ordered regions containing only small amounts of free volume.
- (3)  $T_2$  can be regarded as the 'crystallite melt temperature' or the rate independent thermodynamic transition temperature predicted by Gibbs and Di Marzio (149) below which the polymer has an equilibrium configurational entropy of zero.

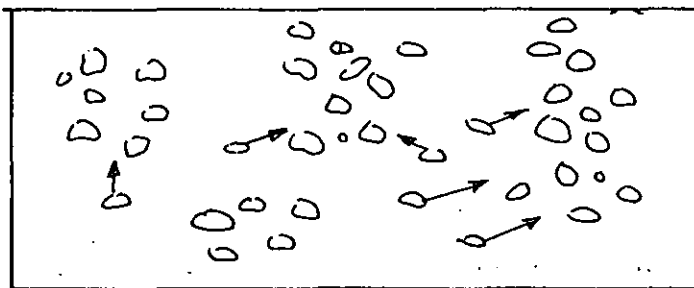
Thus on cooling from above  $T_g$  to room temperature the free volume in UPVC contracts homogeneously until the free volume concentration is such that the polymer 'feels' that it is in equilibrium with  $T_2$ . After this the free volume contraction proceeds by the nucleation and growth of ordered regions (grains) without further change in the free volume concentration of the inter-grain regions. This sequence is demonstrated diagrammatically in Figure 6.7. This process may be aided by a third region between the inter-grain and grain regions which has an intermediate level of molecular order (as in the fringed micellar model (150)). Thus, provided the polymer is held for a sufficient time below  $T_2$  (ie  $45^{\circ}\text{C}$  for UPVC), the maximum free volume concentration in the inter-grain regions will be independent of time and temperature below  $T_2$ . This is compatible with the experimental procedures and conditions adopted in the measurement of  $\Delta R$ , because the UPVC sheet was stored for 2 years at  $20^{\circ}\text{C}$  prior to testing and



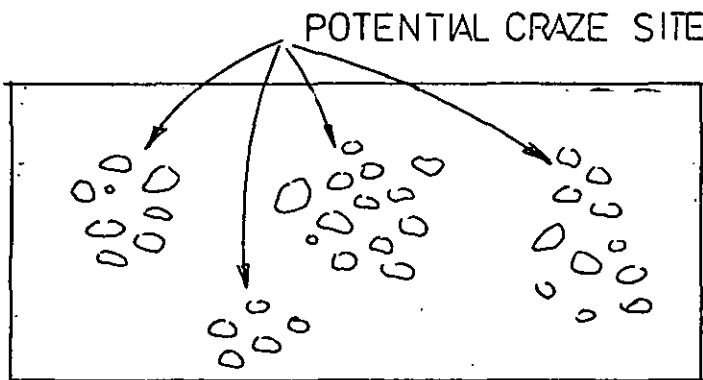
$T_g$   
HOMOGENEOUS  
FREE VOLUME  
DISTRIBUTION



$\geq T_2$   
STILL  
HOMOGENEOUS



$< T_2$   
SEPARATION INTO  
REGIONS OF HIGH  
AND LOW FREE  
VOLUME



LONG TERM  $< T_2$   
FREE VOLUME  
REGIONS IN  
THERMAL  
EQUILIBRIUM  
WITH  $T_2$

Fig. 6.7 Proposed sequence of free volume diffusion on cooling UPVC from  $T_g \rightarrow$  Ambient.

the test temperature did not exceed 45°C.

In conclusion therefore the free volume concentration distribution through the polymer below  $T_2$  could be as shown diagrammatically in Figure 6.8. The regions of maximum free volume are potential sites for craze initiation.

#### 6.5 Fatigue and the Relaxed Strain Criterion

The approach to the dynamic fatigue phenomenon adopted in sections 5.3 and 5.4 ignores actual failure and concentrates on the detailed interaction between successive periods of creep and recovery. It was anticipated that this approach would reveal a pre-failure fatigue criterion.

It has been established that for glassy amorphous polymers repeated interruption of the applied stress reduces the 'isothermal fatigue lifetime' whilst for semi-crystalline polymers the lifetime is extended (90). Thus for glassy polymers the static fatigue lifetime at any stress level or amplitude generally exceeds the dynamic fatigue lifetime (86). For this reason glassy polymers are avoided in service applications involving cyclic loading. This restriction is also becoming recognised in the application of rubber modified glassy polymers which are 'tough' as regards resistance to single impacts but are susceptible to failure under cyclic (multiple impact) load histories (133). It is perhaps relevant to emphasise here that rubber toughening does not increase craze resistance but rather the reverse.

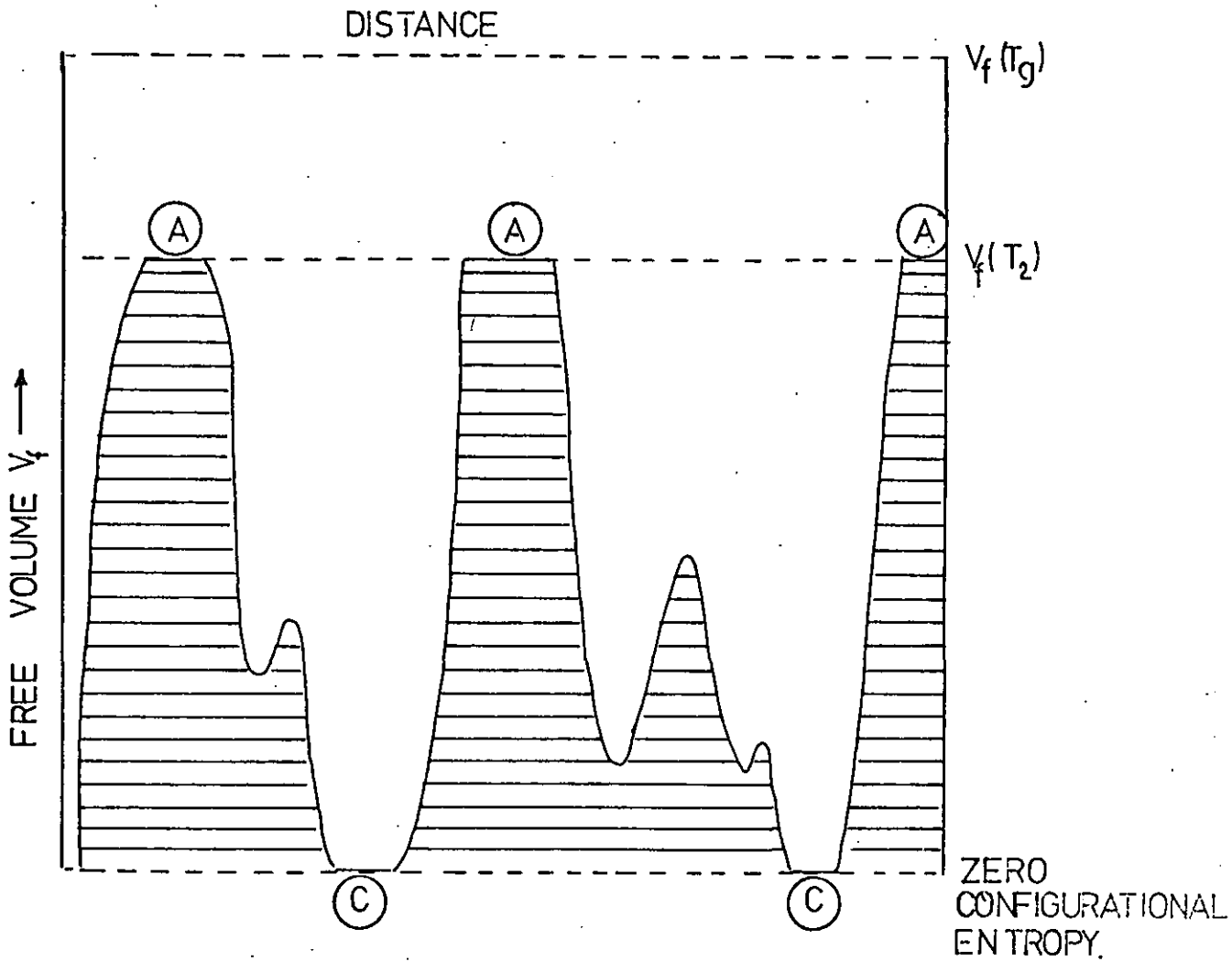


FIGURE 6,8

FREE VOLUME DISTRIBUTION (SCHEMATIC )  
AT A TEMPERATURE BELOW  $T_2$ .

$V_f(T_g)$  EQUILIBRIUM FREE VOLUME AT  $T_g$

$V_f(T_2)$  " " " "  $T_2$

(A) SITES FOR CRAZE INITIATION

(C) REGION OF CRYSTALLINITY

The purpose of the experimental procedure as reported in section 5.3 was to ascertain the effect of the interruption of stress on the damage factor  $\Delta R_{cc}^{(20)}$ . It is observed from Figures 5.11 and 5.12 that for long rest periods  $\Delta R_{cc}^{(20)}$  is considerably reduced compared with  $\Delta R_{cc}^{(20)}$ . This implies that craze healing occurs under zero stress, which is to be expected on the basis of known phenomenology (93) (131). The rate of craze healing increases with temperature, which is also to be expected. However the effect of short rest periods is apparently to increase the damage factor. Obviously craze growth during the short period under zero stress is improbable but craze growth during the first 20 seconds of the second creep period is compatible with the known kinetics of crack growth (89). It is also compatible with Vincent's (88) interpretation (see section 3.3.2.) of the effect of plastic zone recovery on the stress concentration in advance of a crack (and implicitly the intrinsic stress concentration factor of a craze). The partial collapse of crazes during the rest period increases the stress concentration at the craze boundaries during the transient phase of stress re-application. This mechanism applies after any rest period but is only predominant over the beneficial effects of craze healing, when the rest period is short - or in terms of cyclic fatigue, when the frequency is relatively high. On this evidence therefore it could be proposed that the interruption of stress accelerates the growth of crazes and that this is the reason for the reduction in fatigue lifetime under intermittent stressing as compared with the lifetime under uninterrupted stress. It is implied therefore that craze initiation and growth are responsible for the fatigue failure of glassy amorphous polymers.

In section 5.4 the interest in a single rest period graduated to an interest in the interaction of a large number of accumulated creep and recovery cycles. It is apparent from Figures 5.25, 5.26, and 5.27 that the critical tensile strain for craze initiation (transition to positive values of  $\Delta R_{RR}$ ) under cyclic loading is identical to that for static loading. Furthermore the stress amplitude dependency of the critical strain is also identical. It is therefore proposed that the relaxed tensile strain criterion for craze initiation applies equally to dynamic and static load histories.

The growth of strain amplitude under cyclic stressing (Figures 5.13, 5.14, and 5.15) does not exhibit any obvious discontinuity at the strain level for craze initiation. For sufficiently rapid craze growth such a discontinuity would be expected. However the cyclic stress histories with high  $T_c:T_R$  values and low  $T_R$  do exhibit a creep rate that is higher than the creep rate under static stress.

An analysis (Figures 5.16-5.24) of individual cycles reveals that a major source of the additional strain is derived from the progressive increase in the elastic strain component. Which in turn, via the core stress model, suggests that the source of additional strain, is not viscoelastic (or thermally induced) but is the growth of craze damage. The phenomenon is similar to that observed by Benham and Hutchinson (19) for UPVC under cyclic loading. They termed the phenomenon 'cyclic strain softening' and although no mechanism was found to explain it, they did establish that the cause was not thermal instability. Fortunately, Benham et al employed tension/compression

in addition to the tension only cycling adopted here. Under tension/compression cycling the strain softening is very severe and its initiation is readily located by comparing the strain responses to static and cyclic loading. The discontinuity in fact is similar to the sudden acceleration of creep rate caused by solvent crazing (see Figure 5.29). The following observations are made concerning the initiation of cyclic strain softening in UPVC (19).

- ( i ) The induction time for initiation decreases with increasing stress amplitude.
  
- ( ii ) The critical tensile strain for initiation increases with stress amplitude, these being 1.6, 1.3 and 1.1% for stress amplitudes of 42, 35, and 28 MN/m<sup>2</sup> respectively at 0.05 Hz.
  
- (iii) For cycling with a fixed strain amplitude of 1.25% cyclic softening is initiated after a reduction of the modulus by approximately 9%.

The following observations are made concerning the severity of cyclic strain softening:

- ( iv ) The rate of strain softening increases with frequency and stress amplitude.
  
- ( v ) Rapid softening is not observed when the compressive stress amplitude is zero, ie for tension cycling only.



The induction time and critical strain for the initiation of cyclic strain softening are influenced to a similar degree by stress level as is the case with the initiation of crazes. Interpolation of the data in Table 6.1 or Figure 6.4 give critical strains for the initiation of crazing of 1.3%, 1.1% and 0.9% for static stress levels of 42, 35, and 28 MN/m<sup>2</sup> respectively. Although these are lower than the critical strains for the initiation of cyclic strain softening, it is reasonable to suppose that if craze growth is the cause of cyclic softening then craze initiation will precede the detection of softening.

The observation (iii) of cyclic strain softening under conditions of imposed strain amplitude can be used to check the validity of the 0.1% relaxed strain criterion. Equation [21] would predict that for a strain amplitude of 1.25% crazing would be initiated when:

$$\frac{E(t)}{E(0)} = 0.92$$

ie, after an 8% reduction of the modulus due to stress relaxation. This is sufficiently close to the 9% reduction required for the initiation of cyclic strain softening to suggest that both phenomena are controlled by the relaxed strain criterion, and indeed that craze growth and softening are directly linked by cause and effect.

The rate of strain softening increases with frequency and stress amplitude. The rate of craze growth would also increase with stress and decreasing rest period (increasing frequency).

It is known that crazes recover more rapidly under axial compression than under zero stress (131). Thus according to Vincent (88) the stress concentration factor at the craze boundary will be higher during the change from compression to tension than would be the case for tension cycling only. The craze growth under tension/compression cycling would therefore be expected to exceed the growth under tension only cycling. Thus, the comparative severity of cyclic strain softening under reversed tension/compression cycling (V) can be explained, if the phenomenon is associated with craze growth. It is suggested therefore that cyclic strain softening, which may be considered as the onset of dynamic fatigue in UPVC, is caused by craze initiation and growth. Furthermore it is recognised that prior to the initiation of crazes the material behaviour is stable and predictable, whilst the cyclic strain softening stage is unstable (non-isothermal, changing material reference state) and therefore cannot be relied upon to contribute significantly to the service lifetime.

The flexural fatigue failure of UPVC has been studied under controlled load and deformation amplitude by Gotham (86). Fully reversed square wave flexing was used and therefore the outer fibres (skin) were subjected to equal periods of compression and tension. The following characteristics are observed:

- ( vi) The fatigue lifetimes for strain amplitudes of 1.0%, 0.8%, 0.6%, and 0.4% are  $3 \times 10^3$ s,  $7 \times 10^3$ s,  $4 \times 10^4$ s and  $10^6$ s at 0.5 Hz and 20°C.

- (vii) The static and dynamic fatigue characteristics as shown in Figure 2.12, coincide at high stress levels or amplitudes. At lower stress levels and longer fatigue lifetimes the characteristics diverge with dynamic fatigue failure occurring earlier. At the lowest stress amplitude investigated ( $14 \text{ MN/m}^2$ ) the failure strain, as estimated from the isometric stress .v. time characteristics, is 0.55%.
- (viii) Dynamic Fatigue failure after extended lifetimes, ie under low stress or strain amplitude, is by crack propagation.

The strain amplitude, fatigue lifetime data given in (vi) above <sup>are</sup> ~~is~~ presented graphically in Figure 6.9. It would be reasonable to suggest that if a safe strain amplitude exists that this will be in the region of 0.1% to 0.25%. This compares with the predicted safe strain amplitude of 0.1% according to the relaxed criterion for craze initiation. The connection between craze initiation and fatigue failure is further reinforced by the observation that after long (practical) service lifetimes, the dynamic fatigue failure and craze initiation characteristics tend to superpose. For instance the craze initiation strain at  $14 \text{ MN/m}^2$  as estimated from Figure 6.4 is 0.52%, which compares favourably with the apparent failure strain of 0.55% under cyclic stress amplitudes of  $14 \text{ MN/m}^2$ .

The correlation between craze initiation, cyclic strain softening, and dynamic fatigue failure, suggests that the critical condition for fatigue failure, whether this is in the ductile (softening) or brittle (crack propagation) mode is the initiation of crazes.

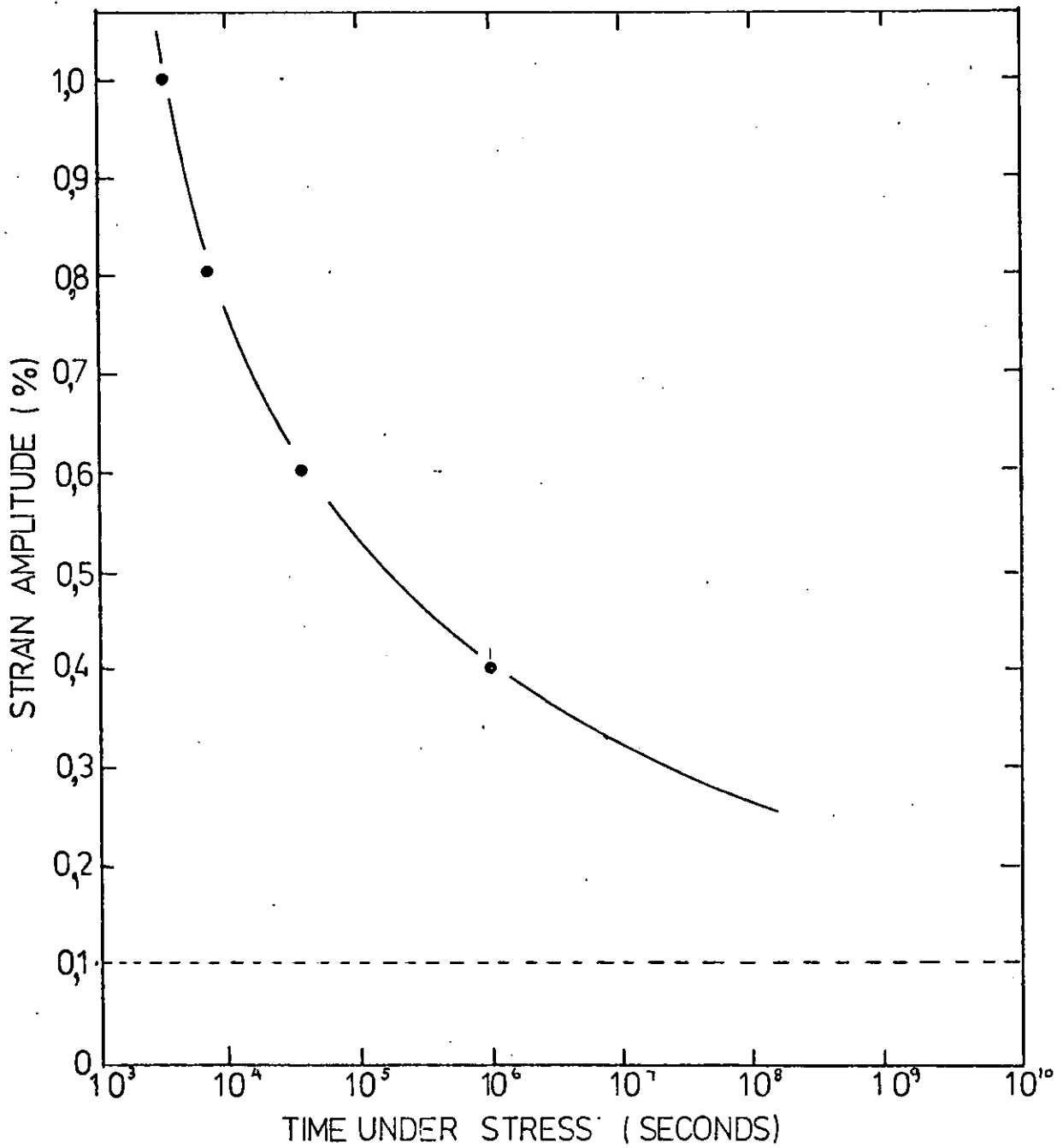


Fig. 6.9 The fatigue lifetime of UPVC at various strain amplitudes (from Gotham (86) ).

## 6.6 An Engineering Design Criterion

The major objective of engineering design is to avoid failure economically. If this objective is to be achieved it is imperative that the cause of failure is known otherwise the design process will be arbitrary. The cause of failure in glassy amorphous polymers is known to be associated with stress and strain history, time, temperature, chemical environment, etc., but has never been isolated and identified. It is perhaps surprising, as failure is not an exclusive response to either stress or strain, that these variables continue to be used as criteria in the design of load bearing plastics components. The adoption of these criteria must be, at least partially due to the influence of traditional design practice. Thus rather than investigate the fundamental cause of failure in plastics, traditional design criteria have been accepted and gradually modified in an attempt to account for the established failure behaviour. For instance in BS 4994 ( 1966 ), total stress or strain criteria are adopted and modified by the use of specific 'safety factors' to account for the effect of time, temperature, chemical environment and material variability. This approach ignores the interaction between the specific variables. Obviously, the approach could evolve to account for variable interaction but the result would be so far removed from traditional design practice, so artificial, and so dependent on fully simulated materials test data that an alternative design criterion would appear attractive.

In anticipation of the limitations of total stress and strain

design criteria, the objective of this thesis has been to investigate and identify the fundamental cause of service failure in UPVC. The emphasis on service failure is made because it is recognised that there is a difference between the service and 'laboratory' performance of UPVC, and indeed of other amorphous and crystalline polymers. Paradoxically, in the laboratory UPVC tends to fail in the ductile mode, but in service, brittle failures predominate. The reasons for this must derive from the lack of simulation of service conditions in the laboratory. For instance:

- example (1) The test duration is generally much shorter than the intended service lifetime.
- example (2) Following from this, the "mechanical stimulation" in a laboratory test is generally more severe than is experienced in service.
- example (3) In service the material is subjected to perturbations which, because of control, do not occur under test. Examples of this are thermally induced stresses or strains due to temperature fluctuation, chance impact loads, and surface contamination.
- example (4) Uniaxial (tensile) stresses are commonly employed in laboratory tests, but in service the stress distribution and component geometry are such that multi-axial stress systems (e.g bi-axial tension) are commonplace.

Examples (1), (2) and (4) above were identified in section 2.6.1, as having a significant effect on the so-called ductile-brittle

transition. Example (3) is introduced as a fundamental difference between test and service conditions and also to accommodate the observed difference between static and dynamic fatigue failure. Laboratory static fatigue tests avoid perturbation and ductile failure is common even when the test duration is long and the applied stress is small (167). At the same stress amplitude, dynamic fatigue failure is brittle (86). Examples (1), (2) and (4) cannot account for this, but if the stress history in a dynamic fatigue test is considered as continual perturbation then the generalisation in example (3) above is applicable. In general therefore, materials tests with constraints on costs and time cannot simulate service performance even to the extent of simulating the failure mode. This severely limits the evaluation of any design criterion based on failure alone. The approach adopted here, therefore, is to consider the act of failure as the end result of the failure process. The initiation of the failure process and the fundamental cause of initiation constitutes the rational, non-arbitrary design criterion.

Craze initiation would appear to be related to the failure process in glassy amorphous polymers. Evidence to support this connection include:

- (a) Brittle failure is inevitably preceded by craze initiation (73). The inherent flaw for brittle failure has been identified as a craze (68).

(b) Mechanical instability often coincides with craze initiation. For example solvent induced softening (see section 3.4 ) and cyclic strain softening (see section 2.2.3.).

(c) The phenomenology of craze initiation and growth can explain the embrittlement of the polymer in service. For instance, with reference to examples (1)-(4) above:

(1) and (2) At low stresses/strains and therefore long service lifetimes, the craze site density is low. This increases the probability of brittle failure at the expense of ductile failure because the stress concentration in advance of individual crazes is increased with low site density (129). Those amorphous polymers which exhibit characteristically high craze site densities tend to be more ductile (100) (150).

(3) Craze initiation is not sensitive to perturbations of the applied stress or strain, but craze growth is. This could explain why dynamic fatigue failure tends to be brittle and premature compared with static fatigue failure.

(4) Craze initiation and growth is a dilatational process and for this reason biaxial and triaxial tension due to applied stresses and/or stress concentrations may be more



severe as regards embrittlement than the uniaxial tensile stress condition. Thus UPVC can be made to fail by crack propagation by notching the specimen (168).

Craze initiation and growth could therefore be responsible for premature brittle failure in service. The sensitivity of craze growth to perturbation suggests that this process is comparatively unstable. Crack growth, cyclic fatigue softening, and solvent craze softening can all be recognised as mechanical instabilities. It is suggested here therefore that craze initiation coincides with the transition from mechanical stability to instability. The duration of the unstable period by its nature cannot be predicted with any confidence and therefore cannot be relied upon to extend the service lifetime. The induction time for crazing can be considered therefore as the safe service lifetime.

On the evidence presented in this thesis, the induction period for craze initiation in UPVC coincides with that required to generate a relaxed tensile strain of 0.1%. This value would appear to be independent of temperature, stress level, stress or strain history, and chemical environment. The 0.1% relaxed strain design criterion has the following advantages over total stress or total strain criteria:

- (i) It is not arbitrary.
- (ii) It automatically includes a margin of safety which is based on rational considerations of stability whilst safety factors when designing on total stress or strain criteria must be modified for each specific application.

are

(iii) Unlike failure data, which ~~is~~ often erratic (possibly because ~~it~~ includes the unstable phase), the generation of a critical level of relaxed strain is an established continuum mechanical process.

Unlike failure data therefore the conditions which combine to generate relaxed strain can be predicted with some confidence. For instance, extrapolation from acceptable laboratory test periods to typical service lifetimes are more justified.

The basic information for designing against brittle failure is creep data and an estimate of the critical relaxed strain ( $\epsilon_{rel}$ )<sub>crit</sub>. The latter can be estimated using the  $\Delta R$  technique adopted here and described in section 4.1, however this was devised as a research tool rather than as a standard materials test. It is admittedly very involved and requires strain measurements of very high resolution. Solvent crazing tests as developed by Kambour et al (135) (136) would appear to be a satisfactory and expedient method of estimating ( $\epsilon_{rel}$ )<sub>crit</sub>. Obviously it would be necessary to ensure that the solvent plasticizing effect was sufficient to reduce the  $T_g$  of the polymer to below the test temperature. The initiation of cyclic softening under conditions of reversed tension/compression cycling (19) is an alternative method of estimating ( $\epsilon_{rel}$ )<sub>crit</sub>.

In combination with tensile creep data at various temperatures, the singular critical relaxed strain can be used to construct a critical surface which defines the stress, temperature and time combinations required to generate ( $\epsilon_{rel}$ )<sub>crit</sub> and which essentially separates the stable (safe) and unstable (unsafe) regimes. This is shown diagrammatically in Figure 6.10. The safe design stress for any specified temperature and service lifetime could be provided by such a diagram. Alternatively a single nomogram might be constructed, this possibility being enhanced

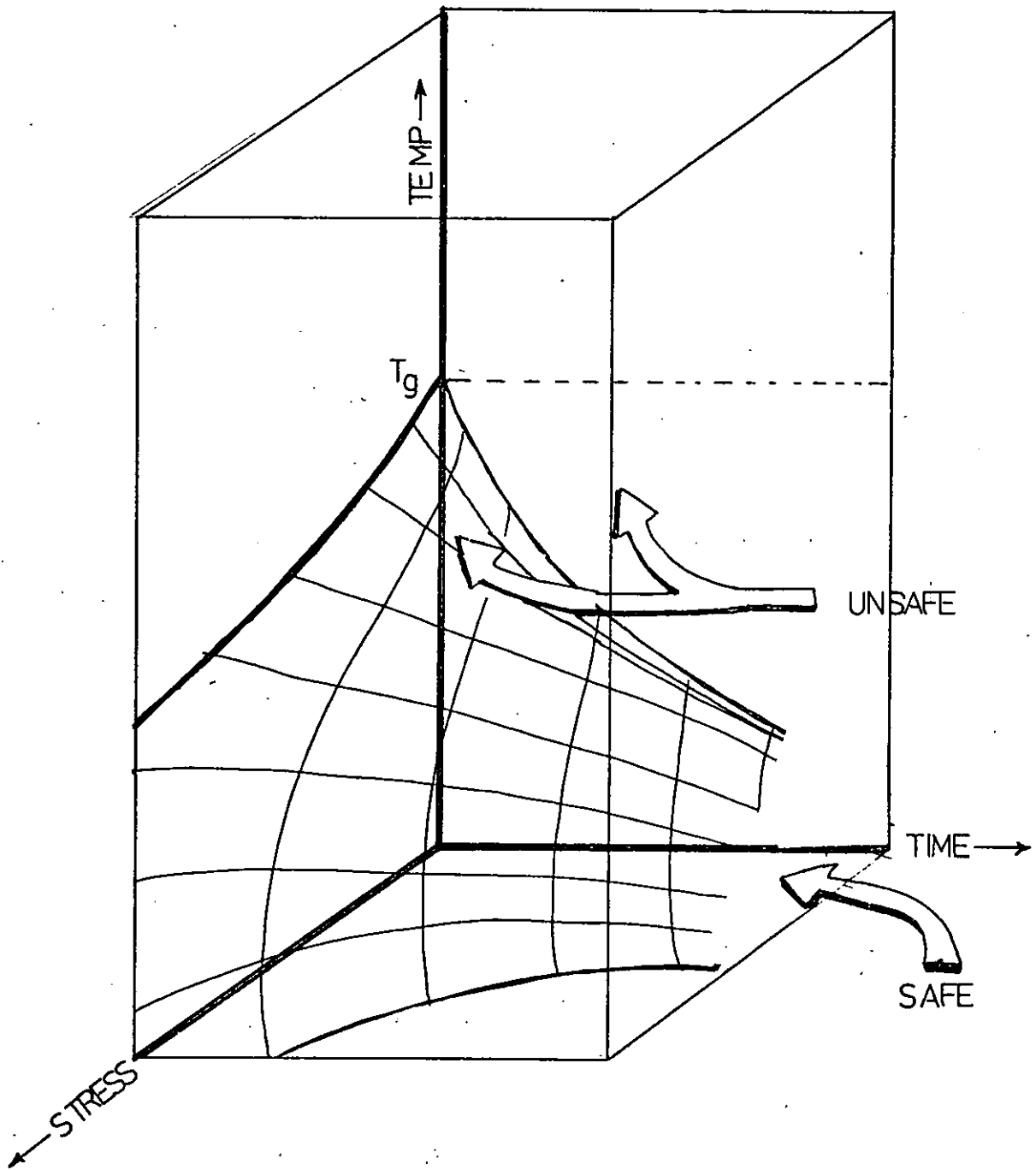


Fig. 6.10 The surface (schematic) separating safe and unsafe service conditions based on the relaxed strain criterion and creep data.

by the evidence that, in the safe regime, the polymer is linear viscoelastic (30). Indeed, the transition from a linear to non-linear behaviour (39) for polycarbonate is apparently triggered by the generation of a relaxed strain of 0.35%. This may well coincide with craze initiation, the growth of which being responsible for the non-linearity. Linearity of response in the safe regime would be a considerable advantage in applying the relaxed strain criterion to design situation involving complex stress histories and stress distributions.

For design applications where solvent plasticization is involved, the relaxed strain design criteria remains valid but only if the degree of solvent plasticization (i.e. the  $T_g$  depression) can be predicted. Data of the type shown diagrammatically in Figure 6.10. could then be employed directly. Alternatively the creep characteristics of the polymer under conditions of solvent saturation could be used to modify the critical surface shown in Figure 6.10. It would be necessary to ensure that solvent penetration was complete prior to creep testing, which implies the use of thin specimens.

For design applications involving intermittent stressing the growth of creep strain and hence the growth of relaxed strain in the safe regime is less than would be the case under static loading (18) (where static stress equals stress amplitude). Thus for any combination of stress and temperature the time required to generate a critical level of relaxed strain is greater under intermittent than under static stress. This is true even if the time is calculated on the basis of total time

under load. Empirical superposition techniques (18) could be used to predict creep under intermittent loading and hence to modify the data in 6.10. Alternatively if the material is reasonably linear, superposition theory can be applied. However it must be emphasised that under intermittent loading and for solvent attack, the in-built safety factor inherent in the relaxed strain design criterion is much reduced as compared with situations involving static stress and a passive chemical environment. This is because the unstable (post-crazing) period is dramatically shortened by dynamic stressing and solvent attack. Under these conditions the relaxed strain criterion may change from a conservative pre-failure criterion to an actual failure criterion.

## 7 Conclusions and Suggested Further Work

### 7.1 Conclusions

1. The coxe stress model introduced in section 4.1 provided two main predictions relating to the effects of surface initiated crazing on the creep and recovery characteristics of a viscoelastic body. These are itemised as:

(a) For craze initiation under constant tensile load the creep rate would increase.

(b) On the removal of load the presence of surface crazing, if this is not severe, would lead to an increase in the elastic (unrelaxed) component of the recovered strain and some retardation of the inelastic (relaxed) recovery process. For severe craze damage the elastic recovered strain component would be decreased and the in elastic recovery process considerably retarded. Severe damage is considered to have been incurred when the cross-section of the specimen is completely covered by craze damage i.e. the area of undamaged core is zero.

2. The predicted increase of the elastic recovery response with craze initiation is of particular interest as a potential mechanical (non-visual) method of detecting craze initiation and assessing craze growth because:

(a) The elastic response is energetic and thus less sensitive to instrument friction than is the inelastic creep and recovery process.

(b) An experimental procedure can be devised whereby the effects of inter-specimen variability and temperature fluctuation can be minimised. In addition the procedure in effect leads to a 'magnification' of the craze induced elastic recovery perturbation. The core stress model in conjunction with classical linear viscoelasticity theory predicts that the strain based function  $\Delta R_{cr}(t)$  will exhibit a transition from near zero negative values to positive values on the initiation of crazing where:

$$\Delta R_{cr}(t) = \epsilon_r(t) - \epsilon_c(t)$$

The procedure thus involves the measurement of  $\epsilon_c(t)$  and  $\epsilon_r(t)$  for a gate input of stress, together with the final creep strain  $\epsilon_c(T)$ .

3.  $\Delta R_{cr}(20)$  was determined for UPVC for a range of stress histories (stress level and creep time) and final creep strain  $\epsilon_c(T)$  at two temperatures, it was observed that:

- (a) With no visible crazing,  $\Delta R_{cr}(20) \sim 0$
- (b) With visible crazing,  $\Delta R_{cr}(20) > 0$
- (c) The critical time (the induction period) for the  $(0 \rightarrow +) \Delta R_{cr}(20)$  transition increased with decreasing stress level and temperature.
- (d) The critical tensile strain for the transition increased with increasing stress level and decreasing temperatures.
- (e) The critical stress, strain and time for the transition decreased with immersion of UPVC in a plasticizing solvent.
- (f) The critical combinations of service variables which combine to generate the  $\Delta R_{cr}$  transition are qualitatively identical and quantitatively similar to those combinations which are known to induce craze initiation.

4. The second transition ( $+ \rightarrow -$ ) in the  $\Delta R_{cr}(z)$  function was observed in UPVC under conditions of severe solvent stress crazing. This transition coincided with the extinction of the undamaged core by the advancing craze fronts. This is in agreement with the predictions of the core stress model.
5. It is proposed therefore that the generation of positive values of  $\Delta R_{cr}$  in glassy polymers is not a reflection of non-linear continuum behaviour but rather a symptom of craze initiation and growth. If this interpretation is correct then it follows that a major source of the non-linearity exhibited by these polymers is a discontinuity which cannot therefore be formalized adequately by the application of continuum mechanics alone. Additional evidence to support this interpretation can be deduced from the failure of the continuum mechanics approach in predicting the deformation response of polymers in the non-linear region particularly when this involves incremental stress reductions. It has also been shown independently that prior to craze initiation the behaviour of glassy amorphous polymers tends to be linear viscoelastic.
6. An analysis of the stress, strain, time and temperature conditions which combine to initiate the ( $0 \rightarrow +$ )  $\Delta R_{cr}$  transition, and by implication to initiate crazing, revealed that for UPVC the initiation coincided with the generation of 0.1% level of relaxed (inelastic) tensile strain. This relaxed strain criterion was shown to be independent of stress level, time, strain, and temperature over the ranges studied.



7. The 0.1% relaxed strain criterion was shown to be valid under conditions of solvent stress crazing. Application of the criterion to previously published solvent crazing data, collected in the stress relaxation mode, revealed that the relaxed strain hypothesis may be valid for all glassy polymers. The criterion, which for the relaxation mode can be formally defined as:

$$\left(\epsilon_s\right)_{cr} \left[ 1 - \frac{E(t_R)}{E(0)} \right] = \left(\epsilon_{rel}\right)_{cr}$$

where  $\left(\epsilon_s\right)_{cr}$  is the apparent crazing strain

$E$  is the relaxation modulus

$t_R$  is the test period

and  $\left(\epsilon_{rel}\right)_{cr}$  is the critical relaxed strain for craze initiation,

emphasises the influence of the test period  $t_R$  on the value of critical (total) strain. If the test period is short (as is commonly the case) the value of  $\left(\epsilon_s\right)_{cr}$  will be optimistically high and quite inadequate in predicting product performance. Basically the critical crazing strain  $\left(\epsilon_s\right)_{cr}$  for an infinite service lifetime is always  $\left(\epsilon_{rel}\right)_{cr}$  whether solvent is present or not. The effect of the solvent, or indeed an increase in test temperature, is to accelerate the rate of relaxation and thereby decrease  $\left(\epsilon_s\right)_{cr}$  at any finite value of test duration or service lifetime.

8. The 0.1% relaxed strain criterion was found to be valid under conditions of intermittent tensile loading. A correlation between craze initiation, the 0.1% relaxed strain criterion, and cyclic strain softening was observed. The initiation of the dynamic fatigue failure process in the absence of any other evidence could well be intimately connected with the initiation of craze damage. Cyclic strain softening and the increase in creep rate with solvent attack may both be regarded as mechanical instabilities which precede failure.

9. The singularity of the relaxed strain criterion suggests that craze initiation is triggered by continuum (molecular) relaxation processes. Surprisingly the elastic stress, strain and strain energy have no direct influence on the craze initiation process although they do indirectly affect the induction period by their effect on the rate of accumulation of relaxed deformation.

The independence of the crazing process to elastic deformation is inconsistent with the traditional concepts of stress induced free volume. The increase in free volume as a result of uniaxial tensile strain has been assumed to be equal to the total (inelastic + elastic) volume expansion of the material. It is reasonable, however, to suppose that the volume increase associated with elastic dilatation increases the occupied volume in preference to the free volume.

If this is correct then the classical free volume yield model could be modified to predict dilatational yielding at a critical level of relaxed strain induced free volume. It follows therefore that if yielding is in response to relaxed deformation then localised pre-craze

yielding could be initiated at a critical level of relaxed dilatational strain. Under uniaxial tensile stress this would lead to an apparent critical relaxed tensile strain for craze initiation.

(10) The independence and singularity of the critical relaxed strain criterion with temperature indicates that the localised free volume has a characteristic maximum. This is not inconsistent with the fringed micellar grain model and the concept of the zero configurational entropy of the glassy state. A molecular model is proposed which explains the mechanism of the formation of free volume maxima with <sup>a</sup> of uniform free volume content.

11. The relaxed strain criterion for craze initiation is a rational design criterion if crazing is the primary cause of brittle failure in service. The long term ductile brittle transition under static load and its acceleration under conditions of intermittent loading can be accounted for in terms of craze initiation and growth. The effect of molecular orientation and solvent attack on service failures can also be rationalised in terms of craze nucleation and growth. It is proposed therefore that by limiting the relaxed strain in service to below a critical level this will reduce or eliminate the probability of brittle failure.

## 7.2 Suggestions for further work

It is appreciated that this thesis includes several propositions that are contentious, particularly where these invite a revision of long established concepts. However it is hoped that even the most conservative research worker in this and related fields will in future be persuaded by the evidence presented here to separate the elastic and inelastic deformation and to test the relaxed strain hypothesis. This simple separation, and awareness of the potential importance of relaxed strain, has recently

proved valuable in the analysis of tensile yield behaviour (13) (55).

In addition to this 'ad hoc' activity, the following specific research topics are suggested:

### 1. Solvent Crazeing

The critical crazing strain of glassy polymers under conditions of pre-equilibrated solvent plasticization, with particular emphasis on the effect of test duration, is a convenient and suitably severe test method for checking the relaxed strain hypothesis and for providing an estimate of the critical relaxed strain.

### 2. Molecular Orientation and Craze Initiation

Although molecular orientation cannot be precisely quantified, it can be reproduced. It is known qualitatively that parallel to the direction of orientation the craze resistance is increased and the creep compliance is decreased. Tensile creep studies in parallel with craze initiation tests would reveal whether the relaxed strain criterion is applicable to oriented materials.

It is also of interest to investigate the effect of annealing oriented materials on craze resistance. Conceptually the annealing process transforms elastic processed-in strain to inelastic relaxed strain and may therefore lead to a reduction of craze resistance. It is known for example that annealing polycarbonate reduces the brittle strength (151).

### 3. Fundamental yield studies

The macroscopic yield and crazing processes may have a common origin in the initiation of microscopic yielded zones. These zones can be detected using electron microscopy with the specimen in a straining jig.

It is of considerable interest to study the nucleation and diffusion characteristics of these zones to establish:

- (a) The nucleation criterion - is this based on relaxed strain?
- (b) And the criteria (nucleation density, diffusion rates, zone interaction mechanics etc) which determine the mode of yielding i.e. normal (crazing) or shear.

#### 4. Thermodynamics of the Glassy State

The stress dependence of  $T_g$  has been studied previously but without reference to deformation and time. A separation of the effects of elastic and inelastic dilatational strain (increase and decrease) would reveal whether the modified free volume model (relaxed strain sensitive) is valid.

#### 5. Craze Initiation under Multiaxial Stress

With uniaxial tensile testing only, it is not possible to delineate the effects of tensile and dilatational deformation. The criterion for craze initiation in UPVC could therefore be either dilatational or tensile relaxed strain. A study of craze initiation under biaxial tension would reveal the generalized criterion.

## BIBLIOGRAPHY

- (1) McCrum, N.G., Read, B.E., & Williams, G.,  
'Anelastic and Dielectric Effects in Polymeric Solids',  
John Wiley & Sons Inc., London (1967).
- (2) Anderson, J.E., Davis, D.D., & Slichter, W.P.,  
Macromolecules, Vol. 2, No. 2, (1969).
- (3) Sternstein, S.S. & Ho, T.C.,  
J. Appl. Phys., Vol. 43, No. 11, (1972).
- (4) Foltz, C.R., & McKinney, P.V.,  
J. App. Polym. Sci., Vol. 13, No. 10 (1969).
- (5) Saito, N., Okano, K., Iwayangi, S.,  
S. Hideshima, T., 'Solid State Physics'  
Vol. 14, Academic Press, New York, (1963).
- (6) Zitek, P., & Zelinger, J.,  
J.App. Polym. Sci., Vol.44, p. 1243, (1970).
- (7) Bauwens - Crowet, C., Bauwens, J.C., & Homes, G.A.,  
J.Polym. Sci., A2, 7, (1969).
- (8) Maxwell, B., & Harrington, J.P.,  
Trans. ASME, p. 569, May (1952).
- (9) Roetling, J.A., Polymer, 6, p. 311(1965).
- (10) Boyer, R.F., Polym. Eng. Sci., 8, p.161, (1968).
- (11) Sternstein, S.S., & Sims, R.,  
Polym. Preprints, 5, p. 422, (1964).
- (12) Heydeman, P., & Guickling, H.D.,  
Kolloid Z., Vol. 193, p. 16, (1963).
- (13) Dibenedetto, A.T., & Trachte, K.L.,  
J.App. Polym. Sci., Vol. 14, p. 2249, (1970).
- (14) Rusch, K.C., & Beck, R.H.,  
J.Macromol. Sci., (Phys.), B3, p. 365, (1969).
- (15) Andrews, R.D., & Kazama, Y.,  
J.Appl. Phys., Vol. 38, No. 11, p. 4118, (1967).
- (16) Bondi, A., J.Polym.Sci., A2, p. 3159, (1964).
- (17) BS4618, 'Recommendations For the Presentation of Plastics  
Design Data', Part 1, (1970).
- (18) Turner, S., Polym. Eng. Sci., Vol. 6, p. 306 (1966).
- (19) Benham, P.P., & Hutchinson, S.J.,  
Plastics & Polymers, p. 259, Aug. (1970).

- (20) Benham, P.P., & Mallon, P.J.,  
Plastics & Polymers p. 22, Feb. (1972).
- (21) Benham, P.P., & Mallon, P.J.,  
Plastics & Polymers, p. 77, April (1972).
- (22) Yannas, I.V., Sung N-H., & Lunn, A.C.,  
J. Macromol. Sci, (Physics), B5(3),  
p. 487, Sept. (1971).
- (23) Yannas, I.V., Proc. Conf. Struct. Mech. Props.  
U.S. Army Natick Labs. Mass. p. 90 (1967).
- (24) Benham, P.P., & McCammond, D.,  
Plastics and Polymers, April (1971).
- (25) Bergen, R.L., SPE Journal, p. 1235, Nov. (1960).
- (26) Turner, S., Br. Plast., Vol 37, p. 682, (1964).
- (27) Bucknall, C.B., & Clayton, D.,  
J. Mat. Sci., Vol 7, p. 202, (1972).
- (28) Christiansen, A.W., Baer, E., & Radcliffe, S.V.,  
Phil. Mag. Vol. 24, p. 451, (1971).
- (29) Boltzmann, L., Pogg. Ann. Physik., Vol. 7, p. 624, (1876).
- (30) Menges, G., & Schmidt, H., PI Conf. Res.  
Eng. Props. Plastics, Paper 15, Cranfield, Jan. (1969).
- (31) Turner, S. British Plastics p. 440 Aug. (1964).
- (32) Benham, P.P., & Hutchinson, S.J.,  
Polym. Eng. Sci., Vol. 11, No. 4, p. 335, (1971).
- (33) Jaksch, A., Kunststoffe, Vol. 55, p. 647, (1965).
- (34) Bergen, R.L., SPE Journal, p. 630, July (1964).
- (35) Bucknall, C.B., Paper 4, 2nd Int. Conf.  
'Yield, Deformation, Fracture, Polymers',  
PI., Cambridge, March (1973).
- (36) Eyring, H., J. Chem. Phys., Vol. 4, p. 283, (1936).
- (37) Oberst, H., & Retting, W.,  
J. Macromol. Sci., (Phys), B5(3), p. 559, (1971).
- (38) Mercier, J.P., Aklonis, J.J., Litt, M., & Tobolsky, A.V.,  
J. Polym. Sci., Vol. 9, p. 447, (1965).
- (39) Yannas, I.V., J. Macromol. Sci., (Phys)  
B6(1), p. 91, (1972).

- (40) Yannas, I.V., Lunn, A.C., & Doyle, M.J.,  
ACS Polym Preprints, Vol. 34, p.96 (1972).
- (41) Ree, T., & Eyring, H., 'Rheology' Vol. II,  
Chapter III, Academic Press, New York, (1958).
- (42) 'Die Physik der Hochpolymeren' (Ed. by H.A. Stuart)  
Springer-Verlag, Berlin, (1956).
- (43) Vincent, P.I., *Plastics* Vol. 27, p. 105, (1962).
- (44) Bryant, G.M., *Textile Research Journal*,  
Vol. 31, p. 399, (1961).
- (45) Litt, K.C., Koch, P.J., & Tobolsky, A.V.,  
*J. Macromol. Sci., (Phys)*, B1, p. 587, (1967).
- (46) Rabinowitz, S., Ward, I.M., & Parry, J.C.,  
*J. Mat. Sci.*, Vol. 5, p. 29, (1970).
- (47) Ainbinder, S.B., Laka, M.G., & Maiors, I. Yu.,  
*Mekhanika Polymerov*, Vol. 1, p. 65, (1965).
- (48) Holliday, L., Mann, J., Pogany, J.A.,  
Pugh, H.D., & Gunn, D.A.,  
*Nature*, Vol 202, p. 381, (1964).
- (49) Coulomb, C.A., *Mem. Math. et Phys.*, Vol. 7, p. 343, (1773).
- (50) Whitney, W., Sc. D. Thesis, M.I.T., Nov. (1964).
- (51) Ender, D.H., *ACS Polym. Preprints*, Vol. 10, No. 2,  
p. 1132, (1969).
- (52) Pampillo, C.A., & Davies, L.A.,  
*J. App. Phys.*, Vol. 42, p. 4674, (1971).
- (53) Bowden, P.B., Chapter 5. 'The Physics of Glassy  
Polymers' (Ed. by R.N.Haward).  
Allied Science Pub. Ltd., London (1973).
- (54) Litt, M.H., & Tobolsky, A.V.,  
*J. Macromol. Sci., (Phys)*, B1, Vol. 3, p. 433, (1967).
- (55) Robertson, R.E., & Patel, M.A.,  
*Polym. Eng. Sci.*, Vol. 12, No. 5, p. 346, (1972).
- (56) Robertson, R.E., *App. Polym. Symp.*, Vol. 7, p. 201, (1968).
- (57) Haward, R.N., Murphy, B.M., & White, E.F.T.,  
*J. Polym. Sci., A-2*, Vol. 9, p. 801, (1967).
- (58) Rehage, G., & Goldbach, G.,  
*Angew, Macromol. Chem.*, Vol. 1, p. 125, (1967).
- (59) Haward, R.N., Murphy, B.M., & White, E.F.T.  
*Proc. Int. Conf. Fracture*, paper 45,  
Brighton, (1969).



- (60) Beuche, F., J. Chem. Phys., Vol. 43, p. 2696, (1968).
- (61) Orowan, E., Rep. Progr. Phys., Vol. 12, p. 185, (1949).
- (62) Irwin, G.R., J. App. Mech., Vol. 24, p. 361, (1957).
- (63) Dugdale, D.S., J. Mech. Phys. Solids, Vol. 8, p. 100, (1960).
- (64) Mills, N.J., Paper 6, 2nd Int. Conf. Yield, Deformation and Fracture of Polymers, P.I., Cambridge, March (1973).
- (65) Griffiths, A.A., Phil. Trans. Roy. Soc., A221, p. 163, (1921).
- (66) Charles, R.J., 'Progress in Ceramic Science' (J.E.Burke, ed.), Vol. 1, page 1., Pergamon Press, New York, (1961).
- (67) Berry, J.P., J. App. Phys., Vol. 34, p. 62, (1963).
- (68) Berry, J.P., J. Polym. Sci., Vol. 50, p. 313, (1961).
- (69) Benbow, J.J., & Roesler, F.C., Proc. Phys. Soc. (London), B70, p. 201, (1957).
- (71) Berry, J.P., Nature Vol. 185, p. 91, (1960).
- (72) Higuchi, M., Rep. Res. Inst. App. Mech., Kushlu Univ. 6 (24), p. 173, (1958).
- (73) Kambour, R.P., J. Polym. Sci., A-2, Vol. 4, p. 349, (1966).
- (74) Murray, J., & Hull, D., J. Polym. Sci., A2, Vol. 8, p. 583 (1970).
- (75) Doyle, M.J., Paper 7, 2nd Int. Conf. on Yield, Deformation and Fracture of Polymers, P.I., Cambridge, March (1973).
- (76) Zhurkov, S.N., Int. Journal of Fracture Mechanics, Vol. 1, p.311, (1965)
- (77) Bueche, F., J. App. Phys., Vol. 28, p.784, (1957)
- (78) Bueche, F., J. App. Phys., Vol. 29, p.1231, (1958)
- (79) Peschansakaya, N.N., & Stepanov, V.A., Soviet Plastics, Vol. 7, p.2402, (1966)
- (80) Hall, M.M., & Wright, D.C., Plastics and Polymers. p.37, Feb. (1974).
- (81) Cooney, J.L., J. App. Polym. Sci., Vol 8, (1964)

- (82) Gaube, E., *Kunststoffe* Vol. 49, Sept. (1959)
- (83) Gotham, K.V., Paper 8, P.I. Conf. Designing to Avoid Mechanical Failure, Cranfield, (1973)
- (84) Forsman, J.P., North, H.C., & Hakala, T.H., *Polym. Eng. Sci.*, April, (1966)
- (85) Andrews, R.D., & Curran, R.J., SPE ANTEC (1965)
- (86) Gotham, K.V., *Plastics & Polymers*, Vol. 37, p.309, (1969)
- (87) Opp, D.A., Skinner, D.W., & Wittorek, R.J., *Polym. Eng. Sci.*, Vol. 9, p.121, (1969)
- (88) Vincent, P.I., Technical Report No. 97, Div. Polym. Sci., Case Western Univ. Cleveland, Ohio
- (89) Brown, H.R., Harris, J.S., & Ward, I.M., Paper 13, P.I. Conf. Yield, Deformation & Fracture, Cambridge, March (1973)
- (90) Lortsch, W., *Kunststoffe*, Vol. 55, p.460, (1965)
- (91) Martin, J.R., & Johnson, J.F., *J. App. Polym. Sci.*, Vol.18, p.257, (1974)
- (92) Sauer, J.A., Marin, J., & Hsiao, C.C., *J. App. Phys.*, Vol. 20, p.507, (1949)
- (93) Spurr, O.K., & Niegisch, W.D., *J. App. Polym. Sci.*, Vol.6, p.585, (1962)
- (94) Kambour, R.P., *Nature*, Vol. 4848, p.1299, (1962)
- (95) Smith, J.W., 'Electric Dipole Moments' Butterworth Sci. Pub., London, (1955)
- (96) Kambour, R.P., *Polymer*, Vol. 5, p.143, (1964)
- (97) Kambour, R.P. & Holik, A.S., ACS Polym. Preprints 10 (2), p.1182, (1969)
- (98) Knight, A.C., *J. Polym. Sci.*, Part A, Vol. 3, p.1845, (1965)
- (99) Kambour, R.P., & Holik, A.S., *J. Polym. Sci.*, A-2, Vol. 7, p.1393, (1969)
- (100) Baer, E., & Wellinghoff, S.T., Paper 3, P.I. Conf. Yield Deformation & Fracture, Cambridge, March, (1973)
- (101) Haward, R.N., Murphy, B.M., & White, E.F.T. *J. Polym. Sci.*, B7, p.157, (1969)

- (102) Knight, A.C., 22nd SPE ANTEC, Vol. 12, (1966)
- (103) Gent, A.N., J. Mat. Sci., Vol. 5, p.925, (1970)
- (104) Menges, G., Kunststoffe Bd, Vol. 63, p.95, (1973)
- (105) Kambour, R.P., & Robertson, R.E., 'Polymer Science'  
Ed. by A.D. Jenkins, Pub. by North Holland, (1972)
- (106) Stewart, C.W., ibid Part A-2, Vol. 8, p.937, (1970)
- (107) Hill, R., 'The Mathematical Theory of Plasticity',  
Clarendon Press, Oxford (1950)
- (108) Drabble, F., Haward, R.N., & Johnson, W.,  
J. App. Phys., Vol. 17, p.241, (1966)
- (109) Haward, R.N., 'Amorphous Materials'  
Edited by R.W. Douglas and B. Ellis, John Wiley,  
London, (1972)
- (110) Irwin, G.R., 'Handbuch der Physik' Vol. VI, Springer  
Berlin, p.551, (1958)
- (111) Natta, G., & Corradini, P.,  
J. Polym. Sci., Vol. 20, p.251, (1956)
- (112) Koenig, J.L., & Druesdow, D., J. Polym. Sci., A-2, Vol. 7,  
p. 1075, (1969)
- (113) Sternstein, S.S., & Ongchin, L.,  
ACS Polym. Preprints, Vol. 10, page 1117, (1959)
- (114) Maxwell, B., & Rahm, L.F.,  
SPE Journal, p.7, Nov. (1950)
- (115) Menges, G., & Schmidt, H.,  
Kunststoffe (Switzerland) Vol. 17, p.393, (1970)
- (116) Menges, G., & Schmidt, H.,  
Kunststoffe, Vol. 57, p.885, (1967)
- (117) Menges, G., Riess, R., & Scharek, H.J.,  
Kunststoffe, Vol. 64, p.200, (1974)
- (118) Menges, G., & Alf, E.,  
Kunststoffe, Vol. 4, p.259, (1972)
- (119) Van Krevelen, D.W., 'Properties of Polymers', Amsterdam  
(1972)
- (120) Bucknall, C.B., & Smith, R.R.,  
Polymer, Vol. 6, p.437, (1965)
- (121) Strella, J., J. Polym. Sci., A-2, Vol. 4, p.527, (1966)

- (122) Matsuo, S., Daane, J.H., Kwei, T.K., & Huseby, T.W.,  
ACS preprints, Vol. 10, p. 1198, (1969).
- (123) Regal, V.R., J. Tech. Phys. (USSR), Vol. 26, p. 359, (1956).
- (124) Sato, Y., High Polymer Chem. (Japan), Vol. 23, p. 69,  
(1966).
- (125) Wang, T.T., Matsuo, M., & Kwei, T.K., J.App. Phys.  
Vol. 42, p. 4188, (1971).
- (126) Goodier, N.J., J. App. Mech. 55, A39, (1933).
- (127) Sauer, J.A., & Hsiao, C.C.,  
Trans. ASME, Vol. 75, p. 895, (1953).
- (128) Knight, A.C., SPE ANTEC, Vol. 12, (1966).
- (129) Cohen, L.A., & Haslett, W.H., SPE Journal p. 246 (1964).
- (130) Kambour, R.P., Le Grand, D.G., & Haaf, W.R.,  
J.Polym. Sci., A-2, Vol. 10, p. 1565, (1972).
- (131) Kambour, R.P. & Kopp, R.W.,  
J.Polym. Sci., A-2, Vol. 7, p. 183, (1969).
- (132) Takahashi, K., J.Polym Sci., (Polym Phys).  
Vol. 12, p. 1697, (1974).
- (133) Bucknall, C.B., Gotham, K.V., & Vincent, P.I.,  
Polymer Science ed. by A.D.Jenkins.  
Pub. by North Holland, (1972).
- (134) Wieser, E., Doctorial Thesis, Aachen, Germany (1959).
- (135) Bernier, G.A., & Kambour, R.P.  
Macromol, Vol. 1, p. 393, (1968).
- (136) Kambour, R.P., Paper 1, PI Conf.  
Yield deformation and Fracture, Cambridge, March, (1973).
- (137) Vincent, P.I. & Raha, S.,  
Polymer, Vol. 13, p. 283, (1972).
- (138) Crook, M., Earl, B.L., Johns, J.H.T.,  
& Loneragan, R.J.  
Polym. Eng. Sci. Vol. 13, p. 390, (1973).
- (139) Hadley, D.W., & Ward, I.M.,  
J. Mech. Phys. Solids, Vol. 13, p. 397, (1965).
- (140) Brereton, M.G., Croll, S.G., Duckett, R.A. & Ward, I.M.,  
J. Mech. Phys, Solids, Vol. 22, p. 97, (1974).
- (141) Lockett, F.J., NPL Report Mat. App. 36, Aug., (1974).
- (142) Dunn., C.M.R., Mills, W.H., & Turner, S.,  
British Plastics, p. 386, July (1964).

- (143) Darlington, M.W., & Saunders, D.W.,  
J.Phys (E) Vol. 3, p. 511, (1970).
- (144) Guild, J., 'The Interference Systems of Crossed  
Diffraction Gratings' Monograph.  
Clarendon Press, Oxford, (1956).
- (145) Shepherd, A.T., Instrument Rev. p. 193, May (1967).
- (146) Hutchinson, J.M., & McCrum, N.G.,  
Nature Phys. Sci., Vol. 236, p. 115, (1972).
- (147) Wright, D.C., RAPRA Members Journal, p. 269, Nov(1974).
- (148) Retting, W. Angew, Makromol. Chem. Vol. 8, p. 87 (1969).
- (149) Gibbs, J.H. & Di Marzio, E.A.,  
J.Chem. Phys., Vol. 28, p. 373, (1958).
- (150) Yeh, G.S.Y., J. Macromol. Sci., Phys., B6(3).  
p. 465, (1972).
- (151) Golden, J.H., Hammant, B.L., & Hazell, E.A.,  
J.App. Polym. Sci., Vol. 11, p. 1571, (1967).
- (152) Matsuo, M., Ibid., Vol. 7, p. 421, (1966).
- (153) Wright, D.C., RAPRA Members Journal. p. 161, June (1974).
- (154) Engineering Prop. of Theromoplastics Ed. By R.M.Ogorkiewicz,  
Wiley Interscience, (1970).
- (155) Alfrey, T., Chem. Eng. News, Vol. 43, p. 64, (1965).
- (156) McCammond, D. & Ward, C.A.,  
Polym. Eng. Sci., Vol. 14, p. 831, (1974).
- (157) Ward, I.M., 'Mechanical Props. Solid Polymers'.  
Wiley Interscience (1971).
- (158) Doolittle, A.K., J. App. Phys. Vol. 22, p. 471,  
(1951).
- (159) Cohen, H.H. & Turnbull, D.,  
J. Chem. Phys., Vol. 26, p. 901, (1959).
- (160) Smith, T.L., Pure and App. Chem., Vol. 23, p. 235, (1971).
- (161) Haward, R.N., & Thackray, G.,  
Proc. Roy. Soc. 1A, Vol. 302, p. 453, (1968).
- (162) Alksne, K.I., Ainbinder, S.B., & Slonimskii, G.L.,  
Polymer Mechanics Vol. 2, No. 3, p. 221, (1966).
- (163) Brady, T.E., & Yeh, G.S.Y.,  
J. Macromol. Sci. Phys., B9(4), p. 659, (1974).

- (164) Geil, P.H., & Yeh, G.S.Y.,  
J. Macromol. Sci., B1(2), p. 235, (1967).
- (165) Bjornhaug, A., Ellefsen, O., & Tonnesen, B.A.,  
J. Polym. Sci., Vol. 12, p. 621, (1954).
- (166) BS4994 Vessels and Tanks in Reinforced Plastics (1973).
- (167) Gotham, K.V., Plastics and Polymers April, (1972).
- (168) Gotham, K.V., PI Conf. Designing & Avoid  
Mechanical Failure, paper 8. Cranfield (1973).

## PATENT SPECIFICATION

(11) 1388 108

1388 108

- (21) Application No. 61834/70 (22) Filed 30 Dec. 1970  
 (23) Complete Specification filed 29 March 1972  
 (44) Complete Specification published 19 March 1975  
 (51) INT CL<sup>3</sup> G01B 5/30 11/16  
 (52) Index at acceptance

G1A 205 207 211 212 21X 21Y 247 248 269 307 357 358  
 369 401 407 409 426 428 42X 42Y 436 438 43X  
 43Y 447 448 457 458 461 463 464 46Y 473 482  
 489 548 549 558 559 578 579 582 589 58Y 675  
 702 70X 70Y 750 780

G1S 1D 1F

(72) Inventor DAVID CHARLES WRIGHT

(54) IMPROVEMENTS IN AND RELATING TO  
EXTENSOMETERS

(71) We, RUBBER AND PLASTICS RESEARCH ASSOCIATION OF GREAT BRITAIN, a British Company, of Shawbury, Shrewsbury, Shropshire, do hereby declare the invention, for which we pray that patent may be granted to us, and the method, by which it is to be performed, to be particularly described in and by the following statement:—

5 The present invention relates to extensometers, that is, to instruments for measuring strains in specimens of a material under test.

15 An object of the present invention is to provide an apparatus for determining the deformation properties of rigid materials, such as thermoplastics materials, and especially the deformation properties of solid materials having non-linear visco-elastic properties.

20 According to the present invention, an extensometer comprises two pairs of elongate bars which are adapted to be symmetrically mounted on either side respectively of a specimen under test, each bar in a pair including a first portion, the first portions of the bars in the pair being mutually parallel and co-planar, a second portion which lies parallel to and laterally spaced from the first portion of the other bar in that pair, said second portions of the bars in the pair also being mutually parallel and co-planar, and an intermediate cross-over portion connecting said first and second portions of the bar, the first and second portions of all four bars being co-planar, a respective roller bearing located between and spacing apart said first and second portions of the bars in each pair, a respective pointer means located adjacent the free end of each of said first portions of said bars for engaging the specimen whereby the two pointer means on the bars in each pair define therebetween a respective gauge length on the specimen, a clamping means adapted to hold together said two pairs of

bars with the specimen therebetween while allowing only relative longitudinal displacement between the two bars in each pair, at least one pair of diffraction gratings carried by respective bars of at least one of said pairs of bars with their grating lines mutually inclined, an optical system which includes a light source arranged for directing a beam of light through said gratings whereby to generate a Moire fringe pattern, and a photoelectric light detector arranged to receive at least a part of said fringe pattern, the arrangement being such that the positions of the light source and light detector means are independent of displacement of the bars due to specimen strain.

60 By this arrangement, when a specimen is engaged by the pointers and the gauge length is increased or decreased due to the subjection of the specimen to a tensile or compressive load respectively, the fringes in said pattern are displaced by an amount proportional to the change in the gauge length. The photoelectric light detector, preferably a photodiode, is thus successively subjected to a plurality of light and dark bands which results in a plurality of electrical pulses proportional in number to the change in the gauge length. These pulses can be recorded automatically, for example on a chart recorder or event timer.

75 The invention will be further described, by way of example, with reference to the drawings accompanying the Provisional Specification in which:—

80 Figure 1 is an end elevation of part of one embodiment of an extensometer constructed in accordance with the present invention, mounted on a specimen under test;

85 Figure 2 is a side elevation of the extensometer of Figure 1; and to the accompanying Figure 3 which is a diagrammatic side elevation of an extensometer in accordance with

[Price 33p]

the invention illustrating the optical system of the instrument.

The extensometer of Figures 1 and 2 comprises two pairs of parallel bars 10a, 10b, 12a, 12b, the bars 10a, 10b having respective central stepped portions 14 and the bars 12a, 12b having respective central stepped portions 16. In addition, the bars 12a, 12b are also provided with respective, laterally offset portions 18, 20 which include the stepped portions 16. As can be seen most clearly in Figure 2, the portions 18, 20 are offset in different directions so that the portion 18 lies in a plane rearwardly of the bars 10a, 10b and the portion 20 lies in a plane in front of the bars 10a, 10b. In this manner, the end portions of all four bars 10a, 10b, 12a, 12b can lie in a single plane although the bars in each pair (10a, 12a, 10b, 12b) are crossed at their central regions so that, at one end of each pair, the bars 10a, 10b lie outside the bars 12a, 12b, but at the other end of the pairs, the positions are reversed.

A respective miniature roller bearing 22 is located between each pair of adjacent end portions of the bars 10a, 10b, 12a, 12b so that the bars in each pair are capable of relative longitudinal displacement. Each miniature roller bearing is flanged by spring loaded washers 23 at each end of that bearing so that the bars are constrained to move in a single plane by preventing relative rotation thereof. Each of the bars 10a, 10b, 12a, and 12b carries an inwardly directed pointer at that one of its end portions which lies inwardly of an end portion of an adjacent one of the bars. Thus, the upper ends of the bars 12a, 12b as viewed in Figure 1, carry pointers 24, 26 and the lower ends of the bars 10a, 10b carry pointers 28, 30. The bars 10a, 10b, 12a, 12b are mounted on a vertically disposed specimen 32 under test with the specimen engaged by the pointers 24, 26, 28 and 30. The bars are held in this position by means of two pairs of clamping arrangements located adjacent the upper and lower ends of the bars respectively. Each clamping arrangement comprises a pair of generally rhomboidal spring strips 34 attached to the outer ones of the bars 10a, 10b, 12a, 12b and interconnected at their projecting ends by means of tie-bars 36. A knurled knob 38 is provided on one screw-threaded end of each tie-bar 36 to enable the spring force holding the bars together to be adjusted, the spring strips being shaped and located such that the lines of action of the rollers and the pointers at the two ends of the bars are substantially coincident.

The specimen 32 is provided with apertures 40, 42 at its two ends whereby one end of the specimen 32 can be attached to a rigidly fixed member while the other end can be attached to a movable member through

which a load can be transmitted to the specimen.

The vertical spacing between the upper and lower pointers provides a gauge length. In fact, there are effectively two "gauge lengths", one between the pointers 24 and 28 on one side of the specimen and another between the pointers 26 and 30 on the other side of the specimen. It will be observed that any change in the first mentioned gauge length will result in a change in the longitudinal spacing of the two bars 10a, 12a and any change in the second gauge length will result in a change in the longitudinal spacing of the two bars 10b, 12b. Clearly, when the specimen is subjected to a simple tensile load, the changes in the two gauge lengths will be substantially the same.

Such changes in the gauge length are detected by means of an optical system utilising the moiré fringe effect. When two identical transmission or diffraction gratings, each having alternate opaque and transparent elements of equal width, are placed face to face with their rulings relatively inclined at a small angle and viewed against a bright background, a pattern of interference fringes of varying light intensity is observed. These fringes are known as moiré fringes. If two such diffraction gratings are constrained to move relative to each other in a direction perpendicular yet coplanar with the rulings, then the moiré fringes will appear to move in a direction perpendicular to their length. The apparent movement of the moiré fringes is proportional to the movement of the grating and can be used to measure this latter movement.

In the extensometer of Figures 1 and 2, associated with the pair of bars 10a, 12a, is a pair of gratings 44a, 46a, and associated with the pair of bars 10b, 12b, is a pair of gratings 44b, 46b. The gratings 44a and 44b are rigidly fixed to the bars 12a, 12b respectively and serve as reference gratings. The gratings 46a, 46b serving as index gratings, are carried by respective supports 50a, 50b which are rotatably mounted on the bars 10a, 10b, whereby the gratings 46a, 46b are rotatable in their own planes. The relative alignment of the pairs of gratings 44a, 46a and 44b, 46b can thus be set so that the lines on the rotatable grating in each pair are at a small angle to those of the fixed grating in that pair.

Attached to each of the bars 10a, 10b by supports 52 is a respective mirror 54, only one of which is shown in Figure 2, the mirrors 54 being pivotably carried by the supports 52 so that their angular position relative to the gratings can be adjusted. Also attached to each of the bars 10a, 10b is a respective reflective prism 56 arranged to direct a light beam applied thereto, in a vertically upward direction from a respective light source (not



shown), through the gratings and onto the mirrors 54. A respective photo-electric light detector comprising an arrangement of photodiodes (not shown) is located beneath each of the mirrors 54 at the bottom of a vertical tube so as to be capable of receiving at least a part of the reflected light beam from its associated mirror. Each photodiode arrangement is connected to an amplifying circuit and thence to a recording device such as a chart recorder, an event timer, or a digital counter.

The operation of the optical system can be understood more clearly by reference to Figure 3 which shows diagrammatically the arrangement of one half the extensometer of Figures 1 and 2. Thus, Figure 3 shows the bars 10b, 12b having the index and reference gratings 44b, 46b mounted thereon respectively. The bar 10b also carries a mirror 54 and a reflective prism 56. A light beam, indicated by the dotted line 60 is generated by a light source 62 and directed onto the prism 56 via a collimating lens 64 and further reflective prism 66, referenced to a fixed supporting structure 70. The gratings 44b, 46b are mounted so that they are separated by a gap D of about 0.003 inches.

When the light beam passes through the two gratings several distinct bands of fringes corresponding to the zero, 1st, 2nd, . . . etc. order fringe patterns are generated and "seen" by the mirror. The tube 67 having an arrangement of photodiodes 67 at the bottom thereof, is located on the fixed support 70 so as to receive the 1st order fringe pattern reflected by the mirror 54. This pattern comprises a series of light and dark bands. It can be seen that when the bars 10b, 12b are now moved longitudinally in the directions of the arrows 72, 74 respectively by virtue of an increase in the specimen length, and hence in the gauge length, the light and dark bands will move in direct relation to the movement of the bars.

It is to be noted that the prism 66 is referenced to the fixed supporting structure 70, whilst the prism 56 is referred to the moving carriage essentially comprising the bars 10a, 10b, 12a, 12b. Provided that the arrangement of photodiodes 68 is approximately vertically below the mirror 54, the axis of the optical system will always pass down the tube 67 irrespective of movement of the carriage members due to strain displacements. By this arrangement, the light source and the photo-electric light detector do not have to be carried by the moving carriage members so that the positions of the light source and light detector are substantially independent of specimen strain. This has the advantages that the carriage can be light and there is no possibility of constraint being made on the movement of the carriage

by the output leads of, for example, the photodiode arrangement 68. Furthermore, only small area gratings are required since only relative grating movement in the direction of strain need be considered.

Pulses are generated by the light detector as each light band passes, the pulses being either recorded on the chart or counted by a counter. The number of pulses recorded is directly proportional to the increase in the gauge length i.e. to the extension undergone by the specimen, the constant of proportionality being determined solely by the line spacing on the gratings which is the same, accurately known amount for each grating. Thus, the instrument provides an "absolute" reading and no calibration is required.

All the parts of the instrument attached to the specimen are preferably constructed of ground flat stock steel so that high machining accuracy and dimensional stability can be attained. By providing an optical system on both sides of the specimen, differences in the strain experienced by each side of the specimen can be detected and an average strain calculated. However, only one pair of gratings may be provided if it is assumed that the aforementioned difference in strain on the two sides of the specimen is not significant.

In one embodiment, the arrangement of photodiodes can comprise two photodiodes connected in parallel at the bottom of the tube 67 and in opposition. The photodiodes are disposed such that when one is in a light field of other is in a dark field. This has the advantage of eliminating the effect of a changing background light level. Furthermore, the effective contrast is doubled.

In a further embodiment two or more photodiodes are provided in the tube 67 and coupled to a logic circuit adapted to indicate whether the gauge length is increasing or decreasing.

Conveniently the grating pitch is about 0.004 m.m.

Although the extensometer described above is for measuring extensions brought about in the specimen by tensile loads, with minor alterations, it could also be used for measuring contractions in length brought about by applying a compressive load to the specimen. It can also be used for retraction measurement (recovery) when a tensile load has been removed.

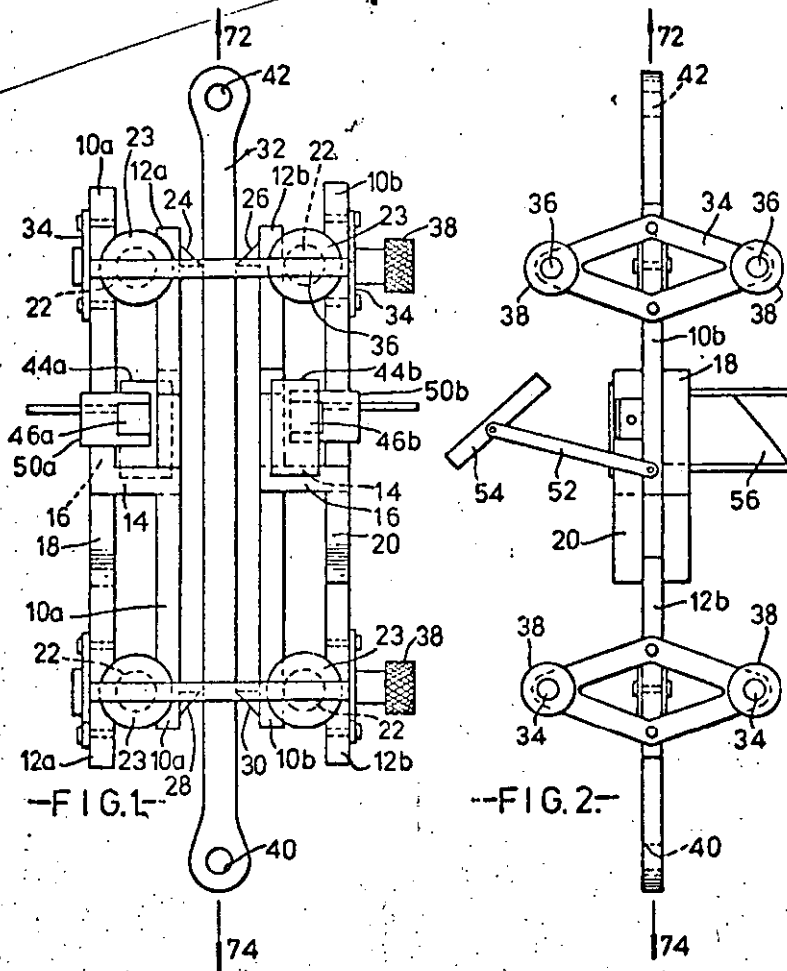
The above described extensometer has the advantages that it provides an absolute reading and can be light in weight (e.g. 100 grams). The long term signal stability is good because the output is inherently digital. Large displacements can be measured without loss of insensitivity. If increments of strain are recorded as a function of time a convenient format is provided for the automatic recording of long term creep and recovery.

## WHAT WE CLAIM IS:—

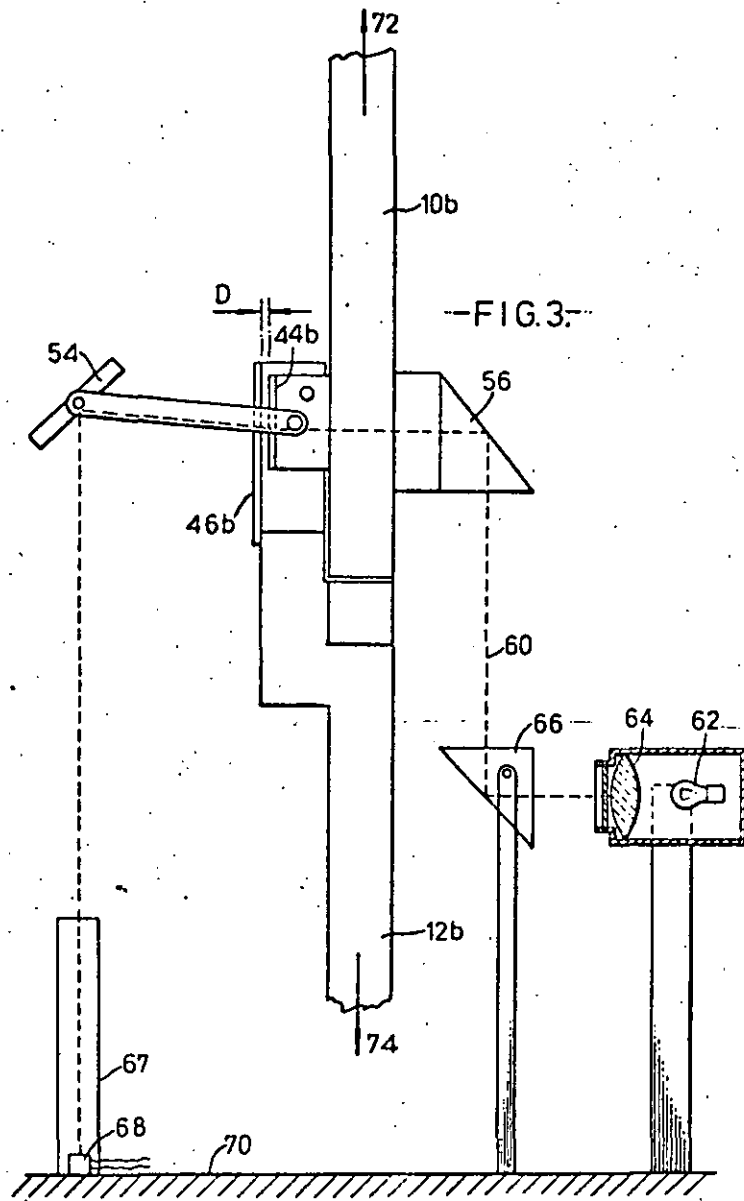
1. An extensometer comprising two pairs of elongate bars which are adapted to be symmetrically mounted on either side respectively of a specimen under test, each bar in a pair including a first portion, the first portions of the bars in the pair being mutually parallel and co-planar, a second portion which lies parallel to and laterally spaced from the first portion of the other bar in that pair, said second portions of the bars in the pair also being mutually parallel and co-planar, and an intermediate cross-over portion connecting said first and second portions of the bar, the first and second portions of all four bars being co-planar, a respective roller bearing located between and spacing apart said first second portions of the bars in each pair, a respective pointer means located adjacent the free end of each of said first portions of said bars for engaging the specimen whereby the two pointer means on the bars in each pair define therebetween a respective gauge length on the specimen, a clamping means adapted to hold together said two pairs of bars with the specimen therebetween while allowing only relative longitudinal displacement between the two bars in each pair, at least one pair of diffraction gratings carried by respective bars of at least one of said pairs of bars with their grating lines mutually inclined, an optical system which includes a light source arranged for directing a beam of light through said gratings whereby to generate a Moire fringe pattern, and a photo-electric light detector arranged to receive at least a part of said fringe pattern, the arrangement being such that the positions of the light source and light detector means are independent of displacement of the bars due to specimen strain.
2. An extensometer as claimed in Claim 1 in which one of said roller bearings is respectively located in the region of each of said four pointer means and said clamping means comprises a pair of spring-loaded clamping devices, the clamping forces applied by one of said spring-loaded clamping devices being arranged to pass substantially through the line for action of two of said pointer means and the roller bearings adjacent thereto, and the other of said pair, through the line of action of the other two pointer means and the roller bearings adjacent thereto, respectively.
3. An extensometer as claimed in Claim 2 in which said spring-loaded clamping devices each comprises a pair of rhomboidal spring strips, one pair of opposite corners of each spring strip being attached to the second portion of a bar of one of said pairs and the other pair of opposite corners receiving respective clamping screws extending from corresponding corners of the other spring plate in the pair which is attached to the second portion of a bar in the other of said pairs of bars.
4. An extensometer as claimed in any of Claims 1 to 3 in which said optical system further includes a first prism rigidly fixed to a reference surface, a second prism attached to one of said bars and arranged to direct a light beam, received from said light source by way of the first prism, through said pair of diffraction gratings, said one bar also carrying a mirror for directing part of the light emanating from the gratings to said light detector.
5. An extensometer as claimed in Claim 1, 2, 3 or 4 which is adapted to be mounted on a vertically oriented, elongate specimen with the two pointers associated with each pair of bars located one above the other to define two said gauge lengths on the specimen.
6. An extensometer as claimed in any of Claims 1 to 5 in which the two pairs of bars on opposite sides of the specimen each have a pair of diffraction gratings mounted thereon whereby the strain on both sides of the specimen can be monitored.
7. An extensometer as claimed in any of Claims 1 to 6 in which one of the diffraction gratings in the, or each, pair of gratings is rigidly fixed to its supporting bar, whereas the other grating in the pair is angularly adjustable relative to its supporting bar and about an axis perpendicular to its plane.
8. An extensometer as claimed in any previous claim in which the photo-electric light detector is connected to a counter or chart recorder whereby the number of electrical pulses generated thereby can be recorded.
9. An extensometer constructed, arranged and adapted to operate substantially as hereinbefore particularly described with reference to and as illustrated in Figures 1 and 2 of the drawings accompanying the Provisional Specification and in Figure 3 of the accompanying drawings.

W. P. THOMPSON & CO.  
12, Church Street,  
Liverpool, L1 3AB  
Chartered Patent Agents.

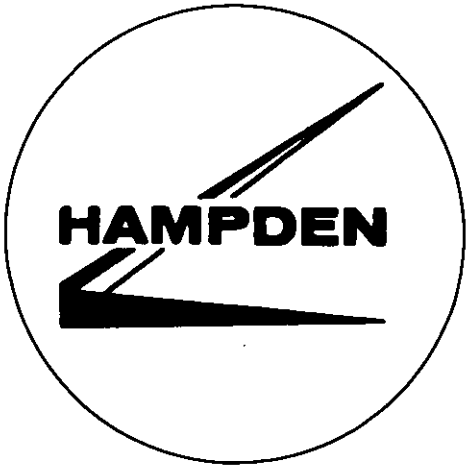
Printed for Her Majesty's Stationery Office, by the Courier Press, Leamington Spa, 1975.  
Published by The Patent Office, 25 Southampton Buildings, London, WC2A 1AY, from which copies may be obtained.



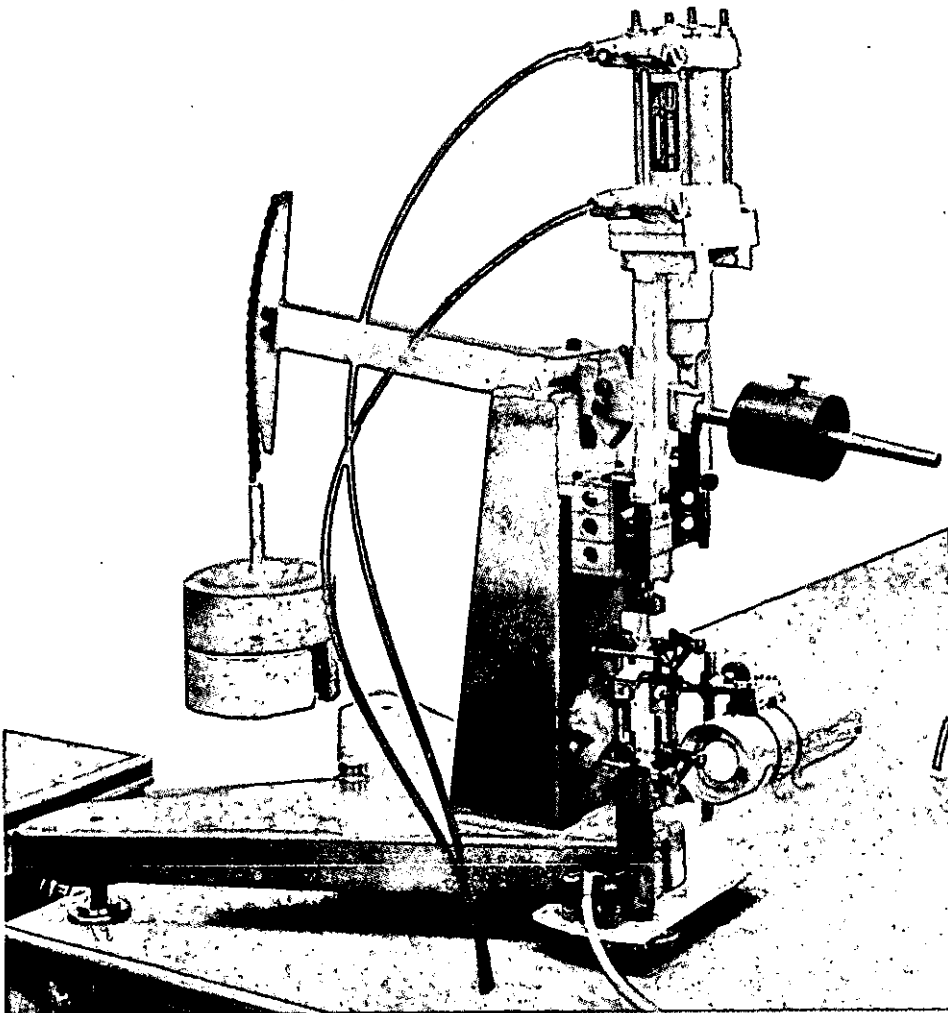
This drawing is a reproduction of the Original on a reduced scale



255



# RAPRA CREEP TESTER



# SPECIFICATION

## Extensometry

Strain sensitivity:	0.0025% (Class A sensitivity-BS 4618)
Gauge Length:	80mm
Diffraction Grating Pitch:	0.004 mm
Total weight of extensometer:	100 grms approx.
Maximum Measurable Strain:	10%
Specimen Dimensions:	130mm x 5mm x 3.3mm (nominal)

## Recording Equipment

Reading Head:	4-M S 9 A Silicon Photo-diodes feeding 2- d.c. operational amplifiers with variable gain, hysteresis and balance.
Output:	10V square pulse per 0.005% strain increment.
Readout:	Bi-directional digital counter.

Stabilised Power Supplies are used for the amplifiers and a 6 Volt Power supply for the Light Source:

N.B. If more than one machine is used a date/time event recorder and logic unit system may prove economical. Flexibility in this respect is provided to satisfy customer's requirements.

## General

Maximum Specimen Load:	1.2 kN
Lever Arm Ratio:	5:1
Alignment System Preload:	5N
Restoring Force at 1% Strain:	5N
Hydro-Pneumatic loading actuator.	

## Services

Mains supply:	230/250V 50 Hz
Air supply:	80-100 p.s.i.

## Laboratory Requirements

Constant Temperature and Humidity Control.  
Heavy Table.

## Dimensions of Instrument

Height:	600mm
Base:	350mm x 350mm
Weight:	15 kg. approx.

### 3. Operating Instructions for the Hampden Creep Tester.

#### 3.1. General Requirements.

The most demanding requirement of the setting-up procedure is that of optimising the Optical system. The optical sequence is light source, lens, large mirror, prism, index grating, reference grating, small mirror and photo-diodes. Apart from the reference grating and the lens all the optical parts are adjustable by rotation.

As the light is transmitted through the grating pair, this being achieved by adjusting the large mirror, a defraction pattern consisting of a central (yellow) image of the source and multiple multi-coloured defraction images on either side. With the small mirror elevated and a white screen placed about 20 cms. from the extensometer, these defraction images can be readily observed, particularly if the ambient light level is low.

Normally the best condition is obtained with the filament horizontal although under certain circumstances individual machines may operate more successfully with filament vertical. (Note : The light filament will normally be in the horizontal position on receiving the tester. The following instructions are for setting the tester up with the filament in the horizontal position. Vertical position settings are the same but a much narrower pattern will be observed).

Unless the angle between the grating lines on the index and reference gratings is very small, the Moire fringes will not be visible. The main target of the setting up process then is to achieve at the photo-diode assembly high contrast fringes in the brighter, lower First order defraction image. The photo-diodes should straddle the visible red and infra-red regions of the image.

#### 3.2. Detailed Setting Up Procedure.

##### Attachment of Extensometer to Specimen.

Fig. 1 & 2 shows the arrangement of the extensometer with respect to the specimen. It is essential that the extensometer knife edges are opposed in pairs symmetrically about the mid-point of the specimen, this can be achieved with the help of a jig (which can be purchased on request from Hampden Test Equipment) which pre-sets the gauge length (distance between knife edges) at 80 mm. Operating instructions for the jig are given in Appendix 1.

The tensioning rods shown in Fig. 1 (4) need only be adjusted if unusually wide or narrow specimens are used. (Normal specimen width is 3 mm.).

##### Insertion of Specimen into Machine.

After attaching the roller bearing pairs and spigots to the ends of the specimen, the low pair (furthest from the grating pair) is inserted into the lower machine based hook, such that the grating pair is furthest away from the body of the machine (Fig.1.) The upper hook is lowered by depressing the cantilever alignment mechanism until specimen can be slotted into this hook. The specimen should now have a slight tensile pre-load applied to it. If it has not then move the balance weight on the lever arm until a slight tensile load is applied.

## Adjustment of the Optical System.

Switch on the mains switch on the electronic console.

Place white screen about 20 cms. from the extensometer on the photo-diode tunnel side. Rotate the large mirror until a light pattern is observed. Obtain the brightest and clearest pattern possible.

To set up the Moiré fringes viewed through the gratings (Fig. 1.9.) use a pin and insert in the small pin hole (Fig. 2.12) at the side of the index grating yoke (Fig. 1.5.) Bring the gratings to the correct position by moving the index grating yoke VERY VERY SLOWLY and the pattern as shown in Fig. 3 should be observed. The correct pattern is 'C'. The sequence A to G below shows the patterns obtained by rotating the index grating.

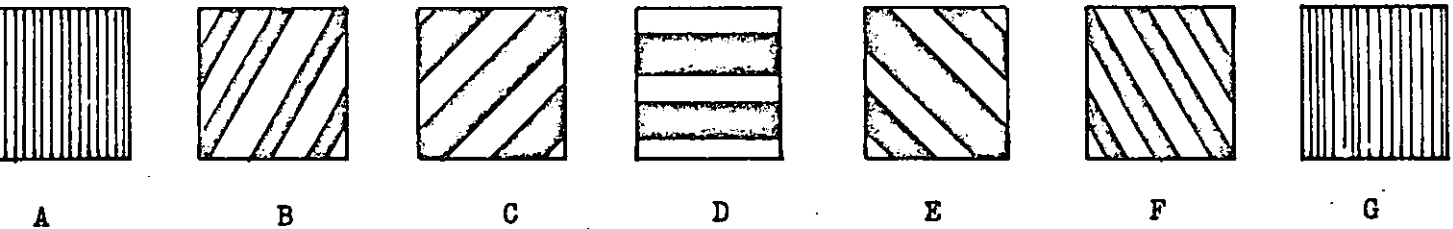


Fig. 3.

Now make sure the Hydraulic Ram is retracted by switching to UP on the hydraulic unit. If the lever arm is gently moved, the Moiré fringes can now be observed easily. Now adjust the small mirror. (Fig. 2.6B). (Note the small screw at the base of the arm (Fig. 2.6A) may have to be tightened periodically), until a bright rainbow pattern is observed, then adjust to bring it to the photo-diode tunnel (Fig. 2.13). Now line up the pattern by the prism (Fig. 2.11) until the light is central down the photo-diode tunnel. Move the small mirror very slightly until the green and violet pattern shown on the photo-diodes. Turn photo-diode tunnel round until the diodes are facing across the pattern (See Fig. 4).

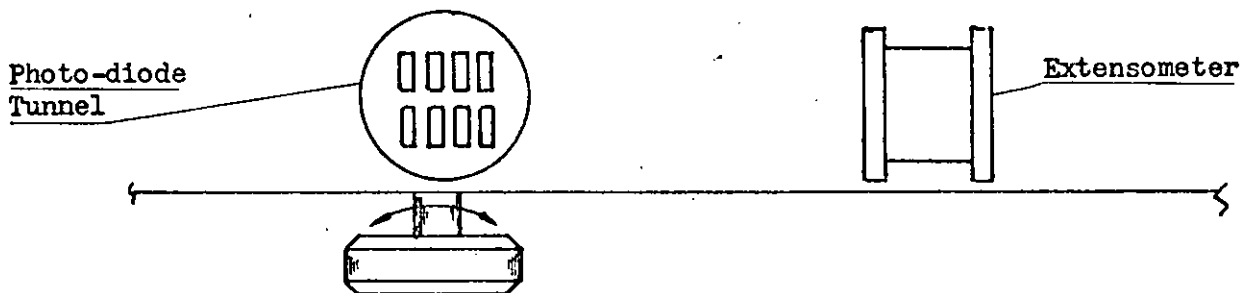


Fig. 4.

## OPTIMISATION USING AN OSCILLOSCOPE.

First ensure gain controls of both amplifiers are fully clock-wise, and both hysteresis controls are fully anti-clockwise.

Set both gain controls  $\frac{1}{4}$  anti-clockwise.

Set both hysteresis controls  $\frac{1}{4}$  clockwise.

Set both Balance Controls to mid-position.

An oscilloscope is required with both X and Y amplifiers. These must both be D.C. coupled. The two monitor I's are connected to the X and Y inputs.

- Set scope to time base = EXT X.X and Y sensitivity = .1 volt/cm. Set both the Avant amplifiers to high band pass.
- Move lever arm up and down and observe the signal on the scope. This will probably be a small circle or ellipse.
- Adjust the small mirror and large mirror alternatively, whilst moving the lever arm up and down until the maximum signal is obtained.



OPTIMISATION USING AN OSCILLOSCOPE continued.

- d) Rotate the photo-diode assembly until the signal is a circle or an ellipse with major and minor axis approximately orthogonal with the X and Y directions.
- e) Connect the MON 1 of one amplifier to the X plates and the MON 2 of the same amplifier to the Y plates. Reduce the Y sensitivity to 10V/cm. The BALANCE, GAIN and HYSTERESIS controls must now be used to obtain the signal patterns shown in Fig. 5.

APPENDIX 2 includes various possible signals.

e) Connect the Monitor one of one amplifier to the X plates and Monitor 2 of the same amplifier to the Y plates. Reduce the Y sensitivity to 10 V per cm. The balance, gain and hysteresis controls must now be used to obtain the signal pattern shown in Fig.5. It is important that the hysteresis 'window' is operative between  $\frac{1}{2}$  and  $\frac{2}{3}$  of the amplitude of the signal and central with it. Also the noise on the signal must be less than half the width of the window. APPENDIX 3.

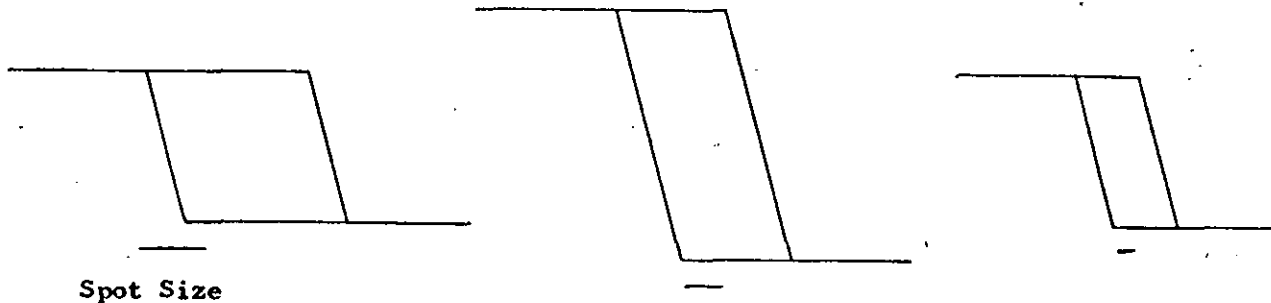


Fig.5

Fig.5. Acceptable oscilloscope patterns for Mon 1, Mon 2, inputs.

INCLUDES VARIOUS POSSIBLE SIGNALS.

(f) Repeat (d) on the second amplifier.

(g) Set the counter to zero. Up and down movement will give a return to zero. Negative counts will signify creep and positive counts recovery or visa versa ; this will depend on how the instrumentation has been set-up. Establish at this stage the meaning of + time and negative readings.

### 3. Loading Procedure.

The restrictor valves in the pneumatic/hydraulic pack vary the rate of load removal or application independently with rubber inserted between the ram bearing and lever arm the loading period should only take about 1 second.

With the pneumatic switch in the UN-load position put appropriate weights on the weight pan. Set counter to zero and load the machine with the pneumatic switch. Each count is equivalent to a strain of 0.000025. After the count rate has slowed sufficiently the low band pass switch can be used - this eliminating much of the noise, and also the effect of any fast stray transients. Before the removal of load this must be switched back to high band pass.

## Appendix 1.

### Extensometer Jig.

This jig centralizes the extensometer about the mid-point of the specimen and also pre-sets the gauge length to 80 mm. If the operation is carried out carefully the gratings should remain at the correct angle and reduce the setting up time for the optical system.

Remove the roller bearings and spigots from the used specimen. Close up the jig. Insert the specimen and extensometer into the jig. Open the jig and remove the specimen. Adjust the extensometer knife edges until in contact with the gauge length templates. After measuring the cross-sectional area of the unused specimen insert this centrally with respect to the extensometer with the aid of the spigots provided and close the jig. After removal some adjustment may be required to centralize on the axis of the specimen.

Appendix 11.

Some Monitor 1/Monitor 1 Signal patterns.

Lever arm moved up/down

Adjust the amplifier balance control  
(on amplifier connected to the Y plates)

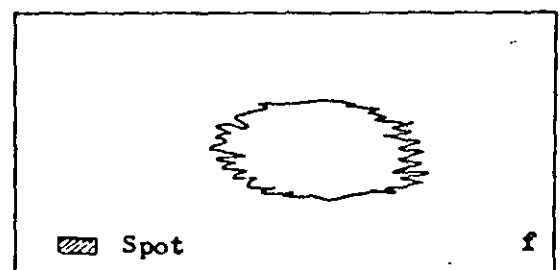
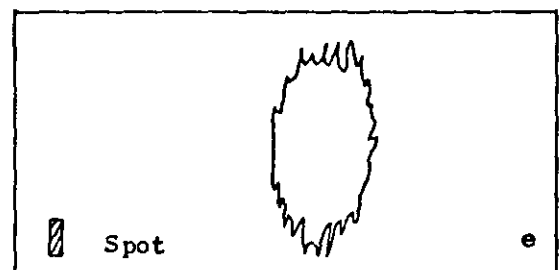
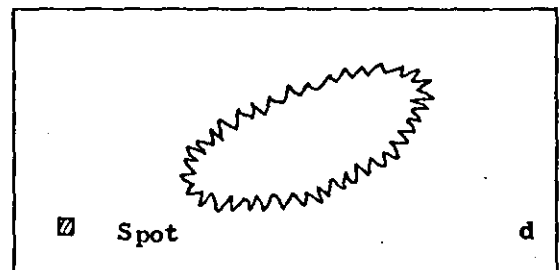
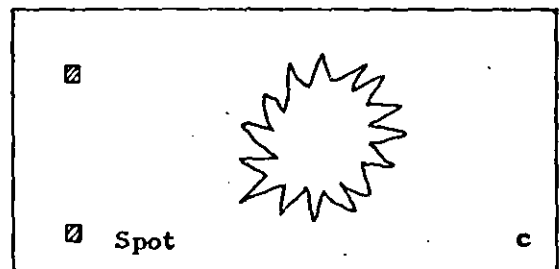
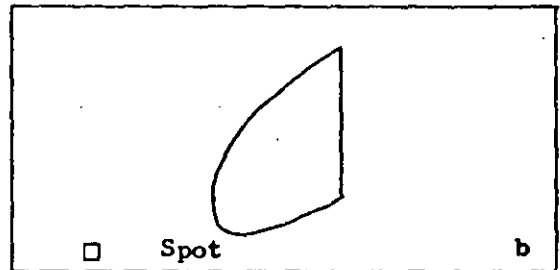
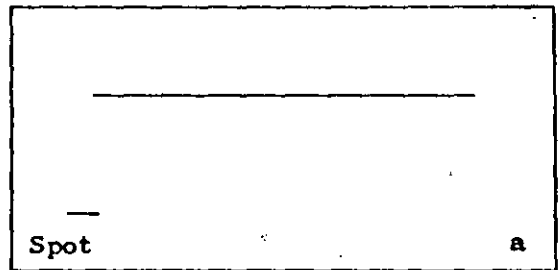
Ditto ..... X plates.

Signal to noise ratio too low  
readjust optical system

Signal strength sufficient but  
readjustment of photo-diode  
assembly is required

O.K.

O.K.

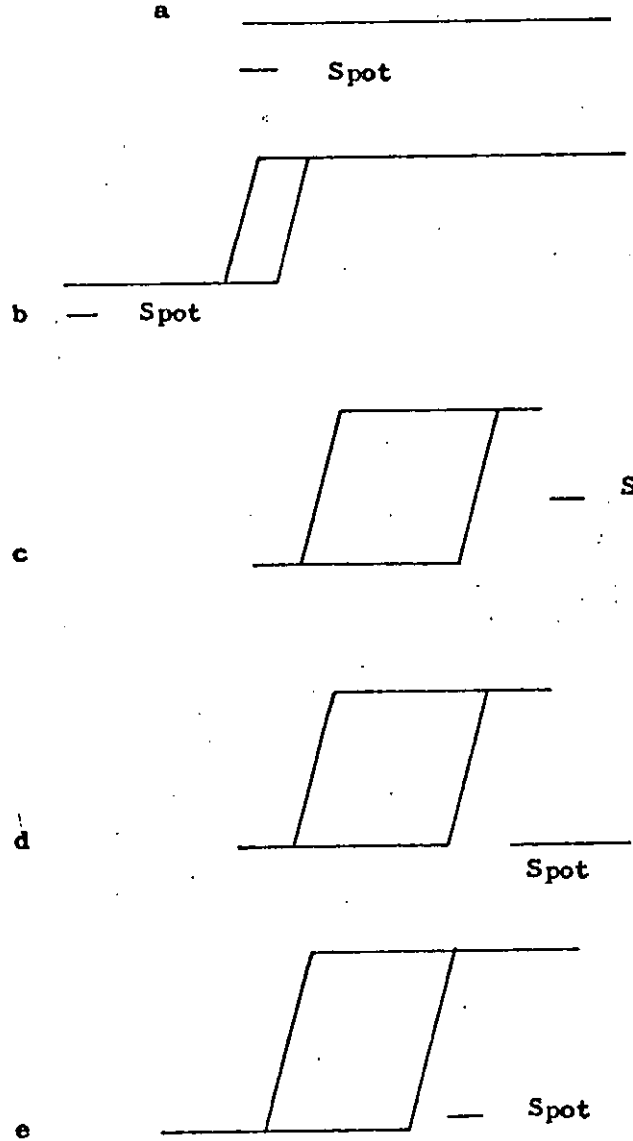


APPENDIX 111.

Some Monitor 1/ Monitor 2 Signal Patterns.

Lever arm moved up/down

- a. Move balance until changes in level is observed.
- b. Centralize with the balance control and increase hysteresis or reduce gain
- c. Decrease hysteresis or increase gain
- d. Correct shape but noise level max. hysteresis level. Original Monitor /1/Monitor/1 signal not sufficient.
- e. O.K.



1/2	CARRIAGE STRUTS
3	LEAF SPRINGS
4	TENSIONING RODS
5	INDEX GRATING YOKE
6A	MIRROR ARM
6B	SMALL REFLECTING MIRROR
7	BEARINGS/FLANGES
8	SUPPORT BEARINGS
9	GRATINGS
10A 10B	INDEX & SCALE GRATINGS
11	REFLECTING PRISM
12	GRATING ADJUST. PIN HOLE
13	PHOTO DIODE TUNNEL
14	LARGE REFLECTING MIRROR
15	SUPPORT HOOKS

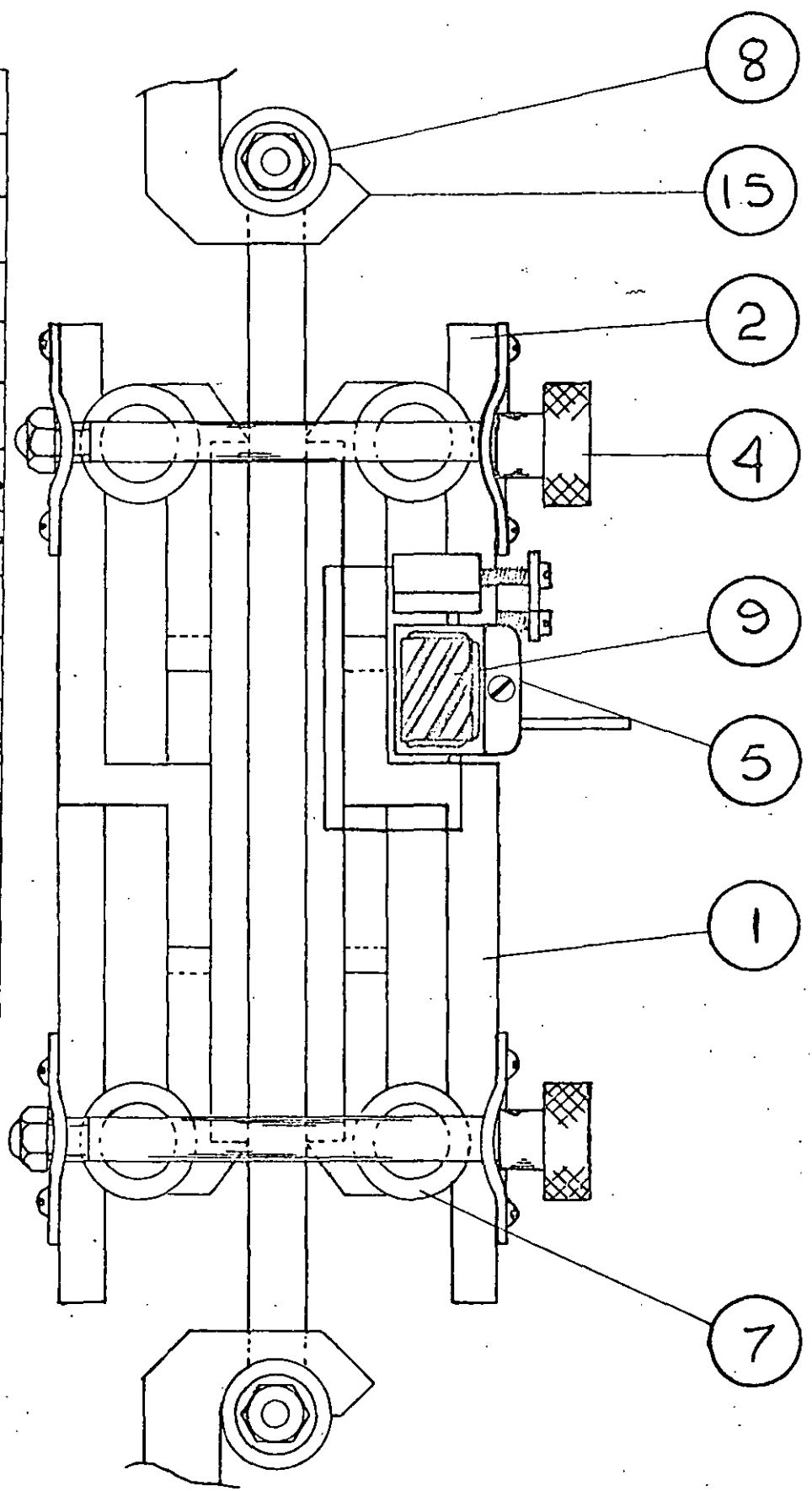


Fig 1

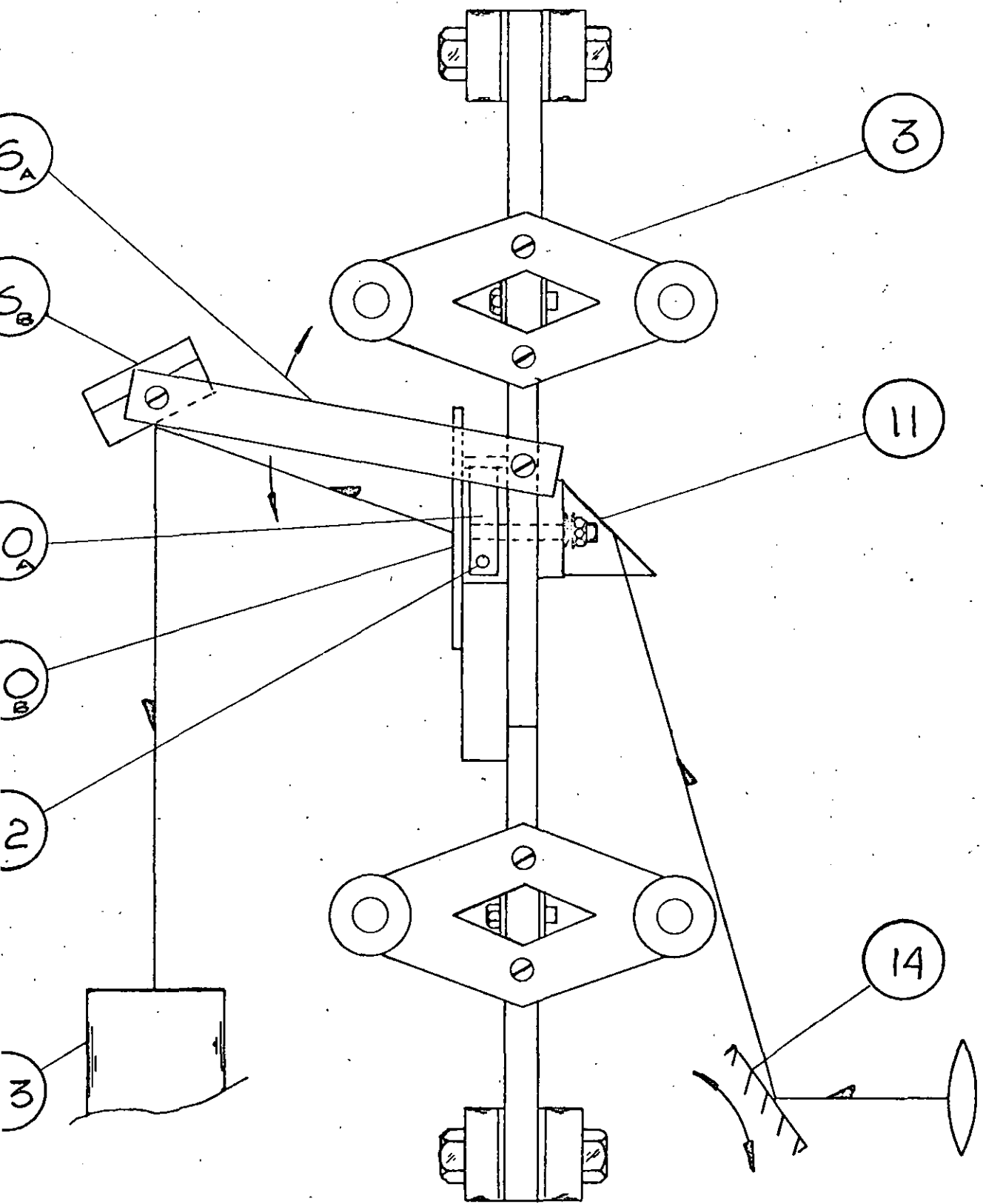


Fig. 2.

# Anomalous Post-Annealing Creep Response of UPVC and PMMA

C. Wright

## SUMMARY

The 20 C creep compliance of UPVC is temporarily increased prior to annealing at temperatures above  $\sim 45$  C and below  $T_g$ . This effect increases with decreasing annealing time. Similar behaviour is observed with PMMA which suggests that this may be a general phenomenon shared by polymers in the 'glassy amorphous state'. The temporary, and therefore unstable nature of the annealed state is inappropriate for a test specimen, particularly for tests of long duration. It is suggested that volume relaxation in UPVC below 45 C proceeds by short-range separation into regions of molecular order and disorder. This state is rapidly disrupted at temperatures above 45 C.

## INTRODUCTION

Thermal conditioning prior to property evaluation is a standard method of minimising batch-batch variability. A relatively severe and recent thermal conditioning treatment supposedly erases the influence of the (often unknown) previous thermal history. This provides an easily accessible materials reference state which however, is almost certainly arbitrary. The reference state in addition may be only a transient one and therefore not stable over the period of test. An arbitrary unstable reference state is particularly inappropriate for creep testing, where long test durations are common and creep data are often intended for use in design calculations.

According to classical concepts of the glassy amorphous state, a polymer at any temperature below its glass transition temperature ( $T_g$ ) undergoes volume relaxation (densification). The rate of this relaxation at temperatures below  $T_g$  is so small that for normal periods of observation the state is apparently stable. At temperatures that approach  $T_g$  the rate of volume relaxation will be increased resulting in a detectable change in the density and properties of the polymer.

Letting (1) investigated the effect on the tensile modulus of UPVC after annealing for various periods at a temperature of ( $T_g - 17$  C). The modulus (25 C) at low strain rates increased substantially with annealing time. At high strain rates the modulus was not significantly affected. Metz and McKinney (2) employed a similar heat treatment of UPVC and attributed the observed increase in the pre-stress transition endotherm to an increase in crystallinity. Burns (3) attributed a similar effect to a decrease in free volume. These observations are compatible with classical expectations. Volume relaxation involves an increase in molecular order; this decreases molecular mobility and therefore increases the long term (low strain rate) modulus. At high strain rate modulus is not primarily dependent on molecular mobility and is therefore not sensitive to annealing.

Turner (4) investigated the effect of pre-conditioning at 60 C on the creep response of UPVC at 60 C. It is reported that the time dependent creep compliance increased with increasing pre-conditioning period. Therefore in this respect the response is apparently

classical and indicative of volume relaxation in the direction of equilibrium.

The procedure adopted here involves room temperature creep testing after annealing periods at various temperatures. Although annealing as compared with pre-conditioning introduces an additional interaction (the cooling cycle) it does offer a distinct advantage. The effect of thermal treatment can only be ascertained unambiguously by comparison with the state or response of the untreated material. The creep behaviour with no-annealing presents no problem, but the zero pre-conditioning state is unattainable.

## EXPERIMENTAL

The following sequence was adopted:

- (i) Calendered sheets of UPVC (Cobex 018 grade supplied by BXL Ltd) were stored for 2 years at 20 C.
- (ii) Creep specimens of nominal dimensions 3mm x 5mm x 140mm were prepared.
- (iii) Creep specimens were stored in ovens at either 60 C  $\pm$  1 C, 50 C  $\pm$  1 C, or 40 C  $\pm$  1 C.
- (iv) After a specified annealing period covering a range between 1 hour and 2000 hours, specimens were removed and cooled (to 20 C) under controlled forced air convection for 30 minutes.
- (v) The cross-sectional areas of the cooled specimens were measured and the specimens prepared for tensile creep testing.
- (vi) 1 hour, 24 hours, or 336 hours after the removal of the specimen from its oven (termed the delay time) a tensile stress of 25MN/m<sup>2</sup> was applied and the creep strain recorded for 10<sup>4</sup>s.

A similar sequence but with only one annealing temperature of 60 C, and one delay time of 1 hour was applied to PMMA (cast Perspex, ICI Ltd).

The tensile creep machines used in the study have been described previously (5). A Moiré fringe extensometer, employing crossed diffraction gratings with a ruling pitch of 4  $\mu$ m provides the means of automatic strain detection. The Moiré fringe image illuminates an assembly of 4 silicon photodiodes. The photodiode signal is amplified and shaped to provide 2 or 4 counter compatible pulses, for each 4  $\mu$ m extension or contraction of the 66.67mm gauge length. Thus strain increments of 0.0015% can be totalised on a bi-directional counter and/or used to trigger a digital event recorder which essentially records the time co-ordinate for each positive or negative strain increment for the duration of the creep test.

## RESULTS

The family of creep curves shown in Figure 1 are for UPVC with various annealing periods at 50 C with a 1 hour delay before testing. The creep characteristic with no thermal treatment is identified by the discontinuous line. Similar data were generated after longer delay times and at different annealing temperatures. The initial creep response tended to be rather erratic for these annealing treatments,



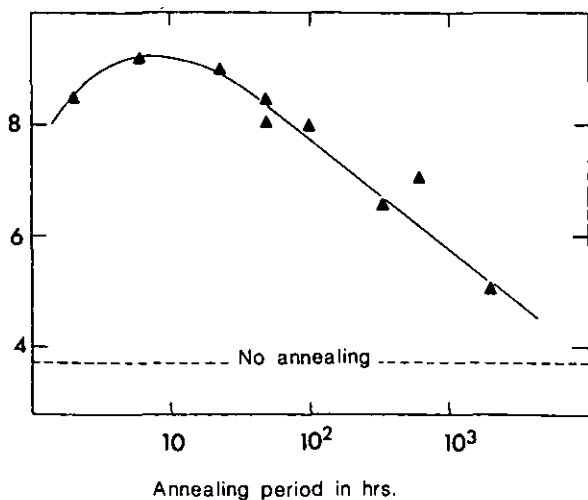


Fig. 5. The time dependent tensile creep compliance  $\Delta C$  of cast A at 20 C v. annealing time at 60 C. The delay time between annealing and testing is 1 hr.

comparison with the non-annealed reference state response. If this response was not known then the data in Figures 2 and 3 would appear to be classical, i.e. a decrease in compliance with increasing annealing time. This is qualitatively similar to the trend observed by Turner and discussed in the introduction.

It would be logical in the absence of any other evidence to seek an explanation for this anomalous behaviour by reference to observed morphological differences between UPVC and that of a classical glassy amorphous polymer. Morphological studies have revealed direct evidence of ordered regions in UPVC (6), (7), (8). These regions might be regarded as small crystallites or regions of molecular orientation with a characteristic cohesive energy and a characteristic melt temperature, or simply as regions of zero configurational entropy which are stable below a particular temperature. Clearly, both aspects describe the same phenomenon but at this stage it is considered preferable to treat each one separately.

Lobst (9) has estimated that the smallest stable unit of molecular order in plasticised PVC would be disrupted at temperatures above 50 C. Larger ordered units have a higher melt temperature but their formation is less probable. Stafford (10) has used the argument that the disruption of 'crystallites' is responsible for the phenomenon of 'reversible stiffening in plasticised PVC'. The compliance of plasticised PVC increases dramatically with annealing but slowly returns to its original stiffness in time after annealing. In this respect the response to annealing is similar to that reported here, but Stafford did not observe the transition in short period annealing effects above 50 C. This transition being close to the minimum 'crystallite' temperature as calculated by Lobst adds considerably to the case for a thermal disruption model. The effect of thermal history on the creep response of UPVC could be explained by the following sequence:

Over extended periods (2 years in this case) at 20 C, small crystallites are formed which are stable at this temperature. The low (or zero) free volume within the crystallite structure is responsible for deformation processes with very long retardation times. Hence the presence of crystallites might be considered as delaying strain response and increasing the creep compliance over long creep times.

After short periods of annealing at 50 C or 60 C the crystallites suffer rapid thermal disruption leading to an increase in creep compliance particularly after long periods

under load.

(3) After long periods of annealing above 45 C the free volume is slowly reduced by the classical process of volume relaxation: As this proceeds the creep compliance will slowly decrease.

(4) With increasing delay time after annealing, crystallites are slowly reformed with an attendant decrease in compliance.

The second approach is to consider the entropy of the system. Gibbs and Di Marzio (11) have proposed that even though the observed  $T_g$  is a kinetic phenomenon there is an underlying thermodynamic transition at a lower temperature  $T_2$ . If the polymer is cooled infinitely slowly then at  $T_2$  the configurational entropy of the specimen as a whole would be zero. Adam and Gibbs (12) calculated that a universal expression for  $T_2$  could be:

$$T_2 = T_g - 53 \text{ C}$$

According to Adam et al the activation volume in the Eyring (13) viscosity equation is identified as the minimum cooperatively re-arranging region. The transition probability, the mobility, and hence the relaxation or creep rate increases as this minimum activation volume decreases. Obviously this cooperative entity must contain free volume for internal re-arrangement, or more precisely a unit value of quantised free volume (hole) must be present. The volume of the cooperative entity, and hence the rate of relaxation and creep might therefore depend significantly on the distribution of free volume or the quantised unit of free volume. At temperatures below  $T_2$  close packing is energetically favourable because the equilibrium configurational entropy is zero. This cannot be achieved on a macroscopic scale within a finite time because this involves large diffusion distances and a high degree of molecular cooperation.

It is proposed here, however, that expulsion of free volume could be achieved within a finite time at the short-range level. The result of such a process would be small regions of aligned molecular segments (crystallites) with zero configurational entropy bounded by a region with a high free volume content. Pictorially this is similar to the fringed micellar grain model of the 'glassy' state adopted by Yeh (14). Therefore it could be envisaged that after a finite period of storage at 20 C the quantised unit of free volume would increase in size with a resultant increase in the minimum volume of molecular cooperation and a decrease in creep compliance. On raising the temperature above  $T_2$  the ordered regions are rapidly disrupted with a resultant decrease in the volume of the cooperative entity and increase in compliance.

Both the energy and entropy approach combine strongly to support the hypothesis that the volume relaxation process below  $\sim 45$  C is quite different from that operating above this temperature. Above 45 C, volume relaxation proceeds classically by a uniform diffusion of free volume. Below  $\sim 45$  C ( $T_2$ ) the uniform diffusion process is no longer energetically favourable and is replaced by a short range process which results in the formation of 'small islands' of order in a matrix of disorder. The short range ordered regions are disrupted rapidly on annealing above 45 C and it is proposed that this is responsible for the anomalous creep behaviour reported here for UPVC.

The existence of two different volume relaxation processes could also explain why in some cases (e.g. Retting (1)) apparently classical effects are observed after annealing. The period at room temperature prior to annealing determines whether sufficient localised volume relaxation has accumulated to give a non-classical response. Thus a recently processed polymer may be expected to react differently to annealing than one stored below  $T_2$  for a long period prior to annealing.

## Acknowledgments

I am indebted to my supervisors Mr. M.J.Stevens and Dr. M.M.Hall for the enthusiasm and advice that have been generously provided by both during the preparation of this thesis.

I would also thank Mr. R.H.Norman of RAPRA for the many useful technical discussions. These have given me the opportunity to assess the credibility of various concepts and hypotheses proposed in this thesis.

The thesis has been typed by Gwladys Tipton, a young lady of cheerful and uncomplaining disposition, combined with professional excellence.

I would also acknowledge the help given by Mr. John Beesley who, as my assistant in the early days, contributed to the design of the creep machine hardware and who is responsible for Figures 4.22 and 4.23.

Finally, I acknowledge the generous provision of funds, facilities and services made by RAPRA, its Council and Management, towards the support of the research work that has been reported here.

